
UNIVERSIDAD DE GRANADA
DEPARTAMENTO DE FÍSICA TEÓRICA Y DEL COSMOS
PROGRAMA DE DOCTORADO EN FÍSICA Y MATEMÁTICAS

---

# POSITION ON THE HERTZSPRUNG-RUSSELL DIAGRAM OF MAGNETICALLY ACTIVE YOUNG STARS

---

**Estefanía Casal López**

INSTITUTO DE ASTROFÍSICA DE ANDALUCÍA
CONSEJO SUPERIOR DE INVESTIGACIONES CIENTÍFICAS

Under the supervision of:

**Dr. Matilde Fernández Hernández**

This dissertation is submitted for the degree of
Philosophiæ Doctor (PhD)

April, 2021


Editor: Universidad de Granada. Tesis Doctorales
Autor: Estefanía Casal López
ISBN: 978-84-1117-313-1
URI: http://hdl.handle.net/10481/74712

# Contents

# Abstract

The magnetic activity of K- and M-type dwarf stars is considered responsible for the "alterations" that are observed in some of them. Stauffer et al. (2003) investigated an anomaly observed in the colour-magnitude diagram (CMD) in stars from the Pleiades cluster. The low-mass stars appeared displaced blueward in the $M_v$ versus $B-V$ representation, an effect that is minimized in the $M_v$ versus $V-I_c$ representation. Similarly, they observed reddening in the $M_v$ versus $V-K_s$ diagram. As a result of this blueward displacement in $M_v$ versus $B-V$ and redward displacement in $M_v$ versus $V-K_s$, it was speculated that this could be due to the presence of spots and plages on the photosphere of the stars. Kamai et al. (2014) took up the study of this hypothesis in stars belonging to the Pleiades cluster. For this they contributed new photometric observations in BVIc filters and used new rotation period measurements provided by Hartman et al. (2010). Kamai et al. (2014) confirmed the systematic blueward displacement in the CMD corresponding to $B-V$ and the redward displacement in $V-K_s$ for the low-mass stars (K and M spectral types). In order to see both effects, they compared their CMDs with the semi-empirical isochrone corresponding to the zero-age main sequence (ZAMS) defined by VandenBerg & Clem (2003). They also showed that the low-mass stars with lower rotation periods showed a trend to increased blueward displacement in the $M_v$ versus B-V CMD and redward displacement in the $M_v$ versus $V-K_s$ CMD.

The aim of our study is to continue the investigation of Stauffer et al. (2003) and Kamai et al. (2014). We wish to check their hypothesis by studying low-mass stars in five open clusters: Alpha Persei, Pleiades, Coma Berenices, Praesepe and Hyades. These clusters have different ages. The phenomenon that is put forward as an explanation of the observations should diminish with advancing age. For this purpose, we have gathered the photometry available in the literature for low-mass stars belonging to the five clusters, in the bands $BVR_cI_c$ and $JHK_s$, from the 2MASS project (Cutri et al. 2003). We have added to the photometry taken from the literature, contributing the photometry we obtained from observations performed over 26 nights at the Sierra Nevada Observatory (OSN), between February 2015 and May 2017. In addition we have compiled the rotation periods available in the literature for each cluster.
We then studied isochrone models, which are used to predict the position of the stars of a stellar cluster with a certain age on the CMD (Bell et al. 2014). As we have not found a stellar model whose isochrones reproduce the CMDs we wish to study ($M_v$ vs $B-V$, $M_v$ vs $V-I_c$, and $M_v$ vs $V-K_s$) we have used the data from the Hyades cluster in order to generate a fiducial in the three CMDs. We have superimposed the fiducial that corresponds to each CMD to the distribution of

points of the three CMDs for each cluster and we have calculated the deviations of the stars with respect to it.
We have confirmed that blueing and reddening are indeed present for stars of the young clusters *alpha* Persei and Pleiades. Regarding the older clusters, blueing is observed in some M-type dwarfs in Praesepe.

The use of colour-magnitude diagrams is not recommendable for identifying non-member stars in young clusters aged less than 1 Gyr unless one takes into account the fact that, depending on age and spectral type, the stars can present this blueing and/or reddening.

Lastly, to represent the absolute magnitudes we have made use of the distances generated from the *Gaia* DR2 parallaxes for each star. These distances have enabled us to detect a contamination of rapidly rotating giant stars in the Coma Berenices cluster. These giants have been classified in other studies as late spectral type member stars of Coma Berenices located on the main sequence. We have shown that this type of contamination can prove to be an inconvenience when it comes to using the gyrochronology technique to derive the ages of clusters. We recommend being sure about the luminosity of the stars used to apply this technique. Having eliminated the Coma Berenices giant stars, our sample indicates that this cluster has an age of $\sim$ 600 Myr, and is therefore younger than the age put forward by Tang et al. (2019) of $\sim$ 800 Myr.

# Resumen

La actividad magnética de las estrellas de tipos espectrales K y M se considera responsable de las "alteraciones" observadas en algunas de ellas. Stauffer et al. (2003) investigaron sobre una anomalía observada en el diagrama Color-Magnitud (CMD) en estrellas del cúmulo Pléyades. Las estrellas de baja masa aparecían desplazadas hacia el azul en la representación $M_v$ frente a $B-V$, este efecto se veía minimizado en la representación $M_v$ frente a $V-I_c$. De modo similar observaron un enrojecimiento en el diagrama $M_v$ frente a $V-K_s$. A raíz de este desplazamiento hacia el azul observado en $M_v$ frente a $B-V$ y hacia el rojo en $M_v$ frente a $V-K_s$ se especuló que podría ser debido a la presencia de manchas y plagas en la fotosfera de las estrellas. Kamai et al. (2014), continuaron la investigación de esta hipótesis en estrellas pertenecientes al cúmulo de las Pléyades, para ello aportaron nuevas observaciones fotométricas en los filtros BVIc y utilizaron nuevas medidas de períodos de rotación proporcionadas por Hartman et al. (2010). Kamai et al. (2014) confirmaron el desplazamiento sistemático hacia el azul en el CMD correspondiente a $B-V$ y hacia el rojo en el $V-K_s$ para las estrellas de baja masa (tipos espectrales K y M). Para ver ambos efectos compararon sus CMDs con la isocrona semiempírica correspondiente a la secuencia principal de edad cero (ZAMS) definida por VandenBerg & Clem (2003). Además, comprobaron que las estrellas de baja masa con menor período de rotación presentaban una tendencia a aumentar el desplazamiento hacia el azul en el CMD de $M_v$ frente a B-V y hacia el rojo en el de $M_v$ frente a $V-K_s$.

El objetivo de nuestro trabajo ha sido continuar la investigación de Stauffer et al. (2003) and Kamai et al. (2014). Queremos comprobar su hipótesis estudiando estrellas de baja masa en cinco cúmulos abiertos: Alpha Persei, Pléyades, Coma Berenices, Pesebre y Híades. Estos cúmulos tienen diferentes edades, el fenómeno que se propone como explicación de las observaciones se debe ir atenuando al aumentar la edad. Con este fin, hemos recopilado la fotometría disponible en la literatura para estrellas de baja masa pertenecientes a los cinco cúmulos, en las bandas $BVR_cI_c$ y también $JHK_s$ del proyecto 2MASS (Cutri et al. 2003). Hemos incrementado la fotometría tomada de la literatura, aportando la obtenida de observaciones realizadas durante 26 noches en el Observatorio de Sierra Nevada (OSN), entre febrero de 2015 y mayo de 2017. Además hemos hecho una recopilación de los períodos de rotación disponibles en la literatura para cada cúmulo. Posteriormente nos hemos familiarizado con modelos de isocronas que se utilizan para predecir la posición de las estrellas de un cúmulo estelar con una edad determinada en el CMD (Bell et al. 2014). Dado que no hemos encontrado un modelo estelar cuyas isocronas reproduzcan los CMDs

que queremos estudiar ($M_v$ vs $B-V$, $M_v$ vs $V-I_c$ y $M_v$ vs $V-K_s$) hemos utilizado los datos del cúmulo Híades para generar un fiducial en los tres CMDs. El fiducial correspondiente a cada CMD lo hemos superpuesto a la distribución de puntos de los tres CMDs para cada cúmulo y hemos calculado las desviaciones de las estrellas con respecto al mismo.
Hemos comprobado que efectivamente se visualiza azulamiento y enrojecimiento para estrellas de cúmulos jóvenes *alpha* Persei y Pléyades. En cuanto a los cúmulos de mayor edad se percibe azulamiento en algunas estrellas de tipo M en el Pesebre.

No es recomendable usar los diagramas color-magnitud para identificar estrellas no miembros en cúmulos jovenes de edades menores que 1 Gyr si no se tiene en cuenta que, en función de la edad y del tipo espectral, las estrellas pueden presentar este azulamiento y/o enrojecimiento.

Además, para representar las magnitudes absolutas hemos hecho uso de las distancias generadas a partir de los paralajes de *Gaia* DR2 para cada estrella. Estas distancias nos han permitido detectar una contaminación de estrellas gigantes rotadores rápidos en el cúmulo Coma Berenices. Estas gigantes habían sido clasificadas en otros trabajos como estrellas miembros de Coma Berenices localizadas en la secuencia principal y de tipos espectrales tardíos. Hemos comprobado que este tipo de contaminación puede ser un inconveniente a la hora de utilizar la técnica de girocronología para derivar edades de los cúmulos. Recomendamos conocer la clase de luminosidad de las estrellas utilizadas para aplicar esta técnica. Una vez eliminadas las estrellas gigantes de Coma Berenices, nuestra muestra nos indica que este cúmulo tiene una edad de $\sim 600$ Myr, y sería por lo tanto más joven que la edad propuesta por Tang et al. (2019) de $\sim 800$ Myr.

# Chapter 1

# Introduction

## Contents

Low-mass stars (below 2 solar masses) arrive at the main sequence showing noticeable brightness variations on timescales of days, weeks and even years. Since the exact location of a star on the Hertzprung-Russell (HR) diagram allows us to determine, using evolutionary tracks, stellar parameters such as mass, temperature, age or metallicity, the variability adds uncertainty to the values of these parameters. The characterization of this effect is the subject of this work.

The variability of young stars is often linked to stellar rotation, which is a consequence of the angular momentum conservation of the dust and gas cloud in which the star was formed. The outer layers of low-mass stars are convective and the interaction of convection, rotation and magnetic fields is the basic ingredient of the stellar magnetic activity. Stellar cold spots are a well-known outcome of this activity; they are similar in nature to Sunspots, are responsible for most of the brightness variations of young stars and are the result of a partial interruption of energy transport to the stellar surface due to the mentioned interaction (convection + rotation + magnetic fields). Stellar spots can last weeks or months on young low-mass stars and make it possible to obtain the rotational period for even very slow rotators.

The low-mass Pleiades stars have been observed since the 1950s (Johnson & Mitchell 1958), and their early studies already showed unexpected positions for many of them on the HR diagram: they look fainter or bluer than they "should" (Herbig 1962). Stauffer and collaborators monitored some samples of stars in order to obtain rotational periods (Stauffer & Hartmann 1987) and, from comparisons with the Praesepe main sequence, they confirmed that Pleiades K dwarfs look subluminous or bluer on the HR diagram. They suggested that this is the consequence of rapid rotation (Stauffer et al. 2003). This hypothesis was confirmed by Kamai et al. (2014), who compiled a sample of low-mass Pleiades stars for which they had photometry and rotational periods. Below, we explain these last two studies in greater detail.
Stauffer et al. (2003) compared photometry from the literature on the Pleiades and Praesepe clusters on the $M_v$ vs $B-V$, $M_v$ vs $V-I_k$ and $M_v$ vs $V-K_s$ CMDs, and observed blueward displacement by the Pleiades K-type stars on the $M_v$ vs $B-V$ diagram. On the $M_v$ vs $V-K_s$ CMD, they detected a redward displacement by the weakest stars from their Pleiades sample (Late-K/early-M dwarfs) and observed how these blueward and redward displacements were minimized in the $M_v$ vs $V-I_k$ diagram. In that study, they explained that this anomaly in the spectral energy distributions of Pleiades could be caused by spots and plages located on the surface of the stars. The plages, due to their high temperature, could cause a blueing in $B-V$ and the cold spots could give rise to the reddening observed in $V-K_s$. Kamai et al. (2014) obtained $BVI_c$ photometry for 350 stars of Pleiades. With these data, they doubled the number of low-mass stars with quality photometry in the Johnson-Cousins filters. They also selected 507 stars with photometry from the literature, making use of the catalogue developed by Stauffer et al. (2007). This catalogue contains all the photometry existing up to the date of their publication in the $BVI_cJHK$ bands for $\sim$ 1400 stars identified as proper motion members of Pleiades.

Kamai et al. (2014) created an empirical isochrone of 100 Myr by using the Pleiades photo-

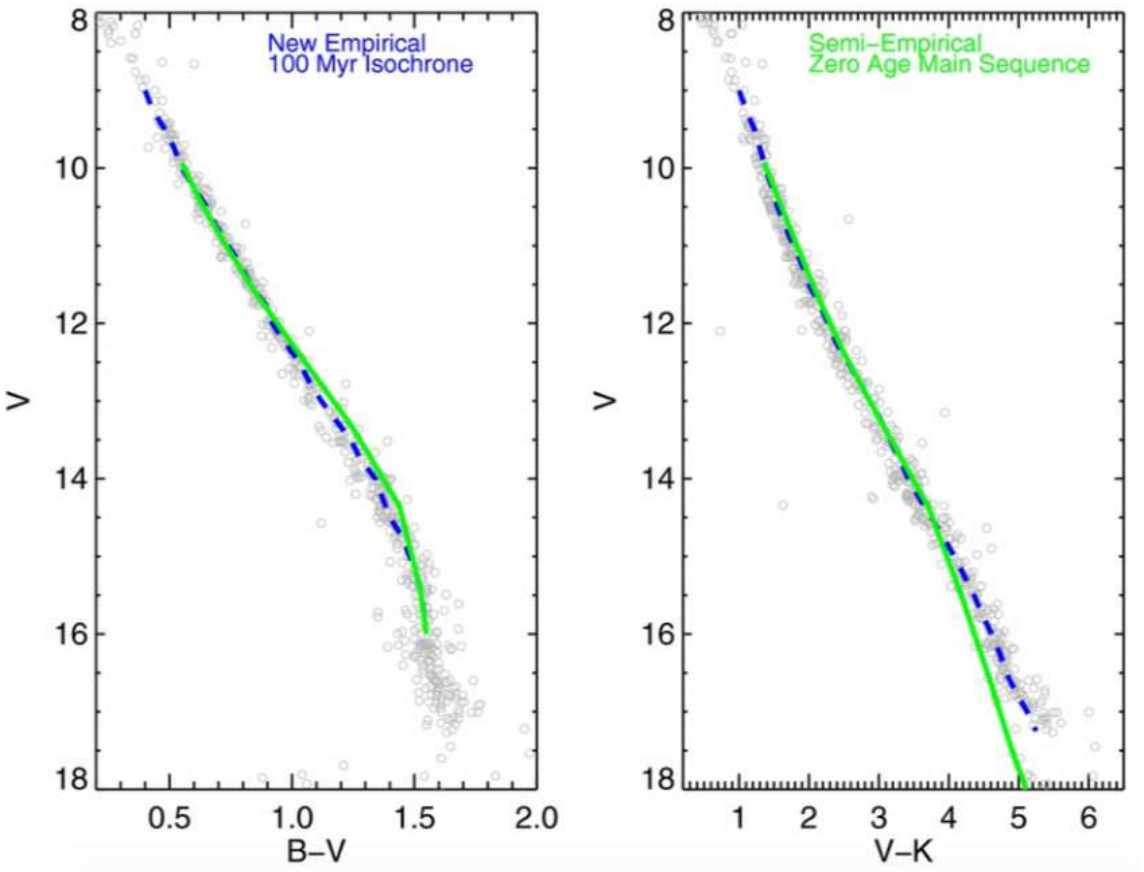


Figure 1.1: Figure 5 represented in Kamai et al. (2014). As they explained, both CMDs contain single Pleiades stars compared with an empirical 100 Myr isochrone defined in their study, and a semi-empirical ZAMS (VandenBerg & Clem 2003). Pleiades with $12.5 < V < 15$ are displaced blueward in the $B - V$ CMD, and stars with $V \gtrsim 14.5$ are displaced redward of the ZAMS in the CMD corresponding to $V - K$.

metric data, and they verified that, in effect, the K and early-M stars with short rotation periods were situated below the isochrone on the $M_v$ vs $B-V$ diagram (Figure 1.1). As is shown in Figure 1.1, they also confirmed that these stars are situated above the ZAMS in the $M_v$ vs $V-K$ diagram, and these blueing and reddening effects are minimized on the $M_v$ vs $V-I_c$ CMD. Lastly, they studied the relation of these deviations with respect to the isochrone, and showed a high correlation between the stars that rotated fastest and the greatest shifts in the $M_v$ vs $B-V$ and $M_v$ vs $B-V$ diagrams (Figure 1.2).

This work deals with the study of the time evolution of this correlation. We needed stars covering an age range from less than 100 Myr to almost one Gyr. Age is very difficult to measure on main-sequence or almost main sequence stars, therefore we have chosen four young open clusters that, as this work began, were thought to cover the age range 70 - 800 Myr: $\alpha$ Per, Coma Berenices, Praesepe and Hyades. For each of these clusters an analysis, similar to the one described for the Pleiades, has been carried out and for the Pleiades the published analysis has

been revised.

## 1.1 GKM stars

Since the effect was discovered on K type stars, this work is focused on stars with spectral types from G to M5 and with solar metallicities. These stars have masses between 1.08 and 0.16 solar masses, effective temperatures between 5920 and 3000 K and theoretical radii between 1.12 and 0.13 solar radii (Pecaut et al. 2012; Pecaut & Mamajek 2013). These stars arrive at the main sequence with ages from 30 Myr, for the G spectral type, to 100 Myr, for the M2.5 spectral type, as estimated from Fig. 4 from D'Antona & Mazzitelli (1994). That is, the lowest mass stars of the $\alpha$ Per and Pleiades clusters are still on the pre-main sequence phase.

Early G type stars consist of a radiative core and a thin convective zone in the outer envelope. This convective zone gets deeper as we go to later spectral types and M3V stars are full convective.

The rotational velocity of high mass main sequence stars (B and A type) can reach 200 km/s but as we move to lower mass stars this velocity is reduced: 95 km/s for F0 type stars and 12 km/s for G type stars (McNally 1965).The young K and M main sequence stars have velocities from 5 to 30 km/s, which correspond to rotational periods of 1 to 10 days (Irwin & Bouvier 2009).

In the early life of a low mass star its rotational velocity changes following a well known behaviour. During the pre-main sequence stage it increases as the star accretes matter from its accretion disk, although the spin up is frequently halted by the magnetic star-disk interaction (Hartmann 2009). Once the inner parts of the accretion disk are cleared up the star is free to spin up as it contracts towards the main sequence. For a 1 solar mass star the maximum rotational velocity is achieved at an age of a few tens of Myr (Bouvier et al. 1997) and declines very slowly after that age. The Sun, 4560 Myr old, has a rotational velocity of 2 km/s. Lower mass stars evolve, in this sense, even slower and 100 Myr old pre-main sequence M stars can still rotate a a speed of 60 km/s (rotational period of less than one day). All stars in this work have been selected from rotational period surveys and are, therefore, biased towards the most active group within each cluster.

Main sequence GKM stars show a binary frequency smaller than main sequence high mass stars. There is a trend from the O stars (binary fraction over 80%), the B (about 60%) and the A stars (about 50%), to the G and K type stars, with binary fractions of about 44%, and the M stars, that show fractions of about 26% (Duchêne & Kraus 2013).

Binary stars can keep higher rotational velocities if there is an orbit-spin synchronization and in these cases the stellar magnetic activity, that usually decreases as the star slows down, does not decline (e.g. BY Dra stars). For this reason and for the fact that the absolute magnitude ($M_v$) of an unresolved binary locates it above the main sequence, binary stars will be removed from the final samples in our study.

### 1.1.1 Disseminated introduction

Before the analysis of each cluster, a brief description of its main characteristics is presented and the section devoted to the Coma Berenices cluster contains a short introduction to gyrochronology, a technique used to determine stellar ages, based on stellar rotational periods.

Finally, an up-to-date summary of the field of isochrones opens the chapter dedicated to the isochrone fitting to the five clusters.

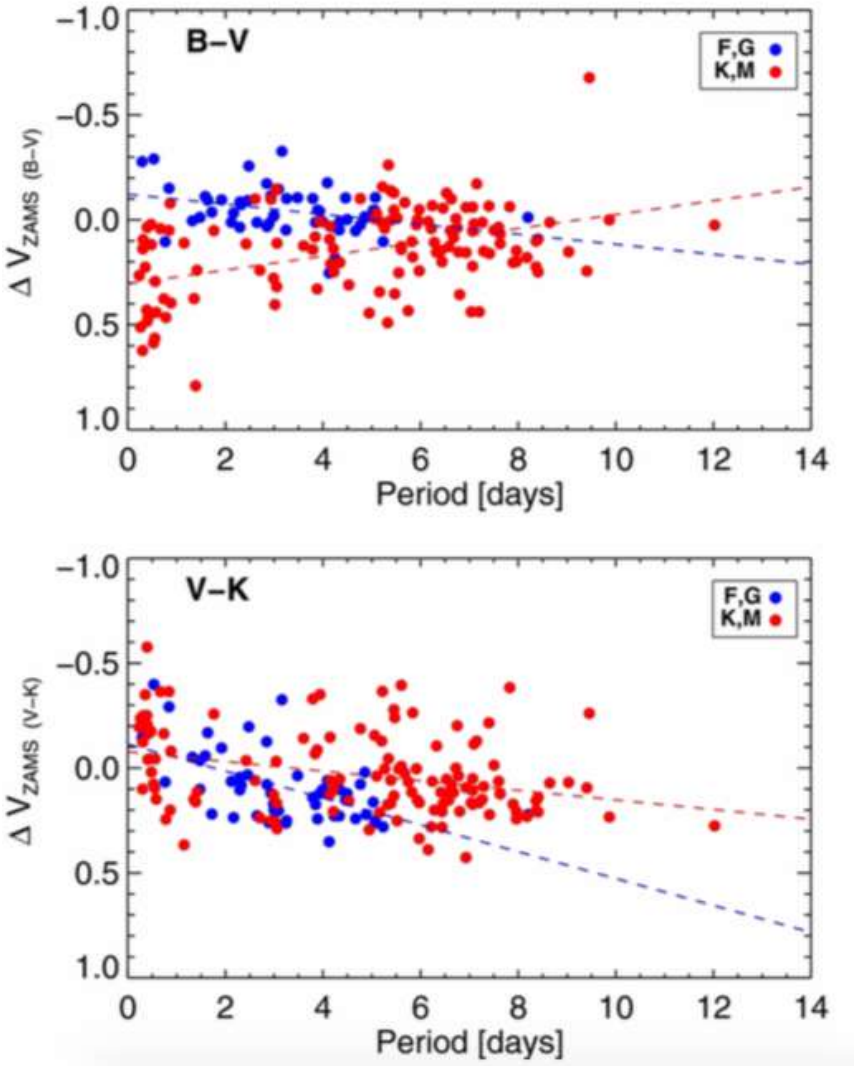


Figure 1.2: Figure 9 represented in Kamai et al. (2014). They shown the correlation of the displacement (relative to the semi-empirical ZMAS) versus rotation period for stars in the $B - V$ CMD (above) and in the $V - K_s$ CMD (bottom). Dashed lines are linear fits. As they explained, in the displacement concerning the $B - V$ CMD, F and G stars do not show a significant correlation, whereas K and M stars show that rapid rotators are more displaced blueward of the ZAMS. Regarding the $V - K$ CMD, both F/G stars and K/M stars show that the rapid rotators are more displaced redward of the ZAMS

# Chapter 2

# Observations and photometry

## Contents

## 2.1 Sample

With the aim of characterizing the phenomenon described in the introduction, and determining the age interval in which it is noticeable, we selected young low-mass stars classified mainly as G, K and M spectral types. We focused on five open clusters with different ages, in order to study stars that have known ages and distances. The clusters in which these low-mass stars are located are: Alpha Persei, Pleiades, Coma Berenices, Praesepe and Hyades.
We selected the stars for which we have been able to find measured rotational periods in the literature. We collected photometry from the literature for these stars in Johnson-Cousins and 2MASS filters, in particular $BVR_cI_c$ and $JHK_s$ respectively.

The collected photometry has been complemented with our photometry of mainly K and M dwarfs taken at Sierra Nevada Observatory (OSN). We measured the absolute brightness for the stars for which we did not find the photometry in the literature, in the required bands. In our study, we used the color indexes $B-V$, $V-I_c$, $V-K_s$ and the $V$ absolute magnitude ($M_v$). We gathered measurements of $V-R_c$ from observations at OSN and from literature, but due to the lack of enough data for that colour, we will present the compiled $V-R_c$ photometry but we will do the study without that measurements.

Some properties of these clusters are summarize in Table 2.1. In the next chapter we will explain these properties in greater detail.

| Cluster | RA J(2000) (hh:mm:ss) | DEC J(2000) (dd:mm:ss) | Distance (pc) | Age (Myr) | OSN |
|---|---|---|---|---|---|
| Alpha Persei | 03 : 20 : 36 | +48 : 10 : 00 | ~170-190 | ~20-95 | 33 |
| Pleiades | 03 : 47 : 00 | +24 : 27 : 00 | ~115-145 | ~70-150 | 2 |
| Coma Berenices | 12 : 25 : 06 | +26 : 06 : 00 | ~80-90 | ~400-800 | 33 |
| Praesepe | 08 : 40 : 24 | +19 : 40 : 00 | ~180 | ~590-790 | 19 |
| Hyades | 04 : 26 : 54 | +15 : 52 : 00 | ~46 | ~550-750 | 31 |

Table 2.1: Open clusters properties

The Table 2.1 presents the name of the cluster (Cluster); coordinates in the J2000 epoch, Right ascension (RA) and Declination (DEC); distance in parsecs (Distance); age in Myr (Age) and number of stars observed at OSN (OSN).The distance and age columns show the range of their values, collected from the literature.

In order to better sample the age range of clusters, we also searched for rotational periods and photometry in the literature for the following open clusters: Collinder 359 (~32 Myr), Mamajek 2 (~125 Myr), Collinder 285 (~199 Myr), Platais 2 (~346 Myr) and Platais 3 (~501 Myr). We did not find photometry and rotational periods measurements for a significant number of stars in these open clusters, therefore we could not add these clusters into our study.

## 2.2 Telescope and detector at Sierra Nevada Observatory

With the purpose of performing our photometric study, we acquired data using the CCD camera of the 1.5 m telescope at the Sierra Nevada Observatory (OSN), operated by the Instituto Astrofísica Andalucía (CSIC) in Granada, Spain.

Some of the CCD properties are the following.

- The CCD camera is a VersArray 2048 x 2048 with a pixel size of 13.5 $\mu$m and a field of view of 7.92$x$7.92 arcminutes.
- The gain is about 1.5 electrons/ADU with a readout noise about 8.23 electrons.
- The chip response is linear up to 54000 photon counts with an accuracy of ~1% photon counts. The chip saturates from 60000 photon counts.
- The filter wheel offers 6 places for 50 mm square filters. We used the $BVR_cI_c$ Johnson-Cousins filters.

## 2.3 Data acquisition

The observing campaigns were carried out over 37 scheduled nights, from February 2015 to January 2017. We required photometric nights to perform the absolute calibration in the Johnson-Cousins $BVR_cI_c$ filters. Unfortunately, due mostly to bad weather, we lost ~90% of the nights, so to compensate for it, we managed to make observations during Director's Discretionary Time (DDT). We also shared few nights with other photometry programs to gather more data. We extended the observations to May 2017. In the end, we gathered useful data for 26 photometric nights.

### Observation plan

Each night observations started with acquisition of bias (frame with the signal produced by the electronics of the CCD at zero second exposure time) and twilight sky flats (exposures of an uniformly illuminated zone in the sky) in the $BVR_cI_c$ filters. Afterwards, we continued observing standard and target stars in the $BVR_cI_c$ filters.

The plan in the observation of standard stars and targets, required measurements of standard stars at different airmass values along every night[1]. We made a calibration plan for each night. We selected a sample of standard stars according to their color, brightness and coordinates (right ascension and declination), with the purpose of covering the colors and airmass of the target stars observed that night.

[1] Each night we had between 10-60 photometric measurements of standard stars (depending on weather conditions).

In order to get the highest accuracy measurements of the extinction coefficient, and its dependence on the color indexes, we intended to observe at least one standard field at three different airmass measurements. The sequence adopted included two measurements at a high airmass value, at the beginning and end of each night, and one measurement at a low airmass value, when the standard stars were culminating. Unfortunately, some nights the weather conditions did not make possible to follow the stipulated plan, so we had to adapt the number of standard stars measurements to these weather conditions.
The standard stars used in the whole campaign are located in the selected areas (SA), chosen by Landolt: SA32, SA92, SA95, SA98, SA101, SA104, SA109, SA114 (Landolt 1992, 2009, 2013).

Integration times have been calculated taking into account a goal of 0.01mag precision. Other factors, that affect in the precision of the photometry, will make our errors between 0.02-0.04mag. The effect on the colors and magnitudes that we want to check, should be perceptible with an error lower or equal than 0.04mag.

## 2.4 Data reduction

### 2.4.1 Image calibration

Each night was processed independently with the IRAF software (Image Reduction and Analysis Facility).

First of all, we checked all the raw frames to look for signs that could have affected the image quality and also we tried to understand their origin, like for example elongated stars due to focusing or guiding problems, reflections on the telescope optics, etc. Several images taken in different nights presented bright bands due to reflections of light coming from bright near objects, like Jupiter or bright stars. We noted that some of those bands had the shape of an interference pattern. Due to non-controlled reflections inside the telescope, the light from a point source illuminating the edge of a reflecting surface, like the tertiary mirror, could produce these interference patterns (Victor Casanova and Fran Aceituno, private communication).

CCD images were calibrated to correct for instrumental signatures across the detector. The science images were corrected for the signal added to each pixel during readout (bias), and for inhomogeneities due to the CCD behavior and distortions in the optical path (flat field frames). We corrected the images for the following inhomogeneities: pixel-to-pixel sensitivity variations (due to non-uniformity in the pixels response), non homogeneous illumination of the detector, and the shadow produced by dust spots located on the telescope optics.

The first step was to correct science and sky flat field images for bias. First of all, we checked possible deviations in the mean value of every bias image, and selected the bias frames with no significant deviations (typically we had between 10-20 measurements). Next, we combined, using

the median, the selected bias frames in order to generate a "master bias". We subtracted the "master bias" from all the science and sky flat images to correct them for the bias offset.

The second step was to carry out the flat field correction, with this purpose, we used the sky flat images that were previously corrected by the "master bias". We combined, using the median, the bias subtracted sky flat frames at each filter $B$, $V$, $R_c$, $I_c$. Therefore, we generated four "master flats", one per filter $B$, $V$, $R_c$, $I_c$. Next, we divided our science images by the normalized[2] "master flat" at their corresponding filters $BVR_cI_c$.

There were no bias for two nights and no flat frames for one night, in such cases, we used the calibration frames from the closest observational night.

Finally, the calibrated images were displayed one by one, in order to check the successful execution of the tasks in the data reduction process.

### 2.4.2 Photometry

#### Aperture photometry

With the aim of determining the instrumental brightness of the stars of our images, we had to obtain the contribution of all pixels illuminated by each star, and subtract the contribution from the sky background. For this purpose, we used the aperture photometry technique.

In order to collect the star flux, we selected a circle (usually called an aperture) centered on the star, and summed the pixel counts within the aperture. The circle radius had to be large enough to include all of the light from the star, but as small as possible in order to reduce the sky background.

The first step in the aperture photometry technique is to determine the optimal aperture radius.

#### Aperture selection method

With the purpose of selecting the most appropriate aperture, we tested three different methods to generate the aperture, and we also tested different aperture values.
It should be noted that we searched for the optimal aperture for each night independently.

The tested methods are:

- Variable aperture: Each star has a different aperture value. For each image, we selected an aperture for each star, that is proportional to its FWHM (Full With Half Maximum).

[2] We normalized each "master flat" to a mean value close to 1, in order to keep the same level of counts between the raw and calibrated science images.

- Fixed aperture: We used the same aperture value for all the stars each night. The aperture is proportional to the average of the FWHM values of all the stars per night.
- Fixed aperture per image: We used one aperture value per image. The aperture is proportional to the FWHM generated by the mean of the FWHM of several stars located in the image.

The procedure used to determine the different aperture values, is explained as follows.

1. We displayed an image corresponding to the photometric night 17/11/2015 (given in the format day/month/year) and obtained at a very high airmass value. We selected one star in the image, and plotted the stellar radial profile using the task *qphot* (IRAF task for quick photometry). We used this task interactively, in such a way that we selected several apertures that contained all of the star flux, and low sky background level.
   Next, we divided these apertures by the FWHM of the selected star, in order to obtain several *aperture factors*. We used these aperture factors to determine different apertures for every night.
   We generated the aperture factors just for the night 17/11/2015, since it was expected that these factors would not change considerably between nights.

2. We made a list with the FWHM values of each star observed the selected night 17/11/2015. We took the FWHM from the output of the IRAF *imexamine* task.
   Afterwards, we determined the required FWHM values conforming to the method: FWHM per star (Variable aperture), mean FWHM of all stars (Fixed Aperture) and mean FWHM per image (Fixed aperture per image).

3. We multiplied the aperture factors calculated in the first step by the FWHM values obtained according to the method, in order to generate several apertures for each star.
   Therefore, we calculated the photometry of each star for several aperture values directly proportional to the FWHM values.

   Once we selected the optimal aperture selection method, we followed the steps 2 and 3 for every night.

The absolute brightness of the standard stars is tabulated (Landolt 1992, 2009, 2013). For each measurement of the standard stars, we calculated the residual value as the difference between the tabulated absolute brightness and the absolute brightness generated from the instrumental magnitude of that measurement. The absolute brightness is generated for each aperture using the procedure explained in Section 2.4.3. Measurements of standard stars for which residuals were much larger than the average were removed. These noisy measurements could distort the sequence of residuals. We removed them one by one, always checking the new list of residuals once one measurement had been removed. We compared the residuals generated from the instrumental magnitudes using the apertures determined from the different methods and aperture factors. We

selected the method and aperture factors from which we obtained the lowest residual values.

For each aperture, we compared the upper limit residual, the highest value of the standard stars residual values, because we decided to use the upper limit residual as the error bar of the absolute brightness of the target stars. In order to show an example of the residual measurements, we represented the residuals for the night 19/11/2015 and for the $V - I_c$ index. We represented the residuals for the ”Variable aperture“ method. The Figure 2.1 presents the residual values for each measurement of a standard star at different apertures, 1.8*FWHM, 2.0*FWHM, 2.2*FWHM, 2.4*FWHM, 2.6*FWHM, and 2.8*FWHM.

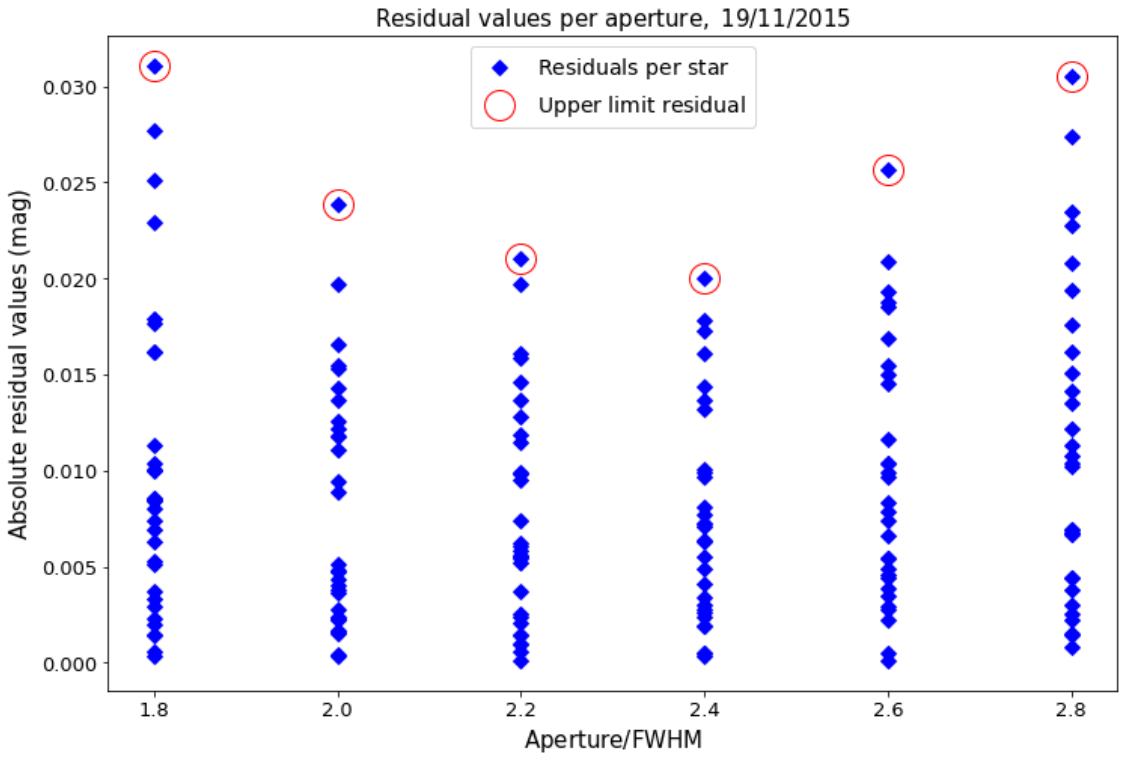


Figure 2.1: Absolute residual values vs Aperture/FWHM at V-I index for the night 19/11/2015. The Y axis represents the absolute value of the residuals for each standard star, while the X axis represents the aperture factor used to calculate the aperture, “Aperture/FWHM”. The diamonds represent the residual values for each measurement of a standard star. The circled diamonds which represent the value at the top of the residuals at each aperture factor, are the upper limit residuals.

In this example, the lowest value of the upper limit residual appears at the aperture 2.4*FWHM with a value = 0.020 mag.

With the purpose of choosing the method and aperture factor used to obtain the optimal aperture, we selected three nights 17/11/2015, 19/11/2015 and 29/11/2015, with a large number of

standard stars measurements (more than 25 measurements), and calculated their instrumental magnitudes following the procedure explained in the Section 2.4.3. This process was repeated for the different aperture values that we generated from the three methods and the aperture factors. We compared the upper limit residual values generated by the apertures obtained from them.

In order to compare the three methods, we represented in Figure 2.2 the absolute upper limit residual values for the three methods at seven aperture factors, for the night 17/11/2015.
The Figure 2.2 shows that the upper limit residual values of all standard stars are mainly lower for the first method "Variable aperture " for the $B-V$ and $V-I_c$ indexes. For $V$ magnitude, the "Fixed aperture per image" method presents slightly lower upper limit residuals. The method "Fixed aperture" shows the lowest upper limit residual values for $V-R_c$ index, but presents the highest values for $V$ and $B-V$, $V-I_c$ indexes.
According to the residual values in all indexes, we decided to use the "Variable aperture" method for all nights.

Once we chose the method, we compared the upper limit residual values for an array of aperture factors, in order to look for the aperture factors range in which the minimum residual value would appear each night. We expected that the position of the minimum residual value would not change considerably from night to night.
We checked the absolute upper limit residual values represented in figures 2.2, 2.3 and 2.4, for aperture factors determined with the "Variable aperture" method, and corresponding to the mentioned nights 17/11/2015, 19/11/2015 and 29/11/2015 respectively.

The figures 2.2, 2.3 and 2.4 show that the minimum appeared between the apertures 1.8*FWHM and 3.0*FWHM. We decided to start doing the aperture photometry using the aperture factors 1.8, 2.0, 2.2, 2.4, 2.6, 2.8 each night.
For several nights, we noted that the minimum residual value mostly appeared for 2.4, 2.6 and 2.8. Therefore we decided to do the photometry every night for the apertures 2.4*FWHM, 2.6*FWHM and 2.8*FWHM.

In summary, we checked the absolute upper limit residual values and selected the "Variable aperture" method and the aperture factors 2.4, 2.6, 2.8 to generate the apertures for which we calculated the instrumental magnitudes each night.
We compared the upper limit residual values generated by the apertures obtained from the range of aperture factors, in order to choose the one that provided the lowest upper limit residuals for the $V$ magnitude, and the $B-V$, $V-R_c$, $V-I_c$ indexes. Each night, we calculated the absolute brightness for target stars in $V$ and $B-V$, $V-R_c$, $V-I_c$ indexes, using the instrumental magnitudes from the aperture generated by the aperture factor providing the lowest upper limit residual for the standard stars.

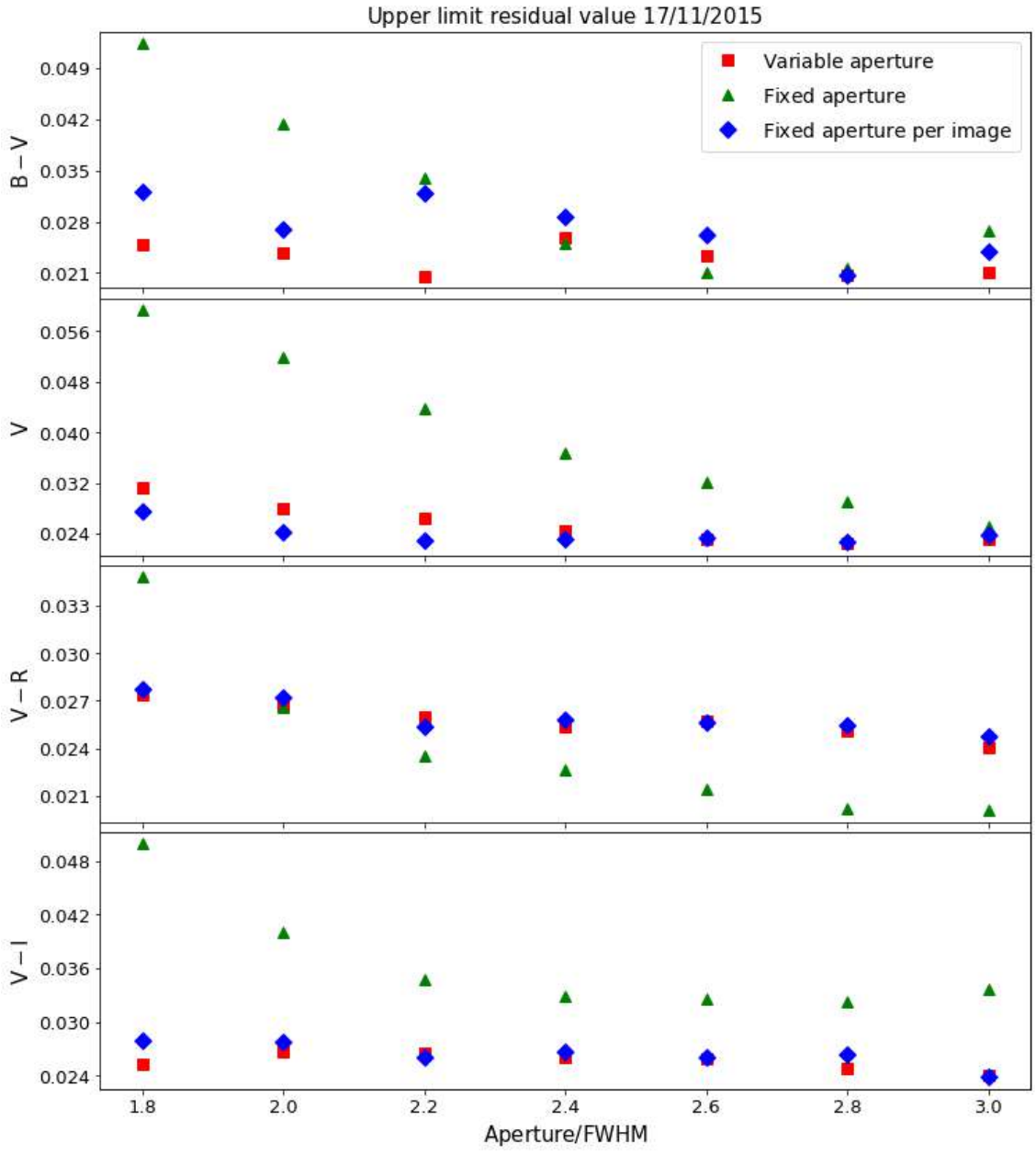


Figure 2.2: Absolute upper limit residual values vs Aperture/FWHM at the different colors and *V* magnitude for the night 17/11/2015. The red squares represent the "Variable aperture" method, the green triangles represent the "Fixed aperture" method and the blue diamonds represent the "Fixed aperture per image" method. The values at the X axis "Aperture/FWHM" are the aperture factors selected to multiply by the FWHM value in order to generate the apertures.

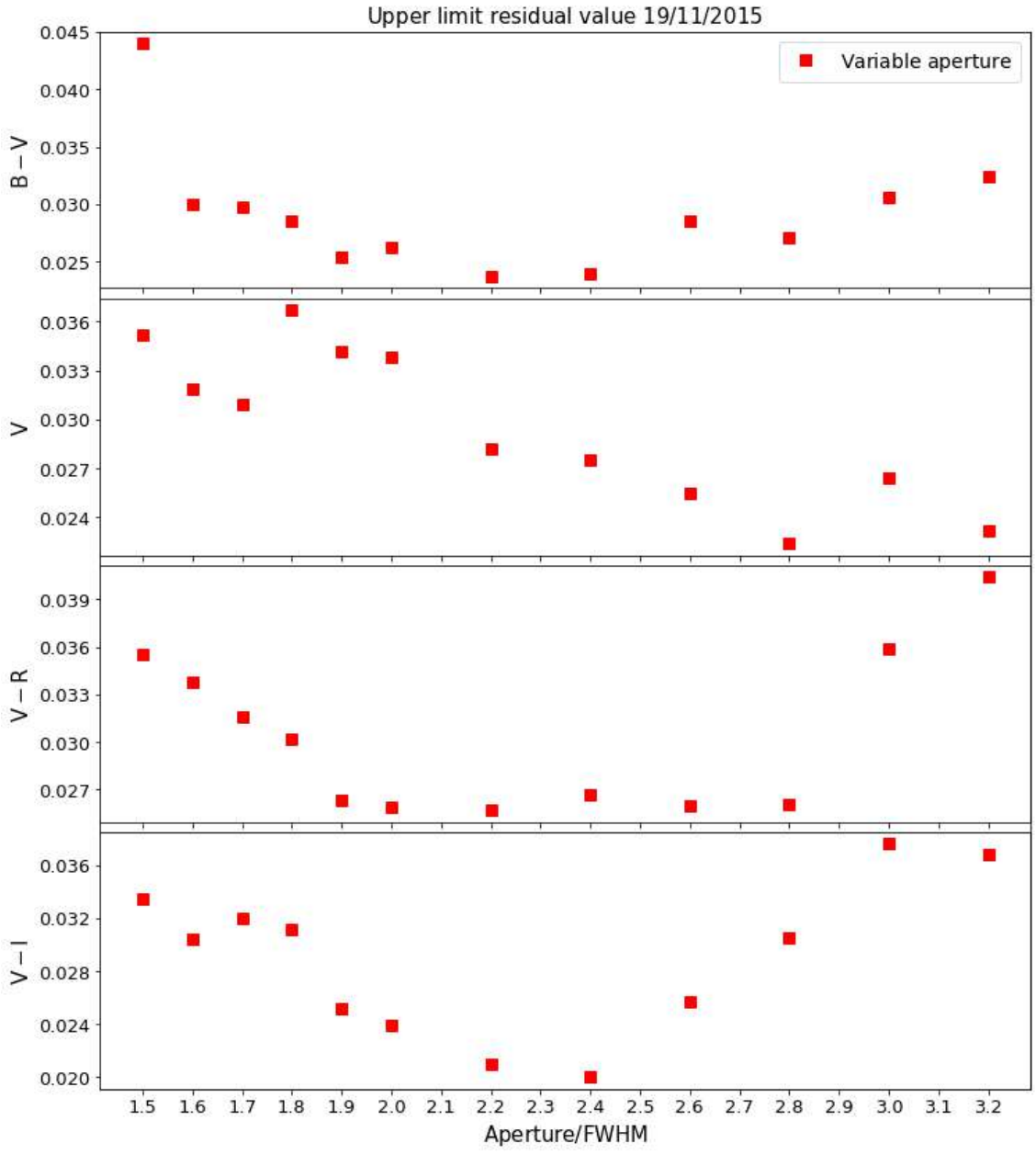


Figure 2.3: Absolute upper limit residual values vs Aperture/FWHM at the different colors and *V* magnitude for the night 19/11/2015. The red squares represent the "Variable aperture" method.

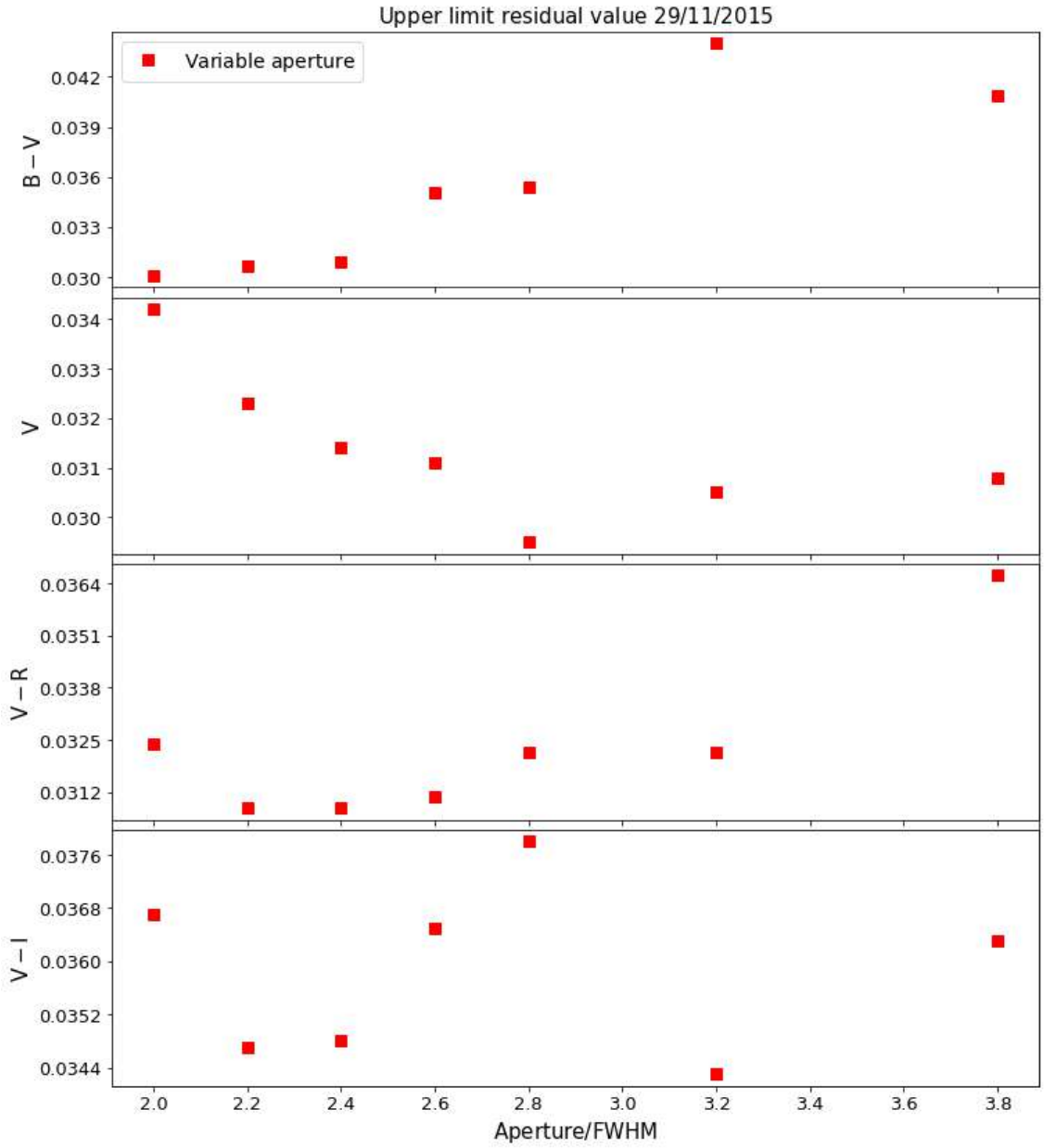


Figure 2.4: Absolute upper limit residual values vs Aperture/FWHM at the different colors and $V$ magnitude for the night 29/11/2015. The red squares represent the "Variable aperture" method.

### Instrumental magnitudes

The instrumental magnitudes were calculated using the aperture photometry technique. As a first step in the aperture photometry procedure, we created a list with all bias corrected and flat-fielded images names. We made copies of the images with two or more stars of interest, in order to have one image per star. All the images from the list were checked using the IRAF *imexamine* task. The stars that presented more than 55000 counts at the peak, were erased from the list. We did not do photometry of these stars because, as we explained before, the chip response is linear up to 54000 photon counts with an accuracy of ~1% photon counts.

Afterwards, we wrote a file containing the name of each image, the pixel star position in the image, and the Moffat FWHM[3] value of each star. This file was used as the input of an IRAF script, written in order to obtain the instrumental magnitudes.

We computed the aperture photometry for science and standard stars. With this purpose, we used the IRAF *qphot* task from our IRAF script, and obtained the instrumental magnitudes at the selected aperture values. In order to obtain the flux from the star, contained in the apertures, the *qphot* task measured and subtracted the contribution of the sky background in each aperture. The sky background was measured in a ring determined by the sky inner radius (*annulus*) with a value of 3∗FWHM pixels, and the sky width (*dannulus*) with a value of 10 pixels.

Each night, we obtained the instrumental magnitudes at the selected apertures, in order to choose the one that presented the lowest upper limit residual value for the standard stars. Therefore, we calculated the absolute brightness of the target stars from the instrumental magnitudes corresponding to the selected aperture.

### 2.4.3 Absolute photometry, transformation to standard photometric system

#### Preparing scripts for absolute photometry

Once the images were calibrated and the instrumental aperture photometry was derived for the science and standard stars, we had to write the following two scripts in Bash programing language before computing the absolute brightness.

The first script was written with the purpose of obtaining the airmass value at half of the exposure time, because the header of each image provided us the airmass value at the beginning of the exposure time. The script generated a table that contained the stellar coordinates (corrected for the effects of precession), the observing date and time of observation, the exposure time and the sidereal time. This table was written in a specific format to be used as the input of a Fortran language program, already written in order to calculate the airmass at half of the exposure time. Due to the format required for the generated table, writing the script was a labourious process.

The second script was written in order to create a table that contains the name of the images, the instrumental magnitudes from the output of the *qphot* photometry and the previously obtained airmass[4]. This table was the input of the program that calculates the coefficients of the transformation to the absolute photometric system, following the method described by Harris et al. (1981). This program had also been written in Fortran language, hence we prepared the input in a specific

[3]The FWHM was calculated using a softened exponential profile to model the PSF (Point Spread Function), (Moffat 1969).

[4]In order to compute the absolute photometry for the $B-V$, $V-R_c$ and $V-I_c$ indexes, we used the airmass average, obtained from the airmass values corresponding to the observational time of the individual measurements of $B, V$; $V, R_c$ and $V, I_c$ respectively.

format.

### Deriving the coefficients for the transformation

With the aim of getting the absolute brightness, the instrumental magnitudes were converted into magnitudes tied to one of the standard photometric systems. Using the Landolt stars (Landolt 1992, 2009, 2013), we determined the $V$ magnitude and the color indexes $B-V$, $V-R_c$ and $V-I_c$ of the Johnson-Cousins photometric system.

We corrected the instrumental magnitudes of the target stars for several factors, in order to obtain the absolute brightness.
First of all, we had to correct them from extinction, that is to convert the instrumental magnitudes measured on the surface of the Earth to the above-atmosphere values. Afterwards, we had to find the zero point of the selected photometric system and to apply the color correction, with the aim of correcting for the different response between the filters used in our observations, and the ones used to determine the tabulated magnitudes of the standard stars.

With the purpose of performing these corrections we used the following transformation equations developed by Harris et al. (1981), for the required Johnson-Cousins filters $BVR_cI_c$:

$$(v-V) = a_1 + a_2X + a_3(B-V) + a_4X(B-V) + a_5(B-V)^2 \tag{2.1}$$

$$(b-v) = b_1 + b_2X + b_3(B-V) + b_4X(B-V) + b_5(B-V)^2 \tag{2.2}$$

$$(v-r_c) = c_1 + c_2X + c_3(V-R_c) + c_4X(V-R_c) + c_5(V-R_c)^2 \tag{2.3}$$

$$(v-i_c) = d_1 + d_2X + d_3(V-I_c) + d_4X(V-I_c) + d_5(V-I_c)^2 \tag{2.4}$$

where the upper case $B$, $V$, $R_c$, $I_c$ denotes the absolute brightness, the lower case $b$, $v$, $r_c$, $i_c$ are the instrumental magnitudes in the $BVR_cI_c$ Johnson-Cousins filters and $X$ is the airmass value. $a_i$, $b_i$, $c_i$, $d_i$ are the coefficients that we had to determine. The first term of the equations represents the zero point correction, the second term the extinction correction, the third and fifth the color correction and the forth term combines color and extinction corrections.

With the aim of obtaining the coefficients, we solved the equations 2.1 - 2.4 for the standard stars, having the coefficients $a_i$, $b_i$, $c_i$, $d_i$ as unknown variables. Since we got more than five measurements of standard stars the system of equations was overdetermined and we searched the best solution applying the least square method. This method searches for the best fit to the tabulated values minimizing the sum of squared residuals for every single equation
The difference between the derived absolute brightness/colors and the tabulated values gives us the residuals, these values provided us with information about the quality of the solution (the set of coefficients) that determined the best fitting, and also about any measurement that might have larger than expected residuals (as shown in Figure 2.5).
As an estimation of the error of our absolute calibration, we adopted the largest remaining residual

(the so called upper limit) after the iterative process by which we removed the noisiest measurements one by one.
The exposure times used, should allow us to reach a precision of a few 0.01 mag. Therefore we tried not to remove measurements with residuals below 0.04 mag.

An example of this method is shown in the Figure 2.5.

```
Lista de residuos ordenados de mayor a menor
 ST  92250     Medida  14: -0.0024
 ST  92330     Medida  10:  0.0026
 ST  98634     Medida  21: -0.0035
 ST  98618     Medida  17: -0.0038
 ST  98618     Medida  27:  0.0057
 ST  98675     Medida  24: -0.0113
 ST  92245     Medida   1: -0.0130
 ST  92250     Medida   4: -0.0131
 ST  92250     Medida   9:  0.0133
 ST  92248     Medida  12:  0.0140
 ST  98676     Medida  25:  0.0147
 ST  92245     Medida   6:  0.0157
 ST  92330     Medida   5: -0.0164
 ST  92245     Medida  11:  0.0177
 ST  92249     Medida   3:  0.0177
 ST  98614     Medida  26:  0.0178
 ST  98624     Medida  18: -0.0178
 ST  98642     Medida  22: -0.0206
 ST  98614     Medida  16: -0.0223
 ST  98624     Medida  28:  0.0227
 ST  92249     Medida  13:  0.0238
 ST  92248     Medida   2: -0.0246
 ST  92248     Medida   7: -0.0251
 ST  98670     Medida  23: -0.0293
 ST  98626     Medida  19:  0.0365
 ST  98627     Medida  20: -0.0368
 ST  92330     Medida  15:  0.0381
Desviacion std de los residuos  0.0204405133
```

Figure 2.5: Example of the list containing the residual values, ordered from lowest to highest. The first and second columns show the name of the standard stars. The third and forth indicate the order in which the image was taken along the night, and the fifth gives the sorted residual values, hence the last measurement in the residual values column, is the upper limit residual value. The bottom quantity represents the standard deviation value of all the residuals.
–la figura si se puede, la cambio por una imagen del programa en ingles.

### Standard stars with anomalous residual values

We dedicate this subsection about two standard stars that presented an abnormal deviation.

During the process of checking the residuals, we found that the standard star SA92-235 presented an anomaly, this star had a high residual value for every night, filter and aperture value. We were using the standard stars table from Landolt (1992).
After several tests and research, we found that Landolt (2009) had written the section “Comments on individual stars” in which he explained that the table of Landolt (1992) provided the star named SA92-235, but this star was in fact SA92-312. The star labeled as SA92-235 presented the identi-

fication chart, right ascension and photometry of SA92-312, but the declination was incorrect. We could not find tabulated photometry values for the star we observed, therefore we removed this star from our standard stars list.

Another star that frequently showed a big deviation in the residuals was SA98-614. In particular, this star presented high residual values for $V$, $V - R_c$ and $V - I_c$ indexes for every night and aperture value. For $B - V$ index, this star presented high residual values in 9 out of 16 nights. An explanation of this kind of deviation could be related with the magnetic activity of the star.

### Absolute brightness of the target stars

In order to perform the final step to obtain the absolute brightness of the target stars in the standard Johnson-Cousins photometric system, we applied the transformation equations 2.1, 2.2, 2.3 and 2.4, to the instrumental magnitudes of the target stars. We implemented into the equations the derived coefficients $a_i$, $b_i$, $c_i$, $d_i$, determined using the instrumental and tabulated magnitudes of the standard stars.
We introduced the instrumental magnitudes of our target stars into this system of equations, and we obtained the photometrically calibrated brightness of the targets. In particular, we determined the $V$ magnitude and the color indexes $B - V$, $V - R_c$ and $V - I_c$ in the standard Johnson-Cousins photometric system.

### Absolute photometry error bars

The errors estimated for the magnitudes obtained from the absolute photometry, were computed according to the following situations:

- For target stars with S/N like the standard stars, we used the upper limit residual value of the standard stars. This value will be the upper limit of the error of the absolute calibration.
- For the target stars whose S/N was worse than that of any standard star, we computed the square root of the squared sum of the mentioned upper limit residual and of the measurement error of the instrumental magnitudes of the target stars, taken from the *qphot* task.

The error values we obtained in the photometry, have shown that we should be able to detect the effect we are looking for in the CMD diagram.

# Chapter 3

# Data of the Five Open Clusters

## Contents

The first step in developing this thesis focused on choosing a sample of stars for each cluster and compiling data for them, such as photometry, distances, membership, etcetera. In this chapter, we will explain the whole process of object selection and the compilation of these data. We will begin by summarizing the process undertaken for the 5 clusters, and then focus on the sample selection for each of them.

**Process followed in the 5 clusters**

We selected stars for which there would be rotation periods available in the literature. Below, given that we also need the stars to have photometry measurements in the Johnson-Cousins $BVI_c$ bands, we have put together this information originating from previous studies, taking into account that we will only use values with an accuracy of at least 0.04 mag, and prioritizing those studies with higher homogeneity in their data. Regarding those stars for which this photometry is unavailable, we selected a subsample with mainly K/M spectral types (since we are more interested in later-type stars), and obtained their absolute magnitudes in $V$, and $B-V$ and $V-I_c$ colours, through observations made at the OSN. As we previously explained, the initial idea was also to provide $V-R_c$ values, but due to lack of observational time, these data have only been obtained for fewer objects than planned. Similarly, to complete the photometric information in other bands ($JHK_s$), we have correlated the tables of the five clusters with the large "Two Micron All Sky Survey" catalogue (Cutri et al. 2003, henceforth referred to as 2MASS), which provides photometry in these bands for some 500 million unique objects. In our study we will use the values of $K_s$ with a precision $\lesssim 0.06$ mag.
Furthermore, with the aim of discarding stars wrongly classified as members of each cluster, data were gathered from studies of membership, proper motions and distances. The last were also used for the representation of the isochrones in the next chapter. The proper motions were compiled using the second *Gaia* release mission data (Gaia Collaboration et al. 2018a, *Gaia* DR2), which contain the highest number of stars ($\sim$ 1.7 billion) with the most accurate astrometric measurements to date. The distances corresponding to each star have been taken from (Bailer-Jones et al. 2018, henceforth, BJ), who calculated distances for more than a billion stars through applying Bayesian inference, making use of the *Gaia* DR2 parallaxes.

## 3.1 Alpha Persei

The Alpha Persei cluster ($\alpha$ Per), also known as Melotte 20 or Collinder 39, and centred on $\alpha_{J2000} = 03^h28^m14.4^s$, $\delta_{J2000} = +49^\circ\ 03'\ 36''$ (Gaia Collaboration et al. 2018a), is situated in the constellation of Perseus and near the galactic plane. It is easy to locate, since it contains one of the 35 brightest stars in the sky: the supergiant star Mirfak (spectral type F5I). $\alpha$ Per is a cluster that is one of the youngest and closest to the Sun, yet both its age and distance have been the subject of debate.

### 3.1.1 Characteristics of the cluster

#### Distance and age

This cluster has been situated at a range of distances of ~ 170-190 pc (for example, Pinsonneault et al. 1998; Robichon et al. 1999; Loktin & Beshenov 2001; Sanner & Geffert 2001; Kharchenko et al. 2005; van Leeuwen 2009). We would like to highlight the work of van Leeuwen (2009), who obtained a mean distance of 172±2.7 pc, using the Hipparcos mission catalogue (Perryman et al. 1997), which was launched in 1994 to take accurate measurements of the parallaxes, positions and proper motions of stars with $V > 9$ mag. Lastly, Lodieu et al. (2019a) derived a similar distance of 177.68±0.84 pc from the *Gaia* DR2 parallaxes.

Over the years, disparate results have been published on its age. Using isochrone fitting, values have been obtained comprising an approximate range of ~ 20-80 Myr (for example, Mermilliod 1981; Meynet et al. 1993; Martín et al. 2001; Sanner & Geffert 2001; Kharchenko et al. 2005; Makarov 2006; Silaj & Landstreet 2014); while using the "lithium depletion boundary" technique, ages in the ~ 65-90 Myr range were obtained (for example, Basri & Martín 1999; Stauffer et al. 1999; Burke et al. 2004; Barrado y Navascués et al. 2004). The former method is commonly used and consists of fitting theoretical isochrones (on a colour-magnitude or Hertzsprung-Russell diagram, CMD and HRD respectively) to the cluster sequence, paying special attention to the highest zone of the cluster's main sequence, which is where the "starting point" is located. This is where we find the most massive stars that have depleted hydrogen reserves in the nucleus. The greater the age of the cluster, the less the mass of stars located at this point. Moreover, in the case of there being giants in the cluster, the isochrone would also fit to these.

The lithium depletion boundary is defined as the observational limit below which the cores of very low-mass objects do not reach high enough temperature for Li destruction. This boundary is used to obtain ages for open clusters and stellar associations younger than 200 Myr.

In our study, we will adopt the age of 70 Myr for the cluster, since this fits within both ranges. It is worth mentioning that the most recent study that used the isochrone method (Silaj & Landstreet 2014) obtained an age of ~ 60 Myr.

#### Membership

Eddington (1910) mentioned the existence of the $\alpha$ Per cluster for the first time. Following this paper, many membership studies have focused on this cluster (for example, Stauffer et al. 1985, 1989b; Prosser 1992; Prosser & Randich 1998; Sanner & Geffert 2001; Lodieu et al. 2005; Makarov 2006; Lodieu et al. 2019a). Compared with other young clusters, it is not a simple task to distinguish between members and non-members in $\alpha$ Per. The mean value of its proper motion is not particularly high ($\mu_\alpha = 22.929 \pm 0.071$ mas/yr y $\mu_\delta = -25.556 \pm 0.095$ mas/yr, Gaia Collaboration et al. 2018a) compared with the field stars. Moreover, it is located at a low galactic latitude (b ~ −6 °; Kharchenko et al. 2009), which complicates selecting its members photometrically due to the high interstellar extinction E(B-V) = 0.09 (Gaia Collaboration et al. 2018a). Lodieu et al.

(2019a), using astrometric data from *Gaia* DR2, estimated that there were 2069 possible members, of which 517 have a high probability of forming part of the cluster.

### 3.1.2 Our sample for $\alpha$ Per

We have compiled 54 stars of $\alpha$ Per, from late-F to intermediate-M ("Mid-M") stars, all with measurements of rotation periods and $BVI_c$ photometry with errors $\lesssim 0.04$ mag (some stars also have $V - R_c$ measurements). Below, we describe the origins of the data that we have compiled. In Table 3.2, we present the sample with the main data: membership, $BVR_cI_c$ photometry, periods and distances.

#### Periods compiled from $\alpha$ Per

Numerous studies have been undertaken to obtain rotation periods for stars from this cluster (see Table 3.1). Several previous studies (Messina et al. 2003; Pizzolato et al. 2003; Jackson & Jeffries 2010) have compiled the measurements available in the literature at the time of their publication. For this study, we initially chose the compilation by Messina et al. (2003), since all the rotation periods currently available in the literature come from studies published before it, with a total of 72 stars of spectral types from F to Mid-M, 54 of these stars will form part of our sample. For these objects, we have checked one by one whether, along with the period selected from the literature by Messina et al. (2003), there were other calculated measurements available from other studies. Where this was so, given the low value of the periods of these stars, if there was a difference $< 0.1$ d, we kept the measurement given by Messina et al. (2003). If, on the other hand, the difference was $\gtrsim 0.1$ d, we chose the measurement that appeared to be the most reliable. Below, we explain the choice made in this latter case.

#### Stars with various measurements of rotation periods with differences $\gtrsim$ 0.1 d

- AP72. Allain et al. (1996) obtain two possible periods for this star: 5.1 d and 6.3 d, of which they choose the latter, which has an amplitude of $A = 0.1$. Prosser & Grankin (1997) obtain a period of 5.1 d with $A = 0.06$ and $FAP = 0.16$ ("False Alarm Probability", a parameter that indicates the probability that the period obtained in not the actual one). We will show the two solutions, since, as there is differential rotation, depending on the latitude that the spot used to obtain the light curve is found at, there can be variations in the value of the period obtained. The differences between these two periods fit in a scenario in which one of the light curves was measured for a spot located near the star's equator, and the other period for a spot situated near the pole.
- AP91. We have noticed that, for this star, Messina et al. (2003) give a period calculated by Messina et al. (2001), which actually corresponds to the star AP93. For this reason, we have adopted the measurement of 0.63 d obtained by Prosser et al. (1993a).

| Literature reference and notation shown in Table 3.2 | |
|---|---|
| Stauffer et al. (1985) | a |
| Stauffer et al. (1987) | b |
| Stauffer et al. (1989b) | c |
| Prosser (1992) | d |
| O'dell & Collier Cameron (1993) | e |
| Prosser et al. (1993b) | f |
| Prosser et al. (1993a) | g |
| O'dell et al. (1994) | h |
| Prosser et al. (1995) | i |
| Allain et al. (1996) | j |
| O'dell et al. (1997) | k |
| Marilli et al. (1997) | l |
| Prosser & Grankin (1997) | m |
| Barnes et al. (1998) | n |
| Messina et al. (2001) | o |

Table 3.1: List of the studies that have measured rotation periods of $\alpha$ Per and the notation we use in Table 3.2 to indicate the source of each period used.

- AP114. Allain et al. (1996) obtain two possible periods: 1.3 d and 4.4 d, selecting the former. Prosser & Grankin (1997) derived $P$ = 4.32 d with an amplitude of $A$ = 0.13 and a very low FAP value: $3.5x10^{-5}$. Hence we chose this last value.
- AP212. Messina et al. (2003) give a period of $P$ = 7.1 d, taken from the study by Prosser et al. (1995). However, an error must have occurred in the former study, because the value that Prosser et al. (1995) actually published for this star is $P$ = 6.2 d, which is the value we will therefore use.

In Table 3.2, we show the period selected for each star in the sample, along with the source for each value (see Table 3.1).

#### Photometry $BVR_cI_c$

Of the photometry measurements compiled for the 54 stars in the sample, 21 were taken from the literature (all in bands $BVR_cI_c$), and 33 were generated from the observations made at the OSN (24 in $BVR_cI_c$ and 9 in $BVI_c$ ). In Table 3.2, we present the sources for the photometry, which we describe below.

#### Photometry compiled from the literature

In the process of searching for photometry in the literature, we started with the table of 72 stars. For these objects, we found data in the following studies:

- Stauffer et al. (1985, 1989b) (henceforth, Stauffer 85/89), provide values of $B-V$, $V$, $V-R_K$ and $V-I_K$ for 35 stars. Thus, both $R$ and $I$ belong to the Kron system and not to the Cousins system, which is what we need. Regarding errors, they are of the same order in both studies: Stauffer et al. (1985) state that the colours and magnitudes obtained might have an accuracy of $1\sigma$ of approximately 0.015 mag, and add that one must bear in mind that both the stars with $V > 16$ mag and some values of $B - V$ have greater errors.
- Kharchenko (2001) builds a catalogue in which he compiles, among other parameters, Johnson $BV$ photometry for $\sim$ 2.5 million stars. The data come from: Hipparcos; the CMC11 catalogue ("Carlsberg Meridian Catalogues"; Belikov et al. 2002) and Tycho-1, Tycho-2 (Høg et al. 2000), although for Tycho-1, Tycho-2 they had to transform the magnitudes to the Johnson system. Overall, ten stars were correlated with this catalogue, for which the $BV$ measurements have mean errors of $\sigma B \sim 0.2$ mag and $\sigma V \sim 0.1$ mag.
- APASS DR9 is a project focused on obtaining Johnson $BV$ photometry, and Sloan $u'$, $g'$, $r'$, $i'$, $z_s$, $Z$ for a large number of stars. It currently provides photometry for 128 million objects. This catalogue provides photometry for 67 stars, although with mean errors of $B - V \sim 0.1$ mag and $V \sim 0.05$ mag.

Given that we seek to maximize the homogeneity of our sample's photometry, and we also need photometric data with errors of $\lesssim 0.04$ mag, these last two catalogues do not meet requirements. We have only correlated them with our objects with the purpose of adding more information to our cluster parameter table and, for some specific cases, to compare their results with those obtained on the OSN. For this reason, we will only consider the data from Stauffer 85/89, because they have estimated the errors of their measurements to be less than 0.04 mag.
Regarding the $V - R_K$ and $V - I_K$ values from Stauffer 85/89, we have transformed them to the Cousins system, using the transformation equations of Bessell & Weis (1987), obtained through fits between both Kron and Cousins systems, with standard errors of fits for $(V - I)_c$ and $(V - R)_c$ of 0.014 and 0.013 mag, respectively.
In Table 3.2, we show the data derived from the Stauffer 85/89 photometry. However, these do not present errors for every star; the only information available in this regard is that explained previously. For these studies, as we will see in the next section, we cannot ensure that they meet the criterion established for presenting errors, of $\lesssim 0.04$ mag.
Moreover, although 35 of the 72 stars have photometry from Stauffer 85/89, as we will explain below, we have obtained photometric measurements from the OSN for 14 of those 35 objects. Thus in our sample of 54 stars, 21 objects will only have photometry sourced solely from the literature.

### Photometry obtained from OSN observations

From the observations made at the OSN, we have obtained the magnitudes in band $V$ and colours $B - V$ and $V - I_c$ for 33 stars from the list with rotation periods, of spectral types K0 to M3, and

we have derived values of $V - R_c$ for 24 of those stars. The mean values of the upper limit error are: e$B - V \sim 0.023$ mag, e$V \sim 0.021$ mag, e$V - R_c \sim 0.017$ mag and e$V - I_c \sim 0.022$ mag.
The observations took place over 18 nights spread over the period between October 2015 and April 2017. Due mainly to technical problems during some nights of observation, and to meteorological conditions that prevented the night from being photometric, for some stars measurements were taken over several nights, in order thus to compare and use the most reliable values. To decide which measurement to take into account from among those that were repeated, we used the following procedure: we calculated the mean of the measurements in the event that the brightness and the colours obtained on these nights did not differ by more than 0.04 mag; if this was not the case, we selected the results from the most reliable night. Unfortunately, for some stars, we have not been able to decide which measurement was the most reliable. Therefore, we have kept all the values obtained for those stars. For the purpose of discovering which were the most reliable measurements, we focused on the following aspects for each observation night:

- The upper limit errors of brightness in $V$ and colours $B - V$, $V - R_c$, $V - I_c$.
- The signal to noise of the stars of interest and the residuals of the standard stars.
- We check that the range of airmasses of the standard stars covers the range of airmasses of the cluster, thus ensuring that we obtain a reliable value for the atmospheric extinction.
- We also check that there is a minimum number of standard stars available, which is needed to ensure the correct functioning of the program that generates the transformation equation coefficients.
- Additionally, we check the atmospheric conditions of every observation night, taking special night of the extinction value in $B-V$, $V$, $V-R_c$ and $V-I_c$, and of the transformation equation coefficients related to this parameter.
- Similarly, we bear in mind that the stars observed at airmasses greater than 2 can give less accurate measurements, due to the high value of the atmospheric extinction in these cases.

In Appendix A, we show the transformation equation coefficients and the extinction values for each night, as well as the ranges of airmasses of the standard stars and of the clusters.

Below, we explain the reasons for deciding to repeat the observation of the aforementioned stars and the measurements that were finally selected.

- AP100. The first observation took place on a photometric night, 21/10/2015, but due to pointing problems, we wished to check that the data obtained were correct, so the measurements were repeated on 29/11/2015. Once again there were technical problems and it was not possible to complete the observation of this star, and only images in band $V$ were taken, the value of which differs by only $\sim 0.002$ mag compared to that obtained on the first night of observation. To decide whether the data obtained on 21/10/2015 were correct, we have compared them with those obtained in the literature. This star was observed by Stauffer

et al. (1989b), and their $B - V$ value differs by less than 0.01 mag, although it should be stated that there is a greater difference in $V$ of $\sim$ 0.06 mag. However, as we have seen, the $V$ measurement made at the OSN is very similar on the two nights, with the value also coinciding with that provided by APASS DR9, with a difference of $\sim$ 0.004 mag compared to that obtained on the first night (although APASS DR9 does not give errors for this datum). Thus, given that the only issue on the night of 21/10/2015 was due to pointing, we have decided to take this night's measurements.

- AP120. The first measurement was taken on a photometric night, 19/11/2015, a night that met the requirements for providing reliable data. However, this star was observed at a lower airmass than the standard stars observed. Although we consider that the difference in airmasses was not so high as to pose a problem, we wished to check it, and so we decided to repeat the measure. It was observed again on 15/01/2017, but it proved to be a night with very poor seeing, and the extinction coefficient "K" in $V - I_c$ has a negative value. Furthermore, bias images were not taken, therefore we have to use those from the previous observation night. Hence, it was observed again on 04/04/2017, although data could not be taken for this star at an airmass lower than 2. Therefore, we could not use new reliable measurements to compare with those taken at the start, which are the ones we ended up using. Neither could we compare our results with those of other catalogues due to their high errors for this star.

- AP124. This star was first observed on photometric night 19/12/2015. Due to technical problems with the 1.5-metre telescope, the observations were made with the 0.9-metre telescope (also at the OSN). Given the lower size of the telescope and the fact that the CCD that it has installed presents interference patterns (fringing) in the $I_c$ filter, several images were obtained for each filter and star, with the idea of combining them to increase the signal to noise and try to reduce the fringing effect.

  For this reason, the $BVR_cI_c$ photometry of this star was generated from the images produced from this combination. We checked the difference between the residuals derived by combining and not combining the repeated images, and we observed that there was barely any difference between the $V$ magnitude and $B - V$ and $V - R_c$ colours. The greatest difference observed was 0.01 mag in $V - I_c$, which could be due to the reduction of the fringing effect when combining the images.

  Nevertheless, we wished to compare the results from the night of 19/12/2015 with data taken on the 1.5-metre telescope, and we repeated the observation of this star on 05/01/2017, taking images in filters $B$, $V$ and $I_c$. There was indeed a discrepancy in the $V - I_c$ values for both measurements, with a difference of $\sim$ 0.06 mag. However, for $B - V$ and $V$, the values are very close, with differences lower than 0.01 mag. The night of 05/01/2017, when the measurements were repeated, was photometric, with reasonable coefficient and extinction values in $V - I_c$. We therefore kept the photometry obtained on this night. For this star, the $V - R_c$ value was obtained using the images attained on the night of 19/12/2015, which we include in the table, specifying that this data was obtained with the observations made on

this night and not on the night selected (05/01/2017).

- AP169. The first observation took place on the night of 19/12/2015, which, as we have already seen for AP124, was undertaken with the 0.9-metre telescope, and the photometry was obtained by combining the images. Just as for AP124, new data were taken with the 1.5-metre telescope, in this case on the night of 02/03/2016. However, due to the presence of cirrus clouds on this night, the observation could not be completed, and as a result it was not possible to obtain images in the $B$ filter. Therefore, it was decided to repeat the observation of this star on the night of 07/01/2017, which in principle was photometric and with lower total errors than the night of 19/12/2015. The two observations present results with differences greater than 0.04 mag in $B - V$ and $V - I_c$, and we were not able to compare this photometry with catalogues in the literature due to their high errors for this star. Therefore, we could not find sufficient reasons to choose the measurements of one of the two nights, and so we will show the values obtained on both nights in Table 3.2.

- AP139. As with the two previous stars, AP139 was observed on the night of 19/12/2015 using the 0.9-metre telescope, and the photometry was attained combining the images. Likewise, its observation was repeated on the 1.5-metre telescope on the night of 07/01/2017. The differences between the results of the two nights differ by more than 0.04 mag in $B-V$. For the same reasons as for star AP169, we utilize the data from both nights.

- AP201. This star was also observed for the first time on 19/12/2015 on the 0.9-metre telescope and its photometry was obtained by combining the repeated images. As undertaken in the previous cases, data were taken again on another photometric night on the 1.5-metre telescope, on 06/01/2017. In this case, for the $V$ magnitude and $V - I_c$ colour, the differences between the results of the two nights are less than 0.04 mag, although unfortunately in $B - V$ there is a disparity of $\sim$ 0.2 mag. Due to this discrepancy, we proceeded to decide from which night the photometry should be taken. As we could not compare our results with the catalogues in the literature, due to their high errors, and because there are no clear indicators of one night being significantly more reliable than other, we consulted the table "A Modern Mean Dwarf Stellar Color and Effective Temperature Sequence" (version 2019.3.22). This table was created by Eric Mamajek (http://www.pas.rochester.edu/~emamajek/EEM_dwarf_UBVIJHK_colors_Teff.txt) and contains tabulated values of magnitudes and colours for main-sequence stars (range of spectral types from O3 to Y2). Star AP201 appears in the SIMBAD database (Wenger et al. 2000) catalogued as a K5. In order to check what spectral type the $V$ and $V - I_c$ values obtained on the two nights ($\sim$ 13.1 mag and $\sim$ 1.3 mag respectively) correspond to, we consulted Mamajek's table, and it appears to be an intermediate K (K3-K4). With this in mind, below we have checked which of the two $B - V$ values calculated using the data from both nights would correspond to an intermediate K. The $B - V \sim 0.87$ mag obtained on 19/12/2015 would suggest that it is an early K-type (~K1), whereas the value of $B - V \sim 1.05$ mag attained on 06/01/2017 would correspond to an intermediate K (K3). Hence, we have adopted the values from the night of 06/01/2017. We will also show the $V - R_c$ value obtained in the observations from

the night of 19/12/2015 in Table 3.2. We should mention that prior to using the Mamajek table we took into account the value of reddening for $\alpha$ Per corresponding to each magnitude and colours. We specified the values of reddening for the cluster in the next chapter.

In Table 3.2, we show the results of our observations of $\alpha$ Per with their upper-limit errors and observation dates.

**Discrepancy between our measurements taken at the OSN and the literature**

Given that in principle Stauffer 85/89 provide values with errors lower than 0.04 mag, we wished to check our photometry with theirs. There are 14 stars measured both by Stauffer 85/89 and at the OSN, of which 12 present differences above 0.04 mag in some $B-V$, $V$ and $V-I_c$ values. Nine of these measurements were observed at the OSN on photometric nights (18/11,2015, 21/10/2015, 11/11/2016 and 29/11/2015) and present good values in the transformation and extinction coefficients, as well as presenting a considerable number of measurements of standard stars and low residuals. As a consequence, we adopt our photometry. The 3 remaining stars (AP75, AP91 and AP93) do not appear to have reliable measurements from the OSN. During the observation of AP75, on the night of 16/11/2015, measurements were taken of a number of standard stars that proved to be insufficient to obtain a robust extinction value, while the stars AP91 and AP93 were observed at an airmass greater than 2, on the nights of 05/04/2017 and 06/04/2017, respectively.

For these three stars, we checked whether the Stauffer 85/89 measurements are more reliable than those taken at the OSN, for which we compared the $B-V$ and $V$ from Stauffer 85/89 and from OSN with APASS DR9 (since Kharchenko (2001) does not provide data for these stars). For AP91 and AP93, APASS DR9 presents errors in $B-V$ and $V$ of $\sim$ 0.035 mag and $\sim$ 0.03 mag, respectively; for AP75, the errors are greater: $B-V$ = 0.199 mag and $V$ = 0.064 mag. The differences in $B-V$ between the APASS DR9 and Stauffer 85/89 measurements for the three stars are $\sim$ 0.04 mag, and in $V$ they are more than 0.04 mag except for AP75, although for this star the errors in APASS DR9 are high, as we have seen. Between the APASS DR9 and OSN measurements, the differences are all higher than 0.04 mag except for the $V$ value for the star AP91. In principle, it seems that the Stauffer 85/89 measurements could be more accurate than the OSN ones, but with these data, it is impossible to draw any conclusion. At last we compared the photometry of these three stars with the values tabulated by Erik Mamajek; for the AP75 AND AP93 we could still not decide which measurement to take. However, for AP91, the value of $K_s$ was very helpful while using the tabulated photometry. We looked for the values of $B-V$, $M_v$ and $V-I_c$ corresponding to the absolute magnitude $M_{Ks}$ in order to check which measurements were closer to these values, with no doubt the OSN measurements followed the tabulated values. For this reason we will use the OSN photometry for AP91. In Table 3.2 we show the data from the OSN and from Stauffer 85/89 for these three stars.

### Membership of our sample of $\alpha$ Per

The objects contained in our sample have been classified as probable members by one, or several, of the following studies that are prior to the catalogue from which we have selected the stars with rotation periods (Messina et al. 2003): Stauffer et al. (1985, 1989b) and Prosser & Randich (1998). We wish to check, by reviewing later membership studies, whether the stars we selected from $\alpha$ Per were indeed still considered to be members of the cluster.
Before the Gaia era, new membership studies of $\alpha$ Per were carried out: Deacon & Hambly (2004), Lodieu et al. (2005), Lodieu et al. (2012), Zuckerman et al. (2012), Nunez (2018). However, given the accuracy and completeness of *Gaia* DR2, we decided only to take into account those studies that were able to make use of its astrometric data (for example, Gaia Collaboration et al. 2018a; Lodieu et al. 2019a; Cantat-Gaudin & Anders 2020).

As we wish to ensure that the stars selected for our study are cluster members, we decided to consider mainly the results of Lodieu et al. (2019a). This study, following those by Perryman et al. (1998) y Luri et al. (2018), obtained a tidal radius for $\alpha$ Per of 9.5 pc (with an efficiency of 4 $\sigma$). This parameter is extremely useful for our objective, since it concerns the distance to the centre of the cluster that includes the stars with a very high percentage of being members, since they would be joined to the cluster gravitationally. From this radius, the greater the distance the less the probability of forming part of the cluster. Bearing this in mind, we considered the stars from our sample with a tidal radius close to or less than 9.5 pc as members of $\alpha$ Per. For those objects with a higher radius, we took the value of three times the tidal radius (28.5 pc) as the limit. Stars with values higher than 28.5 pc were marked as having a high probability of being non-members. Those that fell within the range 9.5 pc $< R <$ 28.5 pc were taken into account as possible members. Lastly, several stars in our sample are not included in the Lodieu et al. (2019a) catalogue, because they were rejected at the start of their study as they were not considered to be clear members of the cluster, and therefore we have marked them as non-members.

Our sample of 54 stars contains 37 that we have marked as members, 10 as possible members ($9.5 < R < 28.5$), 1 with a high probability of not forming part of the cluster ($R > 28.5$) and 6 that are not members.

### Table with our selection for $\alpha$ Per

As the table has many columns, in this section we will show the data that was essential for the development of this study.

| *Name* | $\alpha_{J2000}$ (h:m:s) | $\delta_{J2000}$ (o:′:″) | *Notes memb.* | $B-V$ (mag) | e$B-V$ (mag) | $V$ (mag) | e$V$ | $M_v$ (mag) | $V-Rc$ (mag) | e$V-Rc$ (mag) | $V-Ic$ (mag) | e$V-Ic$ (mag) | $Ks$ (mag) | e$Ks$ (mag) | *Notes phot.BVRI* | *Date Obs.OSN* | $D_{BJ,Gaia}$ (pc) | *Period* (days) | *Notes period* | *Spect. Types* |
|---|---|---|---|---|---|---|---|---|---|---|---|---|---|---|---|---|---|---|---|---|
| AP120 | 03:17:38 | +49:54:48 | 1 | 1.548 | 0.027 | 15.151 | 0.026 | 9.024 | 1.083 | 0.019 | 2.301 | 0.021 | 10.517 | 0.017 | OSN | 19/11/2015 | 168.025 | 0.3 | m | M2.0 |
| AP122 | 03:18:09 | +49:18:55 | 1 | 1.482 | 0.015 | 15.226 | 0.016 | 8.977 | 0.99 | 0.014 | 1.989 | 0.021 | 11.093 | 0.017 | OSN | 21/10/2015 | 177.722 | 0.231 | m | M1.0 |
| HE373 | 03:18:27 | +47:21:15 | 1 | 0.77 | | 11.5 | | 5.369 | 0.473 | | 0.891 | | 9.352 | 0.024 | STAUFFER | | 168.369 | 0.333 | f | G3 |
| AP91 | 03:18:50 | +48:16:03 | 2 | 1.066/0.93 | 0.024/ | 12.743/12.59 | 0.028/ | 6.864/6.697 | | | 1.203/1.133 | 0.024/ | 10.0 | 0.018 | OSN/STAUFFER | 05/04/2017 | 149.895 | 1.508 | g | MID-K* |
| AP124 | 03:18:59 | +48:50:42 | 2 | 1.169 | 0.012 | 13.529 | 0.017 | 7.425 | 0.769 | 0.018 | 1.519 | 0.015 | 10.235 | 0.016 | OSN | 05/01/2017** | 166.291 | 0.183 | f | K5 |
| AP93 | 03:19:03 | +48:11:00 | 4 | 0.943/0.93 | 0.03/ | 11.759/11.99 | 0.026/ | 5.536/5.746 | | | 1.034/1.104 | 0.032/ | 9.363 | 0.016 | OSN/STAUFFER | 06/04/2017 | 175.642 | 0.62 | g | EARLY-K* |
| AP95 | 03:19:58 | +49:52:07 | 1 | 0.88 | | 12.28 | | 6.094 | 0.515 | | 0.978 | | 9.917 | 0.018 | STAUFFER | | 172.66 | 0.353 | c | EARLY-K* |
| AP127 | 03:20:01 | +46:53:01 | 2 | 0.941 | 0.031 | 12.592 | 0.03 | 6.473 | | | 1.18 | 0.031 | 9.9 | 0.016 | OSN | 18/03/2017 | 167.443 | 0.347 | f | EARLY-K* |
| AP96 | 03:20:39 | +50:15:50 | 1 | 1.571 | 0.015 | 14.483 | 0.016 | 8.301 | 1.014 | 0.014 | 2.027 | 0.021 | 10.225 | 0.023 | OSN | 21/10/2015 | 172.363 | 0.346 | m | EARLY-M* |
| AP97 | 03:20:42 | +48:24:38 | 1 | 0.87 | | 12.08 | | 5.96 | 0.507 | | 0.949 | | 9.884 | 0.021 | STAUFFER | | 167.456 | 4.8 | m | G6.5 |
| AP98 | 03:21:07 | +48:26:13 | 1 | 1.0 | | 12.8 | | 6.603 | 0.572 | | 1.056 | | 10.327 | 0.020 | STAUFFER | | 173.524 | 6.2 | j | G9 |
| AP100 | 03:21:16 | +48:35:07 | 4 | 1.125 | 0.015 | 12.745 | 0.016 | 6.523 | 0.703 | 0.014 | 1.385 | 0.021 | 9.603 | 0.022 | OSN | 21/10/2015 | 175.558 | 0.229 | e | MID-K* |
| AP102 | 03:21:20 | +48:45:27 | 1 | 0.8 | | 11.96 | | 5.775 | 0.473 | | 0.891 | | 9.887 | 0.020 | STAUFFER | | 172.603 | 4.3 | m | LATE-G* |
| AP101 | 03:21:22 | +49:57:03 | 1 | 1.275 | 0.015 | 13.989 | 0.011 | 7.775 | 0.785 | 0.01 | 1.539 | 0.013 | 10.648 | 0.021 | OSN | 11/11/2015 | 174.902 | 3.2 | j | K6 |
| AP104 | 03:22:05 | +48:49:37 | 4 | 0.78 | | 12.06 | | 3.854 | 0.456 | | 0.862 | | 10.138 | 0.022 | STAUFFER | | 437.631 | 0.409 | l | G3.5 |
| AP139 | 03:22:07 | +47:34:07 | 1 | 0.916/0.922 | 0.034/0.023 | 12.051/12.096 | 0.036/0.019 | 5.79/5.835 | 0.558 | 0.018 | 1.124/1.112 | 0.031/0.02 | 9.364 | 0.223 | OSN | 19/12/2015$^{++}$-07/01/2017 | 178.692 | 0.258 | e | K2 |
| HE520 | 03:22:22 | +49:08:28 | 1 | 0.79 | | 11.69 | | 5.443 | 0.465 | | 0.891 | | 9.64 | 0.016 | STAUFFER | | 177.58 | 0.607 | n | G6V |
| AP108 | 03:23:37 | +48:58:53 | 1 | 0.99 | 0.024 | 12.904 | 0.023 | 6.741 | 0.591 | 0.024 | 1.115 | 0.024 | 10.309 | 0.022 | OSN | 29/11/2015 | 170.855 | 3.85 | m | EARLY-K* |
| AP109 | 03:24:07 | +49:24:52 | 1 | 1.547 | 0.024 | 15.893 | 0.023 | 9.597 | 1.071 | 0.024 | 2.214 | 0.024 | 11.415 | 0.017 | OSN | 29/11/2015 | 181.618 | 0.25 | m | M3 |
| HE601 | 03:24:17 | +49:39:00 | 2 | 0.73 | | 11.43 | | 5.173 | 0.421 | | 0.795 | | 9.622 | 0.018 | STAUFFER | | 178.376 | 3.6 | m | G6 |
| AP15 | 03:24:25 | +48:48:21 | 1 | 1.268 | 0.024 | 14.201 | 0.023 | 7.959 | 0.812 | 0.024 | 1.562 | 0.024 | 10.758 | 0.020 | OSN | 29/11/2015 | 177.137 | 0.622 | o | K5 |
| AP110 | 03:24:56 | +49:26:02 | 4 | 0.92 | | 12.27 | | 5.554 | 0.531 | | 1.008 | | 12.6 | 0.023 | STAUFFER | | 220.424 | 5.519 | l | G8 |
| AP25 | 03:25:16 | +48:22:24 | 1 | 0.88 | | 12.25 | | 6.088 | 0.498 | | 0.949 | | 10.01 | 0.020 | STAUFFER | | 170.769 | 3.7 | m | K0 |
| AP112 | 03:25:32 | +48:30:11 | 1 | 1.184 | 0.015 | 13.654 | 0.011 | 7.478 | 0.738 | 0.01 | 1.383 | 0.013 | 10.601 | 0.016 | OSN | 11/11/2015 | 171.888 | 2.67 | m | MID-K* |
| AP28 | 03:25:54 | +48:31:09 | 1 | 1.05 | | 13.09 | | 6.864 | 0.603 | | 1.162 | | 10.433 | 0.019 | STAUFFER | | 175.863 | 3.47 | m | MID-K* |
| AP33 | 03:26:13 | +48:09:09 | 1 | 1.04 | | 12.94 | | 6.686 | 0.587 | | 1.085 | | 10.395 | 0.020 | STAUFFER | | 178.135 | 6.4 | m | K0 |
| AP37 | 03:26:16 | +48:50:28 | 1 | 0.975 | 0.024 | 12.931 | 0.023 | 6.764 | 0.601 | 0.024 | 1.167 | 0.024 | 10.214 | 0.020 | OSN | 29/11/2015 | 171.141 | 2.45 | m | EARLY-K* |
| HE699 | 03:26:22 | +49:25:38 | 1 | 0.71 | | 11.27 | | 5.036 | 0.421 | | 0.814 | | 9.414 | 0.020 | STAUFFER | | 176.537 | 0.491 | n | G2-3V |
| AP41 | 03:26:25 | +48:20:07 | 1 | 0.85 | | 12.03 | | 5.729 | 0.473 | | 0.911 | | 9.875 | 0.019 | STAUFFER | | 182.043 | 5.5 | j | G5 |
| AP43 | 03:26:28 | +49:02:12 | 4 | 0.97 | | 12.84 | | 6.597 | 0.587 | | 1.153 | | 10.11 | 0.017 | STAUFFER | | 177.291 | 0.582 | o | EARLY-K* |
| AP114 | 03:27:20 | +47:59:25 | 1 | 1.071 | 0.024 | 13.377 | 0.021 | 7.207 | 0.676 | 0.015 | 1.345 | 0.021 | 10.468 | 0.020 | OSN | 18/11/2015 | 171.413 | 4.32 | j | K2 |
| AP56 | 03:27:23 | +48:22:25 | 1 | 1.0 | | 13.0 | | 6.754 | 0.595 | | 1.153 | | 10.339 | 0.022 | STAUFFER | | 177.49 | 0.36 | a | EARLY-K* |
| AP60 | 03:27:39 | +48:24:59 | 1 | 1.549 | 0.015 | 15.711 | 0.016 | 9.542 | 1.116 | 0.014 | 2.451 | 0.021 | 10.9 | 0.023 | OSN | 21/10/2015 | 171.281 | 0.318 | g | EARLY-M* |
| AP63 | 03:27:51 | +49:12:10 | 1 | 0.927 | 0.024 | 12.468 | 0.023 | 6.207 | 0.566 | 0.024 | 1.119 | 0.024 | 9.86 | 0.022 | OSN | 29/11/2015 | 178.697 | 0.225 | f | K2 |
| AP167 | 03:28:11 | +47:25:26 | 1 | 1.112 | 0.023 | 13.488 | 0.019 | 7.19 | | | 1.257 | 0.02 | 10.443 | 0.020 | OSN | 07/01/2017 | 181.77 | 0.408 | i | K5.3 |
| AP70 | 03:28:19 | +48:39:48 | 1 | 1.0 | | 12.83 | | 6.648 | 0.564 | | 1.075 | | 10.331 | 0.025 | STAUFFER | | 172.32 | 6.4 | j | K0 |
| APX158 | 03:28:22 | +50:36:06 | 1 | 0.922 | 0.024 | 12.315 | 0.023 | 6.088 | 0.56 | 0.024 | 1.089 | 0.024 | 9.845 | 0.025 | OSN | 29/11/2015 | 175.937 | 0.26 | d | K0 |
| AP72 | 03:28:23 | +49:14:29 | 1 | 0.99 | | 12.78 | | 6.598 | 0.564 | | 1.066 | | 10.383 | 0.024 | STAUFFER | | 172.382 | 6.3 | j | K0 |

(Continued).

| *Name* | $\alpha_{J2000}$ (h:m:s) | $\delta_{J2000}$ (°:′:″) | *Notes memb.* | $B-V$ (mag) | e$B-V$ (mag) | $V$ (mag) | e$V$ (mag) | $M_v$ (mag) | $V-Rc$ (mag) | e$V-Rc$ (mag) | $V-Ic$ (mag) | e$V-Ic$ (mag) | $Ks$ (mag) | e$Ks$ (mag) | *Notes phot.BVRI* | *Date Obs.OSN* | $D_{BJ.Gaia}$ (pc) | *Period* (days) | *Notes period* | *Spect. Types* |
|---|---|---|---|---|---|---|---|---|---|---|---|---|---|---|---|---|---|---|---|---|
| AP169 | 03:28:24 | +47:36:50 | 2 | 1.086/1.139 | 0.034/0.023 | 13.272/13.263 | 0.036/0.019 | 7.109/7.1 | 0.677 | 0.018 | 1.261/1.227 | 0.031/0.02 | 10.392 | 0.020 | OSN | 19/12/2015$^{++}$-07/01/2017 | 170.805 | 5.1 | j | K7 |
| AP75 | 03:28:47 | +49:16:28 | 4 | 1.353/1.27 | 0.017/ | 13.958/13.82 | 0.019/ | 7.797/7.650 | 0.792/0.787 | 0.012/ | 1.593/1.596 | 0.013/ | 10.284 | 0.020 | OSN/STAUFFER | 16/11/2015 | 170.658 | 2.79 | m | LATE-K* |
| AP117 | 03:28:48 | +49:11:54 | 1 | 0.95 | | 13.05 | | 6.837 | 0.587 | | 1.114 | | 15.112 | 0.122 | STAUFFER | | 174.858 | 0.471 | f | EARLY-K* |
| AP86 | 03:30:22 | +48:24:41 | 2 | 1.297 | 0.018 | 14.316 | 0.013 | 7.949 | 0.838 | 0.012 | 1.616 | 0.019 | 10.769 | 0.024 | OSN | 10/11/2015 | 187.652 | 0.21 | b | LATE-K* |
| HE935 | 03:31:29 | +48:59:28 | 2 | 0.62 | | 10.05 | | 3.935 | 0.368 | | 0.727 | | 8.46 | 0.022 | STAUFFER | | 167.120 | 0.275 | l | F9.5V |
| AP196 | 03:32:19 | +47:04:27 | 1 | 0.896 | 0.024 | 12.332 | 0.023 | 6.122 | 0.532 | 0.024 | 1.019 | 0.024 | 10.123 | 0.019 | OSN | 29/11/2015 | 174.603 | 4.54 | m | K3 |
| AP118 | 03:32:31 | +49:10:35 | 1 | 0.81 | | 11.98 | | 5.804 | 0.482 | | 0.901 | | 9.767 | 0.018 | STAUFFER | | 171.88 | 0.31 | e | G8 |
| AP201 | 03:32:51 | +49:50:44 | 1 | 1.053 | 0.016 | 13.081 | 0.015 | 6.867 | 0.626 | 0.018 | 1.296 | 0.015 | 10.138 | 0.022 | OSN | 06/01/2017** | 174.871 | 3.75 | j | K5 |
| AP205 | 03:33:34 | +46:07:26 | 2 | 1.557 | 0.024 | 15.267 | 0.021 | 9.08 | 1.03 | 0.015 | 2.062 | 0.021 | 11.064 | 0.023 | OSN | 18/11/2015 | 172.756 | 0.264 | m | M0.8 |
| AP208 | 03:33:47 | +47:35:31 | 2 | 1.646 | 0.028 | 15.535 | 0.026 | 9.436 | 1.106 | 0.019 | 2.254 | 0.021 | 11.112 | 0.016 | OSN | 19/11/2015 | 165.895 | 0.325 | m | M1.3 |
| AP211 | 03:34:11 | +49:50:26 | 3 | 1.495 | 0.018 | 15.017 | 0.013 | 8.72 | 0.861 | 0.012 | 1.86 | 0.019 | 11.06 | 0.022 | OSN | 10/11/2015 | 181.742 | 0.288 | m | M0.2 |
| AP212 | 03:34:29 | +49:21:43 | 1 | 1.04 | 0.024 | 13.516 | 0.021 | 7.309 | 0.735 | 0.015 | 1.373 | 0.021 | 10.581 | 0.018 | OSN | 18/11/2015 | 174.359 | 6.2 | i | K4 |
| AP220 | 03:35:44 | +49:06:07 | 1 | 0.919 | 0.024 | 12.77 | 0.025 | 6.606 | | | 1.107 | 0.024 | 10.193 | 0.021 | OSN | 08/04/2017 | 170.945 | 1.3 | m | EARLY-K* |
| AP244 | 03:40:34 | +48:04:36 | 1 | 0.972 | 0.036 | 12.991 | 0.033 | 6.719 | | | 1.126 | 0.029 | 10.352 | 0.023 | OSN | 17/03/2017 | 179.678 | 0.463 | o | EARLY-K* |
| AP247 | 03:40:58 | +47:02:37 | 2 | 1.002 | 0.023 | 13.279 | 0.019 | 6.963 | | | 1.17 | 0.02 | 10.517 | 0.018 | OSN | 07/01/2017 | 183.343 | 2.5 | m | K4.5 |
| AP257 | 03:44:03 | +48:39:59 | 1 | 0.985 | 0.023 | 13.117 | 0.019 | 6.943 | | | 1.161 | 0.02 | 10.446 | 0.023 | OSN | 07/01/2017 | 171.708 | 4.83 | m | K4.3 |

Table 3.2: $\alpha$ Per members and non-members with periods and $BVR_cI_c$ photometry. Parameters shown of $\alpha$ Per: name of the stars taken from Messina et al. (2003); coordinates ($\alpha$ y $\delta$); membership notes (1: member, 2: possible member, 3: unlikely member, 4: non-member); $B-V$, $V$, $V-R_c$, $V-I_c$ photometry and their errors; photometry notes that indicate the origin of the data shown; $M_v$ calibrated brightness, obtained using distances from Bailer-Jones et al. (2018); OSN observation date; distances obtained by Bailer-Jones et al. (2018) using Bayesian analysis of Gaia parallaxes ($D_{BJ.Gaia}$); rotation period; origin of selected rotation period; spectral types taken from SIMBAD.

The symbols that appear in certain columns point out: (a) alongside the observation dates, $**$ means that the $V-R_c$ values for those stars were taken on the night of 19/12/2015, and ++ indicates that it was observed on the 0.9 m on that night and that the $V-I_c$ value could be effected by fringing; (b) alongside the spectral types, $*$ means that these spectral types were derived using $B-V$, $V$ and $V-I_c$ values, and the table by Erik Mamajek of tabulated values; (c) next to the rotation periods, the characters indicate the reference from which these periods were extracted. Note that for AP91 we show both OSN and Stauffer measurements, however for this star we will use the OSN photometry in our study.

## 3.2 Pleiades

Popularly known as the "Seven Sisters", due to the group of stars that are visible to the naked eye, it has attracted observers since antiquity and is (along with the Hyades) the open cluster that has been studied the most. Pleiades (M45, Melotte 22), with centre coordinates $\alpha_{J2000} = 03^h47^m00^s$ $\delta_{J2000} = +24°07'00''$ (Dias et al. 2014), is located in the constellation of Taurus and is one of the nearest clusters to the Earth. It is a young cluster that contains a large number of stars. Due to its young age, spectral types later than M2.5 (M2.5 stars arrive at the main sequence at an age of $\sim$ 100 Myr, as estimated from Fig. 4 from D'Antona & Mazzitelli (1994)) are still contracting to reach the main sequence, while those with masses near to 0.4 $M_\odot$ and more masives have already reached this region of the HR diagram, and the higher-mass stars have started to leave the main sequence. Due to this, Pleiades has been a point of reference for reproducing stellar evolution models.

### 3.2.1 Cluster characteristics

#### Distance and age

The distance of Pleiades was the cause of a great controversy that lasted more than 15 years.
In 1997, the first measurement of its distance was published, which used trigonometric parallaxes from the Hipparcos mission. This distance, with a value of $\sim$ 116 pc, surprisingly did not fit with calculations from previous studies, in which they used the main-sequence fitting technique, by means of which the main sequence of the cluster of interest is compared with the main sequence generated from nearby stars with well-defined parallaxes. Several studies had measured the Pleiades distance using this system with an average approximate result of $\sim$ 130 pc (for example, Vandenberg & Bridges 1984; Soderblom et al. 1993), which is a much higher value than that given by Hipparcos. From then on, numerous studies made an effort to try to shed light on this controversy, and new calculations of the cluster distance were made, many of which are shown in Table 3 from van Leeuwen (2009), where the techniques used are also specified. van Leeuwen (2009) calculated the mean of the distances obtained by 11 studies subsequent to the Hipparcos catalogue, obtaining a value of 133.66 pc with standard deviation of 13.06 pc. Furthermore, van Leeuwen (2009) carried out a new reduction of the Hipparcos astrometric data in order to improve the accuracy of the parallaxes and proper motions, and obtained a new distance for Pleiades of $\sim$120 pc. This result, although a little higher, continued not to fit with those provided by the aforementioned studies. This gave rise to new studies focused on resolving the discrepancy (for example, Palmer et al. 2014; Melis et al. 2014; Abramson 2018). Of these, it is worth mentioning the distance obtained by Melis et al. (2014), which, using high-precision parallax measurements and very long baseline interferometry, obtained a distance of 136.2 $\pm$ 1.2 pc, which confirmed the low value of the Hipparcos result. Similarly, Abramson (2018) again calculated the distance of Pleiades, in this case from *Gaia* DR2 parallaxes, and produced a practically identical value to the previous one (136.2 $\pm$ 5.0 pc). Likewise for Lodieu et al. (2019a), who used the *Gaia* DR2 parallaxes and the Bayesian method explained in Luri et al. (2018), and obtained a distance of

135.15 ± 0.43 pc, similar to the above. In short, given the precision of the data utilized in these latest studies, the search for the distance of Pleiades could be declared over.

We would not like to end this subsection without mentioning the study by Krełowski et al. (2019), which gives a possible explanation for the origin of the controversy between the distance obtained by Hipparcos and the rest. In this study, they suggest that the brightest stars of the cluster are located at a greater distance from its centre than expected. Moreover, they are situated between it and us, meaning that their distance to us would be closer to that given by Hipparcos, and this is what might have caused the obtention of shorter distances. In order to check their theory, we have looked for the distances to the centre of Pleiades for the objects that comprise the "Seven Sisters" in the paper by Lodieu et al. (2019a), and the stars Electra and Maia are indeed some 30 pc from the cluster centre and Taygeta is at a distance above 20 pc. Furthermore, the distance of Atlas is greater than 15 pc. As we will see below, the tidal radius of Pleiades has been established at 11.6 pc.

However, the age of Pleiades continues to be the centre of debate. With the isochrone fitting method, ages in the range of 70-135 Myr were obtained (for example, Patenaude 1978; Mermilliod 1981; Steele et al. 1993; Meynet et al. 1993; Sanner & Geffert 2001; Kharchenko et al. 2005; Bell et al. 2014). Its age has also been calculated by fitting on the CMD isochrones generated through stellar models which considered parameters not included in more classical models (Mazzei & Pigatto 1989; Brandt & Huang 2015; Gossage et al. 2018).

These studies have provided values in the range of 120-130± 20 Myr, with the ages also calculated using the lithium depletion boundary technique (Basri et al. 1996; Stauffer et al. 1998b; Burke et al. 2004; Barrado y Navascués et al. 2004).

A later study, carried out by Dahm (2015), revised the positioning of the lithium boundary and proposed a lower age for Pleiades of 112 ±5 Myr. Taking this into account, along with the fact that the common age range obtained using the classical and "non-classical" isochrone methods, and the lithium depletion boundary method, is between 100 and 135 Myr, we therefore take that more recent age of ∼ 112 Myr for Pleiades.

### Membership

With the purpose of choosing its members, both photometrically and astrometrically, many studies undertaken over the years have shown that Pleiades proves to be more simple to study than other open clusters. This is essentially due to the fact that it has a high proper motion compared to the field stars, with an approximate mean value of $\mu_\alpha \sim 19.99$ mas $yr^{-1}$ y $\mu_\delta \sim$ -45.5 mas $yr^{-1}$ (Gaia Collaboration et al. 2018a), and it is not close to the galactic plane (b $\sim -23°$; Kharchenko et al. 2009), hence it has a low interstellar extinction value (E$(B-V) = 0.045$ mag; Gaia Collaboration et al. 2018a).

As Lodieu et al. (2019a) summarize, numerous studies dedicated to selecting Pleiades members have been carried out (for example, Trumpler 1921; Hertzsprung 1947; Artyukhina 1969; Eichhorn et al. 1970; Jones 1981; Turner 1979; Haro et al. 1982; Stauffer 1982b, 1984; van Leeuwen et al. 1986; Jameson & Skillen 1989; Stauffer et al. 1989a, 1991, 1994, 1998a; Simons

& Becklin 1992; Hambly et al. 1993, 1999; Willliams et al. 1996; Cossburn et al. 1997; Zapatero Osorio et al. 1997a,b,c, 1999, 2014, 2018; Martin et al. 1998; Bouvier et al. 1998; Festin 1998; Pinfield et al. 2000; Sanner & Geffert 2001; Adams et al. 2001; Moraux et al. 2001, 2003; Jameson et al. 2002; Dobbie et al. 2002; Deacon & Hambly 2004; Bihain et al. 2006, 2010; Casewell et al. 2007, 2011; Lodieu et al. 2007, 2012; Bouy et al. 2013; Sarro et al. 2014; Barrado et al. 2016; Gaia Collaboration et al. 2018a). Stauffer et al. (2007) compiled 1416 candidates for cluster membership using previous studies (see Table 1 of this article); by means of a probability selection method, Bouy et al. (2015) identified a total of 2107 stars with a high probability of being members; Olivares et al. (2018) analysed the membership of Pleiades and provided the longest and least contaminated list of members up to the date of its publication, contributing 2151 stars with the probability of being members higher than 75%; lastly, we should again highlight the study by Lodieu et al. (2019a), who, using the method explained in the section on $\alpha$ Per, obtained a tidal radius of 11.6 pc, which produced a total of 1248 stars. In addition, Lodieu et al. (2019a) calculate a total of 947 possible members at a distance from the centre of 11.6 pc $< d <$ 34.8 pc.

### 3.2.2 Our sample for Pleiades

We have compiled 281 stars from intermediate-F to intermediate-M, with known rotation periods and photometry in the $BVI_c$ bands. However, as we will explain, for one of the stars we will not be able to use the collected period. Below, we explain in detail the origin of the data shown in Table 3.2.2 on membership, $BVI_c$ photometry, periods and distances.

#### Periods

In order to form our sample, we began with the tables from Covey et al. (2016) and Rebull et al. (2016), both with rotation periods of Pleiades candidate members.

- Covey et al. (2016) compile 495 stars that include 383 rotation periods from the catalogue by Hartman et al. (2010) plus their own robust measurements of 132 rotation periods (of which 112 are new measurements). These periods had to fulfil the following two criteria to be defined as robust: one single peak on the periodogram and one "peak power" > 30. Hartman et al. (2010) used the member compilation of Stauffer et al. (2007) and selected 407 probable candidates of forming part of the cluster, for which they measured periods by making use of light curves from data taken with the "Hungarian-made Automated Telescope Network" (HATNet, Bakos et al. 2004). They obtained 368 periods for stars with masses between ~0.4 $M_\odot$ and ~1.3 $M_\odot$. They also compiled 15 periods from the literature.

  Like Covey et al. (2016), where a star has measurements from both studies, we prioritize those from the list of robust periods from Covey et al. (2016).

- Regarding Rebull et al. (2016), they have presented more than 500 new periods from Pleiades, generated from observations from the NASA K2 space mission (Howell et al. 2014, hence-

forth K2), which, using the Kepler instrument (Borucki et al. 2003), provided rotation periods for low-mass stars with the highest precision available at that time. In accordance, in the event that a star has periods obtained by more than one of the studies mentioned, we have prioritized the measurements by Rebull et al. (2016) over the previous studies.

In total, we have compiled 821 stars of Pleiades with rotation periods and spectral types from A0. Below we explain the acquisition of the photometry data for these objects, and we will select the stars whose measurements fulfil the established criteria.

#### Photometry $BVI_c$

Of the 281 stars from the final Pleiades sample, 279 have $BVI_c$ photometry taken from the literature and 2 have been observed at the OSN in the same filters. Except for four objects, in principle all fulfil the criterion of presenting photometry with errors $\lesssim 0.04$ mag in the three bands.

#### Photometry coming from the literature

With the aim of correlating the set of stars with rotation periods with the available photometry in the literature, we have taken the most homogeneous and accurate list of measurements in the $BVI_c$ bands of Pleiades stars that has been obtained thus far, with V values in the range of 9 mag $< V \lesssim$ 17 mag. This photometry was provided by Kamai et al. (2014), who obtained measurements in the $BVI_c$ bands for 350 stars with typical errors in $V$, $B-V$ and $V-I_c$ of 0.023 mag, 0.019 mag and 0.019 mag, respectively.

In order to increase the number of stars in the sample with photometry information, we also used the catalogue from Stauffer et al. (2007), which gives a compilation of $BVI_c$ from the literature for their list of 1416 Pleiades candidates. As we need the most homogeneous compilation of photometry possible, and with the most reliable measurements, we followed the same criterion as Kamai et al. (2014) and we have taken their selection of 507 stars from the Stauffer et al. (2007) catalogue (this selection was sent by B.L. Kamai through private communication, as it is not available in her article). The photometry measurements of these stars fulfil the criterion of not having been done either by photographic plate or with filter sets lacking appropriate calibration to the Johnson-Cousins and Kron systems. This is because many of the stars had been observed in other photometric systems, including Walraven, Geneva, Kron and Johnson. Neither Stauffer et al. (2007), nor Kamai et al. (2014) provide $V-R_c$ data.

Of the 821 stars with rotation periods, 469 have $BVI_c$ photometry in the literature. Among these 469 objects, 242 have photometry obtained from Kamai et al. (2014) and 227 from Stauffer et al. (2007). From this selection of 469 stars, we took those that have photometry for which we knew the magnitude and colour errors, without surpassing ~0.04 mag. In total, there are 279 stars that meet this criterion, 236 with photometry from Kamai et al. (2014) and 43 from Stauffer et al. (2007). We want to mention that before the later selection we removed those stars classified in Simbad as spectral types with luminosity class different than V. As we can see, the number of stars

with photometry coming from Stauffer et al. (2007) has been reduced considerably. This is because they did not give errors for every measurement, only the references that they used to make their photometry compilation. Since we are more interested on late spectral types, we selected stars G6 or later spectral types from the 227 stars with measurements by Stauffer et al. (2007), in order to search for the errors of the photometric values. We found a total of 15 references for our selection of 177 stars and searched for photometry errors in each of the 15 references and confirmed that either the measurements had errors higher than 0.04 mag, or the magnitudes and colours had been obtained by calculating the mean of data given in various studies and the resulting error had not been provided. The 43 stars with photometry from Stauffer et al. (2007) that have been kept in our sample have values of magnitudes and colours that come from Stauffer (1982b) and Stauffer & Hartmann (1987), with errors $\lesssim$0.04 mag except for four stars – HCG 150, HCG 323, HCG 372 and HCG 427 – which have errors in $V - I_K$ (I in the Kron system) of $\sim$ 0.05 mag. We decided to keep them because these are early-mid M dwarfs, and in $B - V$ and $V$ the errors are not above 0.04 mag. Stauffer (1982b) and Stauffer & Hartmann (1987) provide $I$ in the Kron system, and Stauffer et al. (2007) transformed these colours to the Cousins system using the equations from Bessell & Weis (1987). We must bear in mind that the $V - I_c$ measurement errors obtained by Stauffer et al. (2007) are somewhat greater than those we show, as these are the $V - I_K$ errors (in the Kron system), and the Kron/Cousins fit by Bessell & Weis (1987) presents an error value of 0.014 mag.

To summarize, we have a sample of 279 stars with rotation periods and photometry from the literature with errors $\lesssim$ 0.04 mag (except in the $V - I_c$ error for four M stars), 236 objects have $BVI_c$ photometry from Kamai et al. (2014) and 43, also in $BVI_c$, from Stauffer (1982b) and Stauffer & Hartmann (1987) compiled in Stauffer et al. (2007). In addition, for Pleiades, 2MASS has surpassed the precision in $JHK_s$, thanks to its "2MASS 6X" measurements ("2MASS 6X Point Source Working Database" Cutri et al. 2012). These data are also included in Stauffer et al. (2007). Where a star has measurements from 2 MASS and 2MASS 6X, we prioritize the latter.

#### Photometry obtained at the OSN

As we have already mentioned, we carried out observations for two stars from our Pleiades selection with rotation periods. One of these is a Late-K dwarf (2MASS J03373212+2612137) and the other a Mid-M dwarf (Cl* Melotte 22 HHJ 249). The observations were made on two photometric nights, 21/10/2015 and 10/11/2015 respectively. The upper limit errors for the star 2MASS J03373212+2612137 are e$B - V \sim$ 0.015 mag, e$V \sim$ 0.016 mag, e$V - R_c \sim$ 0.014 mag and e$V - I_c$ $\sim$ 0.021 mag. The upper limit errors for the star star Cl* Melotte 22 HHJ 249 are, following the same order, 0.039 mag, 0.016 mag, 0.017 mag and 0.022 mag. For the latter star, we specify its signal to noise in Table 3.2.2 as it is below the required (S/N=100) in the $B$ band.

#### Membership of our sample

With one exception, all the stars in our sample are included in the list of member candidates of Stauffer et al. (2007). The remaining star is one of those observed at the OSN (2MASS J03373212+2612137) whose only period measurement comes from the catalogue in Hartman

et al. (2010). Searching for a possible reason for which this star was not included in the catalogue of Stauffer et al. (2007), we saw that the name that Hartman et al. (2010) gives for this star comes from the SIMBAD database, yet the star we have observed at the OSN does not appear in this database (we obtained its name from 2MASS). We believe that the period that Hartman et al. (2010) provide actually corresponds to another object that is different from the one for the coordinates they provide. Fortunately, as we will see below, this star remains a possible member of the cluster. Therefore, we will show the OSN measurements for this star but we cannot use any period value.

In order to verify that all the objects we selected do indeed belong to Pleiades, we proceeded in the same way as with $\alpha$ Per and considered the tidal radius obtained by Lodieu et al. (2019a) for Pleiades. We took as highly probable cluster members those stars with a distance to the centre that is less than or equal to the tidal radius (11.6 pc, 206 stars) and as possible members those stars with a distance between the tidal radius and three times its value: 11.6 pc $< d <$ 34.8 pc (41 stars). We considered as unlikely members those objects with a distance to the centre greater than 34.8 pc (four stars), and we discarded those stars not included in the catalogue in Lodieu et al. (2019a) (23 stars). Furthermore, there are seven stars that do not have membership data in this study. This is because *Gaia* DR2 has not provided distances (an essential parameter in their study) for these objects. We would like to mention that the stars observed at the OSN have a distance to the centre of $\sim$ 4 pc (Cl* Melotte 22 HHJ 249) and $\sim$ 25 pc (2MASS J03373212+2612137).

**Table with our Pleiades sample**

Below we show the main collected data for our selection of Pleiades stars.

| *Name* | $\alpha_{J2000}$ (h:m:s) | $\delta_{J2000}$ ($\circ$:$'$:$''$) | *Notes memb.* | $B-V$ (mag) | e$B-V$ (mag) | $V$ (mag) | e$V$ (mag) | $M_v$ (mag) | $V-Ic$ (mag) | e$V-Ic$ (mag) | $Ks$ (mag) | e$Ks$ (mag) | *Notes phot.BVI* | $D_{BJ.Gaia}$ (pc) | *Period* (days) | *Notes period* | *Spect. Types* |
|---|---|---|---|---|---|---|---|---|---|---|---|---|---|---|---|---|---|
| "Cl* Melotte 22 DH 001" | 03:27:36 | +24:31:43 | 0 | 1.38 | 0.016 | 13.61 | 0.013 | 7.958 | 1.779 | 0.019 | 9.892 | 0.019 | Kamai | | 7.262 | H10 | LATE-K* |
| "Cl* Melotte 22 DH 007" | 03:28:49 | +26:29:58 | 2 | 0.88 | 0.012 | 12.016 | 0.011 | 6.089 | 0.958 | 0.018 | 9.924 | 0.019 | Kamai | 153.253 | 6.484 | H10 | EARLY-K* |
| "Cl* Melotte 22 DH 011" | 03:30:34 | +26:12:57 | 2 | 1.171 | 0.013 | 13.224 | 0.013 | 7.417 | 1.333 | 0.019 | 10.279 | 0.018 | Kamai | 145.034 | 4.816 | H10 | MID-K* |
| "Cl* Melotte 22 DH 014" | 03:31:12 | +25:09:54 | 1 | 1.431 | 0.009 | 14.513 | 0.009 | 8.86 | 1.866 | 0.014 | 10.602 | 0.017 | Kamai | 135.09 | 8.034 | H10 | EARLY-M* |
| "Cl* Melotte 22 DH 015" | 03:31:15 | +25:58:52 | 1 | 1.514 | 0.035 | 15.341 | 0.024 | 9.69 | 2.145 | 0.023 | 11.091 | 0.02 | Kamai | 134.946 | 2.411 | H10 | EARLY-M* |
| "Cl* Melotte 22 PELS 008" | 03:31:34 | +26:15:56 | 2 | 0.652 | 0.019 | 10.709 | 0.023 | 4.885 | 0.752 | 0.019 | 9.068 | 0.017 | Kamai | 146.182 | 3.242 | H10 | EARLY-G* |
| "Cl* Melotte 22 PELS 109" | 03:32:00 | +23:46:30 | 1 | 1.33 | 0.009 | 13.832 | 0.009 | 8.132 | 1.575 | 0.014 | 10.52 | 0.018 | Kamai | 138.061 | 8.367 | H10 | LATE-K* |
| "Cl* Melotte 22 DH 023" | 03:32:51 | +25:34:46 | 4 | 1.315 | 0.015 | 13.933 | 0.013 | 8.166 | 1.657 | 0.019 | 10.323 | 0.018 | Kamai | 142.379 | 2.087 | H10 | LATE-K* |
| "Cl* Melotte 22 DH 025" | 03:33:00 | +25:59:46 | 2 | 1.176 | 0.013 | 13.059 | 0.012 | 7.413 | 1.32 | 0.019 | 10.128 | 0.018 | Kamai | 134.674 | 9.078 | H10 | MID-K* |
| "Cl* Melotte 22 PELS 004" | 03:33:06 | +22:08:03 | 1 | 0.811 | 0.01 | 11.36 | 0.022 | 5.724 | 0.865 | 0.016 | 9.425 | 0.02 | Kamai | 134.002 | 5.766 | R16 | LATE-G* |
| "Cl* Melotte 22 PELS 123" | 03:33:14 | +23:00:23 | 1 | 0.939 | 0.011 | 11.98 | 0.022 | 6.48 | 1.028 | 0.017 | 9.669 | 0.014 | Kamai | 125.864 | 7.649 | R16 | EARLY-K* |
| "Cl* Melotte 22 PELS 005" | 03:34:02 | +24:52:51 | 1 | 0.718 | 0.019 | 10.869 | 0.023 | 5.136 | 0.768 | 0.019 | 9.178 | 0.018 | Kamai | 140.184 | 4.333 | H10 | MID-G* |
| "Cl* Melotte 22 DH 040" | 03:34:55 | +22:04:47 | 1 | 1.39 | 0.017 | 16.169 | 0.016 | 10.437 | 2.4 | 0.018 | 11.566 | 0.02 | Kamai | 140.066 | 0.827 | R16 | EARLY-M* |
| "Cl* Melotte 22 DH 042" | 03:35:09 | +24:14:20 | 1 | 1.534 | 0.033 | 15.28 | 0.025 | 9.648 | 2.135 | 0.022 | 11.029 | 0.02 | Kamai | 133.776 | 1.509 | H10 | EARLY-M* |
| "Cl* Melotte 22 PELS 124" | 03:35:32 | +22:49:25 | 1 | 0.517 | 0.019 | 9.858 | 0.023 | 4.263 | 0.617 | 0.019 | 8.541 | 0.017 | Kamai | 131.518 | 2.795 | R16 | LATE-F* |
| "Cl* Melotte 22 DH 050" | 03:35:56 | +25:22:00 | 1 | 1.505 | 0.014 | 16.252 | 0.013 | 10.622 | 2.493 | 0.016 | 11.524 | 0.021 | Kamai | 133.653 | 0.366 | H10 | EARLY-M* |
| "Cl* Melotte 22 DH 054" | 03:36:16 | +25:08:49 | 2 | 1.565 | 0.016 | 16.348 | 0.018 | 10.403 | 2.647 | 0.02 | 11.306 | 0.023 | Kamai | 154.553 | 0.389 | C16 | MID-M* |
| "Cl* Melotte 22 AK II-293" | 03:36:18 | +21:53:39 | 4 | 0.717 | 0.01 | 10.998 | 0.022 | 5.389 | 0.793 | 0.016 | 9.25 | 0.018 | Kamai | 132.37 | 4.252 | H10 | MID-G* |
| "Cl* Melotte 22 DH 056" | 03:36:24 | +22:37:26 | 1 | 1.358 | 0.03 | 14.137 | 0.018 | 8.457 | 1.764 | 0.022 | 10.563 | 0.026 | Kamai | 136.753 | 11.181 | R16 | LATE-K* |
| "Cl* Melotte 22 PELS 189" | 03:36:30 | +24:00:44 | 1 | 0.989 | 0.013 | 12.262 | 0.011 | 6.511 | 1.065 | 0.018 | 9.903 | 0.02 | Kamai | 141.351 | 7.551 | R16 | MID-K* |
| "Cl* Melotte 22 DH 061" | 03:36:41 | +27:49:57 | 2 | 1.348 | 0.009 | 13.965 | 0.009 | 8.244 | 1.624 | 0.014 | 10.542 | 0.02 | Kamai | 139.349 | 8.484 | H10 | LATE-K* |
| "Cl* Melotte 22 HCG 6" | 03:37:03 | +24:44:36 | 1 | 1.544 | 0.015 | 16.24 | 0.019 | 10.616 | 2.52 | 0.014 | 11.439 | 0.018 | Kamai | 133.315 | 0.208 | C16 | MID-M* |
| "Cl* Melotte 22 PELS 009" | 03:37:12 | +21:28:05 | 1 | 0.998 | 0.013 | 12.392 | 0.013 | 6.727 | 1.097 | 0.019 | 9.946 | 0.018 | Kamai | 135.84 | 7.262 | H10 | MID-K* |
| "Cl* Melotte 22 PELS 003" | 03:37:24 | +22:21:04 | 4 | 0.502 | 0.019 | 9.223 | 0.023 | 3.616 | 0.609 | 0.019 | 7.902 | 0.027 | Kamai | 132.268 | 3.388 | R16 | LATE-F* |
| "2MASS J03373212+2612137" | 03:37:32 | +26:12:14 | 2 | 1.360 | 0.015 | 14.321 | 0.016 | 8.334 | 1.618 | 0.021 | | | OSN | 157.544 | | | LATE-K* |
| "Cl* Melotte 22 DH 075" | 03:37:36 | +26:32:49 | 1 | 1.402 | 0.017 | 15.068 | 0.02 | 9.39 | 2.076 | 0.018 | 10.842 | 0.02 | Kamai | 136.645 | 0.325 | H10 | EARLY-M* |
| "Cl* Melotte 22 DH 082" | 03:38:09 | +21:14:49 | 1 | 1.472 | 0.011 | 14.995 | 0.014 | 9.362 | 2.021 | 0.016 | 10.926 | 0.017 | Kamai | 133.839 | 1.726 | H10 | EARLY-M* |
| "Cl* Melotte 22 DH 083" | 03:38:09 | +27:35:10 | 2 | 1.357 | 0.01 | 14.028 | 0.012 | 8.171 | 1.694 | 0.016 | 10.466 | 0.018 | Kamai | 148.379 | 7.826 | H10 | LATE-K* |
| "Cl* Melotte 22 HHJ 418" | 03:38:23 | +23:06:29 | 1 | 1.48 | 0.033 | 15.246 | 0.024 | 9.627 | 2.132 | 0.021 | 11.036 | 0.019 | Kamai | 132.986 | 3.748 | R16 | EARLY-M* |
| "Cl* Melotte 22 PELS 015" | 03:38:23 | +22:29:59 | 1 | 0.542 | 0.019 | 10.065 | 0.023 | 4.375 | 0.645 | 0.019 | 8.696 | 0.018 | Kamai | 137.423 | 2.112 | R16 | LATE-F* |
| "Cl* Melotte 22 HCG 12" | 03:38:49 | +25:11:20 | 1 | 1.42 | 0.016 | 14.164 | 0.013 | 8.471 | 1.914 | 0.02 | 10.231 | 0.023 | Kamai | 137.574 | 0.439 | H10 | EARLY-M* |
| "Cl* Melotte 22 HCG 13" | 03:38:53 | +25:14:11 | 1 | 1.372 | 0.01 | 14.152 | 0.009 | 8.602 | 1.722 | 0.014 | 10.614 | 0.018 | Kamai | 128.833 | 6.775 | H10 | LATE-K* |
| "Cl* Melotte 22 PELS 020" | 03:38:57 | +24:34:11 | 1 | 0.618 | 0.019 | 10.51 | 0.023 | 4.793 | 0.716 | 0.019 | 9.041 | 0.02 | Kamai | 139.11 | 2.986 | H10 | LATE-F* |
| "Cl* Melotte 22 HCG 16" | 03:39:08 | +24:46:15 | 2 | 1.591 | 0.018 | 16.32 | 0.02 | 11.153 | 2.747 | 0.023 | 11.239 | 0.021 | Kamai | 108.002 | 0.725 | H10 | MID-M* |
| "Cl* Melotte 22 PELS 018" | 03:39:13 | +24:27:59 | 2 | 0.601 | 0.019 | 10.34 | 0.023 | 4.583 | 0.702 | 0.019 | 8.905 | 0.022 | Kamai | 141.702 | 2.647 | H10 | LATE-F* |
| "Cl* Melotte 22 PELS 011" | 03:39:28 | +23:53:42 | 1 | 0.858 | 0.01 | 11.56 | 0.022 | 5.881 | 0.94 | 0.016 | 9.475 | 0.02 | Kamai | 136.737 | 5.674 | H10 | EARLY-K* |
| "Cl* Melotte 22 HHJ 359" | 03:39:29 | +25:34:56 | 2 | 1.566 | 0.012 | 16.676 | 0.021 | 11.218 | 2.588 | 0.019 | 11.735 | 0.02 | Kamai | 123.506 | 1.188 | H10 | MID-M* |
| "Cl* Melotte 22 HHJ 324" | 03:39:46 | +23:58:53 | 1 | 1.61 | 0.019 | 16.849 | 0.02 | 11.2 | 2.655 | 0.019 | 11.83 | 0.022 | Kamai | 134.856 | 1.138 | R16 | MID-M* |
| "Cl* Melotte 22 HHJ 291" | 03:39:48 | +23:50:57 | 1 | 1.654 | 0.022 | 17.231 | 0.02 | 11.67 | 2.935 | 0.02 | 11.834 | 0.019 | Kamai | 129.485 | 0.385 | R16 | MID-M* |
| "Cl* Melotte 22 PELS 025" | 03:40:03 | +27:44:26 | 2 | 0.5 | 0.019 | 9.573 | 0.023 | 3.86 | 0.552 | 0.019 | 8.373 | 0.027 | Kamai | 138.837 | 0.766 | H10 | MID-F* |
| "Cl* Melotte 22 PELS 138" | 03:40:06 | +26:11:47 | 1 | 0.816 | 0.01 | 11.224 | 0.022 | 5.689 | 0.873 | 0.016 | 9.264 | 0.019 | Kamai | 127.959 | 6.531 | H10 | LATE-G* |

(Continued).

| *Name* | $\alpha_{J2000}$ (h:m:s) | $\delta_{J2000}$ ($\circ$:':'') | *Notes memb.* | $B-V$ (mag) | e$B-V$ (mag) | $V$ (mag) | e$V$ (mag) | $M_v$ (mag) | $V-Ic$ (mag) | e$V-Ic$ (mag) | $Ks$ (mag) | e$Ks$ (mag) | *Notes phot.BVI* | $D_{BJ.Gaia}$ (pc) | *Period* (days) | *Notes period* | *Spect. Types* |
|---|---|---|---|---|---|---|---|---|---|---|---|---|---|---|---|---|---|
| "Cl* Melotte 22 PELS 022" | 03:40:12 | +25:38:32 | 1 | 0.932 | 0.011 | 12.099 | 0.022 | 6.384 | 1.084 | 0.017 | 9.579 | 0.019 | Kamai | 139.01 | 3.602 | H10 | EARLY-K* |
| "Cl* Melotte 22 SK785" | 03:40:15 | +25:19:19 | 1 | 1.53 | 0.018 | 16.135 | 0.017 | 10.499 | 2.393 | 0.014 | 11.507 | 0.018 | Kamai | 134.052 | 7.826 | H10 | M3 |
| "Cl* Melotte 22 AK III-679" | 03:40:22 | +26:04:19 | 4 | 1.003 | 0.011 | 12.154 | 0.022 | 5.381 | 1.177 | 0.017 | 9.516 | 0.021 | Kamai | 226.205 | 7.826 | H10 | MID-K* |
| "Cl* Melotte 22 HCG 33" | 03:40:23 | +25:29:48 | 1 | 1.684 | 0.026 | 17.018 | 0.017 | 11.307 | 2.858 | 0.019 | 11.664 | 0.021 | Kamai | 138.727 | 0.926 | H10 | M3 |
| "Cl* Melotte 22 HCG 34" | 03:40:24 | +24:35:04 | 1 | 1.507 | 0.017 | 16.3 | 0.016 | 10.633 | 2.44 | 0.018 | 11.607 | 0.019 | Kamai | 135.929 | 4.418 | H10 | EARLY-M* |
| "Cl* Melotte 22 SK787" | 03:40:25 | +22:49:00 | 0 | 1.495 | 0.012 | 14.936 | 0.01 | 9.284 | 2.243 | 0.015 | 10.558 | 0.018 | Kamai |  | 9.814 | H10 | EARLY-M* |
| "Cl* Melotte 22 SK775" | 03:40:30 | +23:33:04 | 4 | 1.378 | 0.015 | 14.344 | 0.02 | 8.303 | 1.654 | 0.017 | 10.816 | 0.017 | Kamai | 161.474 | 9.921 | H10 | LATE-K* |
| "Cl* Melotte 22 PELS 019" | 03:40:31 | +24:29:14 | 1 | 0.876 | 0.01 | 11.716 | 0.022 | 6.023 | 0.963 | 0.016 | 9.556 | 0.021 | Kamai | 137.575 | 6.813 | R16 | EARLY-K* |
| "Cl* Melotte 22 SK773" | 03:40:31 | +23:33:02 | 1 | 1.528 | 0.033 | 15.235 | 0.025 | 9.602 | 2.101 | 0.023 | 11.057 | 0.017 | Kamai | 133.816 | 2.337 | R16 | M1.2 |
| "Cl* Melotte 22 PELS 012" | 03:40:34 | +23:40:57 | 1 | 0.742 | 0.019 | 10.901 | 0.023 | 5.263 | 0.802 | 0.019 | 9.148 | 0.017 | Kamai | 134.138 | 4.549 | R16 | LATE-G* |
| "Cl* Melotte 22 DH 146" | 03:40:35 | +20:57:57 | 1 | 1.592 | 0.015 | 15.985 | 0.018 | 10.366 | 2.392 | 0.02 | 11.295 | 0.022 | Kamai | 132.971 | 0.534 | R16 | MID-M* |
| "Cl* Melotte 22 AK III-700" | 03:40:36 | +26:09:05 | 2 | 0.714 | 0.01 | 11.14 | 0.022 | 5.221 | 0.781 | 0.016 | 9.395 | 0.022 | Kamai | 152.651 | 4.126 | H10 | MID-G* |
| "Cl* Melotte 22 HCG 39" | 03:40:43 | +25:42:20 | 1 | 1.066 | 0.012 | 12.857 | 0.011 | 7.208 | 1.239 | 0.018 | 10.134 | 0.022 | Kamai | 134.84 | 6.462 | H10 | MID-K* |
| "Cl* Melotte 22 DH 154" | 03:40:50 | +23:25:06 | 1 | 0.696 | 0.019 | 10.799 | 0.023 | 5.155 | 0.776 | 0.019 | 9.123 | 0.018 | Kamai | 134.548 | 4.395 | R16 | EARLY-G* |
| "Cl* Melotte 22 DH 156" | 03:40:51 | +23:35:54 | 1 | 1.09 | 0.012 | 12.786 | 0.013 | 7.152 | 1.22 | 0.019 | 10.083 | 0.019 | Kamai | 133.922 | 8.325 | R16 | MID-K* |
| "Cl* Melotte 22 HCG 44" | 03:40:55 | +22:20:59 | 1 | 1.571 | 0.014 | 16.281 | 0.02 | 10.588 | 2.511 | 0.014 | 11.441 | 0.021 | Kamai | 137.624 | 1.326 | H10 | MID-M* |
| "Cl* Melotte 22 DH 166" | 03:41:14 | +23:23:06 | 3 | 1.359 | 0.012 | 14.045 | 0.016 | 8.347 | 1.638 | 0.017 | 10.631 | 0.018 | Kamai | 137.906 | 10.023 | R16 | LATE-K* |
| "Cl* Melotte 22 SK729" | 03:41:27 | +24:01:03 | 1 | 1.735 | 0.028 | 17.012 | 0.018 | 11.352 | 2.94 | 0.016 | 11.466 | 0.023 | Kamai | 135.49 | 0.359 | R16 | MID-M* |
| "Cl* Melotte 22 DH 176" | 03:41:28 | +23:42:30 | 2 | 0.791 | 0.01 | 11.178 | 0.022 | 5.53 | 0.839 | 0.016 | 9.313 | 0.018 | Kamai | 134.754 | 5.468 | R16 | LATE-G* |
| "Cl* Melotte 22 PELS 023" | 03:41:36 | +25:37:10 | 1 | 0.557 | 0.019 | 10.064 | 0.023 | 4.357 | 0.691 | 0.019 | 8.593 | 0.023 | Kamai | 138.493 | 1.637 | H10 | LATE-F* |
| "Cl* Melotte 22 SK724" | 03:41:40 | +23:45:47 | 1 | 1.442 | 0.015 | 14.583 | 0.02 | 8.979 | 1.813 | 0.017 | 10.87 | 0.022 | Kamai | 132.08 | 11.006 | R16 | M0 |
| "Cl* Melotte 22 HCG 57" | 03:41:47 | +22:51:25 | 1 | 1.457 | 0.016 | 14.625 | 0.02 | 8.969 | 1.819 | 0.017 | 10.852 | 0.019 | Kamai | 135.241 | 12.104 | H10 | EARLY-M* |
| "Cl* Melotte 22 DH 193" | 03:41:54 | +23:27:29 | 1 | 1.391 | 0.015 | 13.999 | 0.013 | 8.435 | 1.765 | 0.019 | 10.249 | 0.036 | Kamai | 129.641 | 7.15 | R16 | LATE-K* |
| "Cl* Melotte 22 SK709" | 03:41:59 | +23:42:26 | 1 | 1.423 | 0.014 | 14.725 | 0.018 | 9.063 | 1.933 | 0.018 | 10.843 | 0.021 | Kamai | 135.62 | 7.783 | R16 | M0.2 |
| "Cl* Melotte 22 SK701" | 03:42:03 | +24:32:13 | 1 | 1.537 | 0.019 | 16.396 | 0.016 | 10.699 | 2.473 | 0.018 | 11.632 | 0.021 | Kamai | 137.826 | 2.258 | R16 | EARLY-M* |
| "Cl* Melotte 22 HCG 63" | 03:42:03 | +24:12:36 | 1 | 1.453 | 0.017 | 16.404 | 0.016 | 10.74 | 2.478 | 0.018 | 11.606 | 0.021 | Kamai | 135.755 | 0.7 | R16 | M2.7 |
| "Cl* Melotte 22 PELS 028" | 03:42:04 | +22:25:37 | 1 | 0.985 | 0.015 | 11.718 | 0.019 | 5.964 | 1.148 | 0.019 | 9.159 | 0.018 | Kamai | 141.491 | 6.093 | H10 | MID-K* |
| "Cl* Melotte 22 HCG 61" | 03:42:05 | +25:53:09 | 1 | 1.129 | 0.012 | 12.849 | 0.017 | 7.181 | 1.272 | 0.016 | 10.093 | 0.021 | Kamai | 136.034 | 2.9 | H10 | MID-K* |
| "Cl* Melotte 22 SK698" | 03:42:05 | +25:39:48 | 1 | 1.572 | 0.021 | 15.737 | 0.021 | 10.077 | 2.451 | 0.018 | 10.896 | 0.023 | Kamai | 135.546 | 0.363 | H10 | MID-M* |
| "Cl* Melotte 22 SK699" | 03:42:09 | +23:35:17 | 1 | 1.547 | 0.015 | 15.796 | 0.018 | 10.125 | 2.301 | 0.019 | 11.313 | 0.022 | Kamai | 136.209 | 3.013 | R16 | M2.2 |
| "Cl* Melotte 22 PELS 029" | 03:42:24 | +22:25:16 | 1 | 0.623 | 0.016 | 10.345 | 0.019 | 4.655 | 0.745 | 0.018 | 8.758 | 0.018 | Kamai | 137.425 | 1.586 | H10 | EARLY-G* |
| "Cl* Melotte 22 PELS 035" | 03:42:24 | +21:28:25 | 1 | 0.53 | 0.019 | 9.841 | 0.023 | 4.287 | 0.628 | 0.019 | 8.526 | 0.019 | Kamai | 129.066 | 2.379 | R16 | LATE-F* |
| "Cl* Melotte 22 DH 225" | 03:42:28 | +25:02:49 | 1 | 1.062 | 0.012 | 12.723 | 0.012 | 7.03 | 1.183 | 0.018 | 10.065 | 0.022 | Kamai | 137.622 | 8.406 | H10 | MID-K* |
| "Cl* Melotte 22 SK671" | 03:42:42 | +24:11:58 | 1 | 1.433 | 0.014 | 14.5 | 0.014 | 8.683 | 1.922 | 0.016 | 10.532 | 0.023 | Kamai | 145.666 | 4.823 | R16 | M0 |
| "Cl* Melotte 22 HCG 85" | 03:42:42 | +23:30:10 | 2 | 1.002 | 0.012 | 12.353 | 0.019 | 6.954 | 1.186 | 0.018 | 9.683 | 0.031 | Kamai | 120.153 | 0.338 | H10 | MID-K* |
| "Cl* Melotte 22 HCG 86" | 03:42:42 | +23:20:22 | 1 | 1.668 | 0.019 | 16.765 | 0.017 | 11.137 | 2.942 | 0.017 | 11.388 | 0.022 | Kamai | 133.565 | 0.269 | R16 | MID-M* |
| "Cl* Melotte 22 SK663" | 03:42:49 | +24:10:16 | 1 | 1.606 | 0.015 | 16.953 | 0.021 | 11.38 | 2.73 | 0.019 | 11.74 | 0.022 | Kamai | 130.197 | 1.459 | R16 | M3.2 |
| "Cl* Melotte 22 HCG 93" | 03:42:57 | +24:04:58 | 2 | 1.559 | 0.018 | 16.238 | 0.02 | 10.773 | 2.694 | 0.023 | 11.228 | 0.022 | Kamai | 123.879 | 0.817 | R16 | M3.5 |
| "Cl* Melotte 22 PELS 030" | 03:42:59 | +22:54:03 | 1 | 0.946 | 0.011 | 12.101 | 0.022 | 6.526 | 1.055 | 0.017 | 9.713 | 0.019 | Kamai | 130.313 | 6.7 | R16 | EARLY-K* |
| "Cl* Melotte 22 DH 249" | 03:43:00 | +22:25:27 | 1 | 1.371 | 0.0090 | 13.984 | 0.0090 | 8.338 | 1.646 | 0.014 | 10.587 | 0.019 | Kamai | 134.671 | 6.536 | R16 | LATE-K* |
| "Cl* Melotte 22 HCG 101" | 03:43:04 | +22:48:04 | 4 | 1.56 | 0.02 | 15.16 | 0.01 | 9.385 | 2.2 | 0.03 | 10.785 | 0.016 | Stauffer07/82 | 142.867 | 0.31 | R16 | EARLY-M* |

(Continued).

| *Name* | $\alpha_{J2000}$ (h:m:s) | $\delta_{J2000}$ (o:′:″) | *Notes memb.* | $B-V$ (mag) | e$B-V$ (mag) | $V$ (mag) | e$V$ (mag) | $M_v$ (mag) | $V-Ic$ (mag) | e$V-Ic$ (mag) | $Ks$ (mag) | e$Ks$ (mag) | *Notes phot.BVI* | $D_{BJ.Gaia}$ (pc) | *Period* (days) | *Notes period* | *Spect. Types* |
|---|---|---|---|---|---|---|---|---|---|---|---|---|---|---|---|---|---|
| "Cl* Melotte 22 HCG 97" | 03:43:06 | +24:49:29 | 3 | 1.523 | 0.015 | 15.609 | 0.016 | 9.909 | 2.539 | 0.015 | 10.789 | 0.021 | Kamai | 138.067 | 0.28 | C16 | EARLY-M* |
| "Cl* Melotte 22 HCG 100" | 03:43:10 | +24:41:33 | 1 | 1.6 | 0.03 | 16.37 | 0.02 | 10.778 | 2.64 | 0.03 | 11.42 | 0.022 | Stauffer07/82 | 131.353 | 2.026 | R16 | MID-M* |
| "Cl* Melotte 22 HCG 102" | 03:43:12 | +24:44:45 | 1 | 1.638 | 0.024 | 17.093 | 0.018 | 11.445 | 2.891 | 0.023 | 11.687 | 0.022 | Kamai | 134.744 | 0.707 | R16 | MID-M* |
| "Cl* Melotte 22 HCG 103" | 03:43:13 | +24:39:19 | 1 | 1.433 | 0.015 | 15.994 | 0.018 | 10.297 | 2.384 | 0.02 | 11.293 | 0.021 | Kamai | 137.865 | 0.256 | R16 | M2.2 |
| "Cl* Melotte 22 DH 257" | 03:43:14 | +25:16:13 | 1 | 0.911 | 0.011 | 12.173 | 0.022 | 6.526 | 1.081 | 0.017 | 9.665 | 0.022 | Kamai | 134.684 | 1.185 | H10 | EARLY-K* |
| "Cl* Melotte 22 PELS 031" | 03:43:19 | +22:26:57 | 0 | 0.953 | 0.019 | 11.49 | 0.023 | 5.838 | 1.094 | 0.019 | 9.026 | 0.02 | Kamai | | 5.024 | R16 | EARLY-K* |
| "Cl Melotte 22 102" | 03:43:25 | +23:13:33 | 1 | 0.71 | 0.01 | 10.52 | 0.01 | 4.809 | 0.84 | 0.01 | 8.646 | 0.017 | Stauffer07/87 | 138.77 | 2.757 | R16 | G1V |
| "Cl* Melotte 22 PELS 056" | 03:43:27 | +25:23:15 | 1 | 0.808 | 0.01 | 11.364 | 0.022 | 5.669 | 0.945 | 0.016 | 9.218 | 0.023 | Kamai | 137.716 | 0.669 | H10 | EARLY-K* |
| "Cl* Melotte 22 SK638" | 03:43:27 | +24:27:10 | 2 | 1.577 | 0.016 | 16.581 | 0.017 | 10.516 | 2.731 | 0.017 | 11.419 | 0.021 | Kamai | 163.336 | 2.162 | R16 | M3.5 |
| "Cl* Melotte 22 PELS 037" | 03:43:31 | +22:09:30 | 1 | 0.654 | 0.019 | 10.406 | 0.023 | 4.755 | 0.801 | 0.019 | 8.777 | 0.021 | Kamai | 134.959 | 2.48 | H10 | EARLY-G* |
| "Cl Melotte 22 120" | 03:43:32 | +23:40:27 | 1 | 0.7 | 0.01 | 10.84 | 0.01 | 5.177 | 0.78 | 0.01 | 9.129 | 0.038 | Stauffer07/87 | 135.718 | 3.991 | R16 | MID-G* |
| "Cl Melotte 22 134" | 03:43:37 | +24:13:56 | 1 | 1.47 | 0.01 | 14.37 | 0.01 | 8.575 | 2.1 | 0.01 | 10.232 | 0.025 | Stauffer07/87 | 144.183 | 0.349 | R16 | EARLY-M* |
| "Cl Melotte 22 152" | 03:43:38 | +23:32:10 | 1 | 0.69 | 0.01 | 10.73 | 0.01 | 5.062 | 0.73 | 0.01 | 9.105 | 0.038 | Stauffer07/87 | 136.024 | 3.888 | H10 | EARLY-G* |
| "Cl* Melotte 22 DH 280" | 03:43:38 | +26:36:45 | 1 | 1.332 | 0.012 | 13.916 | 0.017 | 8.15 | 1.581 | 0.015 | 10.614 | 0.026 | Kamai | 142.317 | 9.506 | H10 | LATE-K* |
| "Cl* Melotte 22 HCG 123" | 03:43:42 | +24:34:23 | 2 | 1.57 | 0.03 | 15.43 | 0.01 | 10.32 | 2.31 | 0.02 | 10.955 | 0.022 | Stauffer07/82 | 105.196 | 1.934 | R16 | EARLY-M* |
| "Cl* Melotte 22 HHJ 374" | 03:43:44 | +24:29:16 | 4 | 1.59 | 0.018 | 16.217 | 0.017 | 10.583 | 2.414 | 0.014 | 11.497 | 0.022 | Kamai | 133.892 | 4.005 | R16 | EARLY-M* |
| "Cl* Melotte 22 SK618" | 03:43:45 | +23:03:21 | 1 | 1.698 | 0.014 | 16.79 | 0.021 | 11.081 | 2.609 | 0.019 | 11.731 | 0.021 | Kamai | 138.581 | 2.323 | R16 | MID-M* |
| "Cl* Melotte 22 PELS 043" | 03:43:49 | +25:43:47 | 1 | 0.912 | 0.013 | 11.963 | 0.011 | 6.366 | 1.018 | 0.018 | 9.719 | 0.018 | Kamai | 131.652 | 6.326 | H10 | EARLY-K* |
| "Cl Melotte 22 193" | 03:43:51 | +24:14:51 | 1 | 0.79 | 0.01 | 11.3 | 0.01 | 5.719 | 0.86 | 0.01 | 9.335 | 0.036 | Stauffer07/87 | 130.683 | 5.364 | R16 | LATE-G* |
| "Cl* Melotte 22 HCG 126" | 03:43:54 | +25:28:30 | 1 | 1.64 | 0.02 | 16.15 | 0.01 | 10.483 | 2.44 | 0.04 | 11.467 | 0.024 | Stauffer07/82 | 135.934 | 0.352 | C16 | MID-M* |
| "Cl Melotte 22 212" | 03:43:56 | +24:25:35 | 1 | 1.366 | 0.014 | 14.339 | 0.018 | 8.736 | 1.8 | 0.015 | 10.645 | 0.023 | Kamai | 131.99 | 4.486 | R16 | K7 |
| "Cl* Melotte 22 HCG 129" | 03:43:57 | +24:59:37 | 1 | 1.436 | 0.017 | 16.147 | 0.017 | 10.506 | 2.383 | 0.014 | 11.511 | 0.02 | Kamai | 134.333 | 3.964 | H10 | EARLY-M* |
| "Cl Melotte 22 248" | 03:44:01 | +23:32:38 | 1 | 0.77 | 0.01 | 11.02 | 0.01 | 5.322 | 0.85 | 0.01 | 9.173 | 0.04 | Stauffer07/87 | 137.929 | 4.02 | R16 | LATE-G* |
| "Cl* Melotte 22 DH 305" | 03:44:01 | +21:16:56 | 1 | 1.068 | 0.013 | 12.979 | 0.012 | 7.342 | 1.301 | 0.019 | 10.047 | 0.019 | Kamai | 134.084 | 0.497 | H10 | MID-K* |
| "Cl* Melotte 22 HCG 131" | 03:44:03 | +25:39:23 | 1 | 1.15 | 0.013 | 13.145 | 0.012 | 7.454 | 1.382 | 0.019 | 10.014 | 0.02 | Kamai | 137.481 | 0.211 | H10 | MID-K* |
| "Cl* Melotte 22 HCG 132" | 03:44:04 | +25:51:23 | 1 | 1.102 | 0.013 | 12.847 | 0.011 | 7.138 | 1.288 | 0.018 | 9.845 | 0.02 | Kamai | 138.604 | 0.537 | H10 | MID-K* |
| "Cl Melotte 22 263" | 03:44:05 | +24:16:32 | 1 | 0.88 | 0.01 | 11.63 | 0.01 | 5.969 | 0.96 | 0.01 | 9.438 | 0.031 | Stauffer07/87 | 135.584 | 4.676 | R16 | EARLY-K* |
| "Cl* Melotte 22 PELS 059" | 03:44:05 | +25:29:02 | 1 | 1.031 | 0.013 | 12.554 | 0.011 | 6.912 | 1.147 | 0.018 | 10.007 | 0.02 | Kamai | 134.381 | 6.93 | H10 | MID-K* |
| "Cl* Melotte 22 HCG 140" | 03:44:10 | +24:16:04 | 1 | 1.557 | 0.015 | 16.358 | 0.014 | 10.703 | 2.513 | 0.016 | 11.53 | 0.022 | Kamai | 135.232 | 1.235 | R16 | MID-M* |
| "Cl* Melotte 22 DH 318" | 03:44:12 | +19:18:19 | 2 | 1.561 | 0.028 | 15.099 | 0.023 | 9.268 | 2.001 | 0.021 | 11.048 | 0.016 | Kamai | 146.604 | 7.489 | R16 | EARLY-M* |
| "Cl Melotte 22 293" | 03:44:14 | +24:46:46 | 1 | 0.7 | 0.01 | 10.79 | 0.01 | 5.121 | 0.77 | 0.01 | 9.089 | 0.023 | Stauffer07/87 | 136.065 | 4.025 | R16 | EARLY-G* |
| "Cl* Melotte 22 PELS 046" | 03:44:15 | +26:19:52 | 2 | 0.767 | 0.01 | 11.083 | 0.022 | 5.38 | 0.813 | 0.016 | 9.269 | 0.022 | Kamai | 138.251 | 4.765 | H10 | LATE-G* |
| "Cl* Melotte 22 HCG 145" | 03:44:18 | +24:26:47 | 1 | 1.51 | 0.021 | 16.59 | 0.018 | 10.921 | 2.568 | 0.023 | 11.686 | 0.022 | Kamai | 136.069 | 0.275 | R16 | MID-M* |
| "Cl Melotte 22 324" | 03:44:22 | +24:46:06 | 1 | 1.07 | 0.01 | 13.01 | 0.01 | 7.347 | 1.31 | 0.01 | 10.062 | 0.061 | Stauffer07/87 | 135.677 | 0.411 | R16 | MID-K* |
| "Cl* Melotte 22 HCG 149" | 03:44:25 | +24:46:06 | 1 | 1.55 | 0.02 | 15.42 | 0.01 | 9.795 | 2.19 | 0.02 | 11.011 | 0.021 | Stauffer07/82 | 133.352 | 0.764 | R16 | M1.5 |
| "Cl Melotte 22 345" | 03:44:26 | +24:35:23 | 1 | 0.827 | 0.01 | 11.461 | 0.022 | 5.817 | 0.941 | 0.016 | 9.274 | 0.029 | Kamai | 134.497 | 0.837 | R16 | G8 |
| "Cl* Melotte 22 HCG 150" | 03:44:26 | +24:40:53 | 1 | 1.51 | 0.04 | 16.66 | 0.02 | 11.148 | 2.65 | 0.05 | 11.651 | 0.021 | Stauffer07/82 | 126.593 | 1.08 | R16 | MID-M* |
| "Cl* Melotte 22 HCG 156" | 03:44:27 | +24:24:32 | 1 | 1.501 | 0.024 | 16.068 | 0.021 | 10.376 | 2.376 | 0.016 | 11.45 | 0.021 | Kamai | 137.552 | 5.88 | R16 | EARLY-M* |

(Continued).

| *Name* | $\alpha_{J2000}$ (h:m:s) | $\delta_{J2000}$ (°:′:″) | *Notes memb.* | $B-V$ (mag) | e$B-V$ (mag) | $V$ (mag) | e$V$ (mag) | $M_v$ (mag) | $V-Ic$ (mag) | e$V-Ic$ (mag) | $Ks$ (mag) | e$Ks$ (mag) | *Notes phot.BVI* | $D_{BJ.Gaia}$ (pc) | *Period* (days) | *Notes period* | *Spect. Types* |
|---|---|---|---|---|---|---|---|---|---|---|---|---|---|---|---|---|---|
| "Cl* Melotte 22 DH 343" | 03:44:28 | +19:11:06 | 2 | 0.905 | 0.011 | 11.84 | 0.022 | 6.042 | 1.068 | 0.016 | 9.418 | 0.02 | Kamai | 144.429 | 0.533 | R16 | EARLY-K* |
| "Cl Melotte 22 357" | 03:44:28 | +24:10:18 | 2 | 1.21 | 0.01 | 13.32 | 0.01 | 8.081 | 1.52 | 0.02 | 10.06 | 0.033 | Stauffer07/82 | 111.661 | 3.8 | R16 | LATE-K* |
| "Cl* Melotte 22 HCG 152" | 03:44:30 | +25:35:47 | 1 | 1.522 | 0.036 | 15.12 | 0.025 | 9.359 | 2.048 | 0.023 | 10.973 | 0.023 | Kamai | 141.946 | 1.791 | H10 | EARLY-M* |
| "Cl Melotte 22 370" | 03:44:32 | +23:52:31 | 1 | 1.511 | 0.011 | 14.441 | 0.009 | 8.773 | 2.064 | 0.016 | 10.452 | 0.023 | Kamai | 136.044 | 17.283 | R16 | EARLY-M* |
| "Cl Melotte 22 390" | 03:44:35 | +24:00:05 | 1 | 1.431 | 0.012 | 14.329 | 0.017 | 8.667 | 1.747 | 0.016 | 10.654 | 0.019 | Kamai | 135.622 | 9.057 | R16 | LATE-K* |
| "Cl* Melotte 22 HCG 161" | 03:44:36 | +23:30:11 | 1 | 1.587 | 0.032 | 16.624 | 0.021 | 10.93 | 2.613 | 0.018 | 11.662 | 0.021 | Kamai | 137.646 | 1.66 | R16 | MID-M* |
| "Cl* Melotte 22 HCG 164" | 03:44:38 | +22:55:16 | 1 | 1.578 | 0.018 | 15.746 | 0.019 | 10.003 | 2.367 | 0.02 | 11.036 | 0.02 | Kamai | 140.82 | 0.315 | R16 | EARLY-M* |
| "Cl* Melotte 22 PELS 034" | 03:44:42 | +22:27:52 | 1 | 0.716 | 0.016 | 10.757 | 0.019 | 5.14 | 0.803 | 0.018 | 9.072 | 0.02 | Kamai | 132.854 | 3.991 | R16 | MID-G* |
| "Cl* Melotte 22 PELS 044" | 03:44:43 | +25:52:32 | 1 | 0.877 | 0.01 | 11.684 | 0.022 | 6.072 | 0.971 | 0.016 | 9.52 | 0.02 | Kamai | 132.554 | 6.626 | H10 | EARLY-K* |
| "Cl* Melotte 22 PELS 041" | 03:44:44 | +25:29:57 | 1 | 0.975 | 0.013 | 12.206 | 0.011 | 6.492 | 1.062 | 0.018 | 9.74 | 0.018 | Kamai | 138.914 | 6.775 | H10 | EARLY-K* |
| "Cl Melotte 22 430" | 03:44:44 | +24:13:52 | 1 | 0.81 | 0.01 | 11.39 | 0.01 | 5.744 | 0.86 | 0.02 | 9.497 | 0.051 | Stauffer07/82 | 134.672 | 5.519 | H10 | G8 |
| "Cl* Melotte 22 DH 356" | 03:44:48 | +26:36:03 | 2 | 1.354 | 0.015 | 14.422 | 0.02 | 8.516 | 1.691 | 0.017 | 10.828 | 0.02 | Kamai | 151.775 | 7.148 | H10 | LATE-K* |
| "Cl* Melotte 22 PELS 137" | 03:44:53 | +26:08:31 | 1 | 1.032 | 0.013 | 12.436 | 0.011 | 6.9 | 1.145 | 0.018 | 9.929 | 0.018 | Kamai | 127.975 | 8.646 | H10 | MID-K* |
| "Cl* Melotte 22 PELS 135" | 03:45:02 | +19:33:34 | 1 | 0.463 | 0.019 | 9.449 | 0.023 | 3.759 | 0.617 | 0.019 | 8.152 | 0.021 | Kamai | 137.427 | 0.937 | R16 | LATE-F* |
| "Cl Melotte 22 514" | 03:45:04 | +25:15:28 | 1 | 0.7 | 0.01 | 10.73 | 0.01 | 5.073 | 0.76 | 0.01 | 9.041 | 0.018 | Stauffer07/87 | 135.313 | 3.79 | H10 | EARLY-G* |
| "Cl* Melotte 22 SK534" | 03:45:05 | +25:29:11 | 1 | 1.553 | 0.015 | 16.152 | 0.015 | 10.472 | 2.401 | 0.016 | 11.484 | 0.018 | Kamai | 136.784 | 3.174 | H10 | EARLY-M* |
| "Cl* Melotte 22 PELS 045" | 03:45:08 | +26:17:33 | 1 | 0.813 | 0.01 | 11.491 | 0.022 | 5.799 | 0.888 | 0.016 | 9.443 | 0.018 | Kamai | 137.525 | 5.263 | H10 | LATE-G* |
| "Cl* Melotte 22 PELS 040" | 03:45:10 | +21:42:17 | 1 | 0.549 | 0.019 | 9.987 | 0.023 | 4.463 | 0.658 | 0.019 | 8.586 | 0.02 | Kamai | 127.278 | 2.932 | R16 | LATE-F* |
| "Cl Melotte 22 554" | 03:45:12 | +24:35:10 | 1 | 1.32 | 0.01 | 13.925 | 0.012 | 8.33 | 1.61 | 0.016 | 10.556 | 0.021 | Kamai | 131.533 | 4.389 | R16 | K5V |
| "Cl* Melotte 22 PELS 047" | 03:45:14 | +26:35:18 | 1 | 0.921 | 0.013 | 12.053 | 0.011 | 6.288 | 1.001 | 0.018 | 9.805 | 0.02 | Kamai | 142.232 | 6.438 | H10 | EARLY-K* |
| "Cl Melotte 22 566" | 03:45:14 | +25:05:20 | 2 | 1.389 | 0.01 | 14.427 | 0.014 | 8.568 | 1.711 | 0.016 | 10.782 | 0.018 | Kamai | 148.526 | 0.527 | H10 | K4V |
| "Cl* Melotte 22 HCG 183" | 03:45:16 | +24:07:16 | 1 | 1.557 | 0.021 | 16.239 | 0.016 | 10.659 | 2.416 | 0.018 | 11.627 | 0.025 | Kamai | 130.608 | 2.185 | R16 | MID-M* |
| "Cl* Melotte 22 HCG 181" | 03:45:17 | +24:34:33 | 1 | 1.57 | 0.03 | 16.18 | 0.01 | 10.641 | 2.48 | 0.03 | 11.43 | 0.021 | Stauffer07/82 | 128.202 | 0.854 | R16 | MID-M* |
| "Cl* Melotte 22 HCG 178" | 03:45:17 | +25:15:48 | 1 | 1.65 | 0.04 | 16.2 | 0.02 | 10.481 | 2.68 | 0.04 | 11.179 | 0.02 | Stauffer07/82 | 139.247 | 0.688 | H10 | MID-M* |
| "Cl Melotte 22 624" | 03:45:23 | +24:51:03 | 1 | 1.472 | 0.016 | 15.349 | 0.018 | 9.647 | 2.186 | 0.015 | 11.037 | 0.021 | Kamai | 138.194 | 1.248 | R16 | M2 |
| "Cl Melotte 22 659" | 03:45:26 | +23:25:49 | 3 | 0.983 | 0.008 | 12.231 | 0.013 | 6.107 | 1.188 | 0.011 | 9.526 | 0.049 | Kamai | 167.842 | 2.804 | R16 | MID-K* |
| "Cl Melotte 22 673" | 03:45:30 | +24:18:46 | 1 | 1.463 | 0.025 | 15.691 | 0.019 | 10.035 | 2.309 | 0.016 | 11.129 | 0.021 | Kamai | 135.247 | 2.193 | R16 | EARLY-M* |
| "Cl Melotte 22 676" | 03:45:30 | +23:45:38 | 1 | 1.226 | 0.031 | 13.385 | 0.022 | 7.698 | 1.494 | 0.026 | 10.341 | 0.038 | Kamai | 137.227 | 7.092 | H10 | MID-K* |
| "Cl* Melotte 22 HCG 194" | 03:45:37 | +24:39:07 | 1 | 1.594 | 0.02 | 16.725 | 0.019 | 11.0 | 2.845 | 0.02 | 11.354 | 0.022 | Kamai | 139.643 | 0.333 | R16 | MID-M* |
| "Cl* Melotte 22 SK490" | 03:46:04 | +25:27:11 | 4 | 1.408 | 0.015 | 14.552 | 0.02 | 8.874 | 1.805 | 0.017 | 10.77 | 0.019 | Kamai | 136.625 | 4.344 | H10 | LATE-K* |
| "Cl* Melotte 22 HCG 214" | 03:46:05 | +22:58:54 | 1 | 1.406 | 0.009 | 14.001 | 0.009 | 8.402 | 1.682 | 0.014 | 10.5 | 0.018 | Kamai | 131.792 | 9.893 | R16 | LATE-K* |
| "Cl* Melotte 22 SK488" | 03:46:06 | +24:36:44 | 1 | 1.535 | 0.013 | 16.145 | 0.016 | 10.498 | 2.461 | 0.015 | 11.442 | 0.023 | Kamai | 134.74 | 1.13 | R16 | M2.7 |
| "Cl* Melotte 22 HHJ 435" | 03:46:07 | +23:50:20 | 1 | 1.681 | 0.02 | 15.613 | 0.015 | 9.891 | 2.245 | 0.017 | 10.919 | 0.02 | Kamai | 139.468 | 3.56 | H10 | MID-M* |
| "Cl* Melotte 22 DH 423" | 03:46:09 | +26:08:20 | 1 | 1.042 | 0.011 | 11.865 | 0.022 | 6.197 | 1.143 | 0.016 | 9.301 | 0.021 | Kamai | 135.992 | 8.069 | H10 | MID-K* |
| "Cl* Melotte 22 HHJ 367" | 03:46:18 | +24:41:10 | 1 | 1.567 | 0.021 | 16.509 | 0.018 | 10.865 | 2.505 | 0.023 | 11.688 | 0.021 | Kamai | 134.524 | 5.517 | R16 | MID-M* |
| "Cl* Melotte 22 PELS 050" | 03:46:19 | +20:52:47 | 1 | 0.84 | 0.012 | 11.562 | 0.018 | 5.882 | 0.928 | 0.016 | 9.519 | 0.018 | Kamai | 136.749 | 5.934 | R16 | EARLY-K* |
| "Cl* Melotte 22 SK474" | 03:46:19 | +26:02:36 | 1 | 1.462 | 0.025 | 14.82 | 0.023 | 9.199 | 1.917 | 0.021 | 10.968 | 0.017 | Kamai | 133.123 | 8.988 | H10 | M0.2 |

(Continued).

| *Name* | $\alpha_{J2000}$ (h:m:s) | $\delta_{J2000}$ (º:′:″) | *Notes memb.* | $B-V$ (mag) | e$B-V$ (mag) | $V$ (mag) | e$V$ (mag) | $M_v$ (mag) | $V-Ic$ (mag) | e$V-Ic$ (mag) | $Ks$ (mag) | e$Ks$ (mag) | *Notes phot.BVI* | $D_{BJ.Gaia}$ (pc) | *Period* (days) | *Notes period* | *Spect. Types* |
|---|---|---|---|---|---|---|---|---|---|---|---|---|---|---|---|---|---|
| "Cl* Melotte 22 HHJ 249" | 03:46:25 | +24:28:47 | 1 | 1.519 | 0.04 | 17.92 | 0.016 | 12.213 | 2.857 | 0.022 | 12.538 | 0.021 | OSN+B+ | 138.458 | 0.891 | R16 | MID-M* |
| "Cl* Melotte 22 DH 446" | 03:46:25 | +21:26:18 | 4 | 1.612 | 0.034 | 17.01 | 0.019 | 5.438 | 2.907 | 0.017 | 11.517 | 0.018 | Kamai | 2062.216 | 1.028 | R16 | MID-M* |
| "Cl Melotte 22 1032" | 03:46:28 | +24:26:02 | 1 | 0.75 | 0.01 | 11.1 | 0.01 | 5.447 | 0.84 | 0.01 | 9.157 | 0.026 | Stauffer07/82 | 135.103 | 1.313 | R16 | LATE-G* |
| "Cl Melotte 22 1095" | 03:46:38 | +24:44:52 | 4 | 0.92 | 0.01 | 11.83 | 0.01 | 6.243 | 0.94 | 0.01 | 9.627 | 0.059 | Stauffer07/87 | 131.03 | 7.18 | R16 | EARLY-K* |
| "Cl* Melotte 22 DH 467" | 03:46:44 | +23:59:43 | 1 | 1.547 | 0.017 | 16.12 | 0.016 | 10.43 | 2.349 | 0.018 | 11.575 | 0.022 | Kamai | 137.433 | 2.234 | R16 | EARLY-M* |
| "Cl* Melotte 22 HCG 236" | 03:46:48 | +24:18:06 | 4 | 1.53 | 0.03 | 16.24 | 0.01 | 9.342 | 2.67 | 0.04 | 11.717 | 0.022 | Stauffer07/82 | 239.657 | 3.697 | C16 | MID-M* |
| "Cl* Melotte 22 HCG 245" | 03:46:49 | +23:04:08 | 1 | 1.527 | 0.015 | 16.155 | 0.016 | 10.419 | 2.466 | 0.017 | 11.423 | 0.021 | Kamai | 140.331 | 0.285 | R16 | EARLY-M* |
| "Cl Melotte 22 1173" | 03:46:49 | +24:36:00 | 1 | 1.53 | 0.03 | 15.1 | 0.01 | 9.424 | 2.05 | 0.03 | 10.996 | 0.022 | Stauffer07/82 | 136.513 | 7.911 | R16 | EARLY-M* |
| "Cl* Melotte 22 HCG 241" | 03:46:54 | +25:14:45 | 1 | 1.65 | 0.03 | 16.19 | 0.01 | 10.457 | 2.43 | 0.03 | 11.489 | 0.022 | Stauffer07/82 | 140.182 | 2.692 | R16 | MID-M* |
| "Cl Melotte 22 1275" | 03:47:01 | +23:29:42 | 1 | 0.83 | 0.01 | 11.45 | 0.01 | 5.822 | 0.87 | 0.02 | 9.56 | 0.036 | Stauffer07/82 | 133.528 | 5.931 | R16 | LATE-G* |
| "Cl* Melotte 22 DH 490" | 03:47:04 | +20:11:45 | 2 | 1.439 | 0.013 | 14.621 | 0.017 | 9.059 | 1.928 | 0.016 | 10.679 | 0.016 | Kamai | 129.548 | 8.944 | H10 | EARLY-M* |
| "Cl Melotte 22 1305" | 03:47:07 | +23:13:35 | 1 | 1.19 | 0.01 | 13.52 | 0.01 | 7.84 | 1.43 | 0.02 | 10.397 | 0.059 | Stauffer07/82 | 136.78 | 0.389 | R16 | MID-K* |
| "Cl Melotte 22 1321" | 03:47:09 | +23:44:32 | 1 | 1.47 | 0.03 | 15.22 | 0.01 | 9.545 | 2.37 | 0.02 | 10.656 | 0.021 | Stauffer07/82 | 136.436 | 0.845 | R16 | EARLY-M* |
| "Cl* Melotte 22 HCG 258" | 03:47:14 | +23:49:53 | 1 | 1.35 | 0.04 | 15.78 | 0.02 | 10.106 | 2.47 | 0.03 | 11.086 | 0.021 | Stauffer07/82 | 136.377 | 0.533 | R16 | EARLY-M* |
| "Cl* Melotte 22 PELS 142" | 03:47:15 | +25:22:19 | 1 | 0.819 | 0.01 | 11.524 | 0.019 | 5.928 | 0.931 | 0.018 | 9.517 | 0.022 | Kamai | 131.572 | 4.145 | H10 | LATE-G* |
| "Cl* Melotte 22 SK432" | 03:47:15 | +25:06:55 | 0 | 1.66 | 0.024 | 16.701 | 0.017 | 11.049 | 2.725 | 0.015 | 11.485 | 0.02 | Kamai | | 1.125 | R16 | MID-M* |
| "Cl* Melotte 22 SK428" | 03:47:21 | +25:05:12 | 1 | 1.622 | 0.042 | 15.699 | 0.025 | 10.012 | 2.3 | 0.022 | 11.136 | 0.018 | Kamai | 137.191 | 3.694 | R16 | EARLY-M* |
| "Cl* Melotte 22 PELS 060" | 03:47:21 | +25:31:33 | 1 | 0.539 | 0.019 | 9.826 | 0.023 | 4.155 | 0.673 | 0.019 | 8.435 | 0.033 | Kamai | 136.192 | 0.844 | H10 | LATE-F* |
| "Cl* Melotte 22 HCG 276" | 03:47:29 | +22:22:36 | 1 | 1.444 | 0.013 | 14.769 | 0.012 | 8.983 | 2.068 | 0.018 | 10.596 | 0.02 | Kamai | 143.638 | 1.286 | H10 | EARLY-M* |
| "Cl* Melotte 22 HCG 273" | 03:47:31 | +24:22:14 | 1 | 1.495 | 0.015 | 15.795 | 0.018 | 10.139 | 2.293 | 0.019 | 11.371 | 0.026 | Kamai | 135.293 | 2.763 | R16 | EARLY-M* |
| "Cl* Melotte 22 HCG 277" | 03:47:33 | +23:41:33 | 0 | 1.47 | 0.03 | 15.74 | 0.01 | 10.088 | 2.58 | 0.03 | 10.929 | 0.021 | Stauffer07/82 | | 0.423 | R16 | EARLY-M* |
| "Cl Melotte 22 1454" | 03:47:34 | +24:41:03 | 1 | 1.073 | 0.02 | 12.809 | 0.017 | 7.164 | 1.282 | 0.02 | 10.076 | 0.033 | Kamai | 134.584 | 8.598 | R16 | K5 |
| "Cl* Melotte 22 PELS 066" | 03:47:34 | +21:44:49 | 1 | 1.016 | 0.013 | 12.325 | 0.011 | 6.741 | 1.101 | 0.018 | 9.895 | 0.018 | Kamai | 130.862 | 7.555 | R16 | MID-K* |
| "Cl* Melotte 22 SK409" | 03:47:38 | +24:49:11 | 1 | 1.571 | 0.02 | 16.533 | 0.017 | 10.813 | 2.493 | 0.023 | 11.697 | 0.026 | Kamai | 139.293 | 2.323 | R16 | MID-M* |
| "Cl Melotte 22 1593" | 03:47:48 | +23:13:05 | 1 | 0.77 | 0.01 | 11.15 | 0.01 | 5.481 | 0.82 | 0.01 | 9.298 | 0.027 | Stauffer07/87 | 136.112 | 5.137 | R16 | G7V |
| "Cl* Melotte 22 HCG 295" | 03:47:51 | +24:30:19 | 1 | 1.521 | 0.016 | 16.116 | 0.016 | 10.445 | 2.384 | 0.014 | 11.467 | 0.025 | Kamai | 136.235 | 1.418 | R16 | EARLY-M* |
| "Cl* Melotte 22 PELS 143" | 03:47:58 | +26:37:45 | 1 | 0.873 | 0.01 | 11.655 | 0.022 | 6.022 | 0.927 | 0.016 | 9.609 | 0.017 | Kamai | 133.857 | 6.462 | H10 | LATE-G* |
| "Cl* Melotte 22 HCG 309" | 03:48:06 | +23:02:03 | 1 | 1.69 | 0.03 | 16.16 | 0.01 | 10.492 | 2.42 | 0.04 | 11.55 | 0.021 | Stauffer07/82 | 136.042 | 1.562 | R16 | MID-M* |
| "Cl* Melotte 22 DH 550" | 03:48:08 | +25:18:55 | 1 | 1.272 | 0.014 | 13.942 | 0.012 | 8.356 | 1.637 | 0.019 | 10.336 | 0.017 | Kamai | 130.963 | 0.446 | R16 | LATE-K* |
| "Cl* Melotte 22 DH 554" | 03:48:10 | +23:00:04 | 2 | 1.383 | 0.021 | 14.553 | 0.023 | 8.524 | 1.711 | 0.02 | 11.004 | 0.018 | Kamai | 160.62 | 6.548 | R16 | LATE-K* |
| "Cl* Melotte 22 DH 556" | 03:48:10 | +19:18:09 | 1 | 1.204 | 0.012 | 13.1 | 0.011 | 7.525 | 1.352 | 0.018 | 10.217 | 0.02 | Kamai | 130.297 | 4.262 | H10 | MID-K* |
| "Cl* Melotte 22 HCG 304" | 03:48:12 | +26:35:02 | 1 | 1.273 | 0.014 | 13.586 | 0.012 | 7.969 | 1.466 | 0.019 | 10.36 | 0.019 | Kamai | 132.841 | 4.704 | H10 | LATE-K* |
| "Cl* Melotte 22 HHJ 336" | 03:48:15 | +23:42:04 | 1 | 1.65 | 0.021 | 17.11 | 0.021 | 11.129 | 2.829 | 0.023 | 11.778 | 0.02 | Kamai | 157.081 | 0.367 | R16 | M3.5 |
| "Cl* Melotte 22 HCG 318" | 03:48:16 | +22:32:41 | 2 | 1.399 | 0.012 | 14.667 | 0.017 | 8.654 | 1.913 | 0.015 | 10.695 | 0.017 | Kamai | 159.408 | 0.215 | H10 | LATE-K* |
| "Cl* Melotte 22 DH 568" | 03:48:20 | +23:36:12 | 1 | 1.54 | 0.017 | 16.117 | 0.017 | 10.44 | 2.377 | 0.014 | 11.472 | 0.02 | Kamai | 136.581 | 1.033 | R16 | EARLY-M* |
| "Cl* Melotte 22 HCG 323" | 03:48:23 | +22:52:22 | 1 | 1.5 | 0.04 | 16.14 | 0.02 | 10.563 | 2.47 | 0.05 | 11.484 | 0.02 | Stauffer07/82 | 130.446 | 1.139 | R16 | EARLY-M* |
| "Cl* Melotte 22 HCG 317" | 03:48:26 | +25:14:41 | 1 | 1.554 | 0.043 | 15.463 | 0.026 | 9.849 | 2.214 | 0.024 | 11.089 | 0.017 | Kamai | 132.694 | 1.634 | R16 | EARLY-M* |

(Continued).

| *Name* | $\alpha_{J2000}$ (h:m:s) | $\delta_{J2000}$ ($\circ$:$'$:$''$) | *Notes memb.* | $B-V$ (mag) | e$B-V$ (mag) | $V$ (mag) | e$V$ (mag) | $M_v$ (mag) | $V-Ic$ (mag) | e$V-Ic$ (mag) | $Ks$ (mag) | e$Ks$ (mag) | *Notes phot.BVI* | $D_{BJ.Gaia}$ (pc) | *Period* (days) | *Notes period* | *Spect. Types* |
|---|---|---|---|---|---|---|---|---|---|---|---|---|---|---|---|---|---|
| "Cl* Melotte 22 HCG 329" | 03:48:26 | +22:12:42 | 2 | 1.239 | 0.021 | 14.023 | 0.015 | 8.113 | 1.544 | 0.019 | 10.602 | 0.017 | Kamai | 152.047 | 0.399 | R16 | LATE-K* |
| "Cl* Melotte 22 HCG 332" | 03:48:27 | +23:11:30 | 4 | 1.648 | 0.028 | 17.45 | 0.021 | 12.659 | 3.327 | 0.022 | 11.361 | 0.022 | Kamai | 90.815 | 0.463 | R16 | MID-M* |
| "Cl* Melotte 22 HCG 339" | 03:48:42 | +25:00:29 | 1 | 1.63 | 0.04 | 16.61 | 0.02 | 10.894 | 2.57 | 0.04 | 11.72 | 0.02 | Stauffer07/82 | 139.057 | 0.337 | R16 | MID-M* |
| "Cl Melotte 22 2027" | 03:48:49 | +24:16:03 | 4 | 0.85 | 0.01 | 10.93 | 0.01 | 5.154 | 0.92 | 0.01 | 8.822 | 0.017 | Stauffer07/87 | 142.952 | 5.092 | R16 | EARLY-K* |
| "Cl Melotte 22 2106" | 03:48:58 | +23:12:04 | 4 | 0.87 | 0.01 | 11.54 | 0.01 | 5.774 | 0.95 | 0.01 | 9.453 | 0.042 | Stauffer07/87 | 142.327 | 6.007 | R16 | EARLY-K* |
| "Cl* Melotte 22 HHJ 353" | 03:48:58 | +23:05:39 | 1 | 1.567 | 0.019 | 16.351 | 0.016 | 10.673 | 2.43 | 0.018 | 11.669 | 0.021 | Kamai | 136.62 | 13.699 | R16 | EARLY-M* |
| "Cl* Melotte 22 HCG 351" | 03:49:01 | +24:54:10 | 1 | 1.579 | 0.021 | 16.954 | 0.02 | 11.325 | 2.717 | 0.019 | 11.814 | 0.022 | Kamai | 133.599 | 1.497 | R16 | MID-M* |
| "Cl* Melotte 22 SK327" | 03:49:09 | +25:53:49 | 1 | 1.546 | 0.015 | 16.115 | 0.018 | 10.453 | 2.442 | 0.02 | 11.384 | 0.025 | Kamai | 135.628 | 0.404 | C16 | M2.5 |
| "Cl* Melotte 22 HCG 370" | 03:49:28 | +24:31:54 | 2 | 1.531 | 0.017 | 15.991 | 0.019 | 10.142 | 2.45 | 0.023 | 11.258 | 0.026 | Kamai | 147.825 | 0.543 | R16 | EARLY-M* |
| "Cl Melotte 22 2311" | 03:49:29 | +23:42:44 | 1 | 0.82 | 0.01 | 11.35 | 0.01 | 5.731 | 0.85 | 0.02 | 9.479 | 0.04 | Stauffer07/82 | 132.984 | 5.714 | R16 | LATE-G* |
| "Cl Melotte 22 2341" | 03:49:33 | +23:47:44 | 1 | 0.72 | 0.01 | 10.93 | 0.01 | 5.223 | 0.74 | 0.01 | 9.191 | 0.038 | Stauffer07/87 | 138.504 | 4.943 | R16 | EARLY-G* |
| "Cl* Melotte 22 HCG 372" | 03:49:33 | +24:32:03 | 1 | 1.52 | 0.04 | 16.58 | 0.02 | 10.925 | 2.59 | 0.05 | 11.738 | 0.022 | Stauffer07/82 | 135.221 | 1.593 | R16 | M3.2 |
| "Cl Melotte 22 2368" | 03:49:35 | +23:27:17 | 2 | 1.357 | 0.011 | 14.348 | 0.01 | 8.472 | 1.869 | 0.015 | 10.42 | 0.022 | Kamai | 149.723 | 1.281 | R16 | LATE-K* |
| "Cl* Melotte 22 HCG 376" | 03:49:36 | +22:09:05 | 1 | 1.417 | 0.015 | 13.977 | 0.013 | 8.246 | 1.912 | 0.02 | 10.022 | 0.018 | Kamai | 140.0 | 0.247 | R16 | EARLY-M* |
| "Cl Melotte 22 2366" | 03:49:37 | +24:17:46 | 1 | 0.82 | 0.01 | 11.49 | 0.01 | 5.834 | 0.86 | 0.01 | 9.578 | 0.057 | Stauffer07/87 | 135.254 | 6.218 | H10 | LATE-G* |
| "Cl Melotte 22 2462" | 03:49:50 | +23:42:20 | 1 | 0.84 | 0.01 | 11.49 | 0.01 | 5.787 | 0.86 | 0.02 | 9.546 | 0.049 | Stauffer07/82 | 138.239 | 6.847 | R16 | EARLY-K* |
| "Cl* Melotte 22 HCG 378" | 03:49:52 | +21:18:26 | 1 | 1.555 | 0.014 | 15.631 | 0.015 | 9.944 | 2.456 | 0.017 | 10.921 | 0.018 | Kamai | 137.24 | 0.472 | R16 | EARLY-M* |
| "Cl* Melotte 22 SK293" | 03:49:58 | +23:42:34 | 1 | 1.523 | 0.018 | 16.333 | 0.016 | 10.673 | 2.476 | 0.018 | 11.567 | 0.021 | Kamai | 135.489 | 1.342 | R16 | M2.5 |
| "Cl* Melotte 22 SK291" | 03:50:02 | +25:24:02 | 4 | 1.571 | 0.016 | 16.175 | 0.016 | 10.841 | 2.523 | 0.014 | 11.459 | 0.019 | Kamai | 116.63 | 2.352 | H10 | MID-M* |
| "HD 23975" | 03:50:18 | +25:22:46 | 1 | 0.413 | 0.015 | 9.733 | 0.019 | 4.044 | 0.613 | 0.019 | 8.382 | 0.017 | Kamai | 137.337 | 1.857 | R16 | MID-F* |
| "Cl Melotte 22 2644" | 03:50:21 | +24:28:00 | 1 | 0.77 | 0.01 | 11.09 | 0.01 | 5.4 | 0.77 | 0.01 | 9.354 | 0.021 | Stauffer07/87 | 137.396 | 5.072 | H10 | LATE-G* |
| "Cl* Melotte 22 AK IV-131" | 03:50:21 | +27:08:40 | 1 | 0.825 | 0.01 | 11.346 | 0.022 | 5.852 | 0.881 | 0.016 | 9.356 | 0.018 | Kamai | 125.56 | 6.239 | H10 | LATE-G* |
| "Cl* Melotte 22 HCG 398" | 03:50:23 | +22:11:18 | 1 | 1.414 | 0.0090 | 14.507 | 0.0090 | 8.842 | 1.87 | 0.014 | 10.585 | 0.02 | Kamai | 135.854 | 1.896 | R16 | EARLY-M* |
| "Cl* Melotte 22 DH 668" | 03:50:25 | +20:42:18 | 2 | 1.443 | 0.012 | 14.686 | 0.014 | 8.687 | 1.814 | 0.018 | 10.935 | 0.021 | Kamai | 158.383 | 17.597 | R16 | EARLY-M* |
| "Cl* Melotte 22 PELS 072" | 03:50:36 | +25:25:35 | 1 | 0.931 | 0.014 | 12.095 | 0.019 | 6.418 | 1.108 | 0.018 | 9.582 | 0.017 | Kamai | 136.611 | 0.314 | R16 | EARLY-K* |
| "Cl* Melotte 22 DH 679" | 03:50:39 | +25:23:38 | 4 | 1.122 | 0.016 | 12.454 | 0.02 | 6.261 | 1.361 | 0.019 | 9.434 | 0.017 | Kamai | 173.236 | 0.579 | R16 | MID-K* |
| "Cl* Melotte 22 SK263" | 03:50:39 | +23:13:03 | 1 | 1.59 | 0.013 | 16.603 | 0.021 | 10.907 | 2.506 | 0.019 | 11.749 | 0.021 | Kamai | 137.791 | 0.889 | R16 | MID-M* |
| "Cl* Melotte 22 DH 686" | 03:50:54 | +22:32:53 | 1 | 1.071 | 0.013 | 12.772 | 0.011 | 7.087 | 1.227 | 0.018 | 9.987 | 0.018 | Kamai | 137.067 | 5.158 | H10 | MID-K* |
| "Cl* Melotte 22 HCG 412" | 03:50:57 | +25:35:07 | 1 | 1.611 | 0.02 | 16.893 | 0.016 | 11.386 | 2.824 | 0.018 | 11.581 | 0.019 | Kamai | 126.301 | 2.079 | R16 | MID-M* |
| "Cl* Melotte 22 DH 696" | 03:51:11 | +26:35:16 | 1 | 1.382 | 0.0090 | 13.988 | 0.0090 | 8.212 | 1.595 | 0.014 | 10.599 | 0.021 | Kamai | 142.933 | 6.651 | H10 | LATE-K* |
| "Cl* Melotte 22 HCG 424" | 03:51:19 | +24:10:13 | 1 | 1.566 | 0.015 | 16.132 | 0.016 | 10.564 | 2.484 | 0.017 | 11.4 | 0.021 | Kamai | 129.91 | 1.866 | H10 | MID-M* |
| "Cl* Melotte 22 DH 706" | 03:51:24 | +22:50:29 | 1 | 1.374 | 0.01 | 14.268 | 0.0090 | 8.63 | 1.745 | 0.014 | 10.595 | 0.022 | Kamai | 134.18 | 3.661 | H10 | LATE-K* |
| "Cl* Melotte 22 HCG 427" | 03:51:24 | +26:03:12 | 3 | 1.67 | 0.04 | 16.68 | 0.02 | 11.071 | 2.66 | 0.05 | 11.678 | 0.025 | Stauffer07/82 | 132.344 | 1.674 | C16 | M3.2 |

(Continued).

| *Name* | $\alpha_{J2000}$ (h:m:s) | $\delta_{J2000}$ (°:′:″) | *Notes memb.* | $B-V$ (mag) | e$B-V$ (mag) | $V$ (mag) | e$V$ (mag) | $M_v$ (mag) | $V-Ic$ (mag) | e$V-Ic$ (mag) | $Ks$ (mag) | e$Ks$ (mag) | *Notes phot.BVI* | $D_{BJ,Gaia}$ (pc) | *Period* (days) | *Notes period* | *Spect. Types* |
|---|---|---|---|---|---|---|---|---|---|---|---|---|---|---|---|---|---|
| "Cl* Melotte 22 HCG 420" | 03:51:24 | +22:06:48 | 1 | 1.172 | 0.012 | 13.189 | 0.011 | 7.492 | 1.361 | 0.018 | 10.196 | 0.019 | Kamai | 137.851 | 6.431 | R16 | MID-K* |
| "Cl* Melotte 22 SK231" | 03:51:24 | +25:05:53 | 1 | 1.625 | 0.017 | 16.521 | 0.02 | 10.841 | 2.458 | 0.023 | 11.768 | 0.024 | Kamai | 136.776 | 4.391 | R16 | MID-M* |
| "Cl* Melotte 22 HCG 430" | 03:51:25 | +23:53:22 | 1 | 1.359 | 0.0090 | 14.06 | 0.0090 | 8.398 | 1.668 | 0.014 | 10.599 | 0.022 | Kamai | 135.653 | 7.148 | H10 | K9 |
| "Cl* Melotte 22 HCG 428" | 03:51:26 | +24:47:39 | 1 | 1.595 | 0.018 | 16.232 | 0.02 | 10.602 | 2.678 | 0.023 | 11.192 | 0.021 | Kamai | 133.665 | 0.307 | C16 | MID-M* |
| "Cl* Melotte 22 PELS 068" | 03:51:42 | +21:40:06 | 1 | 0.848 | 0.01 | 11.485 | 0.022 | 5.765 | 0.918 | 0.016 | 9.452 | 0.018 | Kamai | 139.305 | 5.445 | R16 | EARLY-K* |
| "Cl* Melotte 22 HCG 439" | 03:51:55 | +23:33:32 | 0 | 1.633 | 0.022 | 17.268 | 0.021 | 11.616 | 2.911 | 0.023 | 11.782 | 0.018 | Kamai | | 0.578 | R16 | MID-M* |
| "Cl* Melotte 22 PELS 146" | 03:52:01 | +19:35:49 | 2 | 0.628 | 0.019 | 10.476 | 0.023 | 4.698 | 0.749 | 0.019 | 8.873 | 0.018 | Kamai | 143.095 | 2.454 | H10 | EARLY-G* |
| "Cl* Melotte 22 SK201" | 03:52:06 | +22:34:55 | 4 | 1.559 | 0.017 | 16.194 | 0.017 | 10.604 | 2.44 | 0.014 | 11.483 | 0.018 | Kamai | 131.2 | 1.986 | R16 | MID-M* |
| "Cl* Melotte 22 DH 749" | 03:52:18 | +22:00:54 | 2 | 1.524 | 0.012 | 15.747 | 0.015 | 9.878 | 2.23 | 0.015 | 11.39 | 0.021 | Kamai | 149.241 | 1.994 | R16 | EARLY-M* |
| "Cl* Melotte 22 HCG 458" | 03:52:34 | +22:30:08 | 1 | 1.561 | 0.012 | 15.975 | 0.016 | 10.186 | 2.369 | 0.015 | 11.39 | 0.018 | Kamai | 143.818 | 1.766 | R16 | EARLY-M* |
| "Cl* Melotte 22 HCG 460" | 03:52:49 | +21:42:28 | 1 | 1.429 | 0.028 | 14.757 | 0.021 | 9.228 | 1.984 | 0.022 | 10.656 | 0.017 | Kamai | 127.599 | 0.553 | R16 | EARLY-M* |
| "Cl* Melotte 22 PELS 069" | 03:52:53 | +21:46:55 | 4 | 0.863 | 0.012 | 11.771 | 0.018 | 5.677 | 1.047 | 0.016 | 9.349 | 0.018 | Kamai | 165.531 | 1.753 | R16 | EARLY-K* |
| "Cl* Melotte 22 HCG 463" | 03:52:57 | +22:26:02 | 1 | 1.559 | 0.017 | 16.322 | 0.016 | 10.714 | 2.469 | 0.018 | 11.574 | 0.02 | Kamai | 132.322 | 1.29 | R16 | MID-M* |
| "Cl* Melotte 22 SK145" | 03:52:59 | +24:54:06 | 1 | 1.374 | 0.012 | 14.51 | 0.017 | 8.823 | 1.804 | 0.015 | 10.707 | 0.02 | Kamai | 137.184 | 2.486 | R16 | LATE-K* |
| "Cl* Melotte 22 AK V-088" | 03:53:02 | +21:39:37 | 2 | 0.787 | 0.019 | 10.713 | 0.023 | 5.66 | 0.855 | 0.019 | 8.833 | 0.017 | Kamai | 102.47 | 9.456 | H10 | LATE-G* |
| "Cl* Melotte 22 DH 777" | 03:53:05 | +22:48:05 | 1 | 1.256 | 0.023 | 13.628 | 0.017 | 7.941 | 1.499 | 0.022 | 10.376 | 0.017 | Kamai | 137.246 | 5.436 | H10 | LATE-K* |
| "Cl* Melotte 22 PELS 071" | 03:53:24 | +24:03:54 | 1 | 0.797 | 0.01 | 11.397 | 0.022 | 5.735 | 0.881 | 0.016 | 9.439 | 0.021 | Kamai | 135.658 | 4.065 | R16 | LATE-G* |
| "Cl* Melotte 22 PELS 075" | 03:53:31 | +26:31:41 | 4 | 0.909 | 0.011 | 11.899 | 0.022 | 6.362 | 1.14 | 0.016 | 9.242 | 0.022 | Kamai | 128.047 | 0.396 | H10 | EARLY-K* |
| "Cl* Melotte 22 HCG 473" | 03:53:41 | +24:25:10 | 1 | 1.549 | 0.015 | 16.13 | 0.015 | 10.452 | 2.346 | 0.018 | 11.583 | 0.024 | Kamai | 136.645 | 8.561 | R16 | EARLY-M* |
| "Cl* Melotte 22 DH 792" | 03:53:43 | +20:50:01 | 1 | 1.45 | 0.024 | 14.78 | 0.018 | 9.146 | 1.922 | 0.018 | 10.764 | 0.018 | Kamai | 133.891 | 2.783 | R16 | EARLY-M* |
| "Cl* Melotte 22 PELS 083" | 03:53:50 | +25:57:53 | 2 | 0.724 | 0.01 | 11.054 | 0.019 | 5.027 | 0.811 | 0.018 | 9.299 | 0.02 | Kamai | 160.49 | 3.297 | R16 | MID-G* |
| "Cl* Melotte 22 DH 794" | 03:53:53 | +22:25:07 | 1 | 1.041 | 0.011 | 12.153 | 0.022 | 6.523 | 1.225 | 0.017 | 9.406 | 0.018 | Kamai | 133.686 | 6.335 | R16 | MID-K* |
| "Cl* Melotte 22 DH 795" | 03:53:58 | +20:28:50 | 4 | 1.517 | 0.013 | 15.383 | 0.015 | 9.91 | 2.239 | 0.017 | 10.92 | 0.02 | Kamai | 124.363 | 0.408 | R16 | EARLY-M* |
| "Cl* Melotte 22 AK IV-314" | 03:54:09 | +24:20:01 | 1 | 1.065 | 0.015 | 12.483 | 0.014 | 6.922 | 1.255 | 0.018 | 9.721 | 0.023 | Kamai | 129.488 | 8.119 | R16 | MID-K* |
| "Cl* Melotte 22 DH 800" | 03:54:19 | +25:29:43 | 2 | 1.161 | 0.018 | 12.875 | 0.015 | 7.474 | 1.431 | 0.019 | 9.805 | 0.024 | Kamai | 120.308 | 7.741 | R16 | MID-K* |
| "HD 24463" | 03:54:22 | +24:04:32 | 1 | 0.483 | 0.019 | 9.749 | 0.023 | 4.092 | 0.653 | 0.019 | 8.424 | 0.021 | Kamai | 135.317 | 0.882 | R16 | LATE-F* |
| "Cl* Melotte 22 HCG 489" | 03:54:28 | +23:50:08 | 1 | 1.311 | 0.013 | 13.07 | 0.023 | 7.463 | 1.594 | 0.017 | 9.663 | 0.018 | Kamai | 132.279 | 3.058 | R16 | LATE-K* |
| "Cl* Melotte 22 DH 803" | 03:54:28 | +24:19:16 | 1 | 1.377 | 0.012 | 14.203 | 0.017 | 8.543 | 1.717 | 0.015 | 10.62 | 0.02 | Kamai | 135.548 | 4.62 | R16 | LATE-K* |
| "Cl* Melotte 22 PELS 078" | 03:54:28 | +21:23:23 | 1 | 0.724 | 0.012 | 10.948 | 0.018 | 5.318 | 0.805 | 0.016 | 9.183 | 0.018 | Kamai | 133.634 | 4.548 | R16 | MID-G* |
| "Cl* Melotte 22 HCG 488" | 03:54:35 | +21:53:02 | 1 | 1.519 | 0.016 | 15.512 | 0.019 | 9.861 | 2.229 | 0.022 | 11.178 | 0.018 | Kamai | 134.947 | 2.774 | R16 | EARLY-M* |
| "Cl* Melotte 22 HCG 495" | 03:54:53 | +24:34:34 | 1 | 1.343 | 0.014 | 13.167 | 0.012 | 7.423 | 1.58 | 0.019 | 9.831 | 0.016 | Kamai | 140.839 | 8.798 | R16 | LATE-K* |
| "Cl* Melotte 22 DH 813" | 03:55:14 | +19:30:17 | 1 | 1.595 | 0.021 | 16.738 | 0.018 | 11.093 | 2.672 | 0.023 | 11.721 | 0.021 | Kamai | 134.585 | 2.427 | R16 | MID-M* |
| "Cl* Melotte 22 PELS 192" | 03:55:29 | +23:46:21 | 1 | 1.335 | 0.01 | 14.121 | 0.0090 | 8.418 | 1.666 | 0.014 | 10.593 | 0.02 | Kamai | 138.252 | 3.018 | R16 | LATE-K* |
| "Cl* Melotte 22 PELS 079" | 03:55:32 | +21:04:46 | 2 | 0.773 | 0.019 | 11.037 | 0.023 | 5.598 | 0.844 | 0.019 | 9.174 | 0.018 | Kamai | 122.427 | 5.559 | R16 | LATE-G* |
| "Cl* Melotte 22 HCG 502" | 03:55:49 | +23:55:36 | 0 | 1.48 | 0.015 | 14.813 | 0.012 | 9.161 | 2.25 | 0.016 | 10.44 | 0.018 | Kamai | | 2.948 | R16 | EARLY-M* |
| "Cl* Melotte 22 HCG 504" | 03:55:56 | +25:18:00 | 1 | 1.643 | 0.023 | 16.787 | 0.018 | 11.058 | 2.676 | 0.023 | 11.722 | 0.023 | Kamai | 139.921 | 2.46 | R16 | MID-M* |
| "Cl* Melotte 22 PELS 115" | 03:55:58 | +24:33:00 | 1 | 1.089 | 0.016 | 12.752 | 0.014 | 7.129 | 1.282 | 0.019 | 9.921 | 0.017 | Kamai | 133.21 | 7.226 | R16 | MID-K* |
| "Cl* Melotte 22 DH 823" | 03:55:58 | +21:10:39 | 2 | 1.631 | 0.019 | 16.87 | 0.021 | 11.038 | 2.665 | 0.023 | 11.761 | 0.021 | Kamai | 146.695 | 0.596 | R16 | MID-M* |
| "Cl* Melotte 22 DH 829" | 03:56:11 | +20:34:30 | 2 | 1.591 | 0.02 | 16.897 | 0.02 | 11.498 | 2.701 | 0.019 | 11.84 | 0.022 | Kamai | 120.165 | 1.12 | R16 | MID-M* |

(Continued).

| *Name* | $\alpha_{J2000}$ (h:m:s) | $\delta_{J2000}$ (o:′:″) | *Notes memb.* | $B-V$ (mag) | e$B-V$ (mag) | $V$ (mag) | e$V$ (mag) | $M_v$ (mag) | $V-Ic$ (mag) | e$V-Ic$ (mag) | $Ks$ (mag) | e$Ks$ (mag) | *Notes phot.BVI* | $D_{BJ.Gaia}$ (pc) | *Period* (days) | *Notes period* | *Spect. Types* |
|---|---|---|---|---|---|---|---|---|---|---|---|---|---|---|---|---|---|
| "Cl* Melotte 22 AK V-198" | 03:56:12 | +21:02:27 | 4 | 0.706 | 0.015 | 10.788 | 0.019 | 4.698 | 0.818 | 0.019 | 8.967 | 0.02 | Kamai | 165.173 | 5.392 | R16 | LATE-G* |
| "Cl* Melotte 22 SK22" | 03:56:19 | +23:57:52 | 1 | 1.552 | 0.016 | 15.737 | 0.019 | 10.11 | 2.279 | 0.022 | 11.277 | 0.018 | Kamai | 133.463 | 1.134 | R16 | EARLY-M* |
| "Cl* Melotte 22 HCG 508" | 03:56:23 | +24:49:57 | 1 | 1.323 | 0.0090 | 14.122 | 0.0090 | 8.395 | 1.667 | 0.014 | 10.547 | 0.016 | Kamai | 139.786 | 3.323 | R16 | LATE-K* |
| "Cl* Melotte 22 SK17" | 03:56:25 | +23:05:27 | 1 | 1.495 | 0.03 | 15.297 | 0.024 | 9.641 | 2.121 | 0.021 | 11.078 | 0.017 | Kamai | 135.292 | 14.581 | R16 | EARLY-M* |
| "Cl* Melotte 22 SK18" | 03:56:26 | +24:16:52 | 1 | 1.536 | 0.028 | 15.026 | 0.024 | 9.31 | 2.018 | 0.021 | 11.011 | 0.02 | Kamai | 139.079 | 2.114 | R16 | EARLY-M* |
| "Cl* Melotte 22 DH 851" | 03:57:17 | +24:00:33 | 1 | 1.071 | 0.013 | 12.788 | 0.011 | 7.193 | 1.256 | 0.018 | 9.945 | 0.02 | Kamai | 131.549 | 7.29 | R16 | MID-K* |
| "Cl* Melotte 22 PELS 162" | 03:57:33 | +24:03:11 | 1 | 0.934 | 0.012 | 12.113 | 0.011 | 6.399 | 1.019 | 0.018 | 9.861 | 0.016 | Kamai | 138.927 | 7.798 | R16 | EARLY-K* |
| "Cl* Melotte 22 DH 854" | 03:57:35 | +22:55:33 | 4 | 1.256 | 0.012 | 13.884 | 0.017 | 7.723 | 1.512 | 0.015 | 10.642 | 0.022 | Kamai | 170.67 | 8.907 | R16 | LATE-K* |
| "Cl* Melotte 22 HHJ 439" | 03:57:36 | +23:55:52 | 1 | 1.417 | 0.012 | 14.776 | 0.016 | 9.053 | 1.929 | 0.017 | 10.767 | 0.02 | Kamai | 139.498 | 1.676 | R16 | EARLY-M* |
| "Cl* Melotte 22 DH 856" | 03:57:41 | +25:16:04 | 2 | 1.628 | 0.018 | 16.635 | 0.02 | 10.798 | 2.514 | 0.019 | 11.816 | 0.023 | Kamai | 147.008 | 1.423 | R16 | MID-M* |
| "Cl* Melotte 22 HHJ 366" | 03:59:06 | +25:03:20 | 1 | 1.741 | 0.019 | 16.598 | 0.017 | 10.944 | 2.659 | 0.015 | 11.458 | 0.022 | Kamai | 135.17 | 0.779 | R16 | MID-M* |
| "Cl* Melotte 22 DH 875" | 03:59:23 | +22:34:17 | 1 | 1.41 | 0.01 | 14.333 | 0.0090 | 8.694 | 1.792 | 0.014 | 10.562 | 0.019 | Kamai | 134.212 | 1.884 | R16 | K5V |
| "Cl* Melotte 22 DH 877" | 03:59:28 | +23:07:26 | 1 | 1.119 | 0.016 | 13.381 | 0.015 | 7.696 | 1.446 | 0.019 | 10.13 | 0.017 | Kamai | 137.063 | 0.442 | R16 | MID-K* |
| "Cl* Melotte 22 PELS 173" | 04:00:53 | +23:11:38 | 4 | 0.414 | 0.016 | 9.597 | 0.019 | 3.27 | 0.541 | 0.018 | 8.488 | 0.018 | Kamai | 184.275 | 1.394 | R16 | MID-F* |
| "Cl* Melotte 22 DH 896" | 04:01:04 | +20:22:22 | 2 | 1.555 | 0.021 | 15.47 | 0.021 | 9.766 | 2.357 | 0.018 | 10.906 | 0.018 | Kamai | 138.3 | 5.368 | R16 | EARLY-M* |

Pleiades members and non-members. Parameters shown in this table: names of the stars taken from the SIMBAD database (except for the star 2MASS J03373212+2612137, taken from the 2MASS catalogue); coordinates ($\alpha$ y $\delta$); notes of membership (0: without membership data in Lodieu et al. (2019a), 1: member, 2: possible member, 3: unlikely member, 4: non-member); signal-to-noise value when below 100; $B-V$, $V$, $V-I_c$ photometry with their errors and brightness calibrated in the $V$ ($M_v$) band obtained using the distances from Bailer-Jones et al. (2018); notes of photometry that indicate the origin of the data used; distances derived by Bailer-Jones et al. (2018) by means of Bayesian analysis of Gaia ($D_{BJ.Gaia}$) parallaxes; rotation period; origin of the selected rotation period; spectral types.

**Photometry notes.** "Stauffer07/82": data taken from the compilation of photometry in Stauffer et al. (2007). These values and their errors were calculated by Stauffer (1982b). "Stauffer07/87": the photometry and errors were compiled by Stauffer et al. (2007) and obtained by Stauffer & Hartmann (1987). The +B+ symbols written next to "OSN" indicates that the Signal-to-Noise ratio is inferior to 100 (with a value of $\sim 64$) in the $B$ filter.

**Notes for periods.** H10: Hartman et al. (2010); C16: Covey et al. (2016); R16: Rebull et al. (2016). The symbol $*$ marking the spectral types indicates that they were derived using the $B-V$, $V$ and $V-I_c$ data and the table by Erik Mamajek of tabulated values. The spectral types without this symbol were taken from the SIMBAD database.

## 3.3 Coma Berenices

Instead of following the same schema for the other clusters, below we include an article on Coma Berenices that we published in July 2020 in the journal "Monthly Notices of the Royal Astronomical Society", under the title: **Fast-rotating giant stars behind the Coma Berenices star cluster**. Having compared our selection of Coma Berenices objects with the isochrones, we discovered an unexpected contamination of giant stars in the sample:

### 3.3.1 Abstract

In the frame of a study of the empirical isochrones of young stellar clusters, we have carried out $BVI_c$ Johnson-Cousins photometry of a sample of K and M stars of the Coma Berenices star cluster. All these stars have known rotational periods. Our main goal is to get a valuable reference on the colour-magnitude diagram, $M_v$ vs $B-V$, for stars with ages within 400-800 Myr. For this purpose, we obtained $BVI_c$ photometry with an average upper limit for the precision of about 0.025 mag and used parallaxes from the Gaia Data Release 2. We found that one third of our sample is located well above the cluster main-sequence and these stars are confirmed as background giants by their radial velocities in the Gaia Data Release 2. This misclassification shows that giants with short surface rotational periods can mimic main-sequence stars if they are located at the appropriate distance. We recommend caution when using rotational periods in order to determine cluster membership. Besides, the gyrochronology technique should only be used when the luminosity class of the stars is well known. Finally, our cleared sample supports an age of $\sim$ 600 Myr for Coma Berenices, rather than an age of $\sim$ 800 Myr.

### 3.3.2 Introduction

The Coma Berenices open cluster (Melotte 111, hereinafter Coma Ber) is the second nearest star cluster to the Sun, at a distance of 86.7 pc with a dispersion of 7.1 pc (Tang et al. 2018, hereinafter T18). Centered at $\alpha_{J2000} = 12^h25^m$ and $\delta_{J2000} = 26°06'$ (Dias et al. 2014) it is very close to the North Galactic Pole. The age of Coma Ber was formerly considered to be between 400 Myr and 600 Myr (e.g., Loktin et al. 2001; Kharchenko et al. 2005; Silaj & Landstreet 2014). Using gyrochronology, Collier Cameron et al. (2009) obtained an age of 590.7 ± 40.9 Myr but recently T18 estimated an age of around 800 Myr for the cluster through isochrone fitting. In this article, we discuss the age determination of Coma Ber through both techniques.

Isochrone fitting is the most popular method for estimating the age of clusters and stellar associations. The physics behind this technique was well summarized by Angus et al. (2019): "surface gravity changes resulting from fusion in the core are compared with a set of models that trace stellar evolution across the Hertzsprung-Russell or colour-magnitude diagrams" (HRD and CMD respectively). A coeval population of stars located at same distance and with similar chemical composition should lie on the same curve (isochrone) in the HRD/CMD. A disadvantage encountered in isochrone fitting, as mentioned by Angus et al. (2019), is the difficulty of obtaining the age for GKM dwarfs, since most of their physical and observable properties do not change

rapidly. For these spectral types, gyrochronology might be a better choice to determine their ages.

Empirical age relations are also used to measure ages of stars in open clusters (see review Soderblom 2010). The most commonly used age indicators are: lithium depletion (e.g., Sestito & Randich 2005), chromospheric activity decay (e.g., Pace & Pasquini 2004; Pace et al. 2009) and rotational spindown (gyrochronology).

Gyrochronology, consolidated as a technique by Barnes (2003, 2007), is used to derive stellar ages from the rotational periods of the stars and does not depend on stellar distances. Several studies developed in the 1960s suggested a relationship between both rotation and activity with age. Skumanich (1972) plotted projected equatorial rotation velocities ($v \sin i$) for G stars belonging to the Pleiades and Hyades open clusters and also for the Sun. He showed that rotation decayed as the inverse square root of age. Subsequently, Kawaler (1989) suggested the possibility of determining the age of a late-type star from its rotation and colour.

Barnes (2003, 2007) selected data of stars in open clusters and the Sun to calibrate the relationship between rotational period, colour and age. In this way, gyrochronology moved from $v \sin i$ to rotational periods, getting rid of the extra uncertainty given by $v \sin i$, due to the poor knowledge of the angle between the rotation axis and the line of sight ($i$). Barnes (2003, 2007) plotted period vs $B - V$ for stars of young clusters and older field stars, and observed that coeval stars were placed in two different sequences that he defined as slow/interface/I and fast/convective/C. The I sequence contained the stars with longer rotational periods which followed the Skumanich relationship between rotation and age. Moreover, he characterized each coeval population with a common rotation-age relation that resulted from the fit to the I sequence. Subsequent works performed new calibrations in order to get new empirical rotation-age relations for the I sequence (e.g., Mamajek & Hillenbrand 2008; Meibom et al. 2009). In the last decades, rotational periods for solar and late-type stars have been measured in Coma Ber (Radick et al. 1990; Marilli et al. 1997; Collier Cameron et al. 2009; Terrien et al. 2014) and used to estimate the age of the cluster by using gyrochronology (Collier Cameron et al. 2009; Angus et al. 2015).

Coma Ber has a large sky coverage ($> 13° x 8°$) and for this reason, membership studies struggle with discriminating between members and field stars, as it is clear in the thorough study carried out by Sampedro et al. (2017) on a very large sample of clusters. The first membership study of Coma Ber was performed by Trumpler (1938) who analyzed proper motions, photometry, radial velocities and spectral types and identified 37 bright members and seven fainter probable members. The next notorious effort to increase the number of members (Casewell et al. 2006), made use of proper motions and photometry, confirmed 45 previously known members and identified 60 new late-type candidate members. Subsequent works, Kraus & Hillenbrand (2007), Mermilliod et al. (2008), Collier Cameron et al. (2009), Melnikov & Eislöffel (2012), Terrien et al. (2014), used photometry and several of the kinematic parameters (positions, proper motions, radial velocities) and identified a total of $\sim$ 150 candidate members for Coma Ber before the era of *Gaia*.

*Gaia* provided an improvement on the accuracy of fundamental parameters used in membership studies: Gaia Data Release 1 (*Gaia* DR1, Gaia Collaboration et al. 2016) and Gaia Data Release 2 (*Gaia* DR2, Gaia Collaboration et al. 2018b) which led to more reliable results on the candidate members list of Coma Ber. Gaia Collaboration et al. (2017) employed positions, proper

motions and parallax data from *Gaia* DR1 to analyze a field of 10.4° around the Coma Ber center, and reported 50 possible members. T18, collecting proper motions, photometry data and distance measurements from parallaxes by *Gaia* DR2, provided a list with 192 stellar and substellar member candidates. Within that list, 148 stars were expected to be true members. Moreover, T18 not only undertook their own membership study, they also collected and checked the results of previous membership studies for Coma Ber, except for the membership study by Collier Cameron et al. (2009).

Tang et al. (2019) (hereinafter T19) explained that the previous study of T18 might have included field stars in the candidate members list, due to a large radius cut of 17 mas/yr on the proper motions selection. Furthermore, T19 identified leading and trailing tails of Coma Ber and provided a list of 197 Coma Ber candidate members by making use of *Gaia* DR2 astrometry.

In the frame of our study of the isochrone fitting technique for GKM stars of young/intermediate-age open clusters (30 - 800 Myr), we compiled photometry for late-type (late G to M dwarfs) candidate members of the Coma Ber cluster with available rotational periods. Stellar distances were taken from Bailer-Jones et al. (2018), which were estimated using *Gaia* DR2 data and Bayesian inference (hereinafter BJ distances). These BJ distances reveal that several stars had been wrongly classified as K dwarfs members of Coma Ber. In this article we will discuss the nature of these stars and analyze the consequences of this misclassification for the technique of gyrochronology as an age determination tool.

### 3.3.3 Observations

#### The sample

We selected young low-mass stars (late G to M dwarfs) that had been catalogued as Coma Ber candidate members by one or several of the following membership studies: Casewell et al. (2006), Kraus & Hillenbrand (2007), Collier Cameron et al. (2009) and Terrien et al. (2014). Among them we chose those stars with measured rotational periods in the literature. The selection process was undertaken before 2017. Hence, we did not take into account the membership studies of Gaia Collaboration et al. (2017), Sampedro et al. (2017), T18 and T19.

Our sample contains 34 stars (G8 to M0), 33 of them have rotational periods measured by Collier Cameron et al. (2009) who identified 37 variable stars as late F to M candidate members of Coma Ber with membership probabilities higher than 50%. Among them, 20 stars were regarded as probable new members. They obtained rotational periods for these variable stars measuring the period of their variability through observations by SuperWASP. The rotational period of the remaining star in our sample was determined by Marilli et al. (1997). Three of the stars with periods obtained by Collier Cameron et al. (2009) were also measured by Terrien et al. (2014). For two of these stars we calculated the average of the periods obtained by both studies. For the third star, we kept the period of Collier Cameron et al. (2009), since the one from Terrien et al. (2014) diverged from the expected value for a late-type star.

We were able to obtain $BVI_c$ photometry for 33 out of 34 stars and for the remaining star, we took $B, V$ magnitudes from Kharchenko (2001). In order to include additional photometric

information to our sample, we also collected photometry from $JHK_s$ 2MASS (Skrutskie et al. 2006), Pan-STARRS DR1 (Chambers et al. 2016), UKIDSS-DR9 (Lawrence et al. 2013) and SDSS-III DR12 (Alam et al. 2015). Moreover, we gathered parallaxes, proper motions and radial velocities from *Gaia* DR2 and, as we mentioned before, BJ distances.

Table 3.3 shows the membership, photometry, parallaxes, proper motions, radial velocities and rotational periods of the selected sample. The calibrated magnitude $M_v$ was derived taking into account the BJ distances, also shown in the table. In order to compare these distances with the ones determined by the inverse of *Gaia* DR2 parallaxes, we present the results corresponding to both methods and as expected, the lower the parallaxes, the greater the discrepancies.

### Photometry

Calibrated photometry has been carried out from observations made with the 1.5m telescope at Observatorio de Sierra Nevada (OSN), Spain, during nine nights (from May 2015 to May 2017). We used $BVI_c$ Johnson-Cousins filters and, attached to the telescope, a VersArray 2048$x$2048 CCD with a pixel size of 13.5 $\mu$m and a field of view of 7.92$x$7.92 arcminutes.

Our Coma Ber sample contains stars with $B-V$ values from 0.65 to 1.55 mag. In order to perform the absolute calibration, we carefully selected a sample of standard stars from Landolt (1992, 2009, 2013) and located in the following standard star fields: SA32, SA98, SA101, SA104 and SA109. These standard stars covered the $B-V$ values range from 0.5 to 2.2 mag.

The CCD images were bias and flat-field corrected to remove instrumental signatures across the detector. Each night was processed independently with the IRAF software (Image Reduction and Analysis Facility). We conducted aperture photometry and, in order to obtain the calibrated magnitudes, we applied the transformation equations developed by Harris et al. (1981) to the instrumental magnitudes for the required $BVI_c$ Johnson-Cousins filters.

With the objective to estimate the error of our transformation from the instrumental to the calibrated system we have computed the *internal errors* as defined by Harris et al. (1981). Internal errors (in mag) range from 0.007 to 0.022 for the $B-V$ index, from 0.008 to 0.022 for $V$ and from 0.009 to 0.020 for the $V-I$ index. Average values of the extinction coefficients for $B-V$, $V$ and $V-I$ are 0.060, 0.158 and 0.116 mag/airmass. For the V band we got values as large as 0.22 and 0.26 mag/airmass, which we attribute to dust in the atmosphere, and we also got three very transparent nights with extinction below 0.13 mag/airmass (the OSN lies at 2896 m of altitude).

For each star and filter we have computed an individual error, that is actually an upper limit of the real error. We obtained these individual errors as the square root of the squared sum of the upper limit residual and of the error of the instrumental magnitudes of the stars. The upper limit residual was the highest value among the photometric residuals for the selected standard stars. The mean value of the upper limit errors of the sample for the $V$ magnitude and the $B-V$, $V-I_c$ colours is $\sim$ 0.025 mag.

Results are listed in table 3.3. For the target Cl* Melotte 111 AV 1431, the photometry was taken from Kharchenko (2001). The uncertainty of its colour and magnitude, $B-V$ and $V$, are $\sim$ 0.3 mag and $\sim$ 0.1 mag respectively.

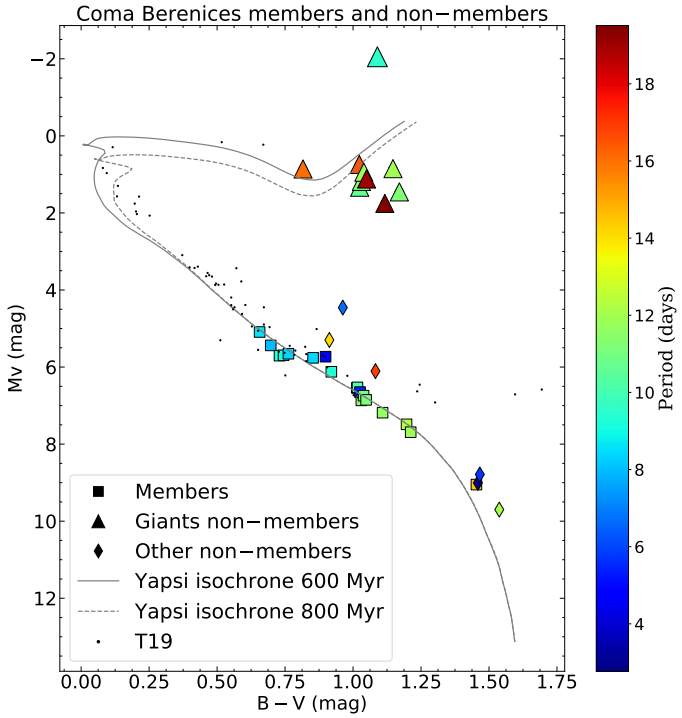


Figure 3.1: CMD for our sample of Coma Ber stars with known periods. We also show the candidate members from T19, represented by dots, with *BV* photometry from Kharchenko (2001). The isochrones correspond to Yapsi evolutionary tracks of 600 Myr and 800 Myr (solid and dashed lines, respectively). Ten stars out of 34 are located well above the main-sequence, one of them is situated over the giant branch, the remaining nine lie close to this branch. Several stars almost overlap and might be difficult to distinguish in the CMD, their periods and photometry can be checked in table 3.3.

### 3.3.4 Results

#### Coma Ber membership in our sample

Fig. 3.1 shows the position of the stars of our sample (mainly K dwarfs) in the CMD. For completeness sake, we included stars with spectral types earlier than K by plotting all the candidate members from T19 with available *BV* photometry from Kharchenko (2001). We overplotted two isochrones that belong to the set of Yale-Potsdam Stellar Isochrones (YaPSI, Spada et al. 2017), and correspond to solar metallicity and ages of 600 Myr and 800 Myr.

Ten stars, with $M_v < 2$ mag, are located well above the cluster main-sequence in the CMD. Nine of them show BJ distances between $\sim$ 950 pc and $\sim$ 1550 pc or, in terms of *Gaia* DR2 parallaxes, between $\sim$ 0.6 mas and $\sim$ 1 mas (the mean *Gaia* DR2 parallax of Coma Ber is $\sim$ 11.6 mas). Considering their calibrated magnitude $M_v$, with values from $\sim$ 0.7 to $\sim$ 1.8 mag, and their colour index $B - V$, from $\sim$ 0.8 to $\sim$ 1.2 mag, we concluded that they might be non-member giant stars (luminosity class III). Unfortunately, neither $V - I$, nor the near-infrared (NIR) colours help discriminating K giants from K dwarfs (Li et al. 2016). Nevertheless, the giant assumption is supported by their radial velocities, since two differentiated groups are presented in the *Gaia*

DR2 radial velocities (RV) of our sample. The RVs in the first group, including only the Coma Ber main-sequence stars, range from $\sim -6$ to $\sim 3$ Km/s. The second group, which contains only the giant stars, has the following RVs range: $\sim -70 <$ RV $< \sim -18$ Km/s and $\sim 12 <$ RV $< \sim 164$ Km/s.

We observe a star with $M_v \sim -2$ mag in our CMD, 2MASSJ12394200+2134578, which is located at a BJ distance of $\sim 5270$ pc and has a *Gaia* DR2 parallax value of $\sim 0.09$ mas. This star is even brighter than the nine stars classified as class III and belongs to the luminosity class II of bright giants. Its radial velocity, 164.51 Km/s, is in agreement with the radial velocity expected for halo stars (Harris & Racine 1979).

After discarding these ten giants, 24 stars remained in our sample. As some of them might have also been misclassified as Coma Ber members, we checked T18 and T19 studies. Both utilized data from *Gaia* DR2, which provided higher accuracy than the catalogs of *Gaia* DR1 and UCAC4 (The fourth United States Naval Observatory CCD Astrograph Catalog, Zacharias et al. 2013) used by Gaia Collaboration et al. (2017) and Sampedro et al. (2017), respectively. Hence, we only took into account the membership information from T18 and T19. A total of 17 stars were identified as candidate members by one of the studies or by both of them. Since T19 reported that their previous work (T18) might have included field stars in their candidate members list, we analyzed the proper motions of the six stars that were considered candidate members by T18 but not by T19. We would keep classifying as candidate members those with proper motions ($\mu$) similar to the mean values for Coma Ber given by Gaia Collaboration et al. (2018a): $\mu_\alpha = -12.111 \pm 0.0048$ mas/yr and $\mu_\delta = -8.996 \pm 0.121$ mas/yr. Three stars satisfied this criterion, while the other three had proper motions that slightly diverged from the mean values of the cluster, with a maximum difference of $\pm 4$ mas/yr. We checked the position of those stars in the CMD and corresponded to that of the candidate members. Therefore, we kept all the 17 stars as candidate members of Coma Ber.

We still had seven stars from our sample of 24 that did not have membership information in any of the studies T18 and T19. In order to avoid a possible misclassification, we checked their BJ distances and *Gaia* DR2 proper motions. We marked out as probable non-members the stars with a distance higher than 94 pc, since Coma Ber has an average measured distance of $86.7 \pm 7.1$ pc (T18). For the stars with BJ distances smaller than 94 pc, we analyzed their proper motions, as described above. We finally classified six out of the seven stars as probable non-members of Coma Ber; four of them were rejected by the distance criterion and the other two by analyzing the proper motions.

In summary, we identified 16 stars as non-members of the cluster, of which ten are giant stars and six are other probable non-members.

Our sample was then originally contaminated because the work by Collier Cameron et al. (2009), although thorough, adopted a wide interval of proper motions. Their candidate members had the following ranges of *Gaia* DR2 proper motions: $\sim -21 < \mu_\alpha < \sim -5$ mas/yr, $\sim 0 < \mu_\alpha < \sim 21$ mas/yr, and $\sim -17 < \mu_\delta < \sim -4$ mas/yr, $\sim 0 < \mu_\delta < \sim 8$ mas/yr.

The proper motions of all the stars in our sample are represented in Fig. 3.2, where we see how candidate members are preferentially concentrated in a region while non-members are more

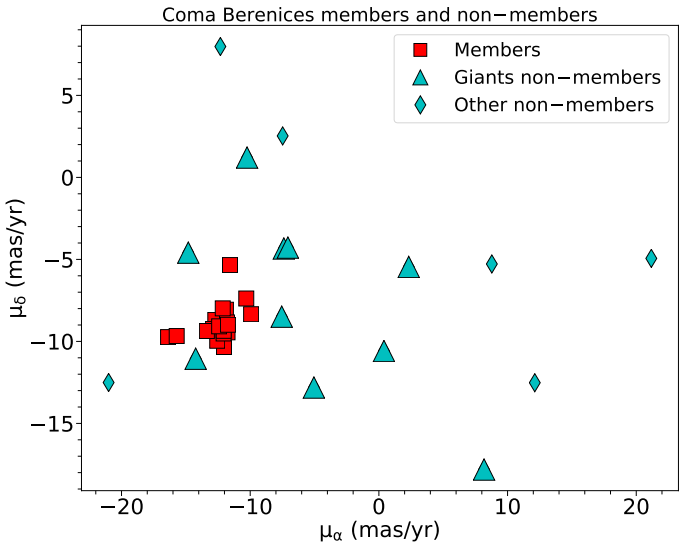


Figure 3.2: Proper motions of Coma Ber candidate members and non-members. Most of the candidate members are concentrated in a differentiated region of proper motions with respect to the stars that do not belong to the cluster.

scattered.

### Rotational periods of the giant stars in our sample

In this section we intend to understand why our sample has been contaminated with giant background stars.

If we compare the surface rotational periods (from 9.77 to 19.51 days) of our subsample of giant stars with those of the giants observed by Kepler and analyzed by Ceillier et al. (2017), we notice that our subsample matches the scarcely populated group of fast rotators, as defined by them.

We want to compute what fraction of the giant population represent the fast rotators, with period below 23 days[1], both for the Kepler giants and for our subsample. The fraction of fast rotators in the Kepler sample can be calculated with the information given by Ceillier et al. (2017), which studied red giants (luminosity class III). In order to compute the fraction for our subsample we have to estimate the size of the whole sample to which our giants belong. Using the *Gaia* DR2 search tool, we looked for all the giant stars that share the spatial, photometric and dynamical space with our nine giants of luminosity class III. Therefore, we selected the stars that are in the ranges covered by the nine giants: *G-band* mean magnitude between 11.20 and 12.10 mag; $BP - RP$ colour index between 1.045 mag and 1.351 mag; $\alpha$, $\delta$ coordinates: $\alpha$ from $11^h\ 48^m$ to $13^h\ 05^m$, and $\delta$ from 19° to 43°; proper motions constrained to the limits used by Collier Cameron et al. (2009) and parallaxes between 0.365 mas and 1.153 mas. This range of parallaxes corresponds to distances from 867 to 2740 pc, which were calculated taking into account the difference in magnitude between early K dwarfs and giants in the CMD: K giants are on average 100 to 1000

[1]This upper limit comes from the bins that Ceillier et al. (2017) used for their Fig.5.

times more luminous, and hence can 'simulate' main-sequence dwarfs if they are located 10 to 32 times further away. We found 628 giants that fulfil all the mentioned requirements.

The nine giants of our subsample represent 1.4% of these 628 giants. This percentage is of the same order than the 0.6% fraction of low-mass red giants that exhibit surface rotational periods with values below 23 days in the Kepler sample analyzed by Ceillier et al. (2017). Therefore, we think we have included in our sample most of the giants that could be mistaken as Coma Ber members because they mimic the Coma Ber main-sequence K stars.

Carlberg et al. (2011) compiled three mechanisms that might explain the high rotational velocities of some giant stars: interactions from a close binary companion; core-envelope differential rotation, where the core rotates much faster than the surface; and a planet spiralling towards the star that inserts angular momentum into the convective envelope of the star.

The Kepler field points through the Galaxy disk and our study has been done along a direction perpendicular to the disk. Interestingly, there seems to be a similar fraction of very fast rotating giants in both directions.

### 3.3.5 Discussion

#### Gyrochronology

Collier Cameron et al. (2009) followed the same method described in Barnes (2007), who considered that the period is inversely proportional to the square root of the age, and determined a period-colour relation for the Coma Ber cluster. They used the periods from Radick et al. (1990) (not included in our study) and Marilli et al. (1997), their periods of stars with membership probabilities higher than 85%, and the 2MASS $J - K$ colours. Using the aforementioned period-colour relation, Collier Cameron et al. (2009) obtained an empirical calibration of period as a function of age and colour and inferred an age of $590.7 \pm 40.9$ Myr for Coma Ber.

In Fig. 3.3 we plotted period vs $B - V$ for our sample of stars, highlighting those that were used for the period-colour calibration by Collier Cameron et al. (2009). We also marked out the stars for which Collier Cameron et al. (2009) used the double of the published period: these are stars for which they analyzed their periods and concluded that the true periods were twice their estimations.

Two groups of giant non-members are shown in Fig. 3.3. The first one contains six out of the ten giants with period values from 9.6 to 11.9 days, which are the fastest rotators among the giants. They fit well within the range of periods of the main-sequence stars (between 9.4 and 14.5 days). This first group mimic the Coma Ber main-sequence stars in colour, period and apparent magnitude. The second group contains the four remaining giants, which are slower rotators (periods from 16.0 to 19.5 days), and does not follow the trend line of the main-sequence members. Both groups might affect the calibration of gyrochronology: the fast rotators would add noise into the fitting of the main-sequence, and the slower rotators might be more problematic, since they can modify the fitting for the calibration in a higher level than the first group.

Regarding the calibration of gyrochronology by Collier Cameron et al. (2009), they made a cut in their candidate members list, and, as we mentioned before, discarded the periods of stars

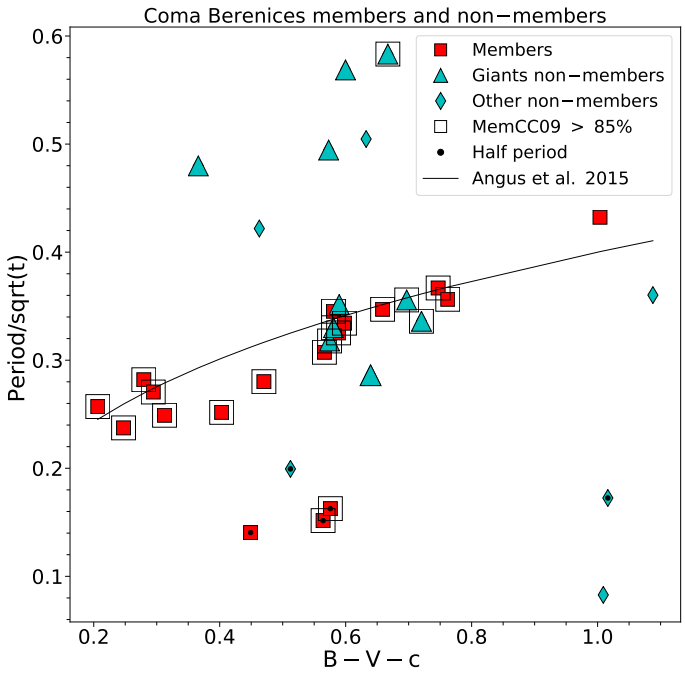


Figure 3.3: Period-colour relation for our Coma Ber sample. In red, we represent the stars we considered members of the cluster and, in cyan, the stars we marked out as non-members. Giant stars are shown by triangles. Inside the hollow square symbol, we show the stars in our sample that were used by Collier Cameron et al. (2009) for their period-colour calibration. Symbols containing a black dot represent the stars with periods considered double their published values by Collier Cameron et al. (2009). The solid line represents the fit of the period-colour relation (eq. 3.1), being $c = 0.45$, from Angus et al. (2015) for an age of $t = 590$ Myr.

with membership probabilities lower than 85%. As a consequence, only five giants contaminated their selected sample for the period-colour calibration. Four giants mimic well the main-sequence members. The remaining giant appears at the top of the plot. They considered the possibility that this star was not a member, and decided to not take it into account for the calibration. For those reasons, the giants in the study by Collier Cameron et al. (2009) barely modified the fit to the main-sequence stars for their calibration of gyrochronology.

Angus et al. (2015), on the other side, used the whole sample of Coma Ber stars selected by Collier Cameron et al. (2009) in order to calibrate their gyrochronology relation:

$$P = A^{0.55} \times 0.40(B - V - 0.45)^{0.31} \tag{3.1}$$

where $P$ is the rotational period (days) and $A$ the age (Myr). They included both the main-sequence and the giant stars, because the giants had not been identified as such. Their Figs. 1 and 2 show for Coma Ber a tail of slower rotators that are slower than the Hyades, although they consider Coma Ber (500 Myr) younger than the Hyades (625 Myr). The three slowest rotators are in fact background giant stars that add noise to the calibration. Fig. 3.3 shows their period-colour relation that corresponds to equation 3.1, for an age of 590 Myr and the result seems to indicate an agreement with the age of $590.7 \pm 40.9$ Myr given by Collier Cameron et al. (2009). Nevertheless, once the giants had been removed, the best-fitting to our data would be a slightly younger age.

In future studies of stellar ages using the gyrochronology technique, one should be aware of this problematic contamination of giants that do not belong to the cluster under study.

#### Age of Coma Berenices

There is a disagreement between the $\sim$ 800 Myr isochronal age obtained by T18 and the gyrochronological age of $590.7 \pm 40.9$ Myr obtained by Collier Cameron et al. (2009).

The isochronal age determination by T18 relied on five evolved stars in the cluster region. One of these five stars (18 Com) was excluded by T18, based on its distance and proper motions. Two evolved stars are binary systems, and another star (16 Com) lied on both the 600 Myr and 800 Myr isochrones. Only one star (14 Com) seems to be an isolated star that supports the 800 Myr estimation. Nevertheless, T19 discarded 14 Com as a candidate member of the Coma Ber cluster.

Our study eliminates the slowest rotators of the rotational periods distribution in the Coma Ber cluster, because they have been identified as background giants. In this way, the Hyades and the Coma Ber period distributions share the shape of the slow rotators tail. Therefore, the age of both clusters should be quite similar.

For all these reasons, we are more confident with the age determination obtained from the gyrochronology technique that gives an age of $590.7 \pm 40.9$ Myr (Collier Cameron et al. 2009).

### 3.3.6 Conclusions

We study the position on the CMD for late-type stars located in the Coma Ber cluster. We obtained $BVI_c$ photometric data from observations and compiled rotational periods from the literature. These are the main results of this work:

1. Distances obtained from *Gaia* DR2 parallaxes have shown nine stars located in the red-giant branch on the CMD and one bright giant, bringing to light the existence of giants previously identified as K dwarfs in our sample. The search of stellar cluster members based on rotational periods needs to take into account the possible contamination of background red giants, by checking their individual parallaxes.

2. Rotational periods of these giant stars show they are fast rotators, and their values do not correspond to the common periods related to their spectral type and luminosity class. Six out of the ten giants have periods that mimic well with the periods of the main-sequence stars. The remaining four stars are slower rotators than the other six giants, and do not follow the trend of the main-sequence stars.

3. The nine K giants of our sample represent, among the giants that share spatial, photometric and dynamical properties with them, a small percentage (1.4%), as the giants with surface rotational periods below 23 days (0.6%) in the whole sample of 17377 oscillating red giants of Ceillier et al. (2017). A similar percentage has also been found by other surveys of giant stars.

4. Contamination of giant stars might be a problem in the process of determining stellar ages from the gyrochronology technique, because the giant stars can add noise to the rotational period distribution. Therefore, before using the gyrochronology technique, it is necessary to confirm the luminosity class of the stars.

5. In the frame of the discrepancy between the ages determined by isochrones and gyrochronology, T19 have discarded as a Coma Ber candidate member, the evolved star that was crucial in T18 for their age estimation of $\sim$ 800 Myr by using the isochrone fitting technique. Besides, after removing the background giants, the rotational period distribution of Coma Ber fits better the age estimated by the gyrochronology technique. Therefore, we are more confident with the result obtained by gyrochonology, which gives an age of 590.7 $\pm$ 40.9 Myr (Collier Cameron et al. 2009) for the Coma Ber cluster.

### 3.3.7 Table of the Coma Ber sample

Table 3.3: Coma Ber members and non-members with measured periods.

| *Name* | $\alpha_{J2000}$ (h:m:s) | $\delta_{J2000}$ (°:′:″) | *Memb. notes* | $B-V$ (mag) | e$B-V$ (mag) | $V$ (mag) | e$V$ (mag) | $M_v$ (mag) | $V-I$ (mag) | e$V-I$ (mag) | *Plx* (mas) | $D_{inv.Gaia}$ (pc) | $D_{BJ.Gaia}$ (pc) | $\mu_\alpha$ (mas/yr) | $\mu_\delta$ (mas/yr) | *RV* (Km/s) | *Period* (days) | *Flag* |
|---|---|---|---|---|---|---|---|---|---|---|---|---|---|---|---|---|---|---|
| 2MASS J11483770+2816305 | 11:48:37.70 | +28:16:30.5 | | 0.75 | 0.03 | 10.39 | 0.03 | 5.70 | 0.78 | 0.03 | 11.20 | 89.29 | 89.06 | -12.06 | -9.36 | 0.50 | 9.43 | b |
| 2MASS J11553336+2943417 | 11:55:33.35 | +29:43:41.7 | | 1.03 | 0.04 | 11.64 | 0.03 | 6.87 | 1.16 | 0.03 | 11.06 | 90.45 | 90.22 | -15.71 | -9.67 | 2.93 | 11.55 | b |
| 2MASS J12005224+2719237 | 12:00:52.24 | +27:19:23.9 | NM | 1.02 | 0.03 | 11.50 | 0.03 | 1.33 | 1.09 | 0.03 | 0.89 | 1120.65 | 1082.84 | -10.24 | 1.21 | 30.84 | 10.63 | b |
| 2MASS J12022298+2254590 | 12:02:22.86 | +22:54:58.7 | NM | 0.91 | 0.02 | 11.72 | 0.02 | 5.30 | 0.92 | 0.02 | 5.17 | 193.54 | 192.48 | -7.48 | 2.53 | | 14.11 | b |
| Cl* Melotte 111 AV 189 | 12:07:57.72 | +25:35:11.3 | | 1.02 | 0.02 | 11.36 | 0.02 | 6.53 | 1.09 | 0.02 | 10.78 | 92.73 | 92.50 | -9.93 | -8.34 | -6.08 | 10.28 | b |
| 2MASS J12083610+3106098 | 12:08:36.10 | +31:06:09.9 | | 1.21 | 0.02 | 12.43 | 0.03 | 7.69 | 1.43 | 0.01 | 11.24 | 88.98 | 88.76 | -11.89 | -8.07 | -0.54 | 11.92 | b |
| 2MASS J12113516+2922444 | 12:11:35.11 | +29:22:44.5 | | 1.01 | 0.02 | 11.29 | 0.02 | 6.54 | 1.03 | 0.02 | 11.19 | 89.33 | 89.11 | -11.80 | -8.84 | 0.91 | (5.07) | b |
| Cl* Melotte 111 AV 523 | 12:12:53.23 | +26:15:01.3 | | 1.03 | 0.02 | 11.32 | 0.03 | 6.65 | 1.07 | 0.02 | 11.59 | 86.29 | 86.08 | -12.07 | -9.52 | 0.59 | (5.44) | b |
| Cl* Melotte 111 AV 1183 | 12:21:15.62 | +26:09:14.0 | | 1.04 | 0.02 | 11.38 | 0.03 | 6.74 | 1.13 | 0.02 | 11.78 | 84.92 | 84.71 | -11.76 | -9.45 | -0.28 | 10.88 | b* |
| Cl* Melotte 111 AV 1404 | 12:23:47.22 | +23:14:44.3 | | 1.05 | 0.02 | 11.50 | 0.03 | 6.85 | 1.16 | 0.02 | 11.75 | 85.10 | 84.89 | -12.56 | -9.96 | 0.55 | 11.18 | b |
| Cl* Melotte 111 AV 1431 | 12:24:06.00 | +26:07:43.0 | | 0.90 | 0.30 | 10.47 | 0.12 | 5.73 | | | 11.25 | 88.90 | 88.67 | -11.73 | -8.99 | -0.04 | (4.7) | a, c |
| 2MASS J12260132+3421084 | 12:26:01.31 | +34:21:08.4 | NM | 1.15 | 0.02 | 11.64 | 0.02 | 0.85 | 1.12 | 0.02 | 0.66 | 1509.69 | 1440.89 | 0.39 | -10.58 | -37.06 | 11.90 | b |
| Cl* Melotte 111 AV 1660 | 12:26:51.03 | +26:16:01.8 | | 1.11 | 0.02 | 11.85 | 0.03 | 7.18 | 1.26 | 0.02 | 11.63 | 85.97 | 85.76 | -12.13 | -7.98 | 0.70 | 11.61 | d |
| 2MASS J12265646+2240542 | 12:26:56.48 | +22:40:54.7 | NM | 1.47 | 0.02 | 15.11 | 0.03 | 8.79 | 1.82 | 0.02 | 5.42 | 184.63 | 183.66 | 8.78 | -5.28 | | (5.77) | b |
| Cl* Melotte 111 AV 1693 | 12:27:20.68 | +23:19:47.4 | | 0.74 | 0.03 | 10.31 | 0.03 | 5.70 | 0.82 | 0.03 | 11.90 | 84.05 | 83.85 | -12.41 | -9.08 | 0.89 | 9.05 | b |
| Cl* Melotte 111 AV 1737 | 12:27:48.29 | +28:11:39.8 | | 0.66 | 0.03 | 9.65 | 0.03 | 5.09 | 0.70 | 0.03 | 12.23 | 81.78 | 81.59 | -13.37 | -9.36 | -0.08 | 8.60 | b |
| Cl* Melotte 111 AV 1826 | 12:28:56.43 | +26:32:57.4 | | 0.92 | 0.03 | 10.75 | 0.02 | 6.12 | 0.95 | 0.02 | 11.86 | 84.35 | 84.15 | -12.88 | -9.24 | 1.30 | 9.37 | d |
| Cl* Melotte 111 AV 1889 | 12:29:42.15 | +28:37:14.6 | NM | 0.82 | 0.03 | 11.28 | 0.02 | 0.86 | 0.90 | 0.02 | 0.79 | 1266.52 | 1216.11 | -7.55 | -8.49 | 61.33 | 16.05 | b |
| 2MASS J12332002+2224234 | 12:33:20.01 | +22:24:23.3 | | 0.76 | 0.03 | 10.27 | 0.03 | 5.65 | 0.82 | 0.03 | 11.92 | 83.93 | 83.73 | -10.30 | -7.38 | -1.81 | 8.33 | b |
| 2MASS J12334186+2914016 | 12:33:41.88 | +29:14:01.7 | NM | 1.08 | 0.04 | 11.48 | 0.03 | 6.11 | 1.19 | 0.03 | 8.37 | 119.47 | 119.07 | 21.17 | -4.94 | -8.03 | 16.88 | b |
| Cl* Melotte 111 AV 2177 | 12:33:42.12 | +25:56:34.0 | | 0.85 | 0.02 | 10.53 | 0.02 | 5.76 | 0.88 | 0.02 | 11.09 | 90.15 | 89.920 | -16.38 | -9.74 | -1.37 | 8.42 | b |
| Cl* Melotte 111 MGM 427 | 12:33:54.22 | +27:08:04.7 | NM | 1.02 | 0.02 | 11.58 | 0.03 | 0.74 | 0.99 | 0.02 | 0.65 | 1547.39 | 1469.82 | -14.81 | -4.59 | 12.81 | 16.54 | b |
| 2MASS J12381145+2333223 | 12:38:11.47 | +23:33:22.2 | | 1.45 | 0.01 | 13.75 | 0.01 | 9.05 | 1.82 | 0.03 | 11.45 | 87.32 | 87.10 | -12.04 | -10.34 | -0.84 | 14.46 | b |
| 2MASS J12394200+2134578 | 12:39:41.99 | +21:34:58.0 | NM | 1.09 | 0.04 | 11.58 | 0.03 | -2.05 | 1.24 | 0.03 | 0.09 | 11587.57 | 5266.94 | -7.07 | -4.28 | 164.51 | 9.57 | b |
| 2MASS J12423510+4105276 | 12:42:35.14 | +41:05:27.7 | NM | 1.04 | 0.02 | 11.83 | 0.01 | 0.94 | 1.07 | 0.02 | 0.63 | 1576.48 | 1503.11 | -7.39 | -4.33 | 15.86 | 11.76 | b |
| 2MASS J12430953+2447052 | 12:43:09.53 | +24:47:05.2 | NM | 1.46 | 0.02 | 13.88 | 0.03 | 9.01 | 2.06 | 0.02 | 10.55 | 94.78 | 94.54 | 12.12 | -12.52 | -1.07 | 2.77 | b |
| 2MASS J12452334+4251041 | 12:45:23.35 | +42:51:04.4 | NM | 1.54 | 0.02 | 14.38 | 0.03 | 9.70 | 2.43 | 0.02 | 11.56 | 86.49 | 86.28 | -21.00 | -12.51 | | 12.05 | b |
| 2MASS J12490041+2521356 | 12:49:00.42 | +25:21:35.6 | | 1.20 | 0.02 | 12.03 | 0.02 | 7.49 | 1.37 | 0.02 | 12.29 | 81.34 | 81.16 | -12.71 | -8.69 | | 12.27 | b |
| 2MASS J12493043+2532109 | 12:49:30.43 | +25:32:11.1 | NM | 1.12 | 0.02 | 11.65 | 0.02 | 1.75 | 1.14 | 0.02 | 1.02 | 979.84 | 952.50 | -14.24 | -11.05 | -21.31 | 19.51 | b |
| 2MASS J12500170+2103121 | 12:50:01.70 | +21:03:12.1 | NM | 0.96 | 0.02 | 11.25 | 0.02 | 4.46 | 0.98 | 0.02 | 4.42 | 226.30 | 228.48 | -12.32 | 7.98 | -24.86 | (6.67) | b |
| 2MASS J12531465+2403135 | 12:53:14.67 | +24:03:13.6 | NM | 1.05 | 0.04 | 12.09 | 0.03 | 1.12 | 1.16 | 0.03 | 0.62 | 1625.96 | 1546.16 | 8.17 | -17.81 | -70.74 | 19.02 | b |
| 2MASS J12573686+2858448 | 12:57:36.86 | +28:58:44.7 | | 0.72 | 0.03 | 10.24 | 0.03 | 5.44 | 0.80 | 0.03 | 10.90 | 91.74 | 91.50 | -11.57 | -5.34 | -0.92 | 7.94 | b |
| 2MASS J12592775+1941150 | 12:59:27.75 | +19:41:15.1 | NM | 1.17 | 0.02 | 11.83 | 0.02 | 1.45 | 1.17 | 0.02 | 0.81 | 1231.36 | 1186.91 | -5.05 | -12.81 | -59.56 | 11.24 | b |
| 2MASS J13054399+2003214 | 13:05:43.99 | +20:03:21.4 | NM | 1.03 | 0.02 | 11.20 | 0.03 | 1.18 | 1.03 | 0.02 | 0.96 | 1041.05 | 1010.34 | 2.32 | -5.46 | -18.84 | 11.04 | b |

Parameters shown in this table in order of appearance: name of the stars, taken from the SIMBAD astronomical database; coordinates ($\alpha$ and $\delta$); membership notes (NM: non-member); OSN photometry with errors, B − V, V, V − I, except for the star Cl* Melotte 111 AV 1431 for which we took photometry from Kharchenko (2001); calibrated magnitude $M_v$, obtained using distances by Bailer-Jones et al. (2018); parallaxes by *Gaia* DR2 (Plx); distances taken from *Gaia* DR2 parallaxes by the inverse of the parallax values ($D_{inv.Gaia}$) and by the Bayesian analysis of Bailer-Jones et al. (2018) ($D_{BJ.Gaia}$); proper motions and radial velocities taken from *Gaia* DR2, and periods taken from literature (see *Notes*). The periods in between "()" were multiplied by two by Collier Cameron et al. (2009).

**Notes.**

[a] Photometry from Kharchenko (2001).

[b] Period from Collier Cameron et al. (2009).

[b*] Period from Collier Cameron et al. (2009), chosen between the values given by Collier Cameron et al. (2009) and Terrien et al. (2014).

[c] Period from Marilli et al. (1997).

[d] Mean value of the periods from Collier Cameron et al. (2009) and Terrien et al. (2014).

## 3.4 Praesepe

### 3.4.1 Characteristics of the cluster

Praesepe (M 44, NGC 2632), also known as "The Beehive", is a cluster rich in stars located in the constellation Cancer, with centre coordinates $\alpha_{J2000}$ : $+08^h40^m19.2^s$, $\delta_{J2000}$ : $+19°40'48''$ (Gaia Collaboration et al. 2018a).

#### Distance and age

Praesepe has been located at an average distance of between ~150 pc and ~200 pc (for example, Vandenberg & Bridges 1984; Pinsonneault et al. 1998; Sanner & Geffert 2001; Kharchenko et al. 2005; van Leeuwen 1999, 2009; Gaia Collaboration et al. 2018a; Lodieu et al. 2019a). Despite the differences in the results of these studies, the distance obtained by Lodieu et al. (2019a) from *Gaia* parallaxes, with a value of 187.35 ± 3.89 pc, agrees with that provided by Hipparcos (188.0 pc ± 14 pc; van Leeuwen 1999) and with that obtained by Gaia Collaboration et al. (2018a), 186.18 pc ± 0.10 pc. However, there is a slight difference of $1\sigma$ with respect to that calculated by van Leeuwen (2009), who obtained a distance of 181.5 ± 6.0 pc in his second reduction of the Hipparcos data.

In spite of the discrepancies in the distance value, this is currently considered a fairly well defined parameter, in contrast to the age of Praesepe, which continues to be the centre of debate. Over the years, isochrone studies have been carried out for this cluster (for example, Allen 1973; Sanner & Geffert 2001; Bonatto et al. 2004; Kharchenko et al. 2005; Fossati et al. 2008; Bell et al. 2014; Gossage et al. 2018) and its age has also been derived using the gyrochronology technique (for example, Delorme et al. 2011a). This is an intermediate-age cluster, comparable to Coma Berenices and Hyades, and much older than $\alpha$ Per and Pleiades. Values of its age have been estimated between 500 Myr and 1.5 Gyr. However, the most commonly accepted range is of 590-790 Myr.
The age we take in this study is the one estimated in the most recent gyrochronology study (Angus et al. 2019), which corresponds to a value of ~650 Myr.

#### Membership

This cluster presents fewer difficulties than others when it comes to discerning between members and non-members. This is due to the high value of the proper motions with respect to the field stars ($\mu_\alpha\ cos\delta$, $\mu_\delta$) ~ (-36.047 ± 0.110, -12.917 ± 0.066) mas $yr^{-1}$ (Gaia Collaboration et al. 2018a), and to the fact that it is far from the galactic plane (b~ 32°, Kharchenko et al. 2009), resulting in a low value of interstellar extinction (~0.027; Gaia Collaboration et al. 2018a).

Numerous studies have been carried out in search of Praesepe members, the first of which was carried out by Klein Wassink (1924, 1927). It is also worth mentioning the great study by Kraus & Hillenbrand (2007), prior to the GAIA era, which studied an area of 300 $deg^2$ and found 1100 candidate members of Praesepe. Lodieu et al. (2019a) consider 1847 possible members and 721 highly probable members at a distance equal to or less than the tidal radius (10.7 pc).

### 3.4.2 Our sample for Praesepe

Starting with the table with rotation periods compiled from the literature, as we have done previously and which we describe below, we have selected those that have photometry in $BVI_c$ bands with errors below or equal to 0.04 mag.We have gathered a total of 197 candidate members of Praesepe of spectral types from A5 to M3.7 that meet these criteria, of which 141 range from early-G to mid-M spectral types. In Section 3.4.2, we will verify their membership.

#### Periods compiled from the literature

There is a total of 905 stars (mainly between F and M spectral types) with rotation periods available in the literature. The rotation periods come from the following studies:

- Douglas et al. (2014) (D14) is a study with a prior compilation of 136 periods from the literature, with data from: Scholz et al. (2011), which analysed light curves obtained on the Isaac Newton telescope (Observatorio Roque de los Muchachos, La Palma) and obtained 49 periods; Delorme et al. (2011b), who monitored $\sim$ 70 members with the superWASP telescope network (Pollacco et al. 2006) and obtained 52 periods; and Agüeros et al. (2011) who, using "The Palomar Transient Factory" telescope (PTF, Law et al. 2009; Rau et al. 2009), monitored $\sim$ 500 members and obtained 40 periods.
  The compilation from this study is not available in the article link, so S. Douglas sent it to me by private communication.
- Kovács et al. (2014) (K14), analysed photometric time series from the HATNet project for 381 objects of Praesepe, and obtained 180 rotation periods.
- Douglas et al. (2017) (D17), analysing K2 curves, studied 794 stars and obtained 677 rotation periods of candidate members of Praesepe. They also carried out a comparative study of their results with those obtained from the literature (that is, D14 and K14 included). D17 reached the conclusion that 75% of their measurements were consistent with previous studies, with a difference of up to 5%, of which half differed by $\lesssim$ 2 %. Where there were differences >10%, they selected the periods they considered the most reliable.
- At a later date, Rebull et al. (2017) (R17), also analysed K2 light curves (a total of 941) and obtained rotation periods for 809 stars of Praesepe. Like D17, they compared their measurements with the periods from the literature (also D14 and K14 included) and confirmed that in the case of measurements similar to their own, there was a mean fractional difference between their periods and those from the literature ($(P_{lit} - P_{R17})/P_{R17}$) in the range of 0.36% and 2.7%. Regarding periods with significant differences compared to their own, they concluded that their results were more reliable.

As we have seen, once D17 had compared their results with those from the literature, they did consider that the latter were more reliable than those obtained by them through the K2 curves, and so opted for the literature results. R17, in turn, concluded that all their measurements were correct. Therefore, if we have stars with periods both from D17 and R17, in the cases where the

measurement given by D17 is from the literature, we choose R17. In contrast, if D17 selected the period from K2 light curves, then we provide the mean of the values from the two studies. We took this decision having calculated the mean fractional difference between the periods obtained by D17 and R17 from K2 light curves and deriving differences in the range of 0.04% - 5.5%.

### $BVR_cI_c$ photometry

In our sample of 197 stars, 189 have measurements that come from the literature and 8 from the observations made at the OSN. Below we describe the origin of this compiled photometry.

#### Photometry compiled from the literature

Although we have found three studies that provide photometry in any of the $BVI_c$ bands for 391 of the 905 stars with rotation periods, it was not possible to find stars with homogeneous measurements in the three filters. Two of these studies correspond to the aforementioned Kharchenko (2001) and APASS DR9, which provide $B-V$, $V$, with mean errors: e$B-V$ = 0.085 mag, e$V$ = 0.038 mag and e$B-V$ = 0.169 mag, e$V$ = 0.085 mag, respectively. The third study is that carried out by An et al. (2007), with measurements in $B-V$, $V$ and $V-I_c$ and errors within the established range (the catalogue is not available in the article, but Deokkeun An sent it via private communication). However, their study is also a compilation of photometry from the literature, in which they gather $B-V$ and $V$ data from Johnson (1952), Dickens et al. (1968), and Castelaz et al. (1991), and gather $V-I_c$ values from measurements by Mendoza (1967), Castelaz et al. (1991), Upgren et al. (1979), Weis (1981), Stauffer (1982a), and Mermilliod et al. (1990). Aside from the aforementioned inhomogeneity of their resulting table, they have had to do a fitting in which they added the quantities +0.002 and +0.006 to $V$ and $B-V$, respectively, to the data from Dickens et al. (1968), so that their system of filters would fit with that from Johnson (1952). Regarding $V-I_c$, because some studies had given $I_K$ – in other words, in the Kron system – they used the transformation equation from Bessell & Weis (1987) to obtain this magnitude in the Cousins system. Despite the inhomogeneity, the data from the literature that we have selected correspond to this last study, in which they provide $BVI_c$ photometry and whose errors are within the established range, unlike the measurements from Kharchenko (2001) and APASS DR9. In Table 3.4.2 of the sample, we have not been able to show the specific origin of every photometric measurement, because the compilation provided by Deokkeun An did not include this information.

Once we removed objects classified in Simbad database as spectral types with luminosity class different than V, we have selected 189 objects with photometry from An et al. (2007) with mean errors: e$B-V$ = 0.006 mag, e$V$ $\sim$ 0.009 mag and e$V-I_c$ $\sim$ 0.009 mag.

#### Photometry obtained at the OSN

At the OSN, we have observed 19 stars of Praesepe, from spectral type K1 to type M4.5, which in principle did not have $BVI_c$ measurements in the literature with the required errors. The observations were made on two consecutive nights in March 2016 and on one night in May 2017. Of these three nights, one was not completely photometric. This was due to the presence of cirrus a

few hours after the start of the observation. It appears not to have affected the measurements of the standard stars but it may have affected the Praesepe stars' data, although it is worth pointing out that the signal to noise for these stars is greater than 100. For the 19 stars, we obtained values of $B-V$, $V$ and $V-I_c$, with the addition of $V-R_c$ for one of them. For 11 of the 19 objects observed, the errors of ourmeasurements surpasses the limit value stipulated. For the other 8, which are spectral types between K1 and M2.8, the mean of the upper limit errors is 0.031 mag, 0.022 mag and 0.024 mag for $B-V$, $V$ and $V-I_c$, respectively. The 11 stars with errors greater than 0.04 mag are not shown in the table of the sample, but we will show the photometry values that we obtained at the OSN in Appendix B.

We noticed that one of our stars (Cl* NGC 2632 JC 141), with photometry obtained at the OSN, was included in the list from An et al. (2007), and apparently with errors that are lower than 0.04 mag in the three $BVI_c$ bands. This has enabled me to verify that the two results are quite similar, with differences for $B-V$, $V$ and $V-I_c$ of 0.014 mag, 0.007 mag and 0.046 mag, respectively. In $V-I_c$, the difference is greater than 0.04 mag, but, due to the fact that our measurements are homogeneous and are not derived from transformations between photometric systems, we will use our data for this object.

### Membership of our sample

The 905 stars of our selection, compiled with rotation periods, have been considered probable members of the cluster by one or more of the following studies: Klein Wassink (1927), Jones & Cudworth (1983), Jones & Stauffer (1991), Adams et al. (2002), Kraus & Hillenbrand (2007), Baker et al. (2010), Boudreault et al. (2012), Khalaj & Baumgardt (2013), Wang et al. (2014).

In the same way as in previous sections, to avoid including non-members of the cluster in our study, we use the tidal radius of Praesepe calculated by Lodieu et al. (2019a), with a value of 10.7 pc. We take as highly probable members those that are located at a distance to the centre of the cluster that is less than this value, possible members those that between 10.7 pc and 3 times its value (32.1 pc), unlikely members those that are located at a distance greater than 32.1 pc, and non-members those stars discarded by Lodieu et al. (2019a). We will also indicate which stars do not have membership data from Lodieu et al. (2019a) due to a lack of measurements of distances in *Gaia* DR2.

For our selected sample of 197 stars with $BVI_c$ photometry and errors less than 0.04 mag:137 are highly probable members, 21 are possible members, 4 are unlikely, 27 non-members and 8 without data from Lodieu et al. (2019a). We should mention that one of the stars observed at the OSN with upper limit errors of $\lesssim$0.04 mag (Cl* NGC 2632 JC 141), is in the category of unlikely member.

### Table with our sample for Praesepe

In this section we show the main collected data for our sample of 197 stars of Praesepe cluster.

| *Name* | $\alpha_{J2000}$ (h:m:s) | $\delta_{J2000}$ (°:′:″) | *Notes memb.* | $B-V$ (mag) | e$B-V$ (mag) | $V$ (mag) | e$V$ (mag) | $M_v$ (mag) | $V-Ic$ (mag) | e$V-Ic$ (mag) | $Ks$ (mag) | e$Ks$ (mag) | *Notes phot.BVI* | *Date Obs.OSN* | $D_{BJ,Gaia}$ (pc) | *Period* (days) | SD *PeriodMean* | *Notes period* | *Spect. Types* |
|---|---|---|---|---|---|---|---|---|---|---|---|---|---|---|---|---|---|---|---|
| ”HIP 42106” | 08:35:00 | +21:05:49 | 1.0 | 0.7 | 0.004 | 11.19 | 0.007 | 4.884 | 0.708 | 0.011 | 9.684 | 0.02 | DE07 | | 182.476 | 8.173 | | K14 | F8.9 |
| ”Cl* NGC 2632 JS 103” | 08:35:55 | +18:08:57 | 1.0 | 0.62 | 0.004 | 10.89 | 0.007 | 4.491 | 0.65 | 0.011 | 9.445 | 0.026 | DE07 | | 190.466 | 7.03 | | K14 | F7.2 |
| ”2MASS J08355696+2049346” | 08:35:57 | +20:49:35 | 2.0 | 0.79 | 0.004 | 11.85 | 0.007 | 5.457 | 0.911 | 0.011 | 9.828 | 0.02 | DE07 | | 189.937 | 1.21 | 0.0 | M | K0V: |
| ”Cl* NGC 2632 JS 116” | 08:36:14 | +19:37:17 | 1.0 | 0.98 | 0.009 | 12.57 | 0.01 | 6.208 | 0.969 | 0.007 | 10.363 | 0.019 | DE07 | | 187.266 | 10.82 | | R17 | K2.1 |
| ”TYC 1395-1646-1 ” | 08:36:16 | +19:32:31 | 0.0 | 0.9 | 0.004 | 11.585 | 0.007 | 5.226 | 0.91 | 0.011 | 9.52 | 0.019 | DE07 | | | 9.249 | | R17 | G9.7 |
| ”Cl* NGC 2632 JS 133” | 08:36:28 | +20:13:43 | 1.0 | 0.95 | 0.009 | 12.65 | 0.01 | 6.276 | 0.998 | 0.007 | 10.441 | 0.019 | DE07 | | 188.242 | 10.334 | | R17 | K1.3 |
| ”BD+19 2045” | 08:36:30 | +18:57:57 | 4.0 | 0.457 | 0.004 | 9.451 | 0.008 | 2.71 | 0.551 | 0.006 | 8.299 | 0.021 | DE07 | | 222.916 | 9.174 | | R17 | F5* |
| ”Cl* NGC 2632 JS 142” | 08:36:40 | +20:36:36 | 1.0 | 0.8 | 0.004 | 11.86 | 0.007 | 5.481 | 0.833 | 0.011 | 10.077 | 0.019 | DE07 | | 188.67 | 8.965 | 0.106 | M | K0V: |
| ”Cl* NGC 2632 JS 146” | 08:36:46 | +20:07:26 | 1.0 | 0.762 | 0.004 | 11.653 | 0.007 | 5.361 | 0.753 | 0.011 | 9.938 | 0.019 | DE07 | | 181.281 | 9.048 | | R17 | G5.0 |
| ”HD 73045” | 08:36:48 | +18:52:58 | 4.0 | 0.316 | 0.004 | 8.647 | 0.008 | 1.405 | 0.333 | 0.006 | 7.944 | 0.034 | DE07 | | 280.813 | 13.011 | | R17 | F0* |
| ”HD 73081” | 08:37:02 | +19:36:17 | 2.0 | 0.466 | 0.004 | 9.217 | 0.008 | 2.731 | 0.527 | 0.006 | 8.062 | 0.02 | DE07 | | 198.202 | 4.413 | | R17 | F6V |
| ”Cl* NGC 2632 S 12” | 08:37:11 | +19:48:13 | 1.0 | 0.71 | 0.004 | 11.29 | 0.007 | 4.924 | 0.714 | 0.011 | 9.686 | 0.02 | DE07 | | 187.565 | 8.242 | | R17 | G |
| ”Cl* NGC 2632 S 13” | 08:37:18 | +19:41:56 | 1.0 | 0.73 | 0.004 | 11.44 | 0.007 | 5.092 | 0.745 | 0.011 | 9.802 | 0.019 | DE07 | | 186.077 | 8.844 | | D14 | G5V |
| ”EPIC 211995288” | 08:37:22 | +20:10:37 | 1.0 | 0.73 | 0.004 | 11.4 | 0.007 | 5.002 | 0.675 | 0.011 | 9.803 | 0.019 | DE07 | | 190.404 | 7.826 | | R17 | G |
| ”BD+19 2050” | 08:37:28 | +19:09:44 | 2.0 | 0.43 | 0.004 | 9.5 | 0.008 | 3.319 | 0.496 | 0.006 | 8.4 | 0.021 | DE07 | | 172.27 | 0.84 | | R17 | F6V |
| ”BD+20 2130” | 08:37:28 | +19:33:45 | 2.0 | 0.56 | 0.004 | 9.79 | 0.008 | 3.22 | 0.598 | 0.006 | 8.464 | 0.02 | DE07 | | 206.049 | 3.619 | 0.001 | M | F6V |
| ”Cl* NGC 2632 S 16” | 08:37:28 | +19:37:03 | 1.0 | 0.775 | 0.004 | 11.65 | 0.007 | 5.398 | 0.846 | 0.011 | 9.806 | 0.018 | DE07 | | 177.968 | 8.873 | | R17 | G8V |
| ”Cl* NGC 2632 JC 106” | 08:37:33 | +18:39:15 | 1.0 | 0.63 | 0.004 | 10.66 | 0.007 | 4.354 | 0.598 | 0.011 | 9.283 | 0.022 | DE07 | | 182.451 | 7.314 | | R17 | G0.0 |
| ”Cl* NGC 2632 VL 465” | 08:37:36 | +19:25:55 | 0.0 | 1.23 | 0.009 | 13.67 | 0.01 | 7.311 | 1.413 | 0.007 | 10.603 | 0.024 | DE07 | | | 11.569 | | R17 | K5V* |
| ”V* BR Cnc” | 08:37:41 | +19:31:06 | 1.0 | 0.238 | 0.004 | 8.262 | 0.008 | 1.889 | 0.279 | 0.006 | 7.662 | 0.018 | DE07 | | 188.155 | 0.087 | | R17 | F0Vn |
| ”BD+19 2052” | 08:37:42 | +19:08:01 | 1.0 | 0.48 | 0.004 | 9.87 | 0.008 | 3.521 | 0.559 | 0.006 | 8.577 | 0.02 | DE07 | | 186.108 | 3.069 | 0.012 | M | F4V |
| ”Cl* NGC 2632 JC 112” | 08:37:46 | +19:35:57 | 1.0 | 0.904 | 0.009 | 12.323 | 0.01 | 6.035 | 0.925 | 0.007 | 10.244 | 0.018 | DE07 | | 180.948 | 9.42 | | R17 | K1V |
| ”Cl* NGC 2632 S 25” | 08:37:47 | +19:26:18 | 1.0 | 0.58 | 0.004 | 10.66 | 0.007 | 4.304 | 0.613 | 0.011 | 9.276 | 0.024 | DE07 | | 186.737 | 5.934 | | R17 | F9V |
| ”Cl* NGC 2632 JC 114” | 08:37:47 | +19:06:25 | 1.0 | 0.907 | 0.009 | 12.28 | 0.01 | 5.96 | 0.911 | 0.007 | 10.202 | 0.018 | DE07 | | 183.67 | 9.361 | | R17 | G8.6 |
| ”Cl* NGC 2632 S 27” | 08:37:50 | +19:53:29 | 2.0 | 0.84 | 0.004 | 11.41 | 0.007 | 5.796 | 0.916 | 0.011 | 9.326 | 0.02 | DE07 | | 132.698 | 6.789 | | R17 | G8V |
| ”Cl* NGC 2632 S 29” | 08:37:52 | +19:59:14 | 1.0 | 0.676 | 0.004 | 11.27 | 0.007 | 4.882 | 0.722 | 0.011 | 9.689 | 0.02 | DE07 | | 189.537 | 7.933 | | R17 | G5V |
| ”Cl* NGC 2632 JC 117” | 08:37:52 | +19:24:53 | 2.0 | 0.98 | 0.009 | 12.92 | 0.01 | 6.286 | 1.017 | 0.007 | 10.621 | 0.024 | DE07 | | 212.224 | 17.47 | 0.015 | M | K2.0 |
| ”Cl* NGC 2632 JC 118” | 08:37:57 | +19:14:10 | 1.0 | 0.793 | 0.004 | 11.84 | 0.007 | 5.496 | 0.811 | 0.011 | 10.038 | 0.02 | DE07 | | 185.676 | 9.082 | | R17 | G8V |
| ”BD+17 1894” | 08:38:08 | +17:03:02 | 1.0 | 0.44 | 0.004 | 9.77 | 0.008 | 3.442 | 0.477 | 0.006 | 8.704 | 0.021 | DE07 | | 184.368 | 0.614 | | R17 | F2 |
| ”Cl* NGC 2632 JS 212” | 08:38:08 | +20:26:22 | 1.0 | 0.782 | 0.004 | 11.718 | 0.007 | 5.372 | 0.769 | 0.011 | 9.932 | 0.019 | DE07 | | 185.895 | 9.172 | | R17 | G6.5 |
| ”Cl* NGC 2632 JS 211” | 08:38:08 | +19:59:16 | 1.0 | 0.913 | 0.009 | 12.095 | 0.01 | 5.804 | 0.959 | 0.007 | 9.898 | 0.02 | DE07 | | 181.184 | 8.976 | | R17 | K1.2 |
| ”Cl* NGC 2632 S 38” | 08:38:14 | +19:21:55 | 4.0 | 0.7 | 0.004 | 10.9 | 0.007 | 5.343 | 0.755 | 0.011 | 9.188 | 0.02 | DE07 | | 129.26 | 7.226 | | R17 | G4V* |
| ”Cl* NGC 2632 JS 220” | 08:38:15 | +20:34:04 | 1.0 | 0.72 | 0.004 | 11.45 | 0.007 | 5.121 | 0.761 | 0.011 | 9.717 | 0.018 | DE07 | | 184.445 | 9.395 | | R17 | G4.5 |
| K2-100 | 08:38:24 | +20:06:22 | 1.0 | 0.583 | 0.004 | 10.553 | 0.007 | 4.171 | 0.621 | 0.011 | 9.182 | 0.018 | DE07 | | 188.959 | 4.255 | | R17 | G0V |
| ”Cl* NGC 2632 JC 125” | 08:38:30 | +19:51:45 | 1.0 | 1.257 | 0.015 | 14.027 | 0.015 | 7.634 | 1.461 | 0.013 | 10.931 | 0.019 | DE07 | | 189.897 | 11.78 | | R17 | K5.3 |

(Continued).

| *Name* | $\alpha_{J2000}$ (h:m:s) | $\delta_{J2000}$ (°:′:″) | *Notes memb.* | $B-V$ (mag) | e$B-V$ (mag) | $V$ (mag) | e$V$ (mag) | $M_v$ (mag) | $V-Ic$ (mag) | e$V-Ic$ (mag) | $Ks$ (mag) | e$Ks$ (mag) | *Notes phot.BVI* | *Date Obs.OSN* | $D_{BJ.Gaia}$ (pc) | *Period* (days) | SD *PeriodMean* | *Notes period* | *Spect. Types* |
|---|---|---|---|---|---|---|---|---|---|---|---|---|---|---|---|---|---|---|---|
| "V* CY Cnc" | 08:38:38 | +19:59:23 | 1.0 | 0.213 | 0.004 | 8.139 | 0.008 | 1.813 | 0.24 | 0.006 | 7.61 | 0.018 | DE07 | | 184.183 | 0.051 | | R17 | F0V |
| "Cl* NGC 2632 JC 132" | 08:38:41 | +19:25:18 | 1.0 | 1.43 | 0.015 | 14.63 | 0.015 | 8.273 | 1.654 | 0.013 | 11.188 | 0.022 | DE07 | | 186.845 | 14.384 | 0.093 | M | K7V |
| "Cl* NGC 2632 JS 247" | 08:38:46 | +20:34:36 | 3.0 | 0.91 | 0.009 | 12.44 | 0.01 | 6.076 | 0.949 | 0.007 | 10.313 | 0.02 | DE07 | | 187.388 | 9.368 | | R17 | K |
| "HD 73397" | 08:38:47 | +19:30:03 | 1.0 | 0.319 | 0.004 | 8.993 | 0.008 | 2.591 | 0.384 | 0.006 | 8.221 | 0.02 | DE07 | | 190.684 | 0.512 | | R17 | F1V |
| "Cl* NGC 2632 S 51" | 08:38:50 | +20:04:03 | 1.0 | 0.603 | 0.004 | 10.805 | 0.007 | 4.491 | 0.621 | 0.011 | 9.367 | 0.018 | DE07 | | 183.154 | 7.175 | 1.789 | M | G0V |
| "Cl* NGC 2632 JC 137" | 08:38:54 | +19:34:17 | 1.0 | 1.32 | 0.015 | 14.21 | 0.015 | 7.916 | 1.524 | 0.013 | 10.965 | 0.022 | DE07 | | 181.48 | 13.635 | 0.487 | M | K6V |
| "Cl* NGC 2632 JC 138" | 08:38:55 | +19:17:02 | 1.0 | 1.52 | 0.015 | 15.96 | 0.015 | 9.623 | 2.14 | 0.013 | 11.741 | 0.018 | DE07 | | 185.138 | 18.154 | 0.062 | M | M0.9 |
| "Cl* NGC 2632 JS 259" | 08:38:57 | +20:10:53 | 2.0 | 1.3 | 0.009 | 13.953 | 0.01 | 7.723 | 1.514 | 0.007 | 10.716 | 0.02 | DE07 | | 176.183 | 11.688 | | R17 | K6V |
| "Cl* NGC 2632 JC 140" | 08:38:58 | +19:36:49 | 4.0 | 1.17 | 0.009 | 13.79 | 0.01 | 7.083 | 1.249 | 0.007 | 11.037 | 0.022 | DE07 | | 219.446 | 13.395 | | R17 | K3.9 |
| "Cl* NGC 2632 JC 141" | 08:39:02 | +19:19:34 | 3.0 | 0.916 | 0.025 | 12.383 | 0.02 | 6.08 | 0.923 | 0.026 | 10.259 | 0.019 | OSN | 07/05/2017 | 182.218 | 9.764 | | R17 | K1V |
| "V* EO Cnc" | 08:39:03 | +20:02:38 | 1.0 | 1.372 | 0.015 | 14.423 | 0.015 | 8.136 | 1.635 | 0.013 | 11.051 | 0.02 | DE07 | | 180.921 | 13.934 | 0.532 | M | K7.5 |
| "Cl* NGC 2632 JC 144" | 08:39:04 | +19:31:22 | 1.0 | 1.21 | 0.009 | 13.79 | 0.01 | 7.414 | 1.346 | 0.007 | 10.857 | 0.016 | DE07 | | 188.454 | 12.631 | | R17 | K5V |
| "HD 73429" | 08:39:05 | +20:07:02 | 1.0 | 0.406 | 0.004 | 9.378 | 0.008 | 3.004 | 0.489 | 0.006 | 8.413 | 0.027 | DE07 | | 188.28 | 0.786 | | R17 | F5V |
| "V* BS Cnc" | 08:39:09 | +19:35:33 | 2.0 | 0.253 | 0.004 | 8.502 | 0.008 | 1.974 | 0.31 | 0.006 | 7.875 | 0.026 | DE07 | | 202.126 | 0.059 | | R17 | A9V |
| "V* AX Cnc" | 08:39:10 | +19:46:59 | 1.0 | 1.488 | 0.025 | 16.087 | 0.023 | 9.711 | 2.398 | 0.023 | 11.347 | 0.02 | OSN | 01/03/2016 | 188.464 | 4.379 | | R17 | M2.0 |
| "HIP 42436" | 08:39:11 | +18:10:33 | 1.0 | 0.56 | 0.004 | 10.25 | 0.007 | 3.95 | 0.592 | 0.011 | 8.994 | 0.02 | DE07 | | 182.006 | 4.198 | | K14 | F7.5 |
| "TYC 1395-1323-1" | 08:39:12 | +19:06:56 | 1.0 | 0.572 | 0.004 | 10.59 | 0.007 | 4.241 | 0.613 | 0.011 | 9.258 | 0.018 | DE07 | | 186.118 | 5.868 | | R17 | F9V |
| "Cl* NGC 2632 S 70" | 08:39:15 | +20:12:39 | 4.0 | 0.704 | 0.004 | 11.31 | 0.007 | 5.011 | 0.738 | 0.011 | 9.649 | 0.02 | DE07 | | 181.892 | 8.123 | | R17 | G4V* |
| "Cl* NGC 2632 JS 706" | 08:39:15 | +19:43:32 | 2.0 | 1.493 | 0.028 | 17.08 | 0.023 | 10.966 | 2.621 | 0.024 | 12.015 | 0.021 | OSN | 01/03/2016 | 167.022 | 0.812 | | D14/S11 | M3.7 |
| "Cl* NGC 2632 JS 280" | 08:39:16 | +20:04:14 | 0.0 | 1.475 | 0.015 | 14.95 | 0.015 | 8.591 | 2.059 | 0.013 | 10.867 | 0.02 | DE07 | | | 7.964 | | R17 | M0V |
| "Cl* NGC 2632 ANM 748" | 08:39:17 | +17:27:46 | 1.0 | 0.77 | 0.004 | 11.69 | 0.007 | 5.362 | 0.795 | 0.011 | 9.965 | 0.02 | DE07 | | 184.339 | 8.981 | | R17 | G8V* |
| "Cl* NGC 2632 JC 155" | 08:39:17 | +19:47:43 | 1.0 | 1.479 | 0.026 | 16.552 | 0.023 | 10.226 | 2.224 | 0.023 | 12.077 | 0.022 | OSN | 01/03/2016 | 184.15 | 19.585 | | R17 | M1.4 |
| "Cl* NGC 2632 JC 158" | 08:39:22 | +19:51:40 | 1.0 | 0.943 | 0.009 | 12.538 | 0.01 | 6.166 | 0.962 | 0.007 | 10.369 | 0.02 | DE07 | | 188.088 | 12.539 | | R17 | K0.0 |
| "BD+19 2061" | 08:39:25 | +19:27:34 | 1.0 | 0.583 | 0.004 | 10.503 | 0.007 | 4.151 | 0.617 | 0.011 | 8.997 | 0.018 | DE07 | | 186.396 | 3.94 | | R17 | F7V |
| "Cl* NGC 2632 KW 184" | 08:39:29 | +19:28:25 | 1.0 | 0.903 | 0.004 | 11.637 | 0.007 | 5.317 | 0.931 | 0.011 | 9.533 | 0.021 | DE07 | | 183.691 | 10.175 | | R17 | K0V |
| "Cl* NGC 2632 JC 163" | 08:39:29 | +19:47:12 | 2.0 | 0.99 | 0.009 | 12.623 | 0.01 | 6.133 | 1.12 | 0.007 | 10.065 | 0.018 | DE07 | | 198.615 | 13.712 | | R17 | K3.0 |
| "BD+20 2146" | 08:39:30 | +20:04:09 | 4.0 | 0.65 | 0.004 | 10.335 | 0.007 | 3.947 | 0.648 | 0.011 | 8.807 | 0.018 | DE07 | | 189.485 | 7.22 | | R17 | F8* |
| "Cl* NGC 2632 JS 298" | 08:39:32 | +19:24:18 | 1.0 | 1.577 | 0.038 | 17.79 | 0.024 | 11.537 | 2.576 | 0.024 | 12.725 | 0.03 | OSN | 01/03/2016$^{++}$ | 178.092 | 9.162 | | R17 | M2.8 |
| "Cl* NGC 2632 S 79" | 08:39:36 | +18:52:37 | 1.0 | 0.59 | 0.004 | 10.74 | 0.007 | 4.421 | 0.644 | 0.011 | 9.329 | 0.02 | DE07 | | 183.537 | 6.684 | | R17 | G |
| "Cl* NGC 2632 JC 166" | 08:39:36 | +19:15:38 | 1.0 | 1.35 | 0.015 | 14.33 | 0.015 | 8.058 | 1.577 | 0.013 | 11.01 | 0.018 | DE07 | | 179.62 | 17.68 | | D17 | K7V |
| "Cl* NGC 2632 JC 165" | 08:39:36 | +19:29:08 | 1.0 | 1.48 | 0.015 | 15.16 | 0.015 | 8.821 | 1.807 | 0.013 | 11.391 | 0.02 | DE07 | | 185.237 | 16.187 | | R17 | M0V |
| "Cl* NGC 2632 JC 167" | 08:39:37 | +19:48:58 | 1.0 | 1.51 | 0.015 | 15.2 | 0.015 | 8.859 | 1.879 | 0.013 | 11.386 | 0.018 | DE07 | | 185.476 | 16.052 | 0.026 | M | K7.8 |
| "TYC 1395-602-1" | 08:39:38 | +18:10:13 | 1.0 | 0.92 | 0.009 | 12.3 | 0.01 | 5.951 | 0.92 | 0.007 | 10.237 | 0.019 | DE07 | | 186.107 | 9.221 | | K14 | K1.0 |
| "Cl* NGC 2632 JC 168" | 08:39:38 | +19:26:27 | 1.0 | 0.968 | 0.009 | 12.627 | 0.01 | 6.278 | 1.032 | 0.007 | 10.286 | 0.02 | DE07 | | 186.097 | 11.328 | | R17 | K3V |
| "Cl* NGC 2632 JS 309" | 08:39:41 | +19:59:29 | 1.0 | 1.425 | 0.015 | 15.38 | 0.015 | 8.949 | 2.007 | 0.013 | 11.323 | 0.019 | DE07 | | 193.293 | 4.165 | | R17 | M0V |
| "Cl* NGC 2632 WJJP 83" | 08:39:46 | +19:22:01 | 1.0 | 0.581 | 0.004 | 10.667 | 0.007 | 4.306 | 0.64 | 0.011 | 9.259 | 0.02 | DE07 | | 187.187 | 5.794 | | R17 | G0 |

(Continued).

| *Name* | $\alpha_{J2000}$ (h:m:s) | $\delta_{J2000}$ (°:′:″) | *Notes memb.* | $B-V$ (mag) | e$B-V$ (mag) | $V$ (mag) | e$V$ (mag) | $M_v$ (mag) | $V-Ic$ (mag) | e$V-Ic$ (mag) | $Ks$ (mag) | e$Ks$ (mag) | *Notes phot.BVI* | *Date Obs.OSN* | $D_{BJ.Gaia}$ (pc) | *Period* (days) | SD *PeriodMean* | *Notes period* | *Spect. Types* |
|---|---|---|---|---|---|---|---|---|---|---|---|---|---|---|---|---|---|---|---|
| "Cl* NGC 2632 JC 172" | 08:39:47 | +19:49:39 | 1.0 | 0.975 | 0.009 | 12.73 | 0.01 | 6.366 | 1.017 | 0.007 | 10.435 | 0.019 | DE07 | | 187.372 | 10.508 | | R17 | K2.6 |
| "Cl* NGC 2632 WJJP 89" | 08:39:52 | +19:18:45 | 1.0 | 0.508 | 0.004 | 10.237 | 0.007 | 3.91 | 0.574 | 0.011 | 9.008 | 0.02 | DE07 | | 184.28 | 3.143 | | R17 | F7V |
| "HD 73597" | 08:39:54 | +20:33:37 | 1.0 | 0.414 | 0.004 | 9.373 | 0.008 | 3.047 | 0.465 | 0.006 | 8.377 | 0.019 | DE07 | | 184.157 | 1.588 | | R17 | F6V |
| "BD+20 2151" | 08:39:55 | +20:03:54 | 1.0 | 0.483 | 0.004 | 10.113 | 0.007 | 3.618 | 0.551 | 0.011 | 8.961 | 0.019 | DE07 | | 199.101 | 3.29 | 0.001 | M | F4V |
| "HD 73616" | 08:39:58 | +20:09:30 | 2.0 | 0.32 | 0.004 | 8.892 | 0.008 | 2.561 | 0.372 | 0.006 | 8.1 | 0.017 | DE07 | | 184.614 | 0.888 | | R17 | F2V |
| "HD 73641" | 08:39:58 | +19:12:06 | 1.0 | 0.417 | 0.004 | 9.488 | 0.008 | 3.109 | 0.485 | 0.006 | 8.482 | 0.018 | DE07 | | 188.743 | 10.284 | | R17 | F3V |
| "BD+20 2155" | 08:39:59 | +20:01:53 | 4.0 | 0.386 | 0.004 | 9.234 | 0.008 | 2.962 | 0.461 | 0.006 | 8.214 | 0.021 | DE07 | | 179.632 | 0.685 | | R17 | F1V* |
| "Cl* NGC 2632 KW 236" | 08:40:00 | +19:34:00 | 0.0 | 0.997 | 0.004 | 11.933 | 0.007 | 5.574 | 1.068 | 0.011 | 9.484 | 0.018 | DE07 | | | 11.501 | | R17 | K |
| "Cl* NGC 2632 JC 177" | 08:40:00 | +19:34:40 | 1.0 | 0.995 | 0.009 | 12.87 | 0.01 | 6.518 | 1.051 | 0.007 | 10.552 | 0.018 | DE07 | | 186.423 | 10.751 | | R17 | K2.3 |
| "Cl* NGC 2632 S 97" | 08:40:01 | +19:48:23 | 1.0 | 0.501 | 0.004 | 10.297 | 0.007 | 3.939 | 0.578 | 0.011 | 9.079 | 0.02 | DE07 | | 186.873 | 2.962 | | R17 | F6V |
| "HD 73640" | 08:40:01 | +20:08:08 | 1.0 | 0.442 | 0.004 | 9.667 | 0.008 | 3.264 | 0.52 | 0.006 | 8.624 | 0.018 | DE07 | | 190.801 | 1.179 | 0.001 | M | F6V |
| "Cl* NGC 2632 JC 180" | 08:40:01 | +19:18:35 | 1.0 | 1.38 | 0.015 | 14.43 | 0.015 | 8.014 | 1.673 | 0.013 | 10.918 | 0.02 | DE07 | | 191.957 | 14.242 | | R17 | K8V |
| "V* TX Cnc" | 08:40:02 | +18:59:59 | 1.0 | 0.64 | 0.004 | 10.2 | 0.007 | 3.843 | 0.691 | 0.011 | 8.698 | 0.018 | DE07 | | 186.849 | 0.19 | | D17 | G0-G1V |
| "2MASS J08400416+1947039" | 08:40:04 | +19:47:04 | 2.0 | 0.832 | 0.009 | 12.06 | 0.01 | 5.499 | 0.901 | 0.007 | 10.004 | 0.02 | DE07 | | 205.17 | 10.442 | | R17 | K0V |
| "Cl* NGC 2632 S 105" | 08:40:06 | +19:27:15 | 4.0 | 0.57 | 0.004 | 10.245 | 0.007 | 3.305 | 0.617 | 0.011 | 8.868 | 0.02 | DE07 | | 244.302 | 5.9 | | R17 | F8* |
| "EPIC 211938860" | 08:40:06 | +19:18:26 | 1.0 | 0.777 | 0.004 | 11.005 | 0.007 | 4.652 | 0.815 | 0.011 | 9.228 | 0.018 | DE07 | | 186.459 | 7.801 | | R17 | G8V |
| "Cl* NGC 2632 KP 103073" | 08:40:06 | +19:01:31 | 1.0 | 1.008 | 0.009 | 12.63 | 0.01 | 6.276 | 1.124 | 0.007 | 10.009 | 0.02 | DE07 | | 186.548 | 4.675 | | R17 | K1V |
| "Cl* NGC 2632 JC 190" | 08:40:10 | +19:37:17 | 1.0 | 0.819 | 0.009 | 12.003 | 0.01 | 5.613 | 0.847 | 0.007 | 10.133 | 0.02 | DE07 | | 189.637 | 7.962 | | R17 | G9V |
| K2-102 | 08:40:13 | +19:46:44 | 1.0 | 1.095 | 0.009 | 13.2 | 0.01 | 6.827 | 1.162 | 0.007 | 10.64 | 0.02 | DE07 | | 188.175 | 11.611 | | R17 | K3.6 |
| "Cl* NGC 2632 HERT 139" | 08:40:15 | +19:27:31 | 1.0 | 1.298 | 0.009 | 13.915 | 0.01 | 7.669 | 1.5 | 0.007 | 10.689 | 0.02 | DE07 | | 177.496 | 12.007 | 0.052 | M | K6V |
| "Cl* NGC 2632 JC 196" | 08:40:16 | +19:54:54 | 1.0 | 1.01 | 0.009 | 12.7 | 0.01 | 6.386 | 1.182 | 0.007 | 10.013 | 0.018 | DE07 | | 183.119 | 10.506 | | R17 | K3.8 |
| "BD+20 2162" | 08:40:18 | +19:47:15 | 0.0 | 0.587 | 0.004 | 9.963 | 0.008 | 3.604 | 0.64 | 0.006 | 8.583 | 0.018 | DE07 | | | 6.754 | | R17 | F9* |
| "Cl* NGC 2632 WJJP 607" | 08:40:19 | +20:11:31 | 0.0 | 1.21 | 0.009 | 12.97 | 0.01 | 6.611 | 1.346 | 0.007 | 10.038 | 0.018 | DE07 | | | 12.001 | | R17 | K4V |
| "Cl* NGC 2632 WJJP 131" | 08:40:23 | +19:27:53 | 1.0 | 0.588 | 0.004 | 10.7 | 0.007 | 4.297 | 0.66 | 0.011 | 9.336 | 0.02 | DE07 | | 190.786 | 6.87 | | R17 | F7.2 |
| "NGC 2632 JC 205" | 08:40:24 | +18:27:13 | 4.0 | 0.82 | 0.004 | 11.6 | 0.007 | 5.236 | 0.911 | 0.011 | 9.599 | 0.018 | DE07 | | 187.439 | 9.652 | | K14 | G8 |
| "TYC 1395-1849-1" | 08:40:26 | +19:28:33 | 1.0 | 0.48 | 0.004 | 9.87 | 0.008 | 3.527 | 0.52 | 0.006 | 8.763 | 0.02 | DE07 | | 185.604 | 0.898 | | R17 | F5V |
| "Cl* NGC 2632 JC 208" | 08:40:26 | +19:13:10 | 1.0 | 1.04 | 0.009 | 12.9 | 0.01 | 6.553 | 1.075 | 0.007 | 10.461 | 0.02 | DE07 | | 185.921 | 10.686 | | R17 | K3V |
| "Cl* NGC 2632 WJJP 628" | 08:40:27 | +19:16:41 | 1.0 | 0.658 | 0.004 | 11.165 | 0.007 | 4.745 | 0.706 | 0.011 | 9.655 | 0.02 | DE07 | | 192.318 | 8.788 | | R17 | G3V |
| "2MASS J08402863+2018449" | 08:40:29 | +20:18:45 | 1.0 | 0.86 | 0.004 | 11.64 | 0.007 | 5.326 | 0.955 | 0.011 | 9.462 | 0.018 | DE07 | | 183.16 | 8.156 | | R17 | K |
| "Cl* NGC 2632 S 129" | 08:40:32 | +20:12:06 | 2.0 | 0.741 | 0.004 | 11.52 | 0.007 | 5.246 | 0.784 | 0.011 | 9.831 | 0.014 | DE07 | | 179.823 | 8.737 | | R17 | G5V |
| "Cl* NGC 2632 S 131" | 08:40:32 | +19:51:01 | 1.0 | 0.765 | 0.004 | 11.63 | 0.007 | 5.297 | 0.8 | 0.011 | 9.911 | 0.018 | DE07 | | 184.717 | 8.451 | | R17 | G9V |
| "UGCS J084032.94+191139.4" | 08:40:33 | +19:11:39 | 1.0 | 0.293 | 0.004 | 8.655 | 0.008 | 2.362 | 0.333 | 0.006 | 7.964 | 0.015 | DE07 | | 181.396 | 0.061 | | R17 | A9V* |
| "Cl* NGC 2632 JC 215" | 08:40:33 | +19:38:01 | 1.0 | 0.881 | 0.009 | 12.193 | 0.01 | 5.841 | 0.916 | 0.007 | 10.169 | 0.018 | DE07 | | 186.372 | 9.701 | | R17 | K0.8 |
| "Cl* NGC 2632 JC 216" | 08:40:34 | +18:40:28 | 2.0 | 0.77 | 0.004 | 11.62 | 0.007 | 5.258 | 0.784 | 0.011 | 9.832 | 0.016 | DE07 | | 187.281 | 9.674 | | R17 | G5.4 |
| "Cl* NGC 2632 KW 547" | 08:40:38 | +18:42:00 | 4.0 | 0.97 | 0.004 | 11.99 | 0.007 | 3.07 | 0.969 | 0.011 | 9.7 | 0.016 | DE07 | | 608.253 | 2.524 | | R17 | K3* |

(Continued).

| *Name* | $\alpha_{J2000}$ (h:m:s) | $\delta_{J2000}$ (°:′:″) | *Notes memb.* | $B-V$ (mag) | e$B-V$ (mag) | $V$ (mag) | e$V$ (mag) | $M_v$ (mag) | $V-Ic$ (mag) | e$V-Ic$ (mag) | $Ks$ (mag) | e$Ks$ (mag) | *Notes phot.BVI* | *Date Obs.OSN* | $D_{BJ.Gaia}$ (pc) | *Period* (days) | SD *PeriodMean* | *Notes period* | *Spect. Types* |
|---|---|---|---|---|---|---|---|---|---|---|---|---|---|---|---|---|---|---|---|
| "Cl* NGC 2632 S 134" | 08:40:40 | +19:40:09 | 4.0 | 0.676 | 0.004 | 10.87 | 0.007 | 4.472 | 0.773 | 0.011 | 9.189 | 0.018 | DE07 | | 190.404 | 7.138 | | K14 | G1V* |
| "Cl* NGC 2632 S 137" | 08:40:42 | +19:13:25 | 4.0 | 0.609 | 0.004 | 10.607 | 0.007 | 3.483 | 0.703 | 0.011 | 9.063 | 0.018 | DE07 | | 265.94 | 6.112 | | R17 | F9* |
| "Cl* NGC 2632 S 138" | 08:40:42 | +19:33:58 | 2.0 | 0.712 | 0.004 | 11.34 | 0.007 | 5.027 | 0.745 | 0.011 | 9.706 | 0.018 | DE07 | | 183.066 | 8.286 | | R17 | G4V |
| "Cl* NGC 2632 WJJP 162" | 08:40:48 | +19:55:19 | 1.0 | 0.644 | 0.004 | 11.02 | 0.007 | 4.685 | 0.706 | 0.011 | 9.507 | 0.02 | DE07 | | 184.921 | 7.932 | | R17 | G2V |
| "Cl* NGC 2632 WJJP 161" | 08:40:48 | +19:39:32 | 1.0 | 0.718 | 0.004 | 11.007 | 0.007 | 4.598 | 0.788 | 0.011 | 9.254 | 0.018 | DE07 | | 191.305 | 7.207 | | K14 | G2V |
| "TYC 1395-1234-1" | 08:40:48 | +18:54:12 | 4.0 | 0.71 | 0.004 | 11.46 | 0.007 | 5.142 | 0.784 | 0.011 | 9.686 | 0.02 | DE07 | | 183.457 | 8.605 | | R17 | G6.8 |
| "TYC 1395-1897-1" | 08:40:53 | +19:28:59 | 1.0 | 0.519 | 0.004 | 10.305 | 0.007 | 3.917 | 0.59 | 0.011 | 9.049 | 0.02 | DE07 | | 189.458 | 3.822 | | R17 | F7V |
| "Cl* NGC 2632 JS 395" | 08:40:55 | +19:56:07 | 1.0 | 0.864 | 0.009 | 12.11 | 0.01 | 5.827 | 0.891 | 0.007 | 10.132 | 0.018 | DE07 | | 180.587 | 9.123 | 0.01 | M | K1V |
| "Cl* NGC 2632 JC 230" | 08:40:57 | +19:44:05 | 1.0 | 0.86 | 0.009 | 12.23 | 0.01 | 5.855 | 0.891 | 0.007 | 10.213 | 0.02 | DE07 | | 188.368 | 9.158 | | R17 | K0.5 |
| "Cl* NGC 2632 JS 404" | 08:41:03 | +20:27:28 | 1.0 | 0.89 | 0.009 | 12.35 | 0.01 | 6.003 | 0.93 | 0.007 | 10.291 | 0.016 | DE07 | | 185.983 | 9.626 | 0.006 | M | G8.5 |
| "BD+19 2076" | 08:41:07 | +19:04:16 | 0.0 | 0.645 | 0.004 | 10.18 | 0.007 | 3.821 | 0.722 | 0.011 | 8.636 | 0.019 | DE07 | | | 7.843 | 0.06 | M | G1* |
| "Cl* NGC 2632 JC 234" | 08:41:07 | +19:26:49 | 1.0 | 0.931 | 0.009 | 12.44 | 0.01 | 6.161 | 0.959 | 0.007 | 10.288 | 0.018 | DE07 | | 180.187 | 9.751 | | R17 | K1V |
| "BD+20 2176" | 08:41:10 | +19:30:32 | 1.0 | 0.51 | 0.004 | 10.105 | 0.007 | 3.761 | 0.578 | 0.011 | 8.908 | 0.02 | DE07 | | 185.735 | 3.058 | | R17 | F7V |
| "Cl* NGC 2632 S 155" | 08:41:10 | +19:49:07 | 1.0 | 0.73 | 0.004 | 11.505 | 0.007 | 5.193 | 0.78 | 0.011 | 9.753 | 0.02 | DE07 | | 183.013 | 9.054 | | R17 | G6.6 |
| "BD+19 2077" | 08:41:10 | +19:51:19 | 1.0 | 0.68 | 0.004 | 10.7 | 0.007 | 4.363 | 0.784 | 0.011 | 8.939 | 0.018 | DE07 | | 185.058 | 3.068 | | R17 | G7.6 |
| "Cl* NGC 2632 JC 237" | 08:41:10 | +19:56:07 | 1.0 | 1.216 | 0.009 | 13.635 | 0.01 | 7.279 | 1.346 | 0.007 | 10.763 | 0.02 | DE07 | | 186.689 | 13.44 | 0.029 | M | K5.6 |
| "HD 73854" | 08:41:11 | +19:49:46 | 1.0 | 0.353 | 0.004 | 9.044 | 0.008 | 2.717 | 0.415 | 0.006 | 8.19 | 0.021 | DE07 | | 184.271 | 0.752 | | R17 | F5V |
| "Cl* NGC 2632 JS 409" | 08:41:11 | +20:49:58 | 4.0 | 0.77 | 0.004 | 11.92 | 0.007 | 5.646 | 0.814 | 0.011 | 10.12 | 0.018 | DE07 | | 179.845 | 17.016 | | R17 | K0V |
| "HD 73872" | 08:41:14 | +19:55:19 | 1.0 | 0.201 | 0.004 | 8.333 | 0.008 | 2.044 | 0.263 | 0.006 | 7.774 | 0.017 | DE07 | | 181.037 | 0.064 | | R17 | A5V |
| "Cl* NGC 2632 JS 420" | 08:41:15 | +20:02:16 | 1.0 | 1.322 | 0.015 | 14.3 | 0.015 | 7.981 | 1.587 | 0.013 | 11.022 | 0.018 | DE07 | | 183.563 | 13.554 | | R17 | K6V |
| "Cl* NGC 2632 HERT 274" | 08:41:20 | +19:38:05 | 1.0 | 1.169 | 0.009 | 13.555 | 0.01 | 7.212 | 1.278 | 0.007 | 10.762 | 0.02 | DE07 | | 185.633 | 11.873 | | R17 | K5V |
| K2-101 | 08:41:23 | +18:56:02 | 4.0 | 1.04 | 0.009 | 12.96 | 0.01 | 6.585 | 1.085 | 0.007 | 10.536 | 0.019 | DE07 | | 188.33 | 10.662 | | R17 | K3 |
| "Cl* NGC 2632 JS 428" | 08:41:24 | +20:14:57 | 2.0 | 1.465 | 0.015 | 14.675 | 0.015 | 8.3 | 1.96 | 0.013 | 10.776 | 0.02 | DE07 | | 188.336 | 15.207 | | R17 | K7V |
| "Cl* NGC 2632 JC 253" | 08:41:24 | +18:14:03 | 2.0 | 1.424 | 0.042 | 15.734 | 0.021 | 9.37 | 2.27 | 0.027 | 11.455 | 0.02 | OSN | 07/05/2017$^{++}$ | 187.392 | 8.356 | | K14 | M1.0 |
| "BD+20 2181" | 08:41:26 | +19:56:37 | 1.0 | 0.597 | 0.004 | 10.733 | 0.007 | 4.355 | 0.652 | 0.011 | 9.329 | 0.02 | DE07 | | 188.642 | 6.785 | | R17 | G0V |
| "BD+20 2180" | 08:41:27 | +19:32:33 | 1.0 | 0.47 | 0.004 | 9.865 | 0.008 | 3.539 | 0.535 | 0.006 | 8.722 | 0.02 | DE07 | | 184.122 | 3.587 | 0.004 | M | F4V |
| "Cl* NGC 2632 S 169" | 08:41:29 | +19:44:48 | 4.0 | 0.626 | 0.004 | 10.943 | 0.007 | 4.615 | 0.761 | 0.011 | 9.469 | 0.018 | DE07 | | 184.304 | 7.563 | | R17 | G1V* |
| "EPIC 211909748" | 08:41:31 | +18:52:19 | 1.0 | 1.0 | 0.009 | 12.97 | 0.01 | 6.662 | 1.211 | 0.007 | 10.154 | 0.021 | DE07 | | 182.619 | 2.422 | | R17 | K3.1 |
| "Cl* NGC 2632 JC 258" | 08:41:32 | +18:30:02 | 1.0 | 0.56 | 0.004 | 10.41 | 0.007 | 4.071 | 0.602 | 0.011 | 9.105 | 0.021 | DE07 | | 185.252 | 4.149 | | K14 | F5 |
| "Cl* NGC 2632 S 171" | 08:41:34 | +19:58:09 | 1.0 | 0.78 | 0.004 | 11.71 | 0.007 | 5.39 | 0.815 | 0.011 | 9.928 | 0.018 | DE07 | | 183.63 | 8.925 | | R17 | G6.7 |
| "HD 73937" | 08:41:36 | +19:08:33 | 4.0 | 0.391 | 0.004 | 9.321 | 0.008 | 2.892 | 0.457 | 0.006 | 8.351 | 0.022 | DE07 | | 193.133 | 1.12 | | R17 | F1V* |
| "Cl* NGC 2632 JC 259" | 08:41:36 | +19:06:25 | 1.0 | 1.29 | 0.015 | 14.17 | 0.015 | 7.834 | 1.5 | 0.013 | 10.978 | 0.018 | DE07 | | 185.017 | 13.543 | 0.089 | M | K7.1 |
| "Cl* NGC 2632 JC 260" | 08:41:37 | +19:31:14 | 1.0 | 1.211 | 0.009 | 13.575 | 0.01 | 7.253 | 1.297 | 0.007 | 10.731 | 0.018 | DE07 | | 183.831 | 13.474 | 0.009 | M | K5V |
| "Cl* NGC 2632 JC 261" | 08:41:39 | +19:15:57 | 3.0 | 1.07 | 0.009 | 13.09 | 0.01 | 6.799 | 1.124 | 0.007 | 10.574 | 0.021 | DE07 | | 181.195 | 10.176 | | R17 | K4V |
| "BD+21 1891" | 08:41:40 | +20:40:20 | 2.0 | 0.45 | 0.004 | 9.68 | 0.008 | 3.264 | 0.496 | 0.006 | 8.586 | 0.016 | DE07 | | 191.933 | 1.062 | 0.002 | M | F6V |
| "BD+20 2184b" | 08:41:44 | +20:13:37 | 1.0 | 0.565 | 0.004 | 10.47 | 0.007 | 4.186 | 0.613 | 0.011 | 9.142 | 0.018 | DE07 | | 180.64 | 5.521 | | R17 | F8V* |
| "Cl* NGC 2632 JC 263" | 08:41:44 | +19:57:44 | 1.0 | 0.842 | 0.009 | 12.355 | 0.01 | 5.941 | 0.92 | 0.007 | 10.258 | 0.019 | DE07 | | 191.798 | 9.457 | | R17 | K1V |
| "BD+19 2081" | 08:41:45 | +19:16:02 | 1.0 | 0.519 | 0.004 | 10.162 | 0.007 | 3.85 | 0.59 | 0.011 | 8.933 | 0.019 | DE07 | | 182.984 | 4.9 | 0.0 | M | F7V |
| "Cl* NGC 2632 JC 268 " | 08:41:48 | +19:27:31 | 4.0 | 1.18 | 0.009 | 13.67 | 0.01 | 7.331 | 1.317 | 0.007 | 10.732 | 0.018 | DE07 | | 185.285 | 11.207 | | R17 | K5V |

(Continued).

| *Name* | $\alpha_{J2000}$ (h:m:s) | $\delta_{J2000}$ (°:′:″) | *Notes memb.* | $B-V$ (mag) | e$B-V$ (mag) | $V$ (mag) | e$V$ (mag) | $M_v$ (mag) | $V-Ic$ (mag) | e$V-Ic$ (mag) | $Ks$ (mag) | e$Ks$ (mag) | *Notes phot.BVI* | *Date Obs.OSN* | $D_{BJ.Gaia}$ (pc) | *Period* (days) | SD *PeriodMean* | *Notes period* | *Spect. Types* |
|---|---|---|---|---|---|---|---|---|---|---|---|---|---|---|---|---|---|---|---|
| "Cl* NGC 2632 JC 269" | 08:41:49 | +19:11:47 | 1.0 | 1.38 | 0.015 | 14.5 | 0.015 | 8.087 | 1.75 | 0.013 | 10.834 | 0.018 | DE07 | | 191.69 | 13.638 | | R17 | K8V |
| "Cl* NGC 2632 JC 270" | 08:41:50 | +19:39:35 | 1.0 | 1.467 | 0.031 | 16.195 | 0.02 | 9.879 | 2.209 | 0.023 | 11.891 | 0.023 | OSN | 02/03/2016$^{+}$ | 183.373 | 18.90 | | D14/A11 | M1.4 |
| "Cl* NGC 2632 JS 461" | 08:41:52 | +20:10:01 | 1.0 | 0.843 | 0.009 | 12.05 | 0.01 | 5.728 | 0.882 | 0.007 | 10.086 | 0.019 | DE07 | | 183.843 | 9.574 | 0.036 | M | K0.0 |
| "HD 73993" | 08:41:53 | +20:09:34 | 1.0 | 0.33 | 0.004 | 8.829 | 0.008 | 2.498 | 0.356 | 0.006 | 7.79 | 0.017 | DE07 | | 184.587 | 0.47 | | R17 | F2Vn |
| "Cl* NGC 2632 S 184" | 08:41:54 | +19:15:27 | 1.0 | 0.723 | 0.004 | 11.385 | 0.007 | 5.039 | 0.823 | 0.011 | 9.643 | 0.019 | DE07 | | 185.881 | 4.184 | | R17 | G8V |
| "TYC 1395-2091-1" | 08:41:56 | +19:41:22 | 2.0 | 0.643 | 0.004 | 11.045 | 0.007 | 4.732 | 0.738 | 0.011 | 9.544 | 0.018 | DE07 | | 183.092 | 8.056 | | K14 | G2V |
| "HD 73994" | 08:41:58 | +18:54:42 | 2.0 | 0.398 | 0.004 | 9.454 | 0.008 | 3.254 | 0.473 | 0.006 | 8.434 | 0.025 | DE07 | | 173.776 | 2.03 | | R17 | F5V |
| "Cl* NGC 2632 JS 465" | 08:41:59 | +20:55:07 | 1.0 | 0.7 | 0.004 | 11.27 | 0.007 | 4.882 | 0.727 | 0.011 | 9.705 | 0.02 | DE07 | | 189.454 | 8.204 | | K14 | G5V: |
| "Cl* NGC 2632 WJJP 792" | 08:41:59 | +20:06:27 | 4.0 | 1.11 | 0.009 | 13.23 | 0.01 | 6.86 | 1.172 | 0.007 | 10.599 | 0.018 | DE07 | | 187.918 | 11.338 | | R17 | K4 |
| "Cl* NGC 2632 JC 274" | 08:41:59 | +19:44:45 | 1.0 | 1.495 | 0.031 | 16.195 | 0.02 | 9.833 | 2.2 | 0.023 | 11.889 | 0.019 | OSN | 02/03/2016$^{+}$ | 187.267 | 16.808 | | R17 | M1.2 |
| "[QWL2012] Pr0211" | 08:42:11 | +19:16:37 | 1.0 | 0.869 | 0.009 | 12.155 | 0.01 | 5.846 | 0.901 | 0.007 | 10.173 | 0.016 | DE07 | | 182.714 | 7.902 | | R17 | K1V |
| "Cl* NGC 2632 JC 279" | 08:42:12 | +19:12:49 | 1.0 | 1.2 | 0.009 | 13.7 | 0.01 | 7.347 | 1.317 | 0.007 | 10.833 | 0.016 | DE07 | | 186.426 | 13.409 | 0.1 | M | K6V |
| "Cl* NGC 2632 JC 280" | 08:42:13 | +19:16:04 | 4.0 | 1.18 | 0.009 | 13.5 | 0.01 | 7.17 | 1.346 | 0.007 | 10.481 | 0.014 | DE07 | | 184.518 | 10.789 | 0.026 | M | K5V |
| "Cl* NGC 2632 WJJP 835" | 08:42:17 | +20:05:32 | 1.0 | 1.3 | 0.015 | 14.26 | 0.015 | 7.885 | 1.538 | 0.013 | 10.989 | 0.018 | DE07 | | 188.323 | 13.636 | | R17 | K7V |
| "Cl* NGC 2632 KW 456" | 08:42:19 | +20:24:35 | 1.0 | 0.93 | 0.009 | 12.42 | 0.01 | 6.114 | 0.969 | 0.007 | 10.194 | 0.019 | DE07 | | 182.503 | 9.87 | | R17 | K2V* |
| "BD+20 2189" | 08:42:20 | +20:02:12 | 4.0 | 0.553 | 0.004 | 9.715 | 0.008 | 1.976 | 0.613 | 0.006 | 8.408 | 0.021 | DE07 | | 353.041 | 7.395 | | R17 | F7* |
| "Cl* NGC 2632 JS 737" | 08:42:23 | +20:07:06 | 4.0 | 0.893 | 0.009 | 12.095 | 0.01 | 5.831 | 0.94 | 0.007 | 9.914 | 0.018 | DE07 | | 178.963 | 12.6 | | R17 | K1.5V* |
| "Cl* NGC 2632 S 197" | 08:42:32 | +19:23:46 | 1.0 | 0.649 | 0.004 | 10.99 | 0.007 | 4.554 | 0.699 | 0.011 | 9.458 | 0.016 | DE07 | | 193.691 | 10.024 | | R17 | G2V |
| "Cl* NGC 2632 WJJP 860" | 08:42:37 | +20:08:32 | 1.0 | 1.27 | 0.009 | 13.99 | 0.01 | 7.645 | 1.452 | 0.007 | 10.871 | 0.019 | DE07 | | 185.798 | 11.97 | | R17 | K6V |
| "Cl* NGC 2632 JS 496" | 08:42:40 | +19:07:59 | 1.0 | 0.852 | 0.009 | 12.145 | 0.01 | 5.804 | 0.862 | 0.007 | 10.186 | 0.018 | DE07 | | 185.398 | 9.386 | | R17 | K0.1 |
| "Cl* NGC 2632 S 199" | 08:42:42 | +19:05:59 | 1.0 | 0.76 | 0.004 | 11.623 | 0.007 | 5.329 | 0.797 | 0.011 | 9.881 | 0.021 | DE07 | | 181.507 | 8.489 | | R17 | G5.8 |
| "BD+20 2193" | 08:42:44 | +19:34:48 | 1.0 | 0.44 | 0.004 | 9.74 | 0.008 | 3.304 | 0.512 | 0.006 | 8.633 | 0.018 | DE07 | | 193.719 | 0.48 | 0.0 | M | F6V |
| "Cl* NGC 2632 JS 499" | 08:42:44 | +19:37:23 | 2.0 | 0.988 | 0.009 | 12.13 | 0.01 | 5.759 | 1.046 | 0.007 | 9.8 | 0.02 | DE07 | | 187.981 | 10.628 | | R17 | K2.6 |
| "Cl* NGC 2632 S 203" | 08:43:01 | +20:20:16 | 1.0 | 0.732 | 0.004 | 11.43 | 0.007 | 5.116 | 0.776 | 0.011 | 9.774 | 0.02 | DE07 | | 183.153 | 8.935 | | R17 | G5V |
| "Cl* NGC 2632 JS 511" | 08:43:02 | +19:10:03 | 1.0 | 0.85 | 0.009 | 12.12 | 0.01 | 5.816 | 0.862 | 0.007 | 10.158 | 0.021 | DE07 | | 182.281 | 9.883 | 0.01 | M | G7.5 |
| "BD+19 2087" | 08:43:06 | +19:26:15 | 1.0 | 0.66 | 0.004 | 9.97 | 0.008 | 3.453 | 0.668 | 0.006 | 8.461 | 0.021 | DE07 | | 201.082 | 4.738 | 0.0030 | M | F8V |
| "HD 74186" | 08:43:07 | +19:04:06 | 1.0 | 0.528 | 0.004 | 9.602 | 0.008 | 3.287 | 0.598 | 0.006 | 8.36 | 0.029 | DE07 | | 183.207 | 4.93 | | R17 | F8V |
| "Cl* NGC 2632 WJJP 895" | 08:43:07 | +19:47:30 | 1.0 | 1.18 | 0.009 | 13.67 | 0.01 | 7.305 | 1.346 | 0.007 | 10.772 | 0.022 | DE07 | | 187.479 | 12.903 | 0.236 | M | K5V |
| "Cl* NGC 2632 WJJP 899" | 08:43:08 | +19:42:48 | 1.0 | 1.15 | 0.009 | 13.33 | 0.01 | 6.99 | 1.211 | 0.007 | 10.667 | 0.017 | DE07 | | 185.39 | 11.710 | | D14/D11 | K4V |
| "Cl* NGC 2632 S 209" | 08:43:11 | +19:31:35 | 1.0 | 0.768 | 0.004 | 11.78 | 0.007 | 5.434 | 0.776 | 0.011 | 10.007 | 0.021 | DE07 | | 185.866 | 9.108 | | R17 | G6.8 |
| "NSV 4211" | 08:43:18 | +20:30:37 | 4.0 | 0.83 | 0.004 | 11.82 | 0.007 | 5.516 | 0.901 | 0.011 | 9.776 | 0.02 | DE07 | | 182.337 | 9.088 | | R17 | K1.0 |
| " Cl* NGC 2632 S 213" | 08:43:20 | +19:46:08 | 4.0 | 0.592 | 0.004 | 10.78 | 0.007 | 4.829 | 0.652 | 0.011 | 9.359 | 0.018 | DE07 | | 154.924 | 6.382 | | R17 | EARLY-G* |
| "BD+22 1980" | 08:43:23 | +21:40:18 | 1.0 | 0.71 | 0.004 | 10.59 | 0.007 | 4.341 | 0.718 | 0.011 | 8.97 | 0.018 | DE07 | | 177.745 | 11.227 | 0.08 | M | G3.7 |
| "Cl* NGC 2632 JS 537" | 08:43:32 | +19:44:38 | 1.0 | 0.92 | 0.009 | 12.35 | 0.01 | 6.104 | 0.949 | 0.007 | 10.218 | 0.022 | DE07 | | 177.471 | 10.006 | | R17 | K0V: |
| "BD+20 2196" | 08:43:36 | +20:11:22 | 1.0 | 0.509 | 0.004 | 10.143 | 0.007 | 3.763 | 0.59 | 0.011 | 8.923 | 0.018 | DE07 | | 188.768 | 3.649 | 0.0020 | M | F6V |
| "2MASS J08434654+1709242" | 08:43:47 | +17:09:24 | 4.0 | 1.07 | 0.009 | 12.84 | 0.01 | 6.798 | 1.153 | 0.007 | 10.349 | 0.025 | DE07 | | 161.552 | 11.664 | | R17 | K3.5V* |
| "BD+19 2089" | 08:43:48 | +18:48:03 | 1.0 | 0.49 | 0.004 | 10.125 | 0.007 | 3.77 | 0.543 | 0.011 | 8.927 | 0.02 | DE07 | | 186.608 | 4.045 | | R17 | F8 |

(Continued).

| *Name* | $\alpha_{J2000}$ (h:m:s) | $\delta_{J2000}$ (°:′:″) | *Notes memb.* | $B-V$ (mag) | e$B-V$ (mag) | $V$ (mag) | e$V$ (mag) | $M_v$ (mag) | $V-Ic$ (mag) | e$V-Ic$ (mag) | $Ks$ (mag) | e$Ks$ (mag) | *Notes phot.BVI* | *Date Obs.OSN* | $D_{BJ.Gaia}$ (pc) | *Period* (days) | SD *PeriodMean* | *Notes period* | *Spect. Types* |
|---|---|---|---|---|---|---|---|---|---|---|---|---|---|---|---|---|---|---|---|
| "Cl* NGC 2632 KW 551" | 08:43:55 | +18:53:37 | 3.0 | 0.96 | 0.009 | 12.67 | 0.01 | 6.317 | 0.998 | 0.007 | 10.412 | 0.018 | DE07 | | 186.496 | 10.297 | | R17 | K1.3 |
| "BD+20 2198 " | 08:44:07 | +20:04:37 | 4.0 | 0.447 | 0.004 | 10.15 | 0.007 | 2.962 | 0.527 | 0.011 | 9.064 | 0.018 | DE07 | | 273.965 | 3.682 | | R17 | F3V* |
| "Cl* NGC 2632 JS 563" | 08:44:17 | +18:44:12 | 1.0 | 0.9 | 0.009 | 12.34 | 0.01 | 5.99 | 0.94 | 0.007 | 10.262 | 0.018 | DE07 | | 186.209 | 11.007 | | R17 | G9.9 |
| "BD+20 2204" | 08:45:04 | +20:21:28 | 1.0 | 0.54 | 0.004 | 10.4 | 0.007 | 4.129 | 0.592 | 0.011 | 9.13 | 0.019 | DE07 | | 179.516 | 3.669 | | R17 | F5 |
| "Cl* NGC 2632 VL 1686" | 08:45:07 | +20:23:42 | 4.0 | 0.83 | 0.004 | 11.91 | 0.007 | 5.582 | 0.843 | 0.011 | 10.05 | 0.02 | DE07 | | 184.367 | 11.093 | | R17 | K0V |
| " Cl* NGC 2632 JS 588" | 08:45:13 | +19:41:12 | 0.0 | 0.72 | 0.004 | 10.92 | 0.007 | 4.561 | 0.785 | 0.011 | 9.158 | 0.019 | DE07 | | | 7.322 | | K14 | G3V* |
| "BD+19 2093" | 08:45:18 | +18:53:25 | 1.0 | 0.46 | 0.004 | 9.51 | 0.008 | 3.225 | 0.563 | 0.006 | 8.601 | 0.021 | DE07 | | 180.758 | 2.292 | 0.003 | M | F5 |
| "HD 74587" | 08:45:28 | +20:23:43 | 1.0 | 0.28 | 0.004 | 8.51 | 0.008 | 2.262 | 0.304 | 0.006 | 7.864 | 0.021 | DE07 | | 177.638 | 0.059 | | R17 | A5 |
| "BD+22 1985" | 08:45:28 | +21:39:13 | 1.0 | 0.56 | 0.004 | 10.56 | 0.007 | 4.166 | 0.611 | 0.011 | 9.257 | 0.019 | DE07 | | 189.977 | 4.912 | | R17 | F6.6 |
| "BD+21 1904" | 08:45:30 | +20:35:25 | 1.0 | 0.46 | 0.004 | 9.82 | 0.008 | 3.498 | 0.496 | 0.006 | 8.765 | 0.02 | DE07 | | 183.81 | 0.951 | 0.001 | M | F8 |
| "HD 74656" | 08:45:47 | +19:02:58 | 1.0 | 0.24 | 0.004 | 8.03 | 0.008 | 1.768 | 0.246 | 0.006 | 7.534 | 0.027 | DE07 | | 178.835 | 1.815 | | R17 | Am |
| "Cl* NGC 2632 JS 638" | 08:46:47 | +19:38:41 | 1.0 | 0.6 | 0.004 | 10.75 | 0.007 | 4.39 | 0.64 | 0.011 | 9.342 | 0.019 | DE07 | | 187.072 | 6.138 | | K14 | G8V: |
| "V* FV Cnc" | 08:48:02 | +18:40:38 | 1.0 | 0.69 | 0.004 | 10.47 | 0.007 | 4.129 | 0.737 | 0.011 | 8.806 | 0.023 | DE07 | | 185.449 | 2.975 | | R17 | G |
| "Cl* NGC 2632 JS 660" | 08:48:28 | +18:20:43 | 1.0 | 0.72 | 0.004 | 11.43 | 0.007 | 5.14 | 0.727 | 0.011 | 9.772 | 0.019 | DE07 | | 181.145 | 9.195 | | K14 | G5.3 |
| "Cl* NGC 2632 ANM 1903" | 08:49:07 | +19:41:11 | 1.0 | 0.81 | 0.004 | 11.93 | 0.007 | 5.557 | 0.804 | 0.011 | 10.068 | 0.021 | DE07 | | 188.164 | 9.723 | | K14 | G9.4 |

Praesepe members and non-members with periods and $BVI_c$ photometry. Parameters shown in this table: names of the stars taken from the SIMBAD database; coordinates ($\alpha$ and $\delta$); membership notes (0: without membership data in Lodieu et al. (2019a), 1: member, 2: possible member, 3: unlikely member, 4: non-member); $B-V$, $V$, $V-I_c$ photometry with their errors and brightness calibrated in $V$ ($M_v$) band, obtained using the distances from Bailer-Jones et al. (2018); notes of photometry that indicate the origin of the data utilized, DE07: An et al. (2007); night on which the data were taken at the OSN; distances derived by Bailer-Jones et al. (2018) using Bayesian analysis of Gaia ($D_{BJ.Gaia}$) parallaxes; rotation period; standard deviation of the mean of the periods from D17 and R17; origin of the selected rotation period; spectral types.

The marks + beside the observation dates indicate the night affected by cirrus clouds; ++ indicates that the Signal-to-Noise ratio of the measurements has a value under 100.

The symbols $*$ placed beside the spectral types shows that they were derived using $B-V$, $V$ and $V-I_c$ values and the table by Erik Mamajek of tabulated magnitudes and colours. The spectral types without these symbols were taken from the SIMBAD database.

**Notes on the origin of the periods.** K14: Kovács et al. (2014), D14: Douglas et al. (2014), S11: Scholz et al. (2011), D11: Delorme et al. (2011b), A11: Agüeros et al. (2011), D17: Douglas et al. (2017), M: mean of the periods from D17 and R17.

## 3.5 Hyades

### 3.5.1 Characteristics of the cluster

Hyades (Melotte 25, Collinder 50, Caldwell 41), with centre coordinates $\alpha_{J2000}$ : $+04^h26^m54^s$, $\delta_{J2000}$ : $+15°52'00''$ (Dias et al. 2014), is the closest open stellar cluster to us and one of the most studied. Its brightest stars, along with the giant star Aldebaran (which is not a member of Hyades), form a "V" in the sky, giving rise to the silhouette of the face of Taurus, the constellation where the cluster is located in the sky.

#### Distance and age

Its mean distance is fairly well defined, with a value of 46-47 pc (for example, Pinsonneault et al. 1998; Perryman et al. 1998; van Leeuwen 2009; Palmer et al. 2014; Lodieu et al. 2019b). Perryman et al. (1998), using the Hipparcos catalogue, derived the mean distance to the cluster from a group of highly probably member stars (located at a distance of up to 10 pc from the cluster centre), and produced a value of 46.34 ±0.27 pc. Lodieu et al. (2019b) repeated this process but using the parameters from *Gaia* DR2, and obtained a mean distance of 47.03 ±0.20 pc. In this study, they concluded that the difference between the distance obtained with parameters from Hipparcos and with those from *Gaia* DR2 might be due to an offset between the two instruments, with a "Gaia-Hipparcos" difference of -0.118 mas (Arenou et al. 2018). Taking this into account, they put the distance generated from Hipparcos in the Gaia system and produced a distance of 46.595 pc. In short, we can state that the mean distance of the cluster is found between 46 and 47 pc.

The age of Hyades has been established at 650 ± 100 Myr. The studies focused on deriving this parameter have mainly used the isochrone fitting method. They have varied in their selection of models and of the stars to which they have fitted the isochrones (stars located at the "starting point", binaries, sequence of white dwarfs, etc.). The large majority of these studies present results within the established range (for example, Mermilliod 1981; Maeder & Mermilliod 1981; Perryman et al. 1998; De Gennaro et al. 2009; Lodieu et al. 2019b; Lebreton et al. 2001; Brandt & Huang 2015; Gossage et al. 2018). Recently, making use of the lithium depletion boundary, ages have been obtained that also show agreement with the established age: Lodieu et al. (2018) obtain a maximum age of 775 Myr, and both Martín et al. (2018) and Lodieu (2020) derive an age of 650 ± 70 Myr.

#### Membership

Hyades is visible to the naked eye, which is why it has been known since antiquity. However, it was not catalogued as a cluster until the twentieth century (Boss 1908).
Hyades is located at a galactic latitude of $b = -22.34°$ (value taken from the galactic open clusters database: WEBDA), with an almost null interstellar extinction $E(B-V) = 0.001$ (Gaia Collaboration et al. 2018a). In addition, its elevated proper motions facilitate its differentiation from field stars ($\mu_\alpha\, cos\delta$, $\mu_\delta$) ~ (101.005 ± 0.171 , -28.490 ± 0.137 ) mas $yr^{-1}$ (Gaia Collaboration et al.

2018a). As we have already seen in previous sections on other clusters, these characteristics have favoured member selection.

As Lodieu et al. (2019b) have explained, a large number of membership studies have been carried out, with different objectives. These were either to find new members, focusing the observations on a zone of the sky located in the centre of the cluster (for example, Hanson 1975; Stauffer et al. 1995, 1994; Leggett et al. 1994; Bouvier et al. 2008; Melnikov & Eislöffel 2018), or to focus their efforts on much larger areas for the purpose of obtaining the list of cluster members (for example, Reid 1992; Röser et al. 2011; Goldman et al. 2013; Lodieu et al. 2019b). Lodieu et al. (2019b), making use of the *Gaia* DR2 astrometric data, estimated 710 possible cluster members, of which 385 are highly probable members located in the area of the tidal radius.
They also carried out spectroscopic studies to confirm candidate members, using techniques such as: chemical tagging, in which they measure the candidates' abundance of chemical elements, based on the fact that the members of a cluster should have a similar composition (for example, Tabernero et al. 2012); or the study of their radial velocities (for example, Mermilliod et al. 2009a), since the member of the same cluster should also present very similar velocity parameters.

### 3.5.2 Our sample for Hyades

For the Hyades cluster, following the same process as with the previous clusters, we have gathered a total of 75 stars that are candidates for being members of the Hyades and late-F to mid-M spectral types, of which 19 are stars M0-M4 spectral type range. Below we explain how this sample has been produced (Table 3.5.2) and the origin of the data compiled. In Section 3.5.2, we specify their membership.

#### Periods compiled from the literature

In order to form our sample, we began with the catalogue provided by Douglas et al. (2019) (sent via private communication), in which they compiled the 232 objects of the Hyades with the rotation periods then available. We have not found new periods published since this study. Of these 232 stars, there are 102 whose rotation periods have already been compiled by Douglas et al. (2014, 2016), with these measurements coming from studies by Radick et al. (1987, 1995), Prosser et al. (1995), Delorme et al. (2011a), Hartman et al. (2011), and A. Kundert & P. Cargile 2014 (whose data they sent to S. Douglas via private communication). Kundert & P. Cargile 2014 measured periods by analysing the light curves from "The All Sky Automated Survey" (ASAS; Pojmanski 2002), which is a project devoted to monitoring stars for the purpose of detecting and investigating any type of photometric variability.
Regarding the 130 remaining stars, 37 have values obtained by Douglas et al. (2016) and 93 by Douglas et al. (2019), with both studies analysing K2 curves. For stars with measurements coming from several studies, Douglas et al. (2019) carried out a very careful analysis and selection of the values they considered the most reliable. We too will consider this selection. In Table 3.5.2, we show the periods of each star and their origin.

### $BVR_cI_c$ photometry

Of the 232 stars with rotation periods, there are 75 with photometry values in the three $BVI_c$ bands whose errors do not go above 0.04 mag, and spectral types from late-F to Mid-M.
44 of these stars have $BVI_c$ data (some also have $V-R_c$) in the literature, and for the 31 remaining stars, we have obtained $BVR_cI_c$ photometry at the OSN. Below we explain the procedure followed for the selection of the data from the literature and for obtaining the photometry at the OSN.

#### Photometry coming from the literature

For the list of 232 stars with rotation periods, we carried out a search for photometry in any of the $BVR_cI_c$ bands and found data for 183 stars using the following studies:

- Pinsonneault et al. (2004), made a compilation of 89 stars with photometry available in the literature, focusing on the Johnson $BV$ bands and the Cousins $I$ band. This study provided photometry for 34 stars, with mean errors for $B-V$, $V$ and $V-I_c$ of $\sim$ 0.004 mag, $\sim$ 0.011 mag and $\sim$ 0.015 mag, respectively. In this study, they gathered $B$ and/or $V$ data from the studies by Johnson & Knuckles (1955), Mendoza (1967), the Hipparcos mission, Weis & Upgren (1977) and Weis et al. (1979). They obtained photometry in the Johnson $I$ band Mendoza (1967), Johnson et al. (1966), Johnson et al. (1968) and Carney & Aaronson (1979). They compiled $V-I$ values in the Kron system from Weis & Upgren (1977), Weis et al. (1979), Weis & Upgren (1982), Upgren et al. (1985) and Weis & Hanson (1988). Furthermore, they obtained data in Johnson $V-I$ from Eggen (1982). As we can see, the main problem they faced in this compilation was not finding values in the $I$ filter in the Cousins system. In order to achieve their objective, they had to transform the data that they found for the $I$ band from the Johnson and Kron systems to the Cousins system, following the procedures used by Bessell (1979) and Bessell & Weis (1987).
- Kharchenko (2001) provides photometry in the $BV$ bands for 94 stars on the list. The mean errors in $B-V$ and $V$ are $\sim$ 0.106 mag and $\sim$ 0.047 mag, respectively.
- Joner et al. (2006), obtained photometric data in the $BVR_cI_c$ bands for 77 stars of the Hyades, by means of observations on the 0.5-metre telescope at the South African Astronomical Observatory (SAAO). This study provides photometry for 27 stars, with mean errors in $B-V$, $V$, $V-R_c$ and $V-I_c$ of $\sim$ 0.004 mag, $\sim$ 0.005 mag, $\sim$ 0.003 mag and $\sim$ 0.003 mag, respectively.
- APASS DR9. It provides $B-V$ and $V$ values for 164 stars on the list, with mean errors in $B-V$ of $\sim$ 0.077 mag and in $V$ of $\sim$ 0.042 mag.

Of these 183 stars with photometry, only 44 have measurements in the three $BVI_c$ bands whose errors do not exceed 0.04 mag. 25 of these stars also have $V-R_c$ values. The photometry data for these 44 stars come from the studies by Pinsonneault et al. (2004) and Joner et al. (2006). Given the homogeneity of the last study, we prioritize their data where stars have photometry from both studies.

### Photometry obtained at the OSN

We have derived photometry for 31 stars of the Hyades that had not previously been observed in the three $BVI_c$ filters, as well as providing $V - R_c$ values for one of them. All the measurements have upper limit errors below 0.04 mag, with their mean for $B - V$, $V$, $V - R_c$ and $V - I_c$ at 0.026 mag, 0.024 mag, 0.019 mag and 0.022 mag, respectively.

These stars were observed over five photometric nights between November and December 2015. All the images were acquired on the 1.5-metre telescope, except for the night of 19/12/2015, when the stars LP 536-63 and LP 416-570 were observed on the 0.9 m. As we have already commented in Section 3.1.2 on $\alpha$ Per, in the case of stars observed on the 0.9-metre telescope, we have tried to increase the signal to noise and decrease the fringing effect of the CCD in the $I_c$ filter. Thus several images were obtained for both stars for each filter, which were combined to derive the resulting magnitudes and colours. Nevertheless, their values in $V - I_c$ may have been affected by fringing in any case.

The star LP 536-63 was previously observed during the night of 16/11/2015, when it proved impossible to take sufficient data for the standard stars in order to generate a robust extinction value. Thus, the measurement was repeated on the night of 19/12/2015. We have compared them and seen that the magnitudes and colours corresponding to both nights differ by less 0.04 mag, with the exception of $V - R_c$. Since the night of 19/12/2015 meets the criteria to be considered an optimal night for producing reliable photometry values, we will show these data for this star, taking into account the possible fringing effect in $V - I_c$.

In addition, the stars HD 285630, UCAC 4525-009613, HD 286798 (observed on 18/11/2015) and V* V994 Tau, HD 285828, HD 283066, TYC 677-227-1, StKM 1-549, HD 286820, HD 285348 (observed 19/11/2015) were observed several times on the same night, thus obtaining duplicated images and in some cases triplicated. Given that we have been able to verify in the test carried out for the night of 19/12/2015 and explained in Section 3.1.2 that the residuals barely varied between combining and not combining the images in the bands unaffected by fringing, we decided not to combine the images. Instead, since the differences in between the resulting magnitudes and colours of each individual measurement were less than 0.04 mag, we have calculated their mean.

### Membership of the stars in our sample

The list with 232 stars that we began with to generate our sample of 75 objects, as we have explained above, was put together by the study from which we extracted the periods (Douglas et al. 2019). Before compiling the periods, this study gathered together the highly probable candidates for Hyades membership, with a total of 786 stars. For this task they used proper motions and Hipparcos parallaxes, and they identified 13 new probable members, to which they added objects from the following membership studies:

- Röser et al. (2011) produced a census of the Hyades, reaching approximately $0.2M_{\odot}$. For this purpose, they analysed the objects located up to 30 pc from the cluster centre, studying their positions and proper motions given in the "Positions and Proper Motion Extra Large catalogue" (PPMXL, Roeser et al. 2010), and they studied isochrones using 2MASS photometry and the $r'$ band from the "Carlsberg Meridian Catalogue 14" (CMC14, Copenhagen University et al. 2006). They presented a total of 724 candidates.
- Goldman et al. (2013), like Röser et al. (2011), searched for candidates at a distance of 30 pc from the cluster centre. In this case, they used proper motions and PPMXL positions and the photometry from Pan-STARRS1 (Kaiser et al. 2002), combining it with the photometry from 2MASS, "Wide-field Infrared Survey Explorer" (WISE, Wright et al. 2010) and "Sloan Digital Sky Survey Data Release 8" (SDSS DR8, Adelman-McCarthy & et al. 2011). They discovered 54 new candidates and produced a sample of 773 candidates, reaching up to $0.1M_{\odot}$

In summary, the stars from our sample of 75 objects were considered to be highly probable members in at least one of the three mentioned studies (Röser et al. 2011; Goldman et al. 2013; Douglas et al. 2019). In order to verify their membership, we followed the same procedure as with the previous clusters, using the results from the study by Lodieu et al. (2019b). We take a tidal radius of $\sim$ 9 pc, which was the radius taken in this study. We take to be members those stars that are located at a distance of less than or approximately equal to 9 pc from the cluster centre (54 stars from the sample), possible members those located between 9 pc and approximately three times this value (30 pc; 10 stars), unlikely members at a distance greater than 30 pc (zero stars). We discard as members those stars that do not appear in the catalogue by Lodieu et al. (2019b) (nine stars). Of these nine non-members, six have been observed at the OSN. Lastly, the objects that do not have parallaxes measured by *Gaia* DR2 we denote as members without membership information from Lodieu et al. (2019b) (two stars, both with photometry from the OSN).

### Table with our Hyades sample

Below, we present the table with the 75 objects, their membership and a selection of the main data compiled.

| *Name* | $\alpha_{J2000}$ (h:m:s) | $\delta_{J2000}$ (°:′:″) | *Notes memb.* | $B-V$ (mag) | e$B-V$ (mag) | $V$ (mag) | e$V$ (mag) | $M_v$ (mag) | $V-Ic$ (mag) | e$V-Ic$ (mag) | $V-Rc$ (mag) | e$V-Rc$ (mag) | $Ks$ (mag) | e$Ks$ (mag) | *Notes phot.BVRI* | *Date Obs.OSN* | $D_{BJ.Gaia}$ (pc) | *Per.* (days) | *Notes period* | *Spect. Types* |
|---|---|---|---|---|---|---|---|---|---|---|---|---|---|---|---|---|---|---|---|---|
| BD+23 465 | 03:32:50 | +23:41:32 | 2 | 0.845 | 0.002 | 8.890 | 0.010 | 5.773 | | | 0.856 | 0.016 | 6.907 | 0.016 | PIN | | 42.018 | 9.390 | K | K1* |
| LP 413-93 | 03:43:47 | +20:51:36 | 2 | 1.505 | 0.027 | 14.649 | 0.026 | 11.37 | 1.169 | 0.019 | 2.644 | 0.021 | 9.612 | 0.022 | OSN | 19/11/2015 | 45.213 | 12.320 | 2 | M2/3* |
| HD 283066 | 03:51:03 | +23:54:13 | 2 | 1.159 | 0.027 | 10.213 | 0.026 | 7.158 | 0.713 | 0.019 | 1.272 | 0.021 | 7.395 | 0.02 | OSN | 19/11/2015$^{M}$ | 40.828 | 12.570 | 2 | K6 |
| LP 413-108 | 03:54:53 | +16:18:56 | 1 | 1.566 | 0.024 | 14.295 | 0.021 | 11.08 | 1.218 | 0.015 | 2.680 | 0.021 | 9.056 | 0.021 | OSN | 18/11/2015 | 43.940 | 6.040 | D | M4.0 |
| HD 286363 | 03:55:01 | +12:29:08 | 1 | 1.070 | 0.008 | 10.12 | 0.010 | 6.807 | | | 1.124 | 0.020 | 7.574 | 0.021 | PIN | | 45.976 | 11.660 | D | K0 |
| HD 285252 | 03:55:07 | +16:59:55 | 1 | 0.906 | 0.003 | 8.964 | 0.004 | 5.903 | 0.492 | 0.003 | 0.915 | 0.003 | 6.91 | 0.021 | JONER | | 40.936 | 9.820 | K | K0 |
| HD 285348 | 04:03:39 | +19:27:18 | 1 | 1.048 | 0.027 | 10.151 | 0.026 | 6.746 | 0.640 | 0.019 | 1.146 | 0.021 | 7.6 | 0.02 | OSN | 19/11/2015$^{M}$ | 47.972 | 11.60 | 2 | K2 |
| HG 7-88 | 04:05:26 | +19:26:32 | 1 | 1.348 | 0.004 | 11.415 | 0.007 | 8.044 | | | 1.577 | 0.020 | 8.107 | 0.026 | PIN | | 47.232 | 13.850 | 2 | K7 |
| HD 285367 | 04:05:40 | +17:56:16 | 1 | 0.893 | 0.005 | 9.310 | 0.015 | 6.008 | | | 0.896 | 0.016 | 7.254 | 0.023 | PIN | | 45.746 | 9.100 | K | K0 |
| HD 27406 | 04:20:13 | +19:14:01 | 1 | 0.572 | 0.003 | 7.444 | 0.003 | 4.119 | 0.313 | 0.003 | 0.618 | 0.005 | 6.124 | 0.018 | JONER | | 46.238 | 5.45 | R | F9V |
| HG 7-92 | 04:06:35 | +13:32:57 | 1 | 1.489 | 0.024 | 13.401 | 0.021 | 9.913 | 1.034 | 0.015 | 2.178 | 0.021 | 9.091 | 0.018 | OSN | 18/11/2015 | 49.843 | 16.680 | D | M1 |
| HD 285507 | 04:07:01 | +15:20:06 | 1 | 1.180 | 0.008 | 10.485 | 0.007 | 7.218 | | | 1.268 | 0.020 | 7.665 | 0.026 | PIN | | 45.029 | 14.030 | K | K4 |
| HD 285482 | 04:07:43 | +16:31:08 | 1 | 1.019 | 0.027 | 9.929 | 0.026 | 6.592 | 0.599 | 0.019 | 1.090 | 0.021 | 7.511 | 0.026 | OSN | 19/11/2015 | 46.500 | 11.600 | K | K0 |
| HD 285478 | 04:08:11 | +16:52:23 | 2 | 1.405 | 0.027 | 11.491 | 0.026 | 8.476 | 0.904 | 0.019 | 1.724 | 0.021 | 7.933 | 0.024 | OSN | 19/11/2015 | 40.087 | 13.630 | D | K7 |
| HD 286554 | 04:08:27 | +12:11:31 | 1 | 1.328 | 0.003 | 11.277 | 0.006 | 7.945 | | | 1.558 | 0.016 | 8.046 | 0.027 | PIN | | 46.381 | 12.960 | D | K5 |
| HG 7-122 | 04:11:28 | +15:59:32 | 1 | 1.561 | 0.024 | 15.157 | 0.023 | 11.77 | 1.204 | 0.025 | 2.722 | 0.026 | 9.941 | 0.021 | OSN | 17/11/2015 | 47.467 | 1.790 | D | M1 |
| HD 26736 | 04:14:32 | +23:34:30 | 1 | 0.664 | 0.004 | 8.047 | 0.008 | 4.745 | 0.356 | 0.002 | 0.691 | 0.004 | 6.516 | 0.02 | JONER | | 45.752 | 8.38 | K | G5V |
| HD 285625 | 04:15:10 | +14:23:54 | 1 | 1.373 | 0.006 | 11.557 | 0.015 | 8.153 | | | 1.630 | 0.011 | 8.128 | 0.017 | PIN | | 47.947 | 13.910 | D | K5 |
| V* V984 Tau | 04:16:33 | +21:54:27 | 1 | 0.814 | 0.002 | 9.147 | 0.006 | 5.608 | | | 0.825 | 0.011 | 7.275 | 0.023 | PIN | | 51.021 | 10.260 | D | G9/K0 |
| HD 285630 | 04:17:25 | +19:01:48 | 1 | 1.181 | 0.024 | 10.833 | 0.021 | 7.436 | 0.751 | 0.015 | 1.351 | 0.021 | 7.909 | 0.023 | OSN | 18/11/2015$^{M}$ | 47.792 | 12.840 | 2 | K5 |
| HG 7-150 | 04:17:28 | +14:54:04 | 1 | 1.537 | 0.024 | 14.458 | 0.023 | 10.987 | 1.126 | 0.026 | 2.501 | 0.026 | 9.621 | 0.019 | OSN | 17/11/2015 | 49.454 | 2.380 | 2 | M3 |
| HD 285690 | 04:18:19 | +16:05:18 | 1 | 0.984 | 0.002 | 9.548 | 0.005 | 6.276 | 0.533 | 0.006 | 0.991 | 0.003 | 7.322 | 0.017 | JONER | | 45.118 | 12.640 | R | K0 |
| V* V893 Tau | 04:18:58 | +19:54:24 | 1 | 0.748 | 0.005 | 8.597 | 0.005 | 5.238 | 0.405 | 0.001 | 0.768 | 0.003 | 6.921 | 0.016 | JONER | | 46.969 | 9.390 | R | G9 |
| HD 27282 | 04:19:08 | +17:31:29 | 1 | 0.730 | 0.003 | 8.427 | 0.006 | 5.071 | 0.393 | 0.003 | 0.752 | 0.006 | 6.787 | 0.016 | JONER | | 46.896 | 8.960 | K | G8 |
| HD 27406 | 04:20:13 | +19:14:01 | 1 | 0.572 | 0.003 | 7.444 | 0.003 | 4.119 | 0.313 | 0.003 | 0.618 | 0.005 | 6.124 | 0.018 | JONER | | 46.238 | 5.45 | R | F9V |
| HD 27732 | 04:23:22 | +21:22:45 | 1 | 0.758 | 0.002 | 8.854 | 0.010 | 5.349 | | | 0.786 | 0.016 | 7.121 | 0.016 | PIN | | 50.226 | 9.130 | 3 | G8* |
| V* V989 Tau | 04:23:25 | +15:45:47 | 1 | 1.237 | 0.003 | 10.499 | 0.020 | 7.410 | | | 1.368 | 0.011 | 7.494 | 0.018 | PIN | | 41.467 | 12.380 | D | K5V |
| HD 27771 | 04:23:32 | +14:40:14 | 1 | 0.866 | 0.003 | 9.097 | 0.005 | 5.759 | 0.466 | 0.002 | 0.875 | 0.004 | 7.145 | 0.017 | JONER | | 46.525 | 10.010 | K | K1.5* |
| LP 535-73 | 04:23:51 | +09:12:19 | 1 | 1.484 | 0.024 | 12.902 | 0.021 | 9.644 | 1.103 | 0.015 | 2.368 | 0.021 | 8.226 | 0.018 | OSN | 18/11/2015 | 44.834 | 5.330 | D | M3.0 |
| Cl* Melotte 25 VR8 | 04:23:59 | +16:43:18 | 1 | 1.464 | 0.024 | 12.558 | 0.021 | 9.244 | 0.982 | 0.015 | 1.976 | 0.021 | 8.561 | 0.018 | OSN | 18/11/2015 | 46.000 | 17.140 | D | M0 |
| V* V990 Tau | 04:24:17 | +18:00:11 | 1 | 1.069 | 0.004 | 9.966 | 0.009 | 6.621 | 0.602 | 0.004 | 1.102 | 0.005 | 7.524 | 0.018 | JONER | | 46.659 | 11.470 | 2 | K5 |
| HD 285742 | 04:25:00 | +16:59:06 | 1 | 1.028 | 0.001 | 10.248 | 0.006 | 6.562 | 0.583 | 0.004 | 1.070 | 0.005 | 7.83 | 0.016 | JONER | | 54.613 | 11.770 | D | K4 |
| HD 27990 | 04:25:48 | +18:01:02 | 4 | 0.939 | 0.009 | 8.989 | 0.003 | 5.867 | 0.520 | 0.002 | 0.978 | 0.002 | 6.767 | 0.021 | JONER | | 42.108 | 8.460 | D | K2 |

(Continued).

| *Name* | $\alpha_{J2000}$ (h:m:s) | $\delta_{J2000}$ (°:′:″) | *Notes memb.* | $B-V$ (mag) | e$B-V$ (mag) | $V$ (mag) | e$V$ (mag) | $M_v$ (mag) | $V-Ic$ (mag) | e$V-Ic$ (mag) | $V-Rc$ (mag) | e$V-Rc$ (mag) | $Ks$ (mag) | e$Ks$ (mag) | *Notes phot.BVRI* | *Date Obs.OSN* | $D_{BJ.Gaia}$ (pc) | *Per.* (days) | *Notes period* | *Spect. Types* |
|---|---|---|---|---|---|---|---|---|---|---|---|---|---|---|---|---|---|---|---|---|
| V* V992 Tau | 04:26:06 | +15:31:28 | 4 | 0.555 | 0.004 | 7.472 | 0.002 | 4.227 | 0.311 | 0.001 | 0.614 | 0.003 | 6.14 | 0.021 | JONER | | 44.562 | 4.83 | R | F9* |
| HD 28099 | 04:26:40 | +16:44:49 | 1 | 0.659 | 0.003 | 8.12 | 0.007 | 4.812 | | | 0.694 | 0.011 | 6.547 | 0.021 | PIN | | 45.885 | 8.68 | K | G2V |
| HD 286798 | 04:26:43 | +12:41:11 | 0 | 1.335 | 0.024 | 10.455 | 0.021 | | 0.870 | 0.015 | 1.652 | 0.021 | 7.03 | 0.024 | OSN | 18/11/2015$^{M}$ | | 12.610 | D | K2 |
| HD 286820 | 04:26:48 | +10:52:16 | 4 | 1.017 | 0.027 | 9.4532 | 0.026 | 6.094 | 0.638 | 0.019 | 1.155 | 0.021 | 6.882 | 0.02 | OSN | 19/11/2015$^{M}$ | 46.966 | 10.400 | D | K0 |
| HD 285828 | 04:27:25 | +14:15:38 | 4 | 1.087 | 0.027 | 10.445 | 0.026 | 6.841 | 0.677 | 0.019 | 1.224 | 0.021 | 7.713 | 0.023 | OSN | 19/11/2015$^{M}$ | 52.594 | 12.810 | K | K2 |
| V* V993 Tau | 04:27:36 | +15:35:21 | 1 | 0.545 | 0.005 | 7.404 | 0.005 | 4.010 | 0.302 | 0.003 | 0.599 | 0.001 | 6.141 | 0.024 | JONER | | 47.725 | 5.87 | R | F8* |
| HD 28237 | 04:27:46 | +11:44:11 | 1 | 0.556 | 0.003 | 7.507 | 0.01 | 4.224 | | | 0.607 | 0.016 | 6.158 | 0.017 | PIN | | 45.348 | 5.14 | K | F8 |
| HD 285830 | 04:27:47 | +14:25:04 | 1 | 0.927 | 0.006 | 9.475 | 0.010 | 6.010 | 0.509 | 0.003 | 0.949 | 0.004 | 7.348 | 0.02 | JONER | | 49.321 | 10.280 | K | K0 |
| HG 7-232 | 04:28:29 | +17:41:46 | 4 | 1.439 | 0.024 | 12.178 | 0.023 | 8.825 | 1.031 | 0.026 | 2.218 | 0.026 | 7.711 | 0.026 | OSN | 17/11/2015 | 46.832 | 2.440 | 2 | M0.5 |
| V* V918 Tau | 04:28:37 | +19:44:26 | 1 | 0.736 | 0.002 | 8.580 | 0.005 | 5.155 | 0.398 | 0.002 | 0.764 | 0.003 | 6.908 | 0.016 | JONER | | 48.413 | 11.480 | K | G7/8* |
| HD 28344 | 04:28:48 | +17:17:08 | 1 | 0.619 | 0.002 | 7.837 | 0.006 | 4.495 | 0.339 | 0.001 | 0.657 | 0.002 | 6.404 | 0.02 | JONER | | 46.599 | 7.38 | R | G2V |
| V* V994 Tau | 04:28:51 | +16:17:20 | 4 | 1.293 | 0.027 | 10.723 | 0.026 | 7.030 | 0.844 | 0.019 | 1.586 | 0.021 | 7.349 | 0.021 | OSN | 19/11/2015$^{M}$ | 54.768 | 3.660 | R | K4V |
| HD 285773 | 04:29:32 | +17:53:35 | 1 | 0.827 | 0.003 | 8.934 | 0.004 | 5.633 | 0.448 | 0.003 | 0.841 | 0.003 | 7.055 | 0.027 | JONER | | 45.729 | 9.550 | K | K0V |
| HD 28462 | 04:29:58 | +16:40:22 | 1 | 0.854 | 0.003 | 9.090 | 0.030 | 5.795 | | | 0.879 | 0.016 | 7.139 | 0.024 | PIN | | 45.609 | 9.390 | K | K1V |
| HG 7-246 | 04:30:34 | +14:44:53 | 1 | 1.585 | 0.024 | 14.739 | 0.023 | 11.245 | 1.170 | 0.026 | 2.618 | 0.026 | 9.712 | 0.018 | OSN | 17/11/2015 | 49.978 | 18.410 | D | M1 |
| HD 285876 | 04:31:52 | +15:29:58 | 1 | 1.293 | 0.003 | 11.055 | 0.015 | 7.754 | | | 1.471 | 0.016 | 7.895 | 0.024 | PIN | | 45.734 | 13.130 | D | K0V |
| V* V997 Tau | 04:32:59 | +15:49:08 | 1 | 0.755 | 0.002 | 8.641 | 0.004 | 5.285 | 0.406 | 0.002 | 0.774 | 0.001 | 6.941 | 0.026 | JONER | | 46.907 | 9.800 | K | G8* |
| V* V697 Tau | 04:33:24 | +23:59:27 | 0 | 1.499 | 0.024 | 12.639 | 0.023 | | 1.074 | 0.026 | 2.349 | 0.026 | 8.028 | 0.026 | OSN | 17/11/2015 | | 17.550 | D | M3.0 |
| HD 284552 | 04:33:37 | +21:09:03 | 1 | 1.236 | 0.004 | 10.687 | 0.015 | 7.483 | | | 1.362 | 0.016 | 7.686 | 0.026 | PIN | | 43.741 | 13.590 | K | K7V |
| HD 28878 | 04:33:38 | +16:45:45 | 1 | 0.897 | 0.003 | 9.357 | 0.005 | 5.925 | 0.483 | 9.0E-4 | 0.901 | 0.004 | 7.351 | 0.024 | JONER | | 48.576 | 9.820 | 3 | K2* |
| HD 285837 | 04:33:42 | +19:00:51 | 1 | 1.198 | 0.003 | 10.737 | 0.015 | 7.343 | | | 1.317 | 0.016 | 7.82 | 0.023 | PIN | | 47.731 | 12.640 | K | K7 |
| TYC 677-227-1 | 04:34:11 | +11:33:29 | 4 | 1.387 | 0.027 | 11.754 | 0.026 | 8.357 | 0.906 | 0.019 | 1.767 | 0.021 | 8.059 | 0.029 | OSN | 19/11/2015$^{M}$ | 47.779 | 11.590 | K | K7 |
| HD 28977 | 04:34:32 | +15:49:39 | 1 | 0.921 | 0.003 | 9.644 | 0.007 | 6.054 | 0.505 | 0.004 | 0.942 | 0.004 | 7.553 | 0.026 | JONER | | 52.245 | 9.160 | 3 | K0 |
| HD 28992 | 04:34:35 | +15:30:17 | 1 | 0.632 | 0.004 | 7.898 | 0.005 | 4.571 | 0.342 | 0.004 | 0.672 | 0.005 | 6.445 | 0.026 | JONER | | 46.285 | 8.93 | K | G0* |
| UCAC 4517-008262 | 04:35:49 | +13:17:17 | 1 | 1.570 | 0.024 | 14.921 | 0.021 | 11.462 | 1.192 | 0.015 | 2.608 | 0.021 | 9.867 | 0.018 | OSN | 18/11/2015 | 49.169 | 13.360 | D | M2.5 |
| HD 29159 | 04:36:05 | +15:41:02 | 1 | 0.867 | 0.009 | 9.345 | 0.005 | 5.844 | 0.467 | 0.004 | 0.886 | 0.003 | 7.373 | 0.015 | JONER | | 50.147 | 9.470 | D | K0 |
| HD 286929 | 04:39:51 | +12:43:43 | 1 | 1.085 | 0.001 | 9.992 | 0.007 | 6.793 | 0.624 | 0.002 | 1.135 | 0.002 | 7.48 | 0.023 | JONER | | 43.633 | 11.300 | K | K7 |
| UCAC 4521-008763 | 04:41:28 | +14:04:34 | 1 | 1.548 | 0.023 | 13.432 | 0.023 | 9.972 | 1.080 | 0.026 | 2.391 | 0.026 | 8.712 | 0.021 | OSN | 17/11/2015 | 49.199 | 1.280 | D | M2.5 |
| PMJ 04414+1200 | 04:41:29 | +12:00:34 | 1 | 1.477 | 0.023 | 12.907 | 0.023 | 9.539 | 0.990 | 0.026 | 2.095 | 0.026 | 8.754 | 0.02 | OSN | 17/11/2015 | 47.164 | 18.000 | D | M1* |
| TYC 694-1183-1 | 04:41:30 | +13:13:16 | 1 | 1.445 | 0.027 | 11.210 | 0.026 | 7.988 | 0.939 | 0.019 | 1.825 | 0.021 | 7.507 | 0.02 | OSN | 19/11/2015 | 44.101 | 15.420 | D | M0.5 |
| StKM 1-512 | 04:46:19 | +03:38:11 | 2 | 1.276 | 0.004 | 10.910 | 0.010 | 7.6 | | | 1.404 | 0.020 | 7.826 | 0.02 | PIN | | 45.101 | 13.250 | D | K4/5 |
| HD 30246 | 04:46:30 | +15:28:19 | 4 | 0.674 | 4.0E-4 | 8.28 | 0.003 | 4.827 | 0.366 | 0.005 | 0.711 | 7.0E-4 | 6.738 | 0.033 | JONER | | 49.054 | 7.95 | D | G5 |
| StKM 1-514 | 04:47:19 | +06:27:12 | 2 | 1.379 | 0.017 | 11.296 | 0.019 | 8.256 | 0.896 | 0.012 | 1.692 | 0.013 | 7.875 | 0.026 | OSN | 16/11/2015 | 40.545 | 14.440 | D | M0.0 |

(Continued).

| *Name* | $\alpha_{J2000}$ (h:m:s) | $\delta_{J2000}$ (°:′:″) | *Notes memb.* | $B-V$ (mag) | e$B-V$ (mag) | $V$ (mag) | e$V$ (mag) | $M_v$ (mag) | $V-Ic$ (mag) | e$V-Ic$ (mag) | $V-Rc$ (mag) | e$V-Rc$ (mag) | $Ks$ (mag) | e$Ks$ (mag) | *Notes phot.BVRI* | *Date Obs.OSN* | $D_{BJ.Gaia}$ (pc) | *Per.* (days) | *Notes period* | *Spect. Types* |
|---|---|---|---|---|---|---|---|---|---|---|---|---|---|---|---|---|---|---|---|---|
| HD 284653 | 04:47:26 | +23:03:03 | 2 | 1.112 | 0.003 | 10.687 | 0.006 | 6.985 | | | 1.184 | 0.016 | 7.995 | 0.033 | PIN | | 54.998 | 11.790 | 3 | K4V |
| LP 416-570 | 04:48:31 | +16:23:19 | 1 | 1.433 | 0.034 | 12.419 | 0.036 | 9.008 | 0.929 | 0.018 | 1.875 | 0.031 | 8.543 | 0.017 | OSN | 19/12/2015$^{+}$ | 48.118 | 15.690 | D | M0* |
| LP 536-63 | 04:49:52 | +06:06:34 | 2 | 1.574 | 0.036 | 14.720 | 0.036 | 11.523 | 1.071 | 0.018 | 2.720 | 0.032 | 9.627 | 0.022 | OSN | 19/12/2015$^{+}$ | 43.581 | 17.120 | D | M3/4* |
| HD 286085 | 04:50:01 | +16:24:43 | 1 | 1.141 | 0.027 | 10.594 | 0.026 | 7.128 | 0.709 | 0.019 | 1.267 | 0.021 | 7.839 | 0.016 | OSN | 19/11/2015 | 49.335 | 11.980 | D | K6 |
| UCAC 4525-009613 | 04:51:02 | +14:58:17 | 1 | 1.373 | 0.024 | 11.713 | 0.021 | 8.661 | 0.903 | 0.015 | 1.808 | 0.021 | 7.967 | 0.02 | OSN | 18/11/2015$^{M}$ | 40.771 | 13.140 | D | M0.5 |
| HD 284930 | 04:52:24 | +18:59:49 | 1 | 1.070 | 0.008 | 10.290 | 0.010 | 6.760 | | | 1.114 | 0.020 | 7.742 | 0.02 | PIN | | 50.754 | 11.340 | D | K0 |
| HD 32347 | 05:03:08 | +13:43:50 | 2 | 0.776 | 0.007 | 8.596 | 0.004 | 4.947 | 0.414 | 0.002 | 0.786 | 0.004 | 7.226 | 0.027 | JONER | | 53.681 | 8.960 | K | K0 |
| StKM 1-549 | 05:11:10 | +15:48:58 | 4 | 1.445 | 0.027 | 12.040 | 0.026 | 8.257 | 0.962 | 0.019 | 1.932 | 0.021 | 9.866 | "" | OSN | 19/11/2015$^{M}$ | 57.086 | 14.940 | D | M1.0 |
| StKM 1-551 | 05:11:19 | +07:54:32 | 2 | 1.206 | 0.027 | 11.246 | 0.026 | 7.459 | 0.752 | 0.019 | 1.358 | 0.021 | 8.301 | 0.026 | OSN | 19/11/2015 | 57.193 | 13.230 | D | K5 |

Parameters shown by order: names of the stars taken from the SIMBAD database; coordinates ($\alpha$ and $\delta$); membership notes (0: without membership date in Lodieu et al. (2019a), 1: member, 2: possible member, 3: unlikely member, 4: non-member); $B-V$, $V$, $V-R_c$, $V-I_c$ photometry with their errors and brightness calibrated in the $V$ ($M_v$) band obtained using the distances from Bailer-Jones et al. (2018); photometry noted that indicate the origin of the data used, PIN: Pinsonneault et al. (2004), JONER: Joner et al. (2006); night when the data were taken at the OSN, the symbol + indicates that during that night the observations were made using the 0.9 m telescope and that the $V-I_c$ value could be affected by fringing, the $M$ next to the observation date indicates that photometry was derived from the mean of the repeated data for this star on the observation night; distances derived by Bailer-Jones et al. (2018) from Bayesian analysis of parallaxes from Gaia ($D_{BJ.Gaia}$); rotation period; origin of the selected rotation period; spectral types, the symbol $*$ indicates that they were derived using the $B-V$, $V$ and $V-I_c$ values and the table by Erik Mamajek of tabulated values. The remaining spectral types were taken from the SIMBAD database.

**Notes of rotation periods.**

References of the rotation periods, showing the same notations as Douglas et al. (2019):

2: Douglas et al. (2016)

3: Douglas et al. (2019)

P: Prosser et al. (1995)

H: Hartman et al. (2011)

D: Delorme et al. (2011b)

K: rotation period by A. Kundert & P. Cargile 2014;

R: period by Radick et al. (1987) or Radick et al. (1995)

# Chapter 4

# Isochrones

## Contents

The aim of this chapter is focused on selecting a reference in the $M_v$ versus $B-V$, $M_v$ versus $V-I_c$ and $M_v$ versus $V-K_s$ colour-magnitude diagrams, in order to study, in the next chapter, which stars deviate from it. The selection of this reference is effected by comparing the data of the five clusters with various stellar evolution models developed to try to reproduce observational data of clusters in colour-magnitude diagrams (CMD). The idea is to choose the stellar model whose isochrones successfully reproduce these data in the three CMDs.
We will begin the chapter with a summary of the origins of modern stellar evolution models, and of how the isochrones are generated from them. We will then explain the behaviour of the isochrones as a function of various physical inputs and the characteristics of the stellar models chosen to compare with the data. We will next show the fits, and lastly we will decide what reference will be chosen. We will show the fits for $M_v$ versus $B-V$, $M_v$ versus $V-I_c$ however our idea is to use the same chosen stellar model for the three CMDs.

## 4.1 Hertzprung-Russell Diagram

In 1911, the Danish astronomer Ejnar Hertzsprung published the representation of apparent magnitudes against the colour of stars belonging to the Pleiades and Hyades clusters. Because they are diagrams of stars that are members of the same cluster – in other words, they are at the same distance – the use of apparent magnitudes is equivalent to the use of absolute magnitudes. In the Hyades diagram, Hertzsprung showed the differentiation between the two groups of stars, which we now call dwarfs and giants.
Two years later, in 1913, Henry Norris Russell used parallaxes for a large number of stars, and thanks to this was able to represent absolute magnitude versus spectral types (related to the colour of the stars), and thus clearly capture this same effect in which two well-differentiated groups appeared (see Figure 4.1a), marking them as dwarfs or giants, names probably coined by Russell himself. Gingerich (2013) explains the history behind the invention of the HR diagram in great detail, of which we have given only a fragment. From these independent studies (Hertzsprung 1911; Russell 1913), the discovery of the diagram was attributed to them both.

In his book "The Internal Constitution of the Stars", Eddington (1926) provided the first stellar model capable of explaining the physics behind the HR diagram. Eddington was also the first to suggest that if stars did not undergo gravitational collapse, this was not only due to the pressure of the gas present in their interior, but that there should be radiation originating from an energy source located in their centre. This theory, added to later knowledge of the chemical composition present in the interior of stars, has served to quantitatively formalize the theory of stellar evolution.

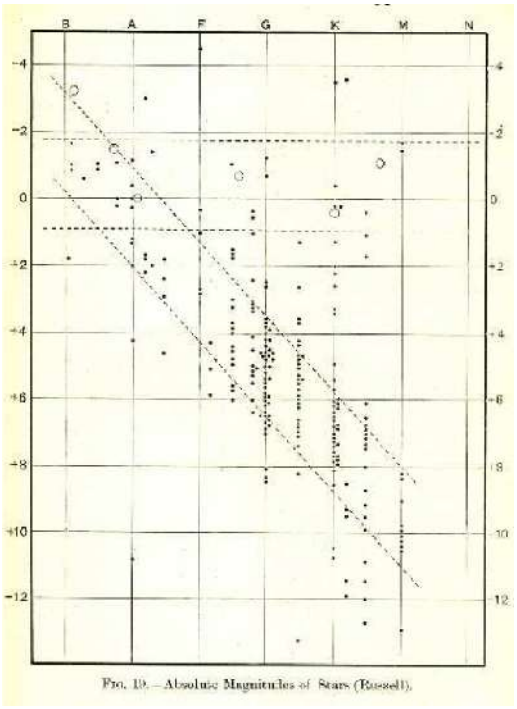


(a) Russell's HR Diagram, representing spectral types-luminosity (Russell 1913).

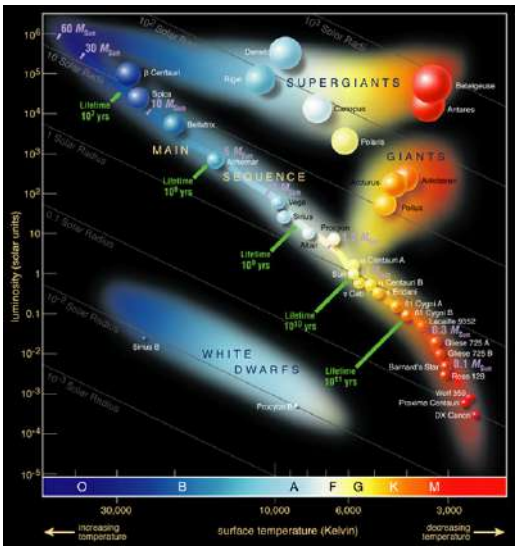


(b) HR Diagram showing some of the evolutionary phases (Image Credit: Pearson Education).

Figure 4.1: HR Diagram

Today, the HR diagram is one of the most used tools in Astrophysics for studying stars and stellar clusters. In this diagram, the temperature of the stars is represented versus their luminosity, although often, instead of using these physical units, it is represented in observational units – absolute magnitude and colour, which diagram we call CMD. As we will see below, making use of modern models of star evolution, the position of each star on the HR diagram provides information on their evolutionary state and their mass (see Figure 4.1b), with it also being possible to estimate the expected values of luminosity and colours for a range of ages.

## 4.2 Evolutionary tracks and isochrones

The codes developed to reproduce the evolution of stars show how a model of a star evolves over a lifetime. Kippenhahn et al. (1967) were the precursors of modern stellar evolution models. They created numerical codes in the FORTRAN programming language in order to solve the equations of stellar structure. Building on their work, other physical properties of stars were added until the current models were developed.

The current codes can generate evolutionary tracks that represent the location of a star on the HR diagram, showing how its luminosity and temperature would change over time (see Figure 4.2a). To use an evolutionary track, one must first provide the initial mass of the star and its initial chemical composition. The tracks are based on a large number of details related to the interior of stars and their atmospheres. Many of these details vary between models: there are several work teams focusing on developing them and each one may adopt different treatments with regard to chemical composition, opacities, equations of state, et cetera. This gives rise to different models possibly producing varying results for the same initial conditions. Furthermore, despite the advances in this field and even though fully convective stars are considered the most simple to describe theoretically (Feiden & Chaboyer 2014), the theory of low-mass stars and brown dwarfs presents different challenges to those faced for more massive stars. The main challenges, as Spada et al. (2017)explain, are the treatment of the boundary conditions of the atmospheres and the equation of state (for example, Allard et al. 1997; Chabrier & Baraffe 1997, 2000). We should also mention the study carried out by the group led by Isabelle Baraffe and Gilles Chabrier, who have developed models focusing on this type of star (Baraffe et al. 1998, 2015).In addition, many authors have concentrated their efforts on trying to improve their models to attain the goal of reproducing the observational data in the regime of low-mass stars, (for example, Dartmouth: Dotter et al. (2008); Padova/PARSEC: Chen et al. (2014); Victoria-Regina: VandenBerg et al. (2006); MESA: Choi et al. (2016); Yapsi: Spada et al. (2017) ).

We derive the isochrones using a group of evolutionary tracks that encompass a range of initial masses and the same initial chemical composition. As we can see in Figure 4.2b, instead of showing on the HR diagram the evolution in time of a star of a particular mass, one isochrone indicates the position on the diagram of the stars of the same age and different masses. This is a much-used tool for studying star clusters that, as we have already explained in this introduction, comprise

objects of different masses, with the assumption that they have the same age and chemical composition. It is worth mentioning the study by Sandage (1962) , who was the first author to use the isochrone fitting method to try to determine the ages of two open clusters and three globular clusters.

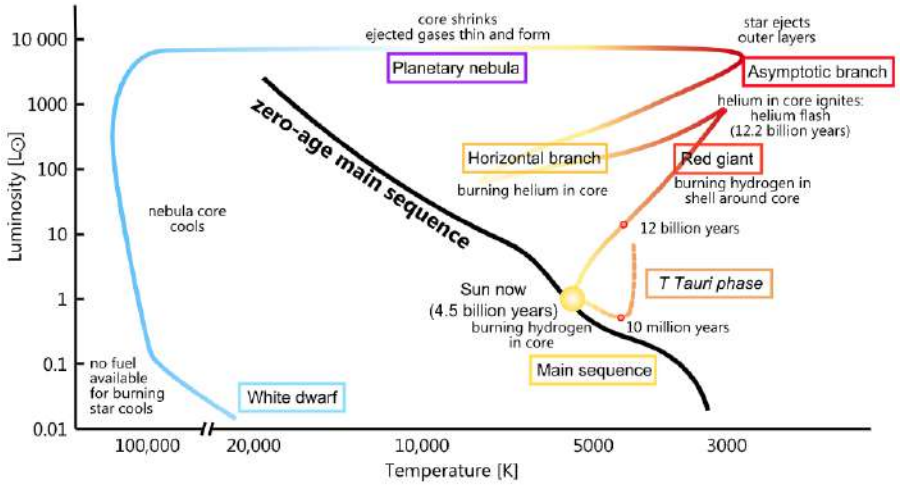


(a) Sun evolutionary track (credit: Wikimedia Commons).

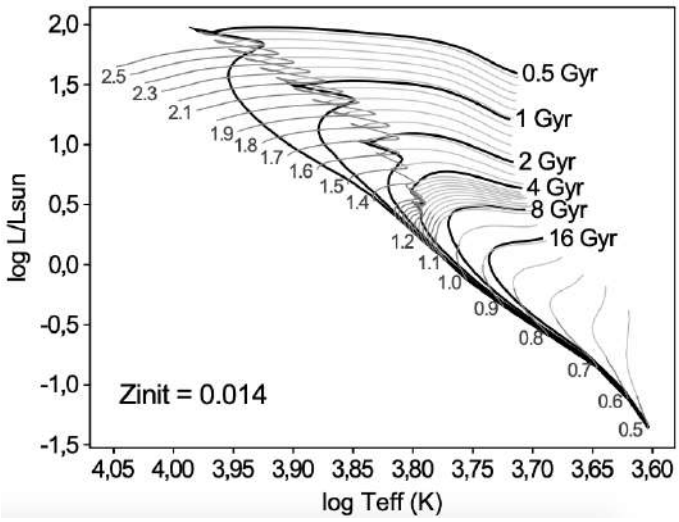


(b) Evolutionary tracks and isochrones (Mowlavi et al. 2012).

Figure 4.2: In the upper figure the evolutionary track of the Sun is shown passing through all its evolutionary phases, where zero-age main sequence is the point in the life of the star when it starts to fuse hydrogen in its core to form helium. In the lower diagram, an example of evolutionary tracks is represented, and isochrones derived from them. *Zinit* indicates the initial chemical composition (metallicity).

As well as the aforementioned difficulties faced by the groups that develop the stellar evolution models and their different treatments, which affect the result of the isochrones, there is a series of parameters, obtained from observational data, whose individual uncertainties contribute to the final uncertainty of the fitting of the isochrone to the cluster stars. These parameters are: the distance of the stars, their membership, the binarity of the sample, reddening, average chemical composition of the cluster (metallicity), and the uncertainty of the fit itself of the isochrone to the data. Fortunately, thanks to *Gaia*, the accuracy of many of these parameters (distance, proper motions, membership, reddening) has been enhanced, and we make use of these in the fits.

Below, we explain some of the parameters used to generate stellar models and isochrones and the effect that the variation of the values of these parameters have on their form.

### 4.2.1 Parameters that affect the form of the isochrones

As we have mentioned above, there are differences between models depending on the factors that their developers take into account regarding the interior of the stars and their atmospheres, which affect the form of the isochrones. Graph 4.3 summarizes the physical inputs and the isochrone zones where they have greater impact. For this reason, before focusing on the characteristics of the selected models, we will explain some of the physical inputs and parameters used to build them and in which zone of the isochrones they have greater relevance.

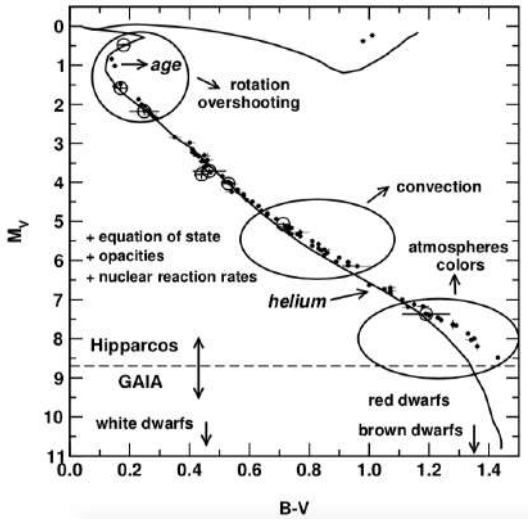


Figure 4.3: Diagram from Lebreton (2005) which shows various physical inputs and parameters and the isochrone zone where they have greater effect. The horizontal line is included to show the magnitude limit of Hipparcos and *Gaia*.

### Mixing Length Parameter

Stellar convection is a complex phenomenon and very difficult to simulate. To simplify its modelling, the mixing length theory (MLT) is used. This holds that the process of convection consists of discrete parcels of fluid, which maintain their temperature and density until they cover a certain distance ($l_{MLT}$) in the interior of the star. Past this distance they disperse in the atmosphere and share their energy with the surroundings.
The mixing length $l_{MLT}$, is proportional to the local pressure scale height $H_P$, and the factor of proportionality is the mixing length parameter, $\alpha_{MLT}$. In other words,

$$l_{MLT} = \alpha_{MLT} * H_p \tag{4.1}$$

. In short, $\alpha_{MLT}$ shows how efficient the convection is, since the higher its value, the higher the area the parcel covers before dispersing. This parameter is determined by comparing the stellar models to a calibrator (usually the Sun) and, in general, a value between 1 and 2 is adopted.

As Lebreton et al. (2014) (henceforth LB14) explain so well, in an overview of the calculation of stellar ages from models, the impact of variations in the value of $\alpha_{MLT}$ in the isochrones is mainly perceived for stars with a convective envelope – spectral type K to F stars. For these, when the $\alpha_{MLT}$ value increases, a displacement of the isochrones toward the blue is observed. This is because the higher the $\alpha_{MLT}$, the more compact the star is, the less the radius and the effective temperature increases, maintaining equal luminosity.

### Convective Overshooting

In stars with mass greater than $\sim$ 1.4 times solar mass, the core is convective and the envelope radiative. Convection in the core is very efficient, thus the value of the mixing length has no effect. For these types of stars, the MLT does not explain the mixing that occurs at the convective boundaries, for the convection extends beyond the boundaries that mark both the convective and radiative regions, penetrating a certain way to the base of the star's radiative envelope. This effect is called convective overshooting.
One of the following methods is usually used to treat this phenomenon:

- The equation that relates the distance covered $d_{ov}$ and the local pressure scale height $H_p$ with the factor $\alpha_{OV}$ is used, which describes the efficiency of the convective overshooting process,

  $$d_{ov} = \alpha_{ov} * H_p \tag{4.2}$$

  The parameter $\alpha_{OV}$ is calibrated by varying its value (it is usually between 0 and 0.4) in the stellar models until it successfully reproduces a selection of observational data.

- The second method is based on the decrease of the displacement velocity of the convective element as it moves away from the convective boundary until it is dispersed in the region of convective overshooting. The parameter $f_{ov}$ is used to describe the mixing efficiency

by convective overshooting, which defines the velocity scale height ($H_v$) of the convective elements at the convective boundary with the following relation:

$$H_v = f_{ov} * H_p \tag{4.3}$$

This parameter is also usually calibrated using observational data.

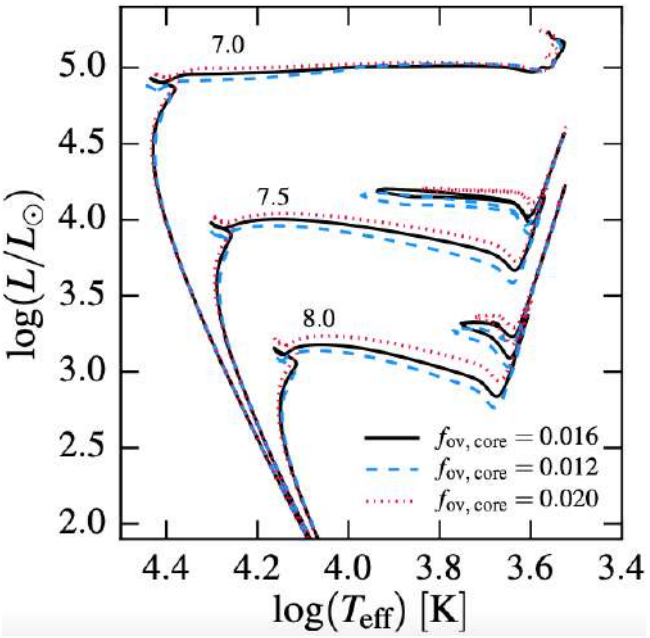


Figure 4.4: MIST isochrones with different values for the parameter $f_{ov}$ (Choi et al. 2016).

Figure 4.4 represents an example that shows how the variation of the parameter of convective overshooting efficiency affects the isochrones. We can see how the higher the value, the longer the main sequence stage, and the position of the turn-off point, frequently used to determine ages, is modified.

### Heavy elements

The chemical elements heavier than hydrogen and helium are designated metals. In the development of the stellar models, it is assumed that the chemical composition of stars is formed by the mass fraction of hydrogen (X), the mass fraction of helium (Y) and the metals (Z), the sum of which is normalized (X + Y + Z = 1).

Neither the initial abundances nor the contents of stars' interiors can be derived from observations. Furthermore, given that observations generally provide abundances relative to hydrogen, in the models it is very common to express a star's abundance of metals by means of the Z/X relation, which is related to the observed abundances using the following equation:

$$[m/H] = log(Z/X)_{star} - log(Z/X)_{\odot} \tag{4.4}$$

[m/H] is the star's metallicity, and $(Z/X)_\odot$ has been determined in many studies, whose resulting values show a dispersion. In Table 3, LB14 show a list of these studies, whose values of $(Z/X)_\odot$ are found between $\sim$ 0.016 and $\sim$ 0.024. Therefore, in the models, one of the values calculated for this parameter must be selected.

Unfortunately, it is not possible to determine the abundances of all the metals of a particular star. Iron is usually used as an indicator of the total metal content, assuming that all the metals vary their abundance proportionally to the abundance variation of Fe. Thus, considering that the metal distribution in a star is the same as in the Sun (solar-scaled distribution) – that is $\{X_i/Z\} = \{X_i/Z\}_\odot$, (the abundance of a given element $i$ is denoted as $X_i$), finally we have,

$$[m/H] = [Fe/H] = log(Z/X)_{star} - log(Z/X)_\odot \tag{4.5}$$

Regarding the variation in the value of $Z$, this affects the form of the isochrones as is shown in Figure 4.5, which we will discuss below. An increase in $Z$ implies a decrease in the temperature and luminosity.

#### $\alpha$ elements

As our study deals with young clusters, the enrichment of elements $\alpha$ (O, Ne, Mg, Si, S, Ar, Ca, Ti) does not have any repercussions. We mention this because in many models it is taken into account as an option for extracting the isochrones.

#### Initial helium abundance

As we have already mentioned and as LB14 explain so well in their review, the initial abundance of helium that is present in the molecular cloud where the Sun was formed cannot be discovered with observational methods, and it is not the same as that observed currently in the Sun's convective envelope.
When the calibration of the models with respect to the Sun is carried out, one takes a star model of 1 $M_\odot$ with the age of the Sun (4.57 Gyr), and one modifies the $\alpha_{MLT}$ values, the initial helium abundance ($Y_{0,\odot}$) values and the initial metals-to-hydrogen ratio $(Z/X)_{0,\odot}$, until the star model presents values of luminosity, radius and surface abundance of metals $(Z/X)_\odot$ as close as possible to those observed for the Sun.

The initial helium abundance $Y_0$ is a free parameter of stellar models, and its value tends to be adopted depending on one of these options:

- Its value is considered the same as that resulting from solar calibration ($Y_{0,\odot}$), which, as we saw, depends on the stellar model.
- It is considered that the initial helium abundance of a model to a given metallicity Z follows this relation:

$$Y_0 = Y_p + Z * (\Delta Y/\Delta Z) \tag{4.6}$$

where $Y_p$ is the primordial helium. The first stars, originating many millions of years after the Big Bang, were formed only with hydrogen y helium. The latter is what is known as primordial helium and its value is fairly well established ($\sim 0.25$, Aver et al. 2013; Cyburt et al. 2008; Coc et al. 2013). $\Delta Y/\Delta Z$ is the helium-to-heavy elements enrichment ratio, which indicates the enrichment of helium and heavy elements in the interstellar medium resulting from Galactic evolution. Its value is not certain, but usually $\Delta Y/\Delta Z = 2 \pm 1$ is adopted. However, as LB14 explain, Gennaro et al. (2010) have shown that in the literature, values from 0.5 to 5, at least, have been adopted.

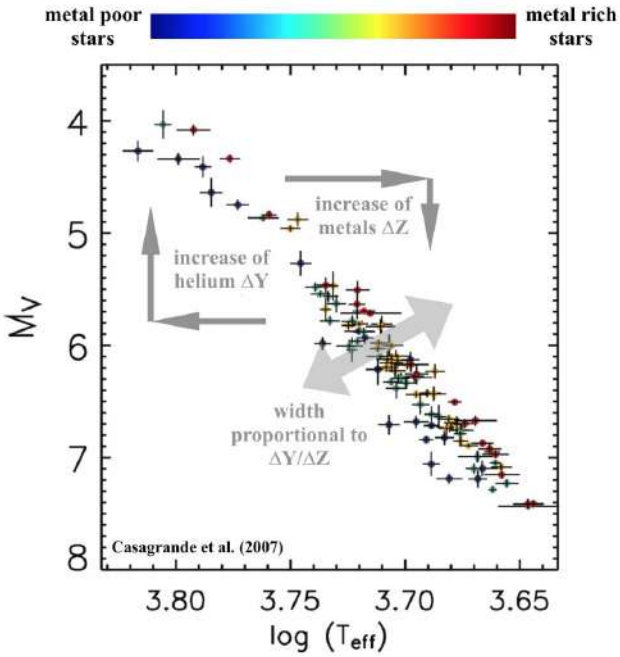


Figure 4.5: Effect of the variations of Y, Z and $\Delta Y/\Delta Z$ on the form of the isochrones. Image from Casagrande et al. (2007).

Following the equation 4.6, the three parameters that modify the isochrones are $Y_0$, $Z$ and $\Delta Y/\Delta Z$, as shown in Figure 4.5 from Casagrande et al. (2007) In this figure, we see how if the value of $Y_0$ is increased to a fixed $Z$, it causes a particular mass in the isochrone to move in the diagram to a hotter and more luminous zone. The result of varying $\Delta Y/\Delta Z$ has an effect as shown in the figure, in which we can see that the higher the value of $\Delta Y/\Delta Z$, the greater the dispersion in luminosity and temperature.

### Rotational-induced mixing

The differential rotation of stars gives rise to a shear effect that generates hydrodynamic instabilities in radiative zones. This causes a turbulence that produces a vertical transport of chemical elements, producing rotational mixing that feeds the convective core of the star with hydrogen. Moreover, as Yoon et al. (2012) explain, it also increases the abundance of helium on the surface. This effect becomes dominant as the star evolves, which leads to greater luminosity and higher

surface temperature than in the models without rotation for most of the time in the main sequence. The effect of the rotation on the isochrones is similar to that produced by convective overshooting. Due to the increase in the convective core, the main sequence is prolonged and the turn-off point position is modified.
To summarize, of the effects that we have discussed, convective overshooting and differential rotation have a greater impact on ~ F-type or later stars, whereas the $\alpha_{MLT}$ value and the Y, Z, $\Delta Y/\Delta Z$ values affect lower-mass stars. However, as L. Casagrande has explained (by private communication), we can affirm that, independently of the age of our stars, spectral types K and later are only affected by variations in Y, Z, $\Delta Y/\Delta Z$.
Additionally, as Feiden & Chaboyer (2014) explains, the properties of fully convective stars derived by stellar models become insensitive to variations of input parameters such as $\alpha_{MLT}$.

### 4.2.2 Stellar models whose isochrones we will fit to the observational data

In the following section, we will fit the isochrones from various stellar evolution models developed by different teams to the observational data compiled for each cluster. The aim is to choose the model that best fits with these data. This model will then be the reference in the next chapter for studying the stars that deviate from the models. First, however, we will explain some details of these stellar models that have been chosen for comparison.

#### Yapsi: Yale-Potsdam stellar isochrones

The Yale-Potsdam stellar isochrones have been developed to improve the Yonsei-Yale (YY, Yi et al. (2003)) models, and are focused on generating stellar models for low-mass stars (Spada et al. 2017).

These isochrones cover a range of ages between 1 Myr and 20 Gyr, a mass range between 0.15 $M_\odot$ and 5 $M_\odot$, and a metallicity [Fe/H] range from -1.5 to +0.3 dex.

For every value of initial metallicity $[Fe/H]_0$, they have calculated evolutionary tracks from which they derived the isochrones, with initial helium abundance values of $Y_0$ = 0.25, 0.28, 0.31, 0.34, 0.37. These initial helium and metallicity values ($Y_0$, $[Fe/H]_0$) have been treated as independent parameters, in such a way that they do not use a fixed value of $\Delta Y/\Delta Z$.
In these models they treat the convective overshoot mixing following the relation from Claret & Torres (2016) between stellar masses and $\alpha_{ov}$. Thus $\alpha_{ov}$ is null for masses lower than 1.35 $M_\odot$. Regarding solar calibration, they derived two $\alpha_{MLT}$ values for two different mass ranges: for masses in the range 0.15 - 0.82 $M_\odot$, $\alpha_{MLT}$ ~ 1.918 and for 0.86 - 5.00 $M_\odot$, $\alpha_{MLT}$ ~ 1.821. To perform this calibration, they took the solar metallicity data from the study by Grevesse & Sauval (1998) with a value of $(Z/X)_\odot$ = 0.0230.
They did not take rotation mixing into account.

To extract their isochrones, one can either access their website, where they have a series of grids for the different metallicities and initial helium abundances, or one can use a routine programmed in FORTRAN language, which they have provided to carry out interpolations in age,

metallicity and helium abundance. We have used this tool to obtain the most suitable Yapsi isochrones for each cluster.

### MESA isochrones and Stellar Tracks (MIST)

As Choi et al. (2016) explain, in their study they have built stellar evolution models using the "Modules for Experiments in Stellar Astrophysics" code (MESA; Paxton et al. 2011, 2013, 2015). Below we describe some characteristics of their solar-scaled models.

The MIST isochrones describe stellar populations of ages between 0.1 Myr and $\sim$ 20 Gyr, masses in the range of $0.1 \leq M/M_{\odot} \leq 300$ and metallicities $-2 \leq [Z/H] \leq 0.5$, being [Z/H] = [Fe/H].

Unlike other studies, they derived the models with solar-scaled composition, taking the proto-solar abundance as reference instead of that currently present in the photosphere, which is $(Z/X)_{\odot}$ = 0.0199 (Asplund et al. 2009). They obtain the initial helium abundance, for a given Z, by means of the relation $Y_0 = 0.249 + 1.5 * Z$, thus adopting a fixed value $\Delta Y/\Delta X = 1.5$.
Regarding processes derived from the convection, they treat the convective overshoot mixing using the second method explained in the previous section, with a value of $f_{ov}$ in the core of 0.016. The fixed value for the mixing length parameter $\alpha_{MLT}$ is 1.82. Lastly, of the models we have used, this is the only one that gives the option of adding the rotation effect on the isochrones.

To obtain these models, they give the options of downloading their grids or using an interpolator, both being available on their website.

### Dartmouth

The Dartmouth Stellar Evolution Program is described in Bjork & Chaboyer (2006), Dotter et al. (2007) and Dotter et al. (2008). These models provide solar-scaled distribution isochrones and also give the option of adding $\alpha$ enhancement, which, as we have explained, we will not be taking into account.

The isochrones generated from their evolutionary tracks cover a range of masses that span from 0.1 $M_{\odot}$ to 4 $M_{\odot}$ and age between 250 Myr and 15 Gyr. With respect to the chemical composition, the metallicity [Fe/H] values are found in the range from -2.5 to 0.5. They obtain the initial helium from the equation $Y_0 = 0.245 + 1.54Z$ – that is $Y_p = 0.245$ and $\Delta Y/\Delta Z = 1.54$. They also give the option of taking another two values of $Y_0$ = 33, 34 for a range of [Fe/H] from 0 to -2.5.

For the treatment of convection, they adopt a value of $\alpha_{MLT} = 1.938$, and they performed the solar calibration using the data from Grevesse & Sauval (1998) with $(Z/X)_{\odot} = 0.0229$.
Regarding the convective overshoot mixing, its value depends on the composition and the stellar mass (see Table 1 of Dotter et al. (2008)). Thus the parameter $\alpha_{ov}$ is equal to 0.05 for a mass that they have defined as minimum, which, as can be seen in the cited Table 1, is not lower than 1.2 $M_{\odot}$ for a solar metallicity. In terms of higher masses, if they exceed the minimum mass by 0.1

$M_\odot$, $\alpha_{ov} = 0.1$, and if they surpass it by 0.2 $M_\odot$, $\alpha_{ov} = 0.2$.

In order to generate the isochrones, we have not been able to use the interpolation program provided on the Dartmouth models website, because, as A Dotter explained by private communication, this tool is only available for ages older than 1 Gyr. For lower ages, there are isochrone grids available on the same website, in which they give different values of metallicity, age, initial helium and $\alpha$ enhancement.

### BCAH15

The models presented in Baraffe et al. (2015) (BCAH15) were developed to improve, update and finally substitute the extremely widely used BCAH98 (Baraffe et al. 1998). These new solar-scaled composition models, like the previous ones, are also based on low-mass stars, from $0.07 M_\odot$ to $1.4 M_\odot$, and provide a range of ages from 0.001 Gyr to 10 Gyr. For all the evolutionary tracks, the metallicity is solar and they consider the initial helium abundance $Y_0 = 0.28$. Moreover, for the solar calibration, they use solar photospheric abundances from Asplund et al. (2009), being $(Z/X)_\odot = 0.0181$, and from this calibration they have derived $\alpha_{MLT} = 1.6$ in the interior of the star. BCAH15 explain that in an ideal situation, the mixing length of the stellar interior is the same as in the atmosphere. In their models, they carry out different considerations in terms of the values $l^{int}_{MLT}$ and $l^{atm}_{MLT}$, although finally they confirm that the greatest differences between the two occur for stars of mass M < 0.2 $M_\odot$, which are insensitive to these variations of mixing length, and therefore we can consider that the value $\alpha_{MLT} = 1.6$. Regarding the convective overshoot mixing, they do not take it into account.
The isochrones we have used are available on the Phoenix/Lyon website.

### PARSEC

The PAdova and TRieste Stellar Evolution Code (PARSEC Bressan et al. 2012; Chen et al. 2014) is an update and improvement of the evolutionary tracks and isochrones of Padova (Bressan et al. 1993; Bertelli et al. 1994, 2008, 2009; Girardi et al. 2000; Marigo 2001). They are scaled-solar composition models, whose isochrones cover a range of ages between 0 Gyr and 15 Gyr, masses between $0.1 M_\odot$ and 350 $M_\odot$, and metallicities -2.2 $\leq [m/H] \leq$ +0.5.

The initial helium abundance is determined by means of the relation $Y_0 = 0.2485 + 1.78Z$, thus $Y_p = 0.2485$ and $\Delta Y/\Delta Z = 1.78$. To treat the convection, they use $\alpha_{MLT} = 1.74$, generated from the calibration of the solar model, using $(Z/X)_\odot = 0.0207$, which value they derived from $Z_\odot$ and $Y_\odot$ taken from Caffau et al. (2011) y Basu & Antia (2004), respectively. Regarding the process of convective overshooting, the parameter $\alpha_{ov}$ varies between 0 and 0.5, depending on the mass and stellar composition, following a similar process to that adopted by the Dartmouth models, the lower the mass the lower the value of $\alpha_{ov}$. The minimum mass of stars with solar metallicity for which they start to consider the overshooting effect is 1.1 $M_\odot$.

To generate the PARSEC isochrones, the group that develops them offers an interface on their website to choose and specify the inputs required. They also show three versions of the code, of which we have used the most recent, "PARSEC version 1.2S".

### 4.2.3 Colour-magnitude diagrams of the isochrone fittings to the cluster data

In this section, we will show the fits of the isochrones of the models selected for the data for the five clusters in two CMDs, $M_v$ versus $B-V$ and $M_v$ versus $V-I_c$ and we will use photometry with errors $\lesssim 0.04$ mag. To calculate absolute magnitude, $M_v$, the BJ distances of the individual stars have been used. For the purpose of seeing the trend of the isochrones in the fits, we have taken into account the cluster samples prior to being trimmed by spectral type, thus including some stars earlier than F-types. Below, we will show the fits carried out for each of the five clusters and then we will describe the conclusions of said fits.

#### $\alpha$ Per

In the fits for this cluster, we have represented 54 stars, 21 with $BVR_cI_c$ photometry from the literature (Stauffer 85/89) and 33 observed at the OSN.
Before representing the isochrones of all the models, we will confirm that the rotation does indeed only affect the form of the isochrones in the upper zone of the main sequence and therefore does not have an impact on our fits. For this, we have first represented the MIST isochrones, whose models provide the option of including this effect, and we show these fits for this cluster with and without the rotation. Additionally, given that when using the Yapsi interpolation tool to generate the isochrones one has to give an initial helium value (in the figures represented, denoted as Y), we will also show various Yapsi isochrones for $\alpha$ Per with values different from Y, in order to select the one that fits best and thus adopt that value to derive the Yapsi isochrones that will be represented with each of the clusters. Regarding the Dartmouth models, as has already been seen, these provide isochrones whose ages begin at 250 Myr, and so we have represented them for Praesepe, Coma Ber and Hyades.

In Figure 4.6, we represent the fits to compare the MIST isochrones with and without rotation, and the Yapsi isochrones with three different Y values: 0.25, 0.28 and 0.30. Indeed, in the two upper diagrams of this figure, we can see that the rotation effect does not impinge on the form of the MIST isochrones in the part of the main sequence that encompasses the low-mass G, K and M stars. Therefore, for all the clusters we will use the MIST isochrones without adding rotation. Regarding the comparison between Yapsi isochrones with different initial helium abundance values, in the lower diagrams, we see that none of the three isochrones is a good fit to $\alpha$ Per in both diagrams. However, in the $M_v$ versus $B-V$ diagram, the isochrone for $Y = 25$, in comparison with the other two, strays further from the trend of the observational data by values of up to $B-V \sim 1.4$ mag, where the three isochrones begin to converge. In the $M_v$ versus $V-I_c$ diagram, it is the isochrone for $Y = 30$ that strays the most, though slightly, from the observational data. In short, although none of the isochrones fits well with this cluster, the extreme values of Y do not appear

to be the best option. Furthermore, BCAH15 use $Y = 28$ for all their isochrones. Therefore, we will use the value $Y = 28$ in the Yapsi isochrones for all the clusters, and we will see how they fit to the data.

Lastly, in Figure 4.7, we represent the CMDs with the isochrones from the stellar evolution models and the data for the cluster, for which we have used the following parameters of $\alpha$ Per:

- For all the clusters, we have adopted the reddening value given by Gaia Collaboration et al. (2018b), which for $\alpha$ Per is $E(B-V) = 0.09$ mag. Using the relations from Bessell & Brett (1988): $E(V-I)_{cousins} = 1.25E(B-V)$ and $E(V-K) = 2.78E(B-V)$, we have generated $E(V-I)_{cousins} = 0.1125$ mag and $E(V-K) = 0.250$ mag. Lastly, we have derived $A_v = 0.279$, according to the equation $A_v = R_v E(B-V)$, being $R_v = 3.1$.
- We took the metallicity of $\alpha$ Per calculated by Netopil et al. (2016) (N16), [Fe/H] = 0.14 ± 0.11. In any case, Carrera et al. (2019) (C19) provide a new metallicity measurement for this cluster ([Fe/H]=0.08 ± 0.04), and so we will compare the isochrones with both metallicity data, except those generated from the BCAH15 models, which, as we have already mentioned, all have metallicities [Fe/H] = 0.
- Regarding its age, as we have explained in a previous chapter, we have adopted the age of 70 Myr for $\alpha$ Per.

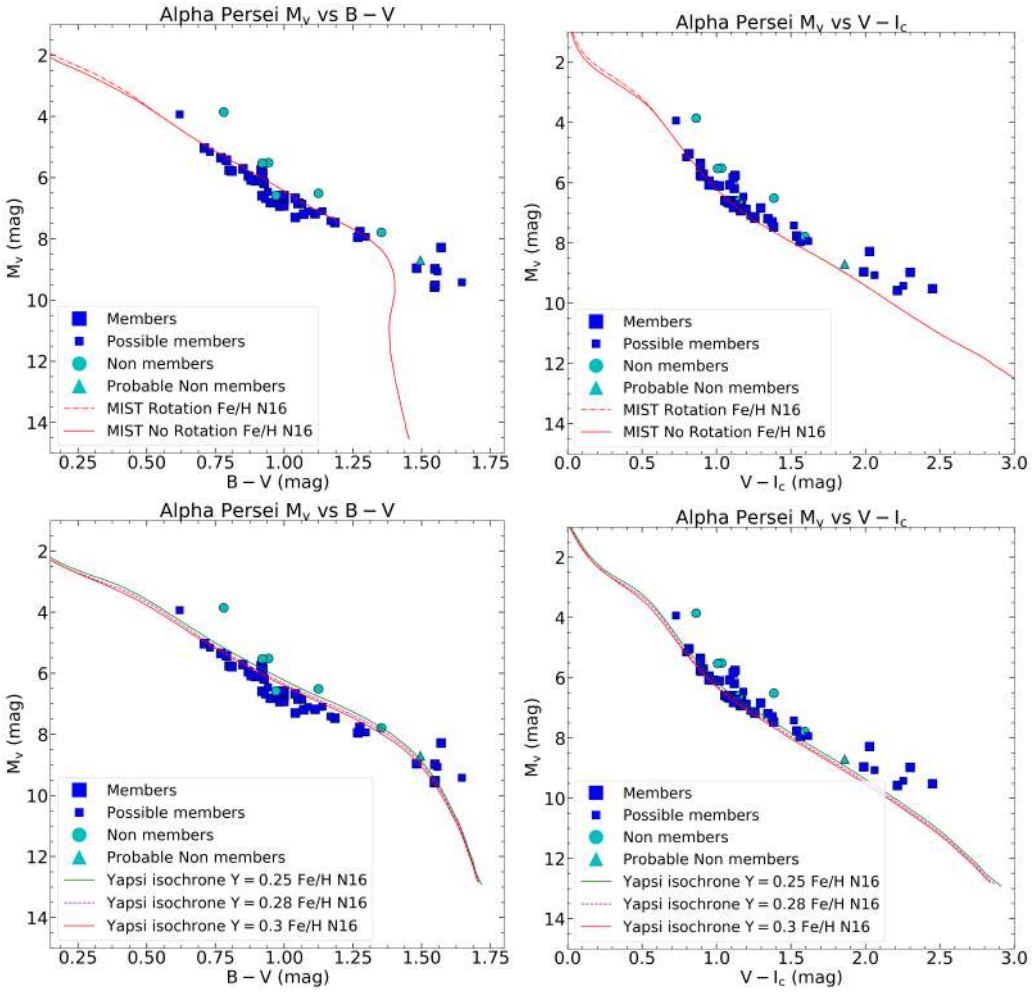


Figure 4.6: CMDs of the objects of $\alpha$ Per, differentiated by their membership, to which the MIST and Yapsi isochrones have been fit. In the upper part, the fits of the MIST isochrones are shown, with the rotation (dotted line) and without (continuous line). In the lower part, the Yapsi isochrones are represented for three different Y values.

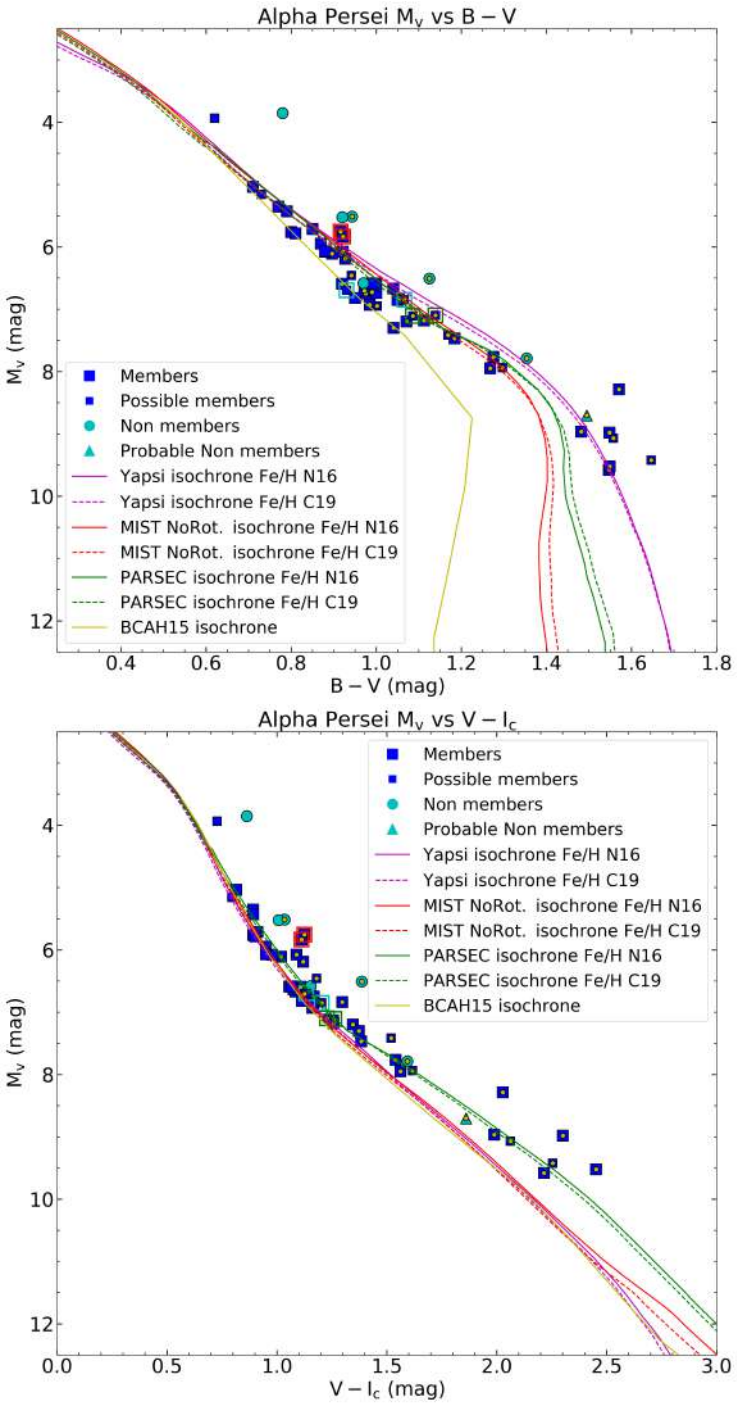


Figure 4.7: CMDs of the isochrones belonging to the Yapsi, MIST, PARSEC and BCAH15 models, fit to the observational data of $\alpha$ Per. The yellow dots mark the stars with OSN measurements. The symbols enclosed by a square represent the stars with two photometry measurements and each color represents a star. The red and green squares indicates that the two measurements were derived from observations at the OSN. The blue squares mark the star with measurements from OSN and Stauffer 85/89. As we explained in the previous chapter, for that star we will use the data from OSN.

Figure 4.7, shows the fit to the $\alpha$ Per data of the isochrones extracted from BCAH15 and Yapsi, MIST without rotation, and PARSEC, the last three represented with metallicities derived by N16 and C19. In the $M_v$ versus $B - V$ diagram, we see how, for the MIST and PARSEC models, the differences between the isochrones of different values of metallicity increase in the lowest zone of the main sequence. In any event, as we can see, these isochrones do not reproduce the observational data in this zone. The BCAH15 isochrone deviates the most from the data, and the Yapsi isochrone, compared with MIST and PARSEC, is a better fit to the zone of lower masses (from $B-V \sim 1.5$ mag) independently of the metallicity value represented, although in comparison with these it strays more from the observational data for higher masses, in the $B-V$ range between $\sim 0.9$ and $\sim 1.4$ mag.

With respect to $M_v$ versus $V - I_c$, the results of the Yapsi, MIST and BCAH15 models are very similar, independently of the metallicity represented. PARSEC is the only model that fits quite well to the data, unlike the other three, which start to stray beyond $V - I_c \sim 1.25$ mag, with no significant differences presented between the metallicities used.

### Pleiades

In the fits performed for Pleiades, 281 stars have been represented, two with photometry derived from the OSN and 279 with measurements from the literature. As we have already seen in the previous chapter, a group of these stars has $BVI_c$ photometry derived by Kamai et al. (2014), and the remaining group forms part of the selection of stars with reliable photometry obtained in that same study and originating from the measurements provided by Stauffer et al. (2007).

Below we proceed in the same way as in the section on $\alpha$ Per, and we describe the Pleiades data used for the representation of the CMDs.

- A reddening value of $E(B - V) = 0.045$ mag has been used, and we have derived, in the same way as in the previous section, $E(V - I)_{cousins} = 0.0562$ mag, $E(V - K) = 0.1251$ mag and $A(V) = 0.1395$ mag.
- For the metallicity, we have compared the isochrones used [Fe/H] = -0.01 ± 0.05 (N16) and [Fe/H] = 0.06 ± 0.00 (C19).
- Although we have decided to use $Y = 28$ as the initial helium value in the Yapsi isochrones, we have also represented the isochrone with $Y = 25$ and metallicity [Fe/H] value obtained by N16, in order to check again the differences between isochrones with different Y values.
- Although the age of Pleiades that we considered most consistent with the results obtained from the literature is 112 Myr, to generate the isochrones we have adopted 100 Myr. This is because when it came to carrying out the representations for this cluster, the age employed by Kamai et al. (2014) – 100 Myr – was used, and because, for the fits that we wish to undertake in the main sequence, a difference of 12 Myr would not be noticed.
- Several stars do not have data from *Gaia* DR2 (these are the same stars that do not have membership information from L19), which is why we have not been able to use the BJ

distances. Instead, we have adopted the mean distance to the cluster of 135 pc to derive their absolute magnitudes.

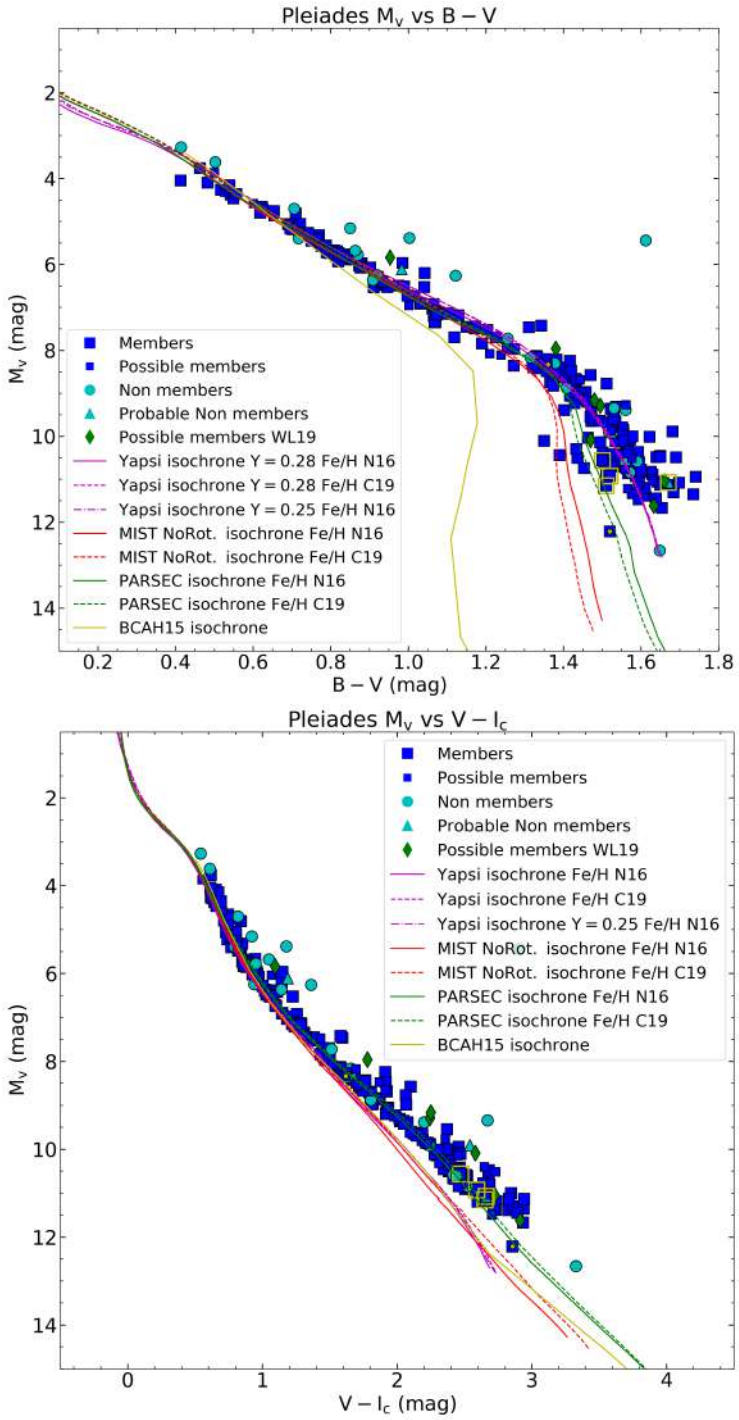


Figure 4.8: CMDs of the isochrones belonging to the Yapsi, MIST, PARSEC and BCAH15 models, fit to the data for Pleiades. The stars represented with a green diamond are those that have no data from *Gaia* DR2 and therefore no membership information from L19. The yellow dots mark the stars with OSN measurements.

Figure 4.8 shows the isochrones from the Yapsi, MIST, PARSEC and BCAH15 models fitted to the observational data. Again, in the $M_v$ versus $B-V$ diagram, the BCAH15 models are those that stray most from the trend demonstrated by the cluster. The other models are very similar for $B-V$ values between $\sim$ 0.3 and $\sim$ 0.8 mag, and beyond the latter value these isochrones begin to diverge. The Yapsi models are those that best fit the lowest part of the main sequence (from $\sim$ 1.4 mag) and, although those that have been generated with a value of $Y_0$=28 and [Fe/H] from N16 seem to fit slightly better, there is no significant difference between the three Yapsi isochrones. The PARSEC and MIST models, however, present differences in the lowest part of the isochrone, with the [Fe/H] varying, and in both models the isochrones with [Fe/H] values from N16 are closer to the cluster data. Although PARSEC reproduces the observational data better than MIST, neither of the two reproduce the behaviour of the cluster in the CMD for $B-V \gtrsim 1.4$ mag. Lastly, for $B-V$ values between $\sim$ 0.8 mag and $\sim$ 1.4 mag, it appears that the PARSEC models reproduce the observational data better.

Concerning the $M_v$ versus $V-I_c$ diagram, the PARSEC isochrones again fit the Pleiades data better, and those that were generated with [Fe/H] derived by C19 fit slightly better, although they are located somewhat below the trend marked by the data. we should point out that binary stars have not been removed, which means that there is a possibility that the fit of this last isochrone would improve if the binaries were not represented.

### Coma Ber

In order to perform the isochrone fitting of the models, we followed the same procedure as in the representation of the CMD explained in the article we published on this cluster. We used the same Coma Ber data that we summarize below, and we have represented, in the $M_v$ versus $B-V$ diagram, 34 stars of Coma Berenices, 33 with measurements from the OSN and 1 star with photometry from Kharchenko et al. 2001. Additionally, we have added the group of stars extracted from T19 with photometry by Kharchenko (2001). Lastly, in the $M_v$ versus $V-I_c$ CMD, we show the 33 stars observed at the OSN, since the photometry provided by Kharchenko (2001) lacks values in the $I$ band.

Below, the CMDs are shown with the fits of the five isochrone models with the following data adopted for Coma Ber:

- The reddening was considered null.
- For the metallicity we adopted that calculated by N16, [Fe/H] = 0.00 ± 0.08.
- For Yapsi, we have again applied the initial helium value $Y_0$=25 and $Y_0$=28 for comparison.
- we will adopt an age of 600 Myr.

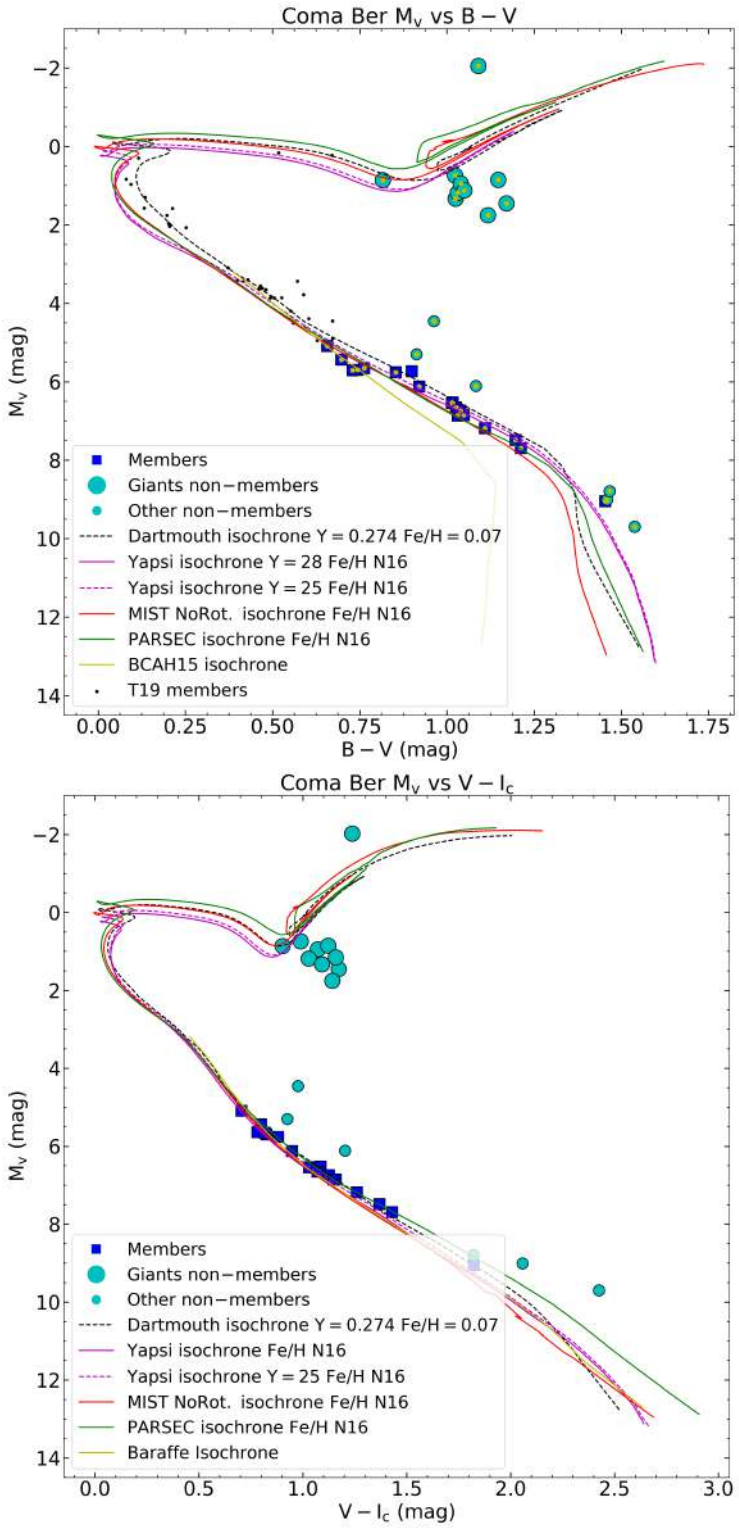


Figure 4.9: CMDs of the isochrones from the Yapsi, MIST, Dartmouth, BCAH15 and PARSEC models fitted to the observational data of Coma Ber. The yellow dots in the CMD $M_v$ versus $B-V$ represent the stars with photometry measurements from OSN. The black dots represent the stars with photometry from T19. All the stars shown in the diagram $M_v$ versus $V-I_c$ have photometry taken at OSN.

Figure 4.9 shows how in the $M_v$ versus $B-V$ diagram, the isochrone that overall seems to fit somewhat better to the data is the one from Yapsi with $Y_0$=28. The MIST, PARSEC and Yapsi ($Y_0$=28) isochrones are very similar, from values of $B-V \sim 0.3$ to $\sim 0.8$ mag. Beyond the latter value, Yapsi separates from the other two models and, unlike them, seems to follow better the trend of the observational data of the lowest part of the main sequence. The BCAH15 isochrone is the worst in reproducing the cluster data and Dartmouth stays above most of the stars, nor does it reproduce the zone of lower-mass stars. The Dartmouth isochrones were previously generated by its authors, and we have chosen those that had a metallicity and value of $Y_0$ closest to those adopted for Coma Ber, although we could not opt for a lower [Fe/H] value, but had to choose the value [Fe/H] = 0.07, which is within the range of uncertainty given by N19. However, we hope that with a value of [Fe/H] = 0 adopted for these isochrones, they would fit better to the observational data from the OSN with $B-V$ from $\sim$ 0.6 mag to $\sim$ 1.2 mag.

In respect of the CMD representing $M_v$ versus $V-I_c$, the isochrone that seems to fit better to the data is the one developed by PARSEC. Aside from the Dartmouth models isochrone, which also follows a similar trend to that of the cluster, the three remaining models – YAPSI, MIST and BCAH15 – as of $V-I_c \sim$1 mag remain below the observational data. We need to bear in mind that we do not have many stars available for this cluster, yet we obtain a similar result to that observed in the CMDs for the Pleiades.

### Praesepe

The isochrones of the five stellar models have been represented in both CMD diagrams with 197 stars of Praesepe, of which 189 have photometry from the literature and eight were observed at the OSN.

To generate and represent the isochrones, we have used the following data for Praesepe.

- Reddening $E(B-V)$ = 0.027 mag, being $E(V-I)_{cousins}$ = 0.0338 mag, $E(V-K)$ = 0.0751 mag and $A(V)$ = 0.0837 mag.
- Metallicity from N16, [Fe/H] = 0.16 ± 0.08
- Age of 650 Myr.
- Again, as with the Pleiades list of objects, we have several stars without data from *Gaia* DR2 and therefore without membership information from L19 and BJ distances, so to derive their absolute magnitudes we have adopted the mean distance to the cluster of 187 pc.

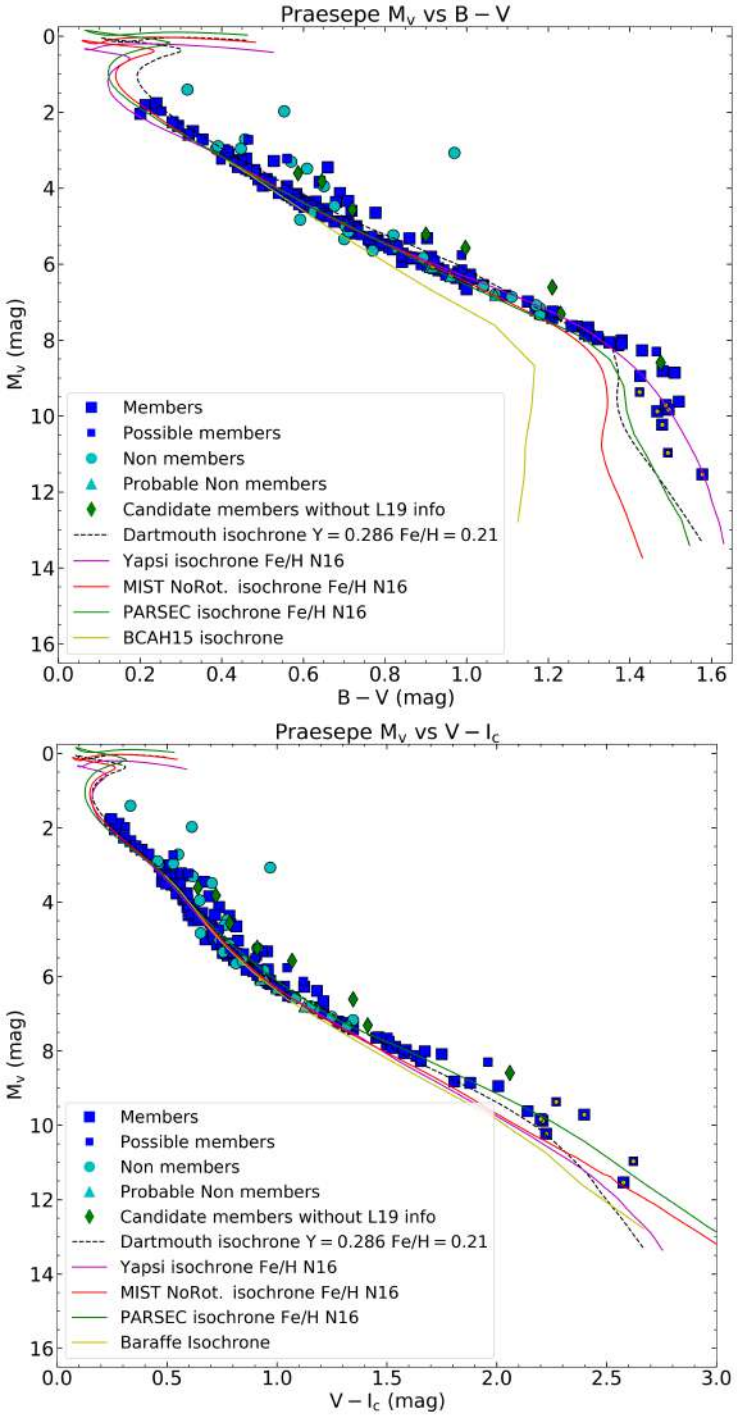


Figure 4.10: CMDs of the isochrones belonging to the Yapsi, MIST, Dartmouth, BCAH15 and PARSEC models, fitted to the observational data of the cluster Praesepe. The objects given the symbol of a green diamond do not have membership information from L19, nor BJ distances. The yellow dots mark the stars with OSN measurements.

Figure 4.10 shows similar results to those observed for the other clusters. In the $M_v$ versus $B-V$ diagram, the Yapsi, MIST and PARSEC isochrones overlap and reproduce the observational data quite well from $B-V \sim 0.4$ to $\sim 0.8$. Beyond the latter value, Yapsi begins to diverge from the other two models, fitting better to the data for the lower-mass stars. The Dartmouth isochrone is again located above practically the whole sequence followed by the objects of the cluster until $B-V \sim 1.2$ mag, from where its luminosity starts to diminish until it falls below the data for the lower-mass stars. The Dartmouth isochrones that we selected are those that were generated with a metallicity value closest to that derived by N16, with [Fe/H] = 0.21, which is within the uncertainty estimated by N16. The BCAH15 isochrone again does not reproduce the data of the cluster in most of the main sequence.

As we have more stars with photometry measurements for Praesepe than for Coma Ber, this $M_v$ versus $V-I_c$ diagram gives a clearer result on the behaviour of the Dartmouth isochrone. Although this isochrone and that from the PARSEC models are the ones that best follow the trend of the cluster in the lower-mass zone, the former is located at lower luminosity values than those shown for the latter, compared to which it also seems to reproduce the observational data worse. In the range of $V-I_c$ values between $\sim 0.5$ mag and $\sim 1$ mag, Yapsi and MIST fit better to the Praesepe data than Dartmouth and PARSEC. The BCAH15 isochrone follows a similar trend to Yapsi and MIST but deviates a little more than these from the cluster data.

### Hyades

Below we show the CMDs of the isochrone models and a total of 75 stars of Hyades, 44 of these stars have measurements from the literature and 31 from observations at the OSN.

For the representation of the isochrones, we have made use of the following data of the cluster.

- Reddening $E(B-V) = 0.001$ mag for which we derived $E(V-I)_{cousins} = 0.00125$ mag, $E(V-K) = 0.0028$ mag and $A(v) = 0.0031$ mag.
- metallicity calculated by N16, [Fe/H] = 0.13 ± 0.05. In the case of Dartmouth, we used an isochrone with the closest metallicity and initial helium abundance values to those of the cluster, [Fe/H] = 0.07 and $Y_0 = 0.274$. As can be seen, [Fe/H] is not within the range of uncertainty of the value given by N16, which would indicate a minimum value of [Fe/H] = 0.08.
- Age 650 Myr.
- There are two stars without data from *Gaia* DR2 that do not have membership information from Lodieu et al. (2019b) (hereinafter, L19H) either. To derive their absolute magnitude, we have adopted a mean distance of 47 pc.

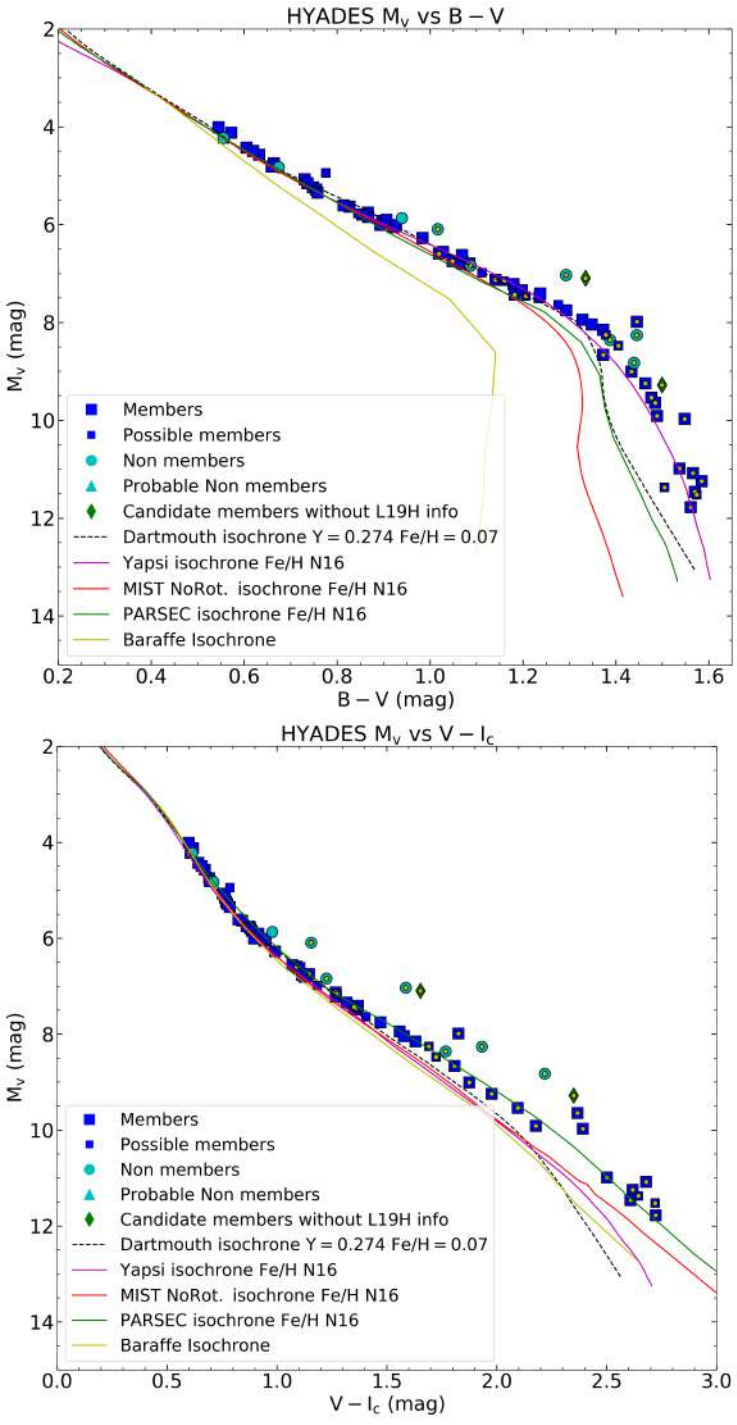


Figure 4.11: CMDs of the isochrones corresponding to the Yapsi, MIST, Dartmouth, BCAH15 and PARSEC models, fitted to the observational data of the cluster Hyades. The objects represented by a green diamond have no membership information from L19H, nor BJ distances. The yellow dots mark the stars with OSN measurements.

In Figure 4.11, there are not many differences compared to the other clusters. In the $M_v$ versus $B-V$ diagram, the Yapsi, MIST and PARSEC isochrones overlap up to $B-V \sim 0.8$ mag, from which point they diverge. Although the Yapsi isochrone does not correctly reproduce the sequence of the cluster stars, and from $B-V \sim 1.25$ mag it is located below it, it is closer to the position of the lower-mass stars. Both PARSEC and MIST are located below the Hyades sequence, almost from the point at which they diverge from Yapsi. The MIST and PARSEC isochrones are very similar up to $B-V \sim 1.15$ mag, at which point they clearly separate, with the PARSEC isochrone straying less from the trend of the lower-mass stars compared to MIST. The Dartmouth isochrone follows a similar path to Yapsi until $B-V \sim 1.3$ mag, from which point on the diagram the Dartmouth isochrones is positioned below the sequence of the cluster stars.

Regarding the $M_v$ versus $V-I_c$ diagram, we can see clearly that the PARSEC isochrone reproduces the cluster data very well and is the one that best fits in comparison with the other models, of which Yapsi, MIST and BCAH15 begin to be located below the sequence from $V-I_c \sim 0.9$ mag and Dartmouth from $V-I_c \sim 1.4$ mag.

### 4.2.4 Conclusions

We have not found any stellar model capable of reproducing the sequences of the clusters in the two CMDs. In the $M_v$ versus $B-V$ diagram, the Yapsi isochrone, although not managing to reproduce the data, is the one that comes close to the trend followed by the lower-mass stars in the five clusters, unlike the other models. However, it strays significantly from the observational data in the $M_v$ versus $V-I_c$ diagram. For this CMD, the model that appears to reproduce the observational data the best is that developed by PARSEC, but, as we have seen, it does not fit correctly to the data in the region of lower-mass stars in the $M_v$ versus $B-V$ diagram. For this reason, we took the decision not to make use of stellar models. Instead, we will proceed in the same way as Kamai et al. (2014), who developed an empirical isochrone using observational data for Pleiades. In this study, we will derive a fiducial for each CMD ($M_v$ versus $B-V$, $M_v$ versus $V-I_c$ and $M_v$ versus $V-K_s$) by using the Hyades data, and we will use this fiducial as a reference in the next chapter.
We have chosen this cluster ahead of the others because it has been well studied, and due to its age – because its stars should not be affected by the variations we are studying in its photometry – and its proximity – because its observational data present fewer uncertainties.

#### Obtaining the fiducial with Hyades data

In order to derive the fiducial from the $M_v$ versus $B-V$, $M_v$ versus $V-I_c$ and $M_v$ versus $V-K_s$ diagrams, having removed the reddening in the $M_v$ magnitude and colours, we will use the group of stars of Hyades employed in the comparison with the isochrone groups, but selecting those that meet the following criteria:

- Stars characterized as singles.
- Stars classified as members of the cluster according to the data from L19H.

- Stars for which their distances have been measured with *Gaia* DR2. As above, we will use the BJ distances.
- The possible member stars whose position in the CMDs follows the same trend as the member stars.
- Lastly, member stars that deviate significantly from the sequence formed by the rest of the objects will be discarded.

**Single stars of Hyades**

In order to distinguish between stars with and without companions, we searched studies in the literature that have focused on this aspect of the Hyades cluster. We found binarity information on our stars in the studies by Kopytova et al. (2016), Patience et al. (1998), Morzinski (2011), Mermilliod et al. (2009b) and the Washington Double Star Catalog (WDS; Mason et al. 2001).

- Kopytova et al. (2016) also derive a fiducial sequence from the Hyades cluster with 250 single stars, spectral types A5 to M6. For this they used data from the literature and from "Lucky Imaging" observations on the Astralux Norte camera mounted on the 2.2 metre telescope at the Calar Alto observatory (Almería), in order to identify stars with no companions.
- Patience et al. (1998) made "speckle-imaging" observations on the Hale telescope at the Palomar observatory (California, USA) and identified 33 binaries.
- Morzinski (2011) used adaptive optics with the Keck (Mauna Kea, USA) and Lick (California) telescopes, observed 75 stars and identified 30 multiple systems.
- Mermilliod et al. (2009b), through observations at the Haute-Provence observatory (France) and ESO La Silla (Chile), obtained spectroscopic data with the principal aim of deriving radial velocities of stars in 13 open clusters, including Hyades. They also identified spectroscopic binary stars in their catalogue.
- The WDS catalogue belongs to the US Naval Observatory and is the largest database of identified multiple systems, with more than 150,000 objects.

Our list of 75 stars of Hyades contains:

- 42 stars classified as singles by Kopytova et al. (2016).
- Three stars identified as singles by Morzinski (2011).
- Two stars (LP 413-108, LP 535-73), that were classified as singles by Kopytova et al. (2016), we identified them photometrically as possible binaries following the procedure explained in section 5.5.1 of the next chapter. These objects are located in three CMDs ($M_v$ versus $V - I_c$, $M_v$ versus $V - K_s$ and $M_{I_c}$ vs $I_c - K_s$) above the trend followed by the rest of the single stars.
- Eight without multiplicity information.

- 20 binaries/multiples identified as such in at least one of the aforementioned studies, with the exception of one star (V* V697 Tau), which we have identified as a possible binary when searching in the Simbad database for stars without binarity information in previous studies.

In Figure 4.12, we represent the 75 stars with their multiplicity and membership.

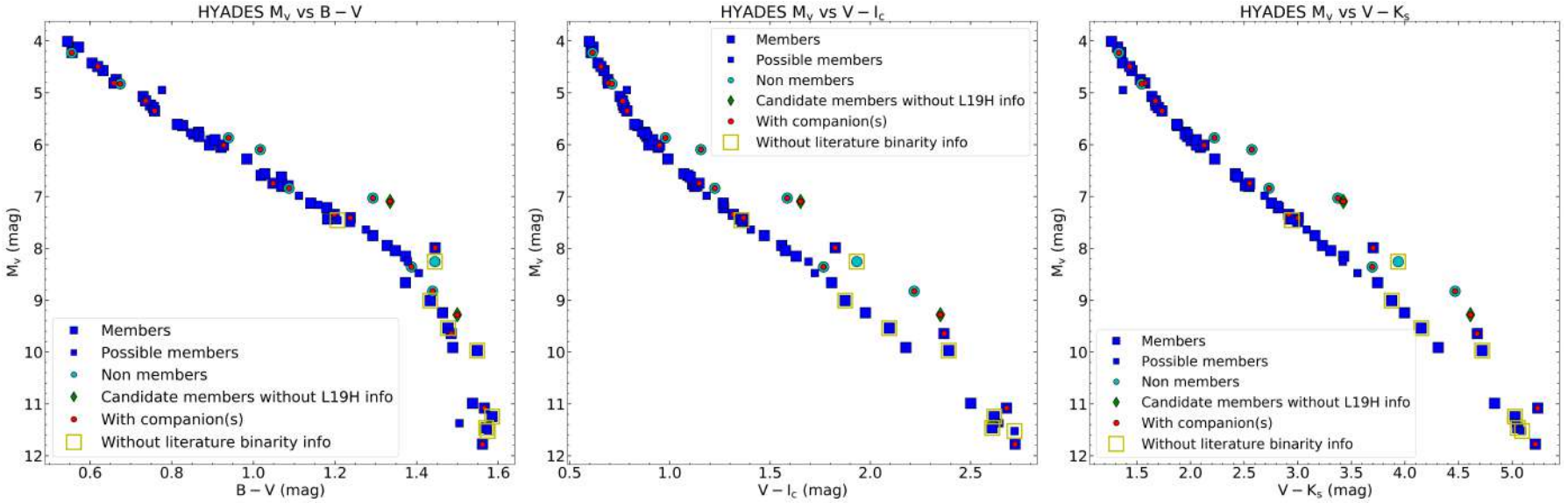


Figure 4.12: Hyades stars with and without binarity/multiplicity information.

Below, we show the fits to the selected Hyades data that meet the aforementioned criteria in the $M_v$ versus $B-V$, $M_v$ versus $V-I_c$ and $M_v$ versus $V-K_s$ diagrams, which we will use as a reference for the three CMDs in the next chapter.

**Fits to Hyades members and single stars**

In each diagram $M_v$ versus $B-V$, $M_v$ versus $V-I_c$ and $M_v$ versus $V-K_s$ of the Figure 4.13 we represent the polynomial that fit best to the data of the objects that have met the requirements. We have marked in red the objects that were discarded for deviating from the trend followed by the rest of the stars in either of the three CMDs. Lastly, given that the lower-mass zone in the CMD is the most complicated to reproduce, in the fit we have used one of the stars that does not have binarity information. This object (UCAC 4517-008262) is a very red star that follows the trend of the objects, that meet the criteria very well, in the three diagrams. In the next chapter we will study photometrically the Hyades members and possible members that do not have binarity information from the literature. In effect, we will catalogue that star as a single object.

Here we show the resulting relations for the three CMDs and the standard deviation of the residuals of the corresponding fit (Root mean square error, RMS). These relations will be used in the next chapter as the fiducial of each CMD. For each diagram the curve that has reproduced the behaviour of the selected stars that best fit the selected data is a fifth-degree polynomial.

Fiducial of the $M_v$ versus $B-V$ diagram, RMS $\sim 0.263$:

$$M_v = 31.725*B-V^5-142.328*B-V^4+251.301*B-V^3-219.7623*B-V^2+100.782*B-V-15.262 \tag{4.7}$$

Fiducial of the $M_v$ versus $V-I_c$ diagram, RMS $\sim 0.102$:

$$M_v = 0.314*V-{I_c}^5-3.288*V-{I_c}^4+13.588*V-{I_c}^3-27.160*V-{I_c}^2+28.920*V-I_c-6.048 \tag{4.8}$$

Fiducial of the $M_v$ versus $V-K_s$ diagram, RMS $\sim 0.065$:

$$M_v = 0.0115*V-{K_s}^5-0.228*V-{K_s}^4+1.786*V-{K_s}^3-6.706*V-{K_s}^2+10.367*V-K_s-5.633 \tag{4.9}$$

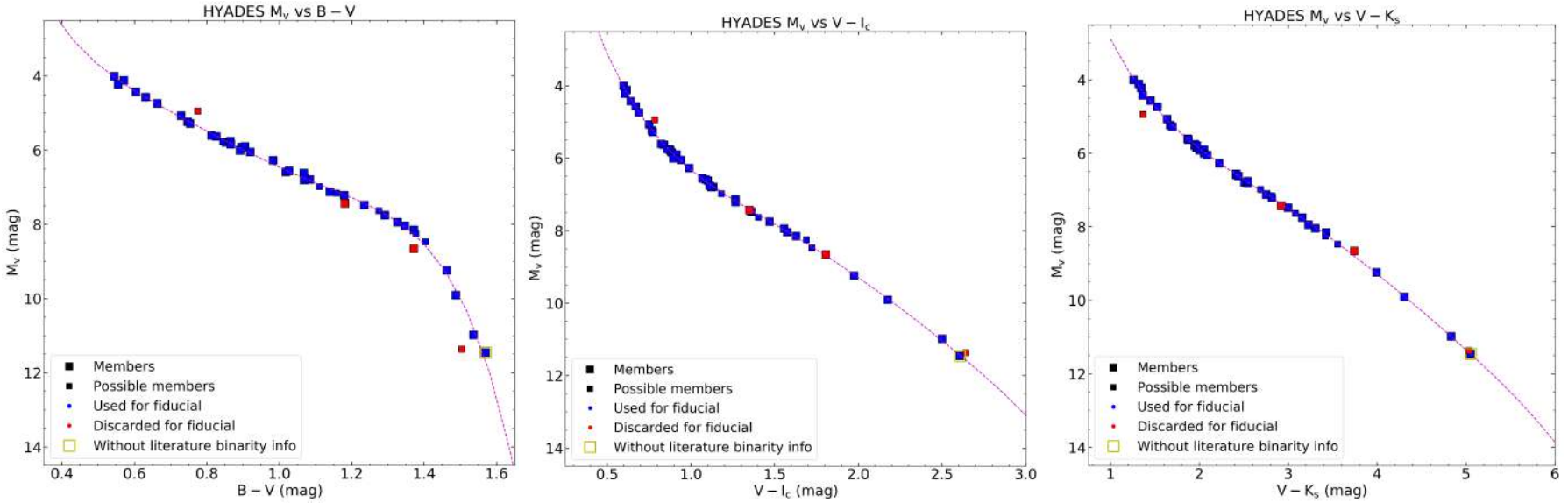


Figure 4.13: Fit of the polynomials that we will use as a fiducial in the $M_v$ versus $B-V$, $M_v$ versus $V-I_c$ and $M_v$ versus $V-K_s$ diagrams. The magenta curve was represented using the stars that meet the specified criteria. The object enclosed by an empty yellow square represents the star for which we have not been able to find information on its binarity but we catalogued it as a single star. The red symbols show those stars thatwere not used for the fits because they deviated from the trend followed by the other stars.

# Chapter 5

# Discussion

## Contents

In this chapter, we will show the results of the fits of the fiducial, obtained using the Hyades cluster, to the four other clusters, $\alpha$ Per, Pleiades, Coma Ber and Praesepe, and also the Hyades cluster itself. The procedure followed for each cluster consists of three parts.

- First, we eliminated the stars classified as non-members, and for the remaining stars we searched the literature in order to identify those that have been catalogued as binary. For those without such information we carried out a photometric classification and characterized the stars as probable singles or binaries. We have represented these stars for each cluster on the $M_v$ vs $B-V$, $M_v$ vs $V-I_c$ and $M_v$ vs $V-K_s$ CMDs, to which we fitted the Hyades fiducial, specifying the value of the periods of each star and marking those classified as binaries.
- For the second step, we carried out a new selection with the aim of only using single stars and reducing the contamination of non-member stars. Thus, we rejected the stars identified as binary, those that had no membership information from L19/L19H and those identified as probable non-members. we then obtained for each cluster a relation between the deviation from their positions on the CMDs with respect to the Hyades fiducial and the value of the stars' rotation periods. In order to obtain this relation, we represented the residuals for each cluster (which we will denote as $\Delta V_{Fiducial}$, following the notation of Kamai et al. (2014)), resulting from the differences in $M_v$ magnitude between the selected stars and the fiducial, on a $\Delta V_{Fiducial}$ vs period diagram. In this diagram, we have only represented the objects whose colours, $B-V$ and $V-I_c$, are located inside the boundaries marked by the colours of the stars that created the $B-V$ and $V-I_c$ Hyades fiducial: 0.54 mag $< B-V <$ 1.6 mag and 0.6 mag $< V-I_c <$ 2.65 mag. These restrictions already included only the stars located within the boundaries given by the colours of the objects that formed the $V-K_s$ fiducial.
- Lastly, we proceeded in a similar way to Kamai et al. (2014) and, with the aim of visualizing those deviations with respect to the fiducial as a function of spectral type, we represented histograms as a function of the variable $\Delta V_{Fiducial}$ for the stars of each cluster grouped according to spectral type.

Below, as with previous chapters, we now show this procedure in detail, cluster by cluster, along with the results obtained.

## 5.1 $\alpha$ Per

### 5.1.1 Binaries in $\alpha$ Per

Once the non-member stars of $\alpha$ Per were eliminated, we were left with a sample of 48 stars, which we had earlier catalogued as members, possible members and probable non-members. For these stars, we found binarity information in the following studies from the literature:

- The WDS catalogue, described in the previous chapter in the section on the identification of binaries in Hyades.

- Patience et al. (2002), who have studied 242 members of the clusters $\alpha$ Per and Praesepe, for the purpose of studying their multiplicity. For this they used speckle imaging observations and images taken directly with the Near Infrared Camera and Multi-Object Spectrometer (NICMOS) installed in the Hubble space telescope. They identified ten binaries in their sample from $\alpha$ Per.

In our sample of 48 stars, 15 were listed in WDS as binaries/multiples, five of which were also identified as such by Patience et al. (2002).
In order to check the binarity of the remaining stars, we followed a similar process to that adopted by Kamai et al. (2014), in which they photometrically identified the possible binaries in Pleiades, representing the stars of the cluster with the fit to their fiducial in four CMDs ($M_v$ vs $B-V$, $M_v$ vs $V-I_c$, $M_v$ vs $V-K_s$ and $M_{I_c}$ vs $I_c-K_s$). They verified the positions of each of the objects that were situated above the fiducial. They took as probable binaries those stars that deviated a $\Delta$V between 0.4 mag and 1.0 mag in three or in the four represented CMDs. They used the $M_{I_c}$ vs $I_c-K_s$ diagram to verify the binarity of the reddest stars with $B-V>1.45$ mag.
We have catalogued four stars that were positioned above the fiducial in three of the four CMDs as probable binaries. Furthermore, we have marked four stars that, independently of their multiplicity, seem to be objects from the pre-main-sequence. We will describe the reasons in the next section.

To summarize, of the 48 objects, we have classified 19 as binary, four as possible pre-main-sequence stars and 25 as singles.

### 5.1.2 Fits of the Hyades fiducial to the cluster $\alpha$ Per

In Figure 5.1, we have represented the $M_v$ vs $B-V$, $M_v$ vs $V-I_c$ and $M_v$ vs $V-K_s$ diagrams of $\alpha$ Per together with the fiducial we obtained in the previous chapter using the data from Hyades. The $M_v$, $B-V$, $V-I_c$ and $V-K_s$ values were represented having previously eliminated the reddening effect corresponding to $\alpha$ Per, for each magnitude and colour. The symbols enclosed by a square represent the stars with two photometry measurements, both derived from observations at the OSN. For these stars we previously had not gathered enough criteria to choose one of the obtained values. Regarding the single star with two OSN measurements, the blueing effect appears in both $B-V$ values and the two values of $M_v$, $V-I_c$ and $V-K_s$ are very similar. For this reason in the next section we derive the mean value. The another object with two OSN measurements is a binary star, hence we will not take it into account in the following sections.
As you can see in the $M_v$ vs $B-V$ diagram, the fiducial is situated above most of the single stars of the cluster. However, in the reddest part, from $B-V>1.4$ mag, those stars are in the position marked by the fiducial or above it. As we stated previously, four stars with $B-V>1.45$ mag lie above this and it is possible that they are objects from the pre-main-sequence. If they were stars from the main sequence, one would expect that, given their short rotation periods, they would be situated below the fiducial. In order to verify that they could indeed be pre-main-sequence stars, we have shown the Figure 3 from the study by D'Antona & Mazzitelli (1994). In this diagram,

they show that the stars with ages corresponding to the $\alpha$ Per cluster ($\sim$ 70 Myr) and with masses that are equal to or lower than 0.5 $M_{\odot}$ (that is to say, $B-V \gtrsim 1.45$ mag) have probably not reached the main sequence. Thus we consider that these objects are probably pre-main-sequence, and we have marked them on both CMDs with a red dot, and we do not use them to obtain the residuals in the next section.

In the $M_v$ vs $V - I_c$ diagram, most of the single stars lie slightly below the fiducial. In other words, the difference in $M_v$ has been reduced in this respect. Regarding the reddest stars (above $V - I_c \sim 1.9$ mag) that have not been marked as pre-main-sequence, they are found slightly above the fiducial.

Lastly, in the $M_v$ vs $V - K_s$ representation, one can see reddening in the single stars that rotate most rapidly, so that those that were situated below the fiducial in the previous diagrams are located above it in this diagram.

In the next section, we show the residuals resulting from the differences between the fiducial and the $M_v$ absolute magnitudes of the cluster stars classified singles, members and possible members.

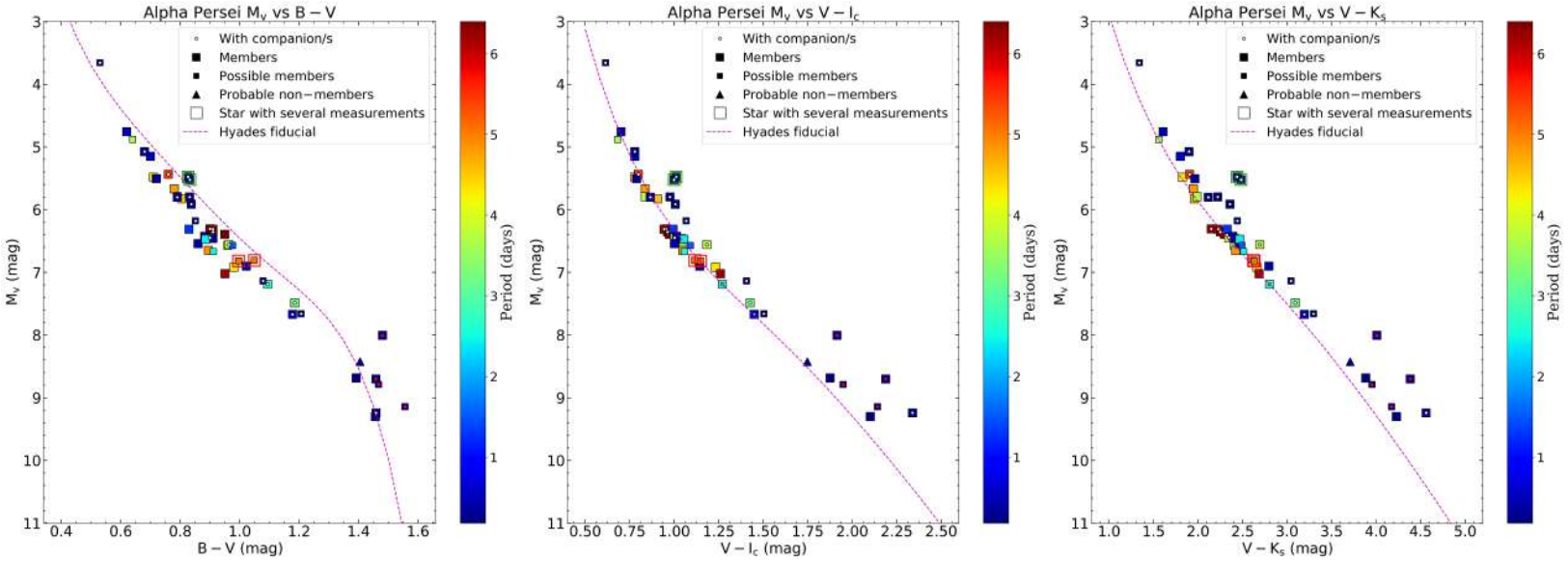


Figure 5.1: Hyades fiducial with stars selected from the $\alpha$ Per cluster and their rotation periods. The symbols enclosed by a square represent the stars with two photometry measurements, both derived from observations at the OSN. Each colour of the squares represents an object. Note that the magnitude and colours were dereddened.

### 5.1.3 Residuals derived from the magnitudes of the $\alpha$ Per stars and the Hyades fiducial

As we have already explained, in order to determine the residuals, we carried out a new selection process and eliminated the binary stars, probable non-members and possible pre-main-sequence stars.The $B-V$ and $V-I_c$ colours of the 24 remaining objects lie within the boundaries marked by the colours of the stars used to generate the Hyades fiducial. Following the procedure explained at the start of the chapter, we obtained the residuals from the differences in the $M_v$ magnitudes of each star of the cluster with respect to the value corresponding to the Hyades fiducial, for each CMD ($M_v$ vs $B-V$, $M_v$ vs $V-I_c$ and $M_v$ vs $V-K_s$).We have represented the ($\Delta V_{Fiducial}$) residuals according to the rotation periods. In these representations, we differentiated the stars by spectral type (the $\alpha$ Per sample is made up of G, K and M stars) and we fit a straight line to each spectral type and to the set of stars formed by K/M spectral types as well. In this way, for each group we have derived a correlation between the rotation periods and the value of said residuals. The coefficients of the straight line fits are shown for each cluster in B.
As you can see in Figure 5.2, the stars with $\Delta V_{Fiducial}$ negative values are those that lie above the fiducial in the corresponding CMD, and those with positive values are situated below. Looking at the residuals from the $M_v$ vs $B-V$ diagram, there does not seem to be a clear correlation between the effect we are studying and the rotation periods. The spectral-type G stars are situated in the positive zone of the residuals but they have no correlation with the rotation period values. The spectral-type K stars similarly lie in the positive values and lean slightly toward increasing values of $\Delta V_{Fiducial}$ as they rotate more rapidly, although there does not seem to be a notable correlation. The M stars (as there are only two we have not fitted a line) present positive residuals but very close to zero. However, these are the most rapid rotators in the sample. For this reason, we would expect a greater deviation of these stars with respect to the fiducial and thus greater positive residuals. Given that these are two objects with $B-V$ values of $\sim 1.4$ mag and $\sim 1.45$ mag, their masses are situated between $\sim 0.5\ M_\odot$ and $\sim 0.6\ M_\odot$. Making use of the diagram from D'Antona & Mazzitelli (1994), these stars may not have reached the main sequence yet; this could be why they do not show the expected deviation.

In the representation of the residuals corresponding to the $M_v$ vs $V-I_c$ diagram, the dispersion observed in the three spectral types is lower than that represented in the previous diagram. The G and K stars are located close to $\Delta V_{Fiducial} = 0$ mag and most of these objects are in the zone of positive residuals. Furthermore, the K stars show a less steep inclination toward greater residuals that we saw in the $M_v$ vs $B-V$ diagram. Regarding the spectral-type M stars, they lie in the negative region of residuals and show a higher deviation than the other stars. However, in the $M_v$ vs $B-V$ diagram their residuals are positive. A possible explanation for this could be that the effect we are studying has become diluted and that there is a prevalence of their being pre-main-sequence stars. Lastly, the dispersion shown in the $B-V$ CMD is greater than that observed in this diagram.

Regarding $M_v$ vs $V-K_s$, one can clearly see a tendency to greater absolute values of the

residuals in their negative zone as the stars rotate more rapidly. Comparing these residuals with those corresponding to $V - I_c$, the large majority of the stars that in that diagram were situated in the region of positive residuals are found in the zone of negative values in this CMD.

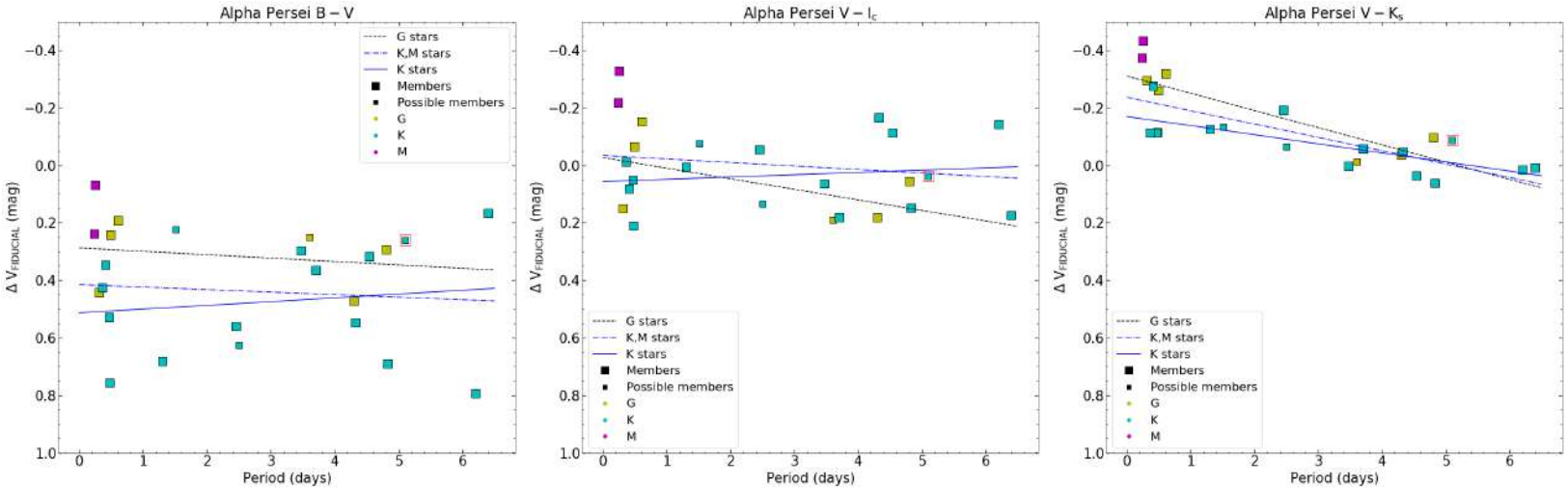


Figure 5.2: Residuals resulting from the differences in $M_v$ between the $\alpha$ Per cluster stars and the Hyades fiducial. The symbol enclosed by a red square represents one of the stars for which we had kept two photometry measurements from the OSN, due to a lack of sufficient criteria to select one of these measurements. In order to calculate the residuals, we decided to use the average of the two measurements.

**Histograms resulting from the residuals of $\alpha$ Per and the Hyades fiducial**

In Figure 5.3, we show the histograms corresponding to the CMDs of the colours $B-V$, $V-I_c$ and $V-K_s$. We have represented them in such a way as to be able to compare the residuals resulting from the $B-V$ CMDs with those from the $V-I_c$. we will also compare the latter with those corresponding to $V-K_s$.

In the histograms that represent the residuals for the $B-V$ colour diagrams, we see how all the stars lie in the zone of positive residuals. The K stars show a greater deviation toward higher residuals, followed closely by mid- and late-G stars. With regard to the residuals corresponding to the $V-I_c$ CMD, as we explained in the previous section, one can clearly see that some of the stars have altered their position toward the region of negative residuals. Moreover, we see that in the case of mid- and late-G and early- and mid-K stars, the dispersion is lower than in the case of $B-V$. Regarding the $V-K_s$ colour, we see how all the stars, with the exception of a small group comprising four mid-K stars and one early-K star, are situated in the region of negative residuals. Additionally, comparing the histograms corresponding to the $V-I_c$ with those of the $V-K_s$ colour, we see that, except for the early-M star, a large number of stars belonging to the other spectral classes have reddened (i.e. moved towards greater absolute values in the region of negative residuals) in $V-K_s$.

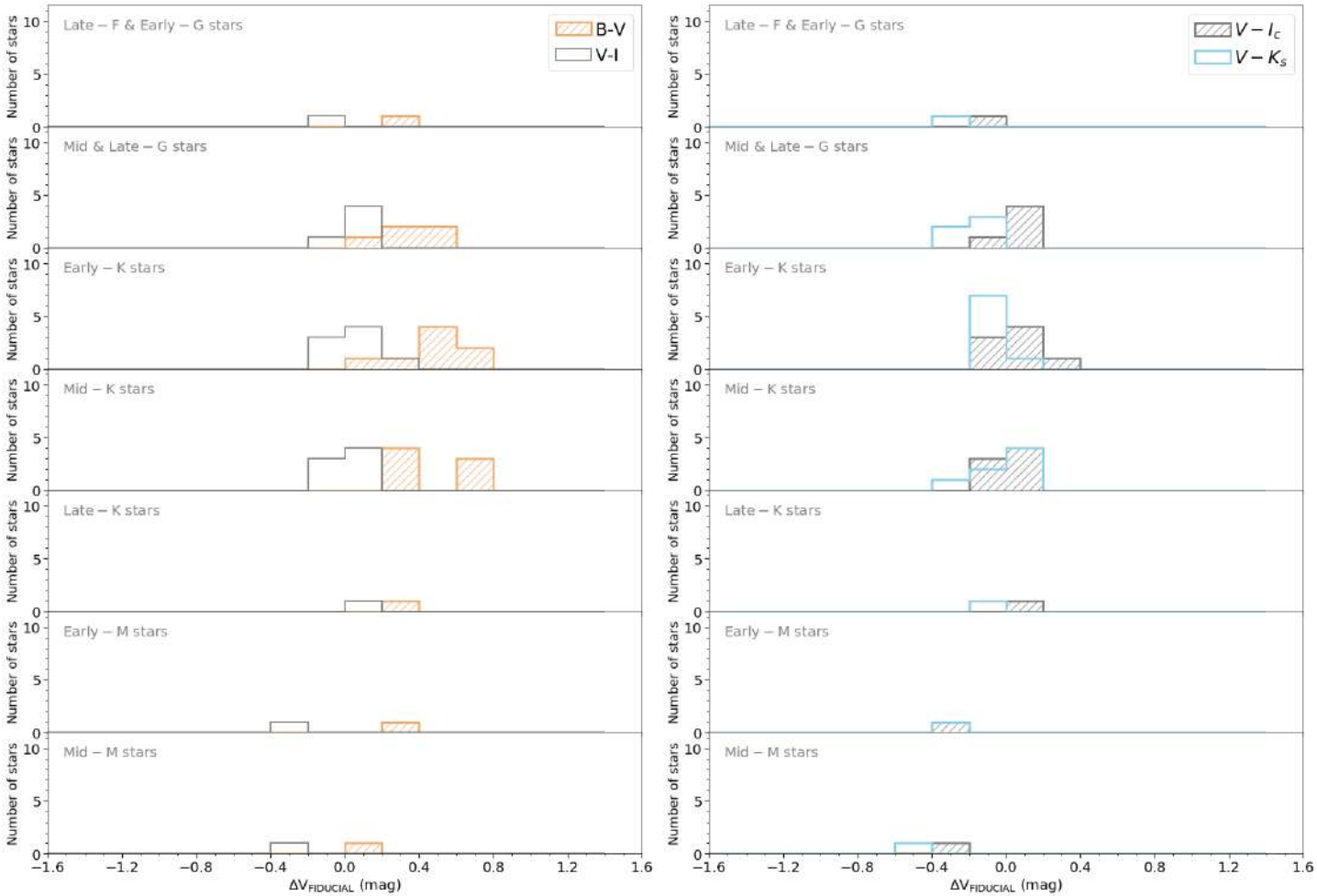


Figure 5.3: Histograms of the resulting residuals for the $\alpha$ Per stars. The residuals corresponding to the $B - V$ colour are represented in orange, $V - I_c$ colour in grey and $V - K_s$ in blue.

## 5.2 Pleiades

### 5.2.1 Binaries in Pleiades

Once the non-member stars have been eliminated, the resulting Pleiades sample contains 258 stars. Furthermore, we will not use the star observed at OSN from which we do not have a value of the rotation period, hence the sample remains with 257 stars. We have found the following papers in the literature that study the multiplicity of these objects:

- WDS Catalogue.
- Mermilliod et al. (2009b), whose study we summarized in the previous chapter, in the section on the identification of binaries in Hyades.
- Kamai et al. (2014), studied the binarity of their own sample for Pleiades, and identified 48 probable binaries. To do so they followed the same procedure explained in the previous section on $\alpha$ Per.
- Hillenbrand et al. (2018), carried out a survey for the clusters Pleiades, Praesepe, and NGC 2264, with the aim of identifying and characterizing multiple systems in them. They obtained images using adaptive optics, using observations with the Robo-AO instrument, installed in the 1.5-metre telescope at the Palomar observatory (California, United States). They identified a total of 32 binaries in Pleiades.

Before studying the binarity of the stars from the Pleiades sample, we made use of Figure 3 from the article by D'Antona & Mazzitelli (1994), and we considered that stars with $B - V \gtrsim 1.6$ mag have a high probability of still being in the pre-main-sequence stage. Thus, independently of their multiplicity, we do not consider them in the calculation of residuals. In total, 22 stars form part of this group.

In order to classify the 235 remaining stars, we have given higher priority to the multiplicity data provided by WDS, Mermilliod et al. (2009b) y Hillenbrand et al. (2018), since the binarity information they provide is more reliable than that from Kamai et al. (2014). As we have explained above, this last study identified the binaries photometrically.
In total, we have catalogued 47 stars as binary/multiple, 45 of which were identified as such in one or more of the four studies. Although catalogued as singles by Hillenbrand et al. (2018), we have photometrically classified the two remaining stars as probable binaries, proceeding in the same way as for the $\alpha$ Per cluster. We have classified the 188 remaining stars as singles. Through our photometric analysis, we confirmed 174 singles previously identified by one or both of the studies by Kamai et al. (2014) y Hillenbrand et al. (2018). We have not found any multiplicity information in the literature for the 14 remaining stars, we have catalogued them as singles through the same analysis of the CMDs.

### 5.2.2 Fits of the Hyades fiducial to the Pleiades cluster

Following the procedure described at the beginning of this chapter, in this section we represent the Pleiades stars, once we removed the non-members, in the $M_v$ vs $B-V$, $M_v$ vs $V-I_c$ and $M_v$ vs $V-K_s$ diagrams together with the corresponding fiducial, and we show their rotation periods. We will mark the binary and pre-main-sequence stars (figure 5.4); however, since the sample contains a high number of objects, we also will represent the CMDs without the probable non-members, candidate members without membership information from L19, binary and pre-main-sequence stars. This "clean" sample (figure 5.5) will lead us to better visualize the position of the stars of interest in the CMDs.
Before proceeding to the representations of the CMDs, we should mention that, due to the fact that only four stars from the sample presented periods that were significantly higher than most of the remaining stars, the method used for showing the values of the periods through a colour bar lost functionality. For this reason, only for the visualization of the diagrams, for these four stars we have replaced their periods with the maximum value ($\sim$ 12.1 days) derived from the large majority of the cluster stars.

In the $M_v$ vs $B-V$ diagram of Figures 5.4/ 5.5, most of the single stars of the cluster are situated below the fiducial, as occurred with the $\alpha$ Per cluster. From $B-V \sim 0.85$ mag most of the rapid rotators are located at a higher distance from the fiducial. As of $B-V > 1.3$ mag are positioned those that move furthest away in $M_v$, all of these objects being rapid rotators. As we can see in Figure 5.4, many stars that have not been catalogued as multiple lie above the fiducial and many of them belong to those we have classified as highly probable pre-main-sequence stars. On the $M_v$ vs $V-I_c$ CMD, many single objects of the cluster are situated slightly below the fiducial, and the distance to it is significantly lower to that observed in the $M_v$ vs $B-V$ diagram. As of $V-I_c \sim 1.85$ mag, the stars begin to be positioned above the fiducial, among which we again see those classified as pre-main-sequence.
Lastly, on the $M_v$ vs $V-K_s$ diagram, in the region of the reddest stars we can see a greater proximity of their positions to the fiducial compared to the $V-I_c$ CMD. The position of the remaining stars with regard to the fiducial are similar to this last CMD, although at first sight one can see several single stars with very short periods and $V-K_s$ values between 2 $\gtrsim$ mag and $\lesssim$ 3.5 mag, which have clearly reddened, meaning that many of these stars that in previous diagrams lie below the fiducial are situated above it in the $V-K_s$ CMD.

On the three CMDs we have enclosed various stars in yellow-sided squares. These stars have errors in $V-I_c = 0.05$ mag. Despite having errors above the established limit of 0.04 mag for this colour, we did not immediately reject them because in $B-V$ they have errors of 0.04 mag and these are quite red stars and hence interesting for our study.

Following the procedure established for each cluster, in the next section we will show the residuals resulting from the differences in $M_v$ between the stars of Pleiades and the Hyades fiducial.

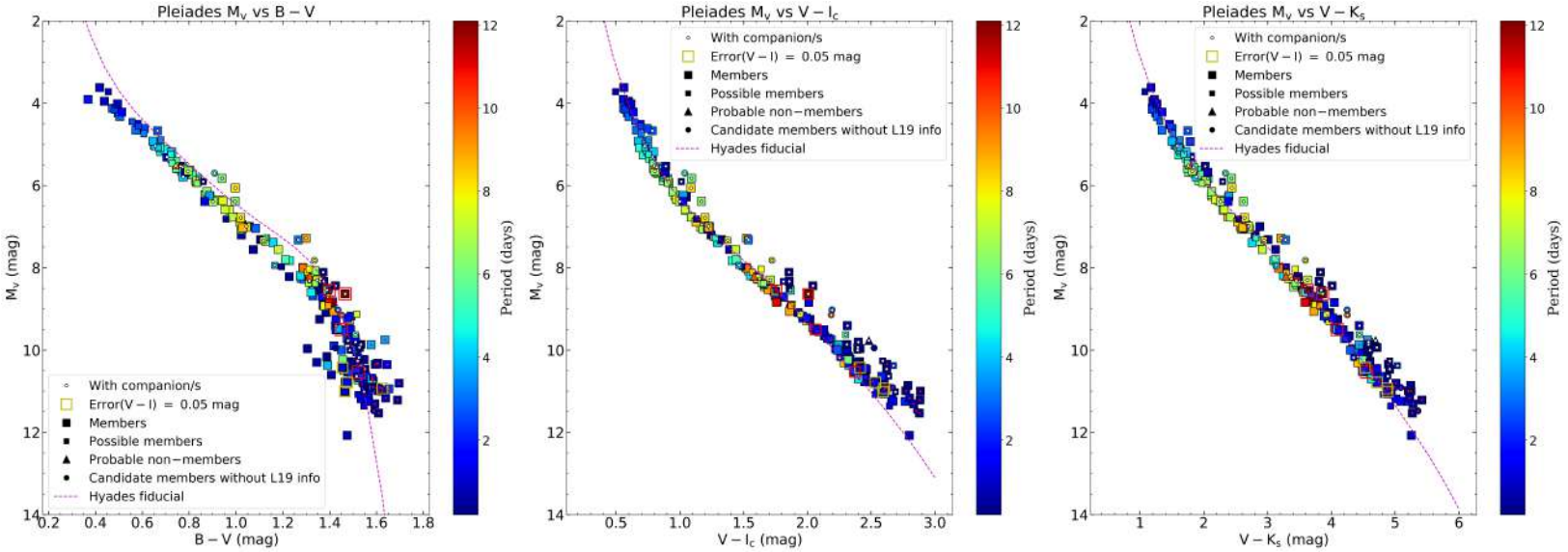


Figure 5.4: Hyades fiducial with the stars selected from the Pleiades cluster and their rotation periods. The symbols enclosed by a red-sided square indicate those stars with rotation periods greater than 12 days. Lastly, the stars marked with a red dot are those we have catalogued as possible pre-main-sequence objects. Note that the magnitude and colours were dereddened.

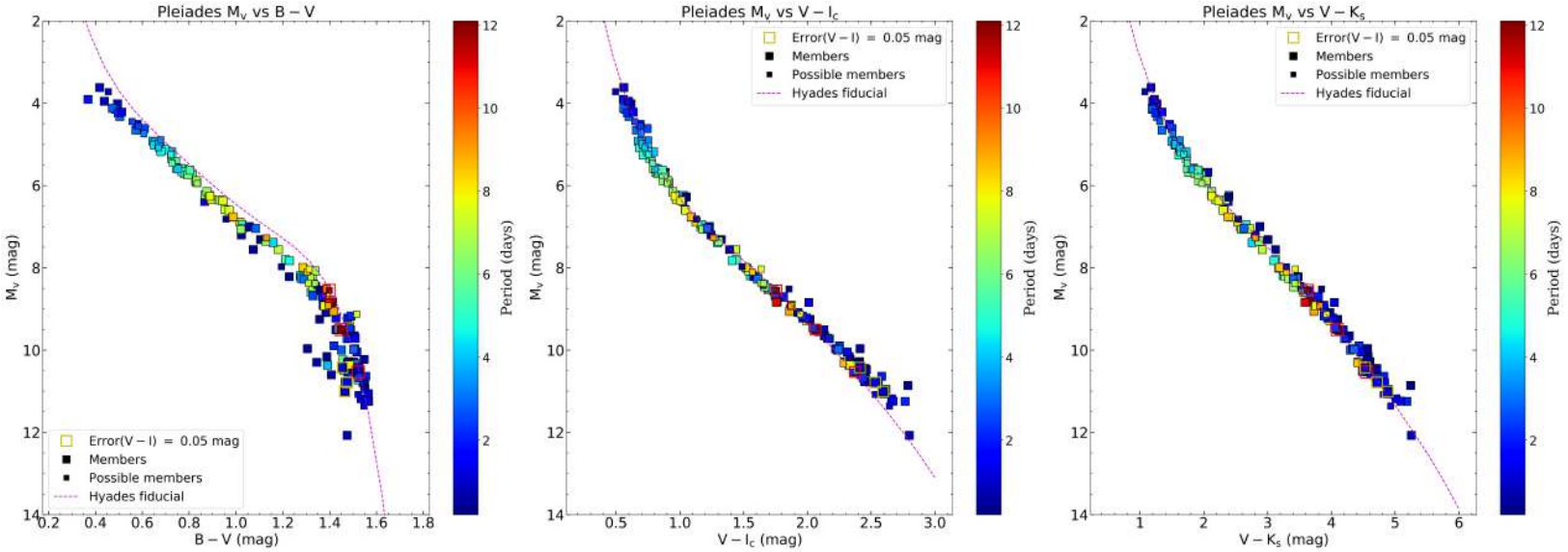


Figure 5.5: Same as Figure 5.4 once we removed the probable non-members, candidate members without membership information from L19, binary and pre-main-sequence stars.

### 5.2.3 Residuals derived from the magnitudes of the stars of Pleiades and the Hyades fiducial

As we have already explained, in order to obtain the residuals, we eliminated binary stars, probable non-members and candidates without membership information from L19. We also discarded the 22 stars classified as objects likely to be found on the pre-main-sequence. Lastly, we have included the boundaries given by the Hyades fiducial. A total of 169 stars remain in the sample. Below we show their residuals with respect to the fiducial.

In order to calculate the correlation between the residuals, rotation periods and spectral classes, we analysed the groupings of the F/G and K/M stars, and also K and M stars separately. In the upper diagram of Figure 5.6, the residuals corresponding to the $M_v$ vs $B-V$ CMD are represented. In this graph, most of the objects are situated in the region of positive residuals, except for a group of M-type stars, which could be binary stars that have not been identified as such, or stars on the pre-main-sequence. Regarding the correlations we wish to examine, the F/G group does not show a relation between the residuals and the rotation periods. The K-type stars, however, noticeably show an effect, which was already observed in a subtle way in the $\alpha$ Per. That is, one can see a greater deviation in the positive residual region for lower rotation period values. As we have already explained in the introduction, this effect has been observed in Pleiades by Stauffer & Hartmann (1987), Stauffer et al. (2003) and Kamai et al. (2014). Regarding the M-stars, if we only take into account those that lie below the fiducial, we see a clear correlation between higher residuals and faster rotators.
In the graph from Figure 5.6, corresponding to the $M_v$ vs $V-I_c$ diagram, this effect is no longer visible. Moreover, both the positive and negative residuals have much lower absolute values than those observed in the previous diagram. For the K stars, we no longer see a correlation between the residuals and the rotation periods, and in the other spectral types the existing correlation indicates a greater deviation toward negative residuals for lower rotation periods. As we can see, very few M-type stars lie below the fiducial and those that do, do not show a correlation with the rotation periods. Furthermore, many of the M stars deviate toward the negative residual region – that is, the effect for these stars is no longer visible and we are probably seeing the deviation of stars that might be binaries or from the pre-main-sequence.
The residuals corresponding to $V-K_s$ show a lesser dispersion with greater clarity when compared with $V-I_c$. We also see a trend in all spectral types toward higher absolute values of the residuals in the negative residual region as the stars rotate more rapidly. Comparing with $V-I_c$, the K dwarfs show a bigger correlation of short rotation periods and greater absolute values of the residuals in the negative region.

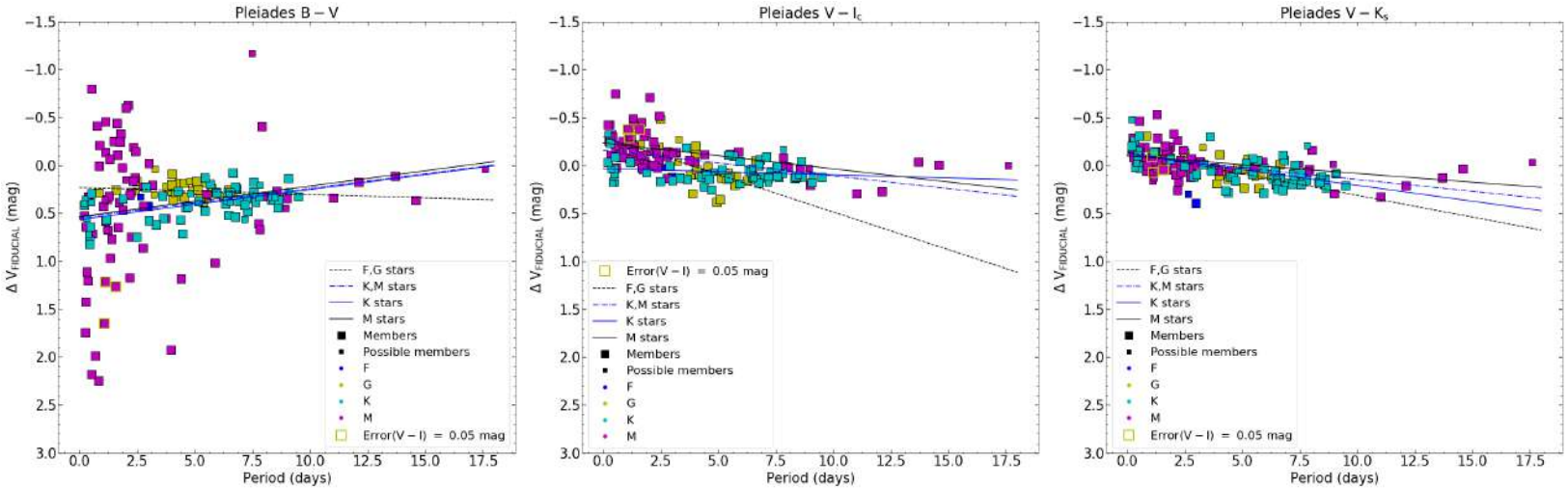


Figure 5.6: Residuals resulting from the differences in $M_v$ between the stars of the Pleiades cluster and the Hyades fiducial.

**Histograms resulting from the Pleiades residuals and the Hyades fiducial**

In Figure 5.7, the histograms of the residuals corresponding to the $B - V$ CMD present a gradual increase in their value, mainly in the positive residual region as we advance toward later spectral types. The exception is the early-M stars, which show a greater dispersion toward higher residuals than the mid-M stars. We should mention that the sample we have of these latter spectral types is notably less than the mid-M dwarfs.

The histograms that represent the $V - I_c$ CMD show a significant decrease in the absolute values of the residuals for most of the stars, particularly the mid-K and later spectral types. As we saw in $\alpha$ Per, many of the stars present residuals that are close to zero or negative. Although most of the mid-/late-G and late-K stars are situated in the positive residual region, the values are lower and with less dispersion than those observed in the $B - V$ CMD histograms.

Comparing the histograms corresponding to $V - K_s$ with those of $V - I_c$, every spectral type from Mid- & late-G to Late-K stars contain stars that have reddened. However, there appears to be blueing of M-type stars.

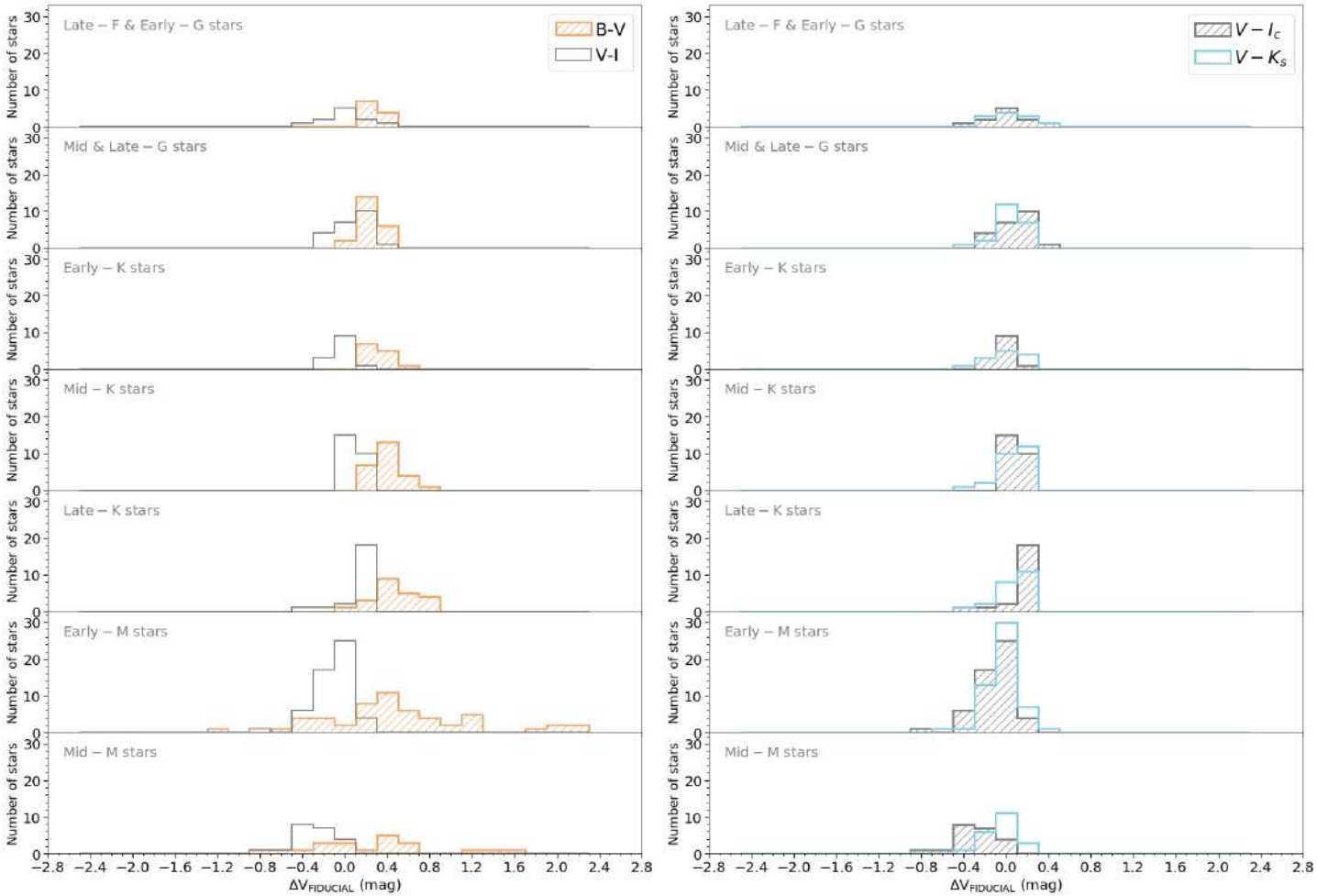


Figure 5.7: Histograms of the resulting residuals for the stars of Pleiades. The residuals corresponding to $B - V$ are represented in orange, $V - I_c$ in grey, and $V - K_s$ in blue.

## 5.3 Coma Ber

### 5.3.1 Binaries in Coma Ber

For this cluster, there was no need to carry out a binarity study. Looking at the CMDs, one sees that the sample does not appear to be affected by binary or multiple stars. Having eliminated the non-member stars, we are left with a sample of 17 stars. We proceed as in the section of Coma Ber in Chapter 3 and for several stars of the sample we used the double of the published periods.

### 5.3.2 Fits of the Hyades fiducial to the Coma Ber cluster

The $M_v$ vs $B-V$ diagram represented in Figure 5.8 shows most of the stars of the cluster lying below the fiducial while the rest fit fairly well with it.
On the $M_v$ vs $V-I_c$ CMD, the deviations that are present in the previous diagram have lessened, except for the reddest star, which in this case is situated below the fiducial.
The $M_v$ vs $V-K_s$ diagram is very similar to the previous one. The two stars lying at the extremes of the diagram, one with a "short" and the other with a "long" period, which in the previous CMDs lay below the fiducial, have moved slightly closer to it. Comparing with the previous diagrams again, several stars that were located on the fiducial or close to it have moved slightly further below it.

Lastly, the three CMDs of Coma Ber show two stars both with two measurements derived from observations at OSN. Following the same criteria as with $\alpha$ Per, in the next section we derive the mean value of both measurements for each star.

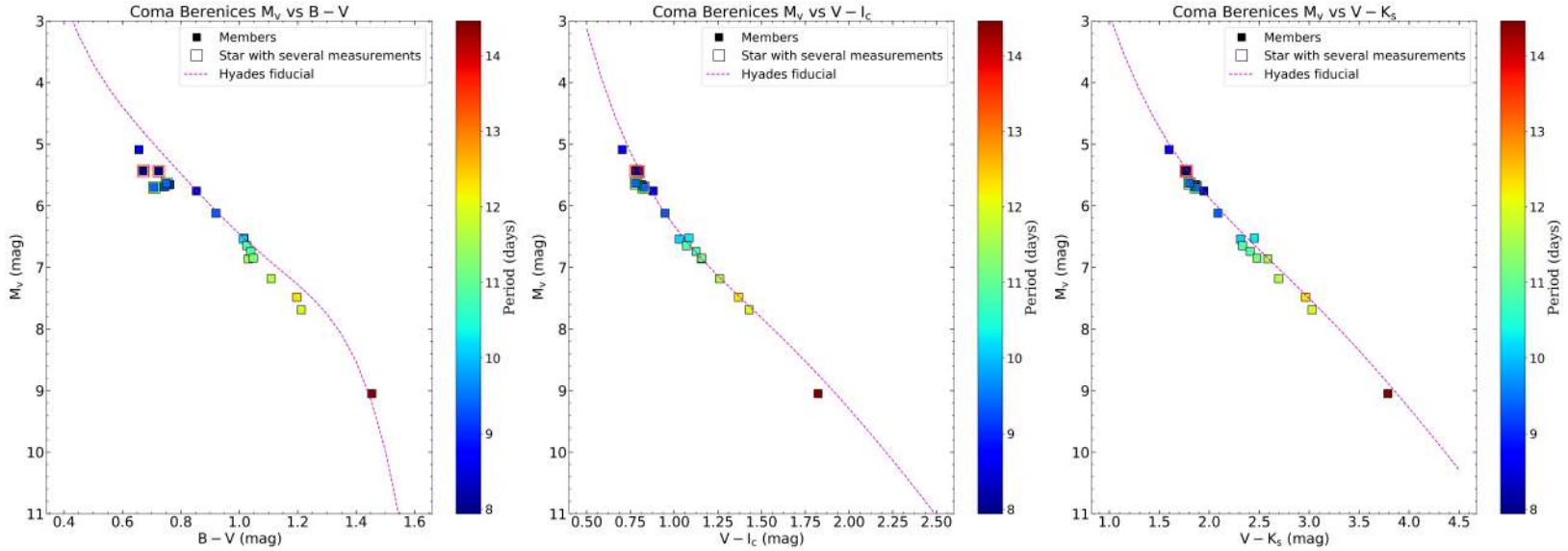


Figure 5.8: Hyades fiducial with selected stars from the Coma Ber cluster and their rotation periods. The symbols enclosed by a square represent the stars with two photometric measurements, both derived from observations at the OSN. Each colour of the squares represents a star.

### 5.3.3 Residuals derived from the magnitudes of the stars of Coma Ber and the Hyades fiducial

For this cluster, there was no need to carry out a new selection process nor apply the limits imposed by the Hyades fiducial. In the representation of the residuals in the $B-V$ and $V-I_c$ diagrams corresponding to Figure 5.9, one can discern three well-differentiated spectral groups that make up the Coma Ber sample (G, K and M). Given the low number of stars, we have obtained the correlations for spectral types G and K. In the residuals diagram of the $M_v$ vs $B-V$ CMD, we can see that most of the stars lie below the fiducial, but we cannot see a correlation that indicates that that deviation is due to their rotation periods. The M-star that is not a rapid rotator is situated in the negative residual region.

The residuals corresponding to the $V-I_c$ CMD show less dispersion and lower values, although many of the stars still lie slightly below the fiducial.

Regarding the residuals corresponding to the $V-K_s$ diagram, compared with the previous diagrams, we see a smaller dispersion. Furthermore, the G-type stars behave in a similar way to the K-types and the residuals of the M star are close to the rest of the stars. Lastly, only two stars are situated in the negative residual region. There is no clearly visible reddening effect related to the rotation periods.

In Coma Ber, for both the G and K stars, very small rotation period intervals are covered, and it is not clear if the effect under study occurs or not. The Pleiades have shown that a large rotation period interval is needed to see this effect. This is due to the dispersion that is seen inherent in the stars. In this cluster, the existing dispersion makes it difficult to detect it.

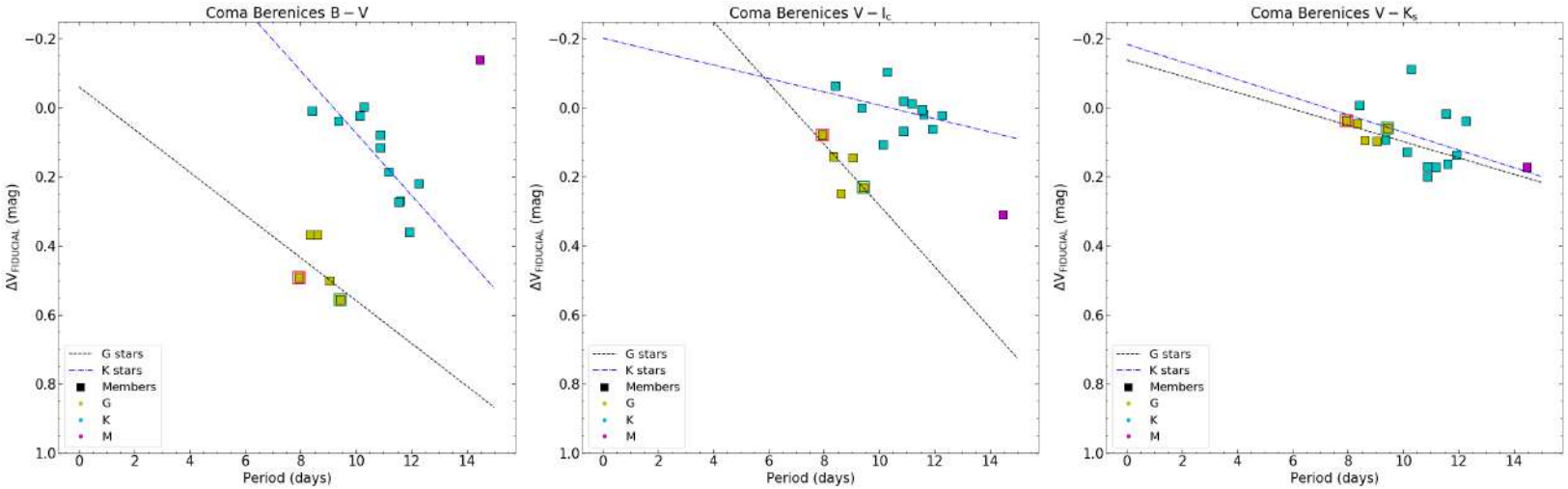


Figure 5.9: Residuals resulting from the differences in $M_v$ between the Coma Ber cluster and the Hyades fiducial.

**Histograms of the residuals from Coma Ber and the Hyades fiducial**

The histograms of Coma Ber represented in Figure 5.10 have been produced, as we have already seen, with the smallest sample of stars of all the clusters in this study, with only 17 stars. In this small sample, the $B - V$ CMD shows that most of the stars have positive residuals, although with values close to zero, with the exception of one mid-K and one early-M dwarf star, whose residuals are negative. The mid-/late-G stars are those that show the largest residuals with some values between 0.4 mag and 0.6 mag.

The histograms corresponding to $V - I_c$ present some early- and mid-K stars in the region of negative residuals, but the rest of the Coma Ber stars have positive residuals, although the majority with values close to zero and showing a smaller dispersion than in the case of the $B - V$ CMD. The residual of the early-M dwarf is positive and slightly larger in absolute value than in the case corresponding to $B - V$, and the early-G star shows a residual with a very similar value to that generated for $B - V$.

The $V - K_s$ histograms are very similar to those for $V - I_c$. When we compare the former with the latter, only two G stars, one mid-K and one early-M have reddened. However, except for the mid-K star, these objects still lie in the region of positive residuals.

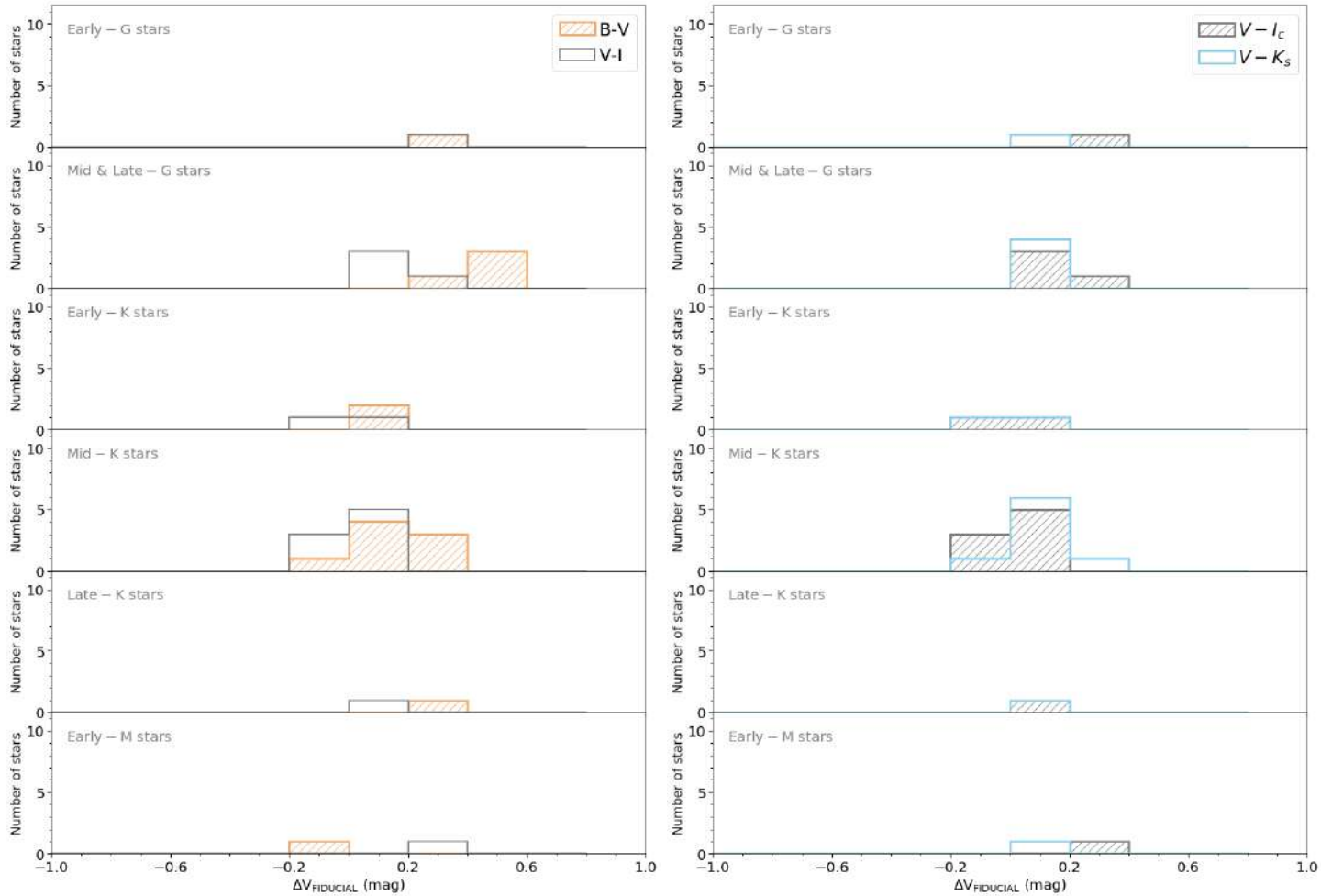


Figure 5.10: Histogram of the resulting residuals for the stars of Coma Ber. The residuals corresponding to $B - V$ are represented in orange, $V - I_c$ in grey and $V - K_s$ in blue.

## 5.4 Praesepe

### 5.4.1 Binaries in Praesepe

Once the non-member stars were discarded, 170 stars remained in the Praesepe sample. In order to check their binarity, we obtained information from the following studies.

- WDS catalogue.
- Patience et al. (2002), who identified 12 binaries in their Praesepe sample.
- Mermilliod et al. (2009b).
- Douglas et al. (2014), who photometrically classified 15 stars as potential binaries among the objects in their Praesepe sample.
- Douglas et al. (2017), who carried out a thorough study of this cluster. This is one of the studies from which we have taken the Praesepe rotation periods. They analysed K2 light curves for 794 cluster members and studied their multiplicity. To achieve their objective, they used various methods: 1. They searched visually for companion stars, for which they studied K2, DDS and SDSS images, and complemented this method by analysing the K2 light curves of these stars. 2. They photometrically analysed the stars using CMD representations. 3. They carried out a search for binaries in previous studies. 4. They analysed the K2 light curves and identified possible eclipsing binaries. In total, they found 82 previously confirmed binaries (or triples) and 262 candidates of multiple systems in their sample.
- Hillenbrand et al. (2018), we have already described this study, in which they identified 8 binaries in their Praesepe sample.

In order to compile the binarity information from these papers, we began the process by using the results from Douglas et al. (2017), as it is a very complete study. For the stars in our sample that were not analysed by Douglas et al. (2017), we searched for their binarity information in the WDS catalogue and in the studies of the literature that Douglas et al. (2017) mention in their Section 4.3. The studies wherein we found multiplicity information are those specified in the list above (Patience et al. 2002; Mermilliod et al. 2009b; Douglas et al. 2014). We identified 53 stars in our sample that have been catalogued as binaries in one or several of these studies. We analysed the 117 remaining stars photometrically, following the same process as for the previous clusters. We classified three stars as probable binaries, for two of which we could not find multiplicity information in the literature, while the third had been catalogued as single in Douglas et al. (2014). We believe that this last star possibly has a companion but that it does not significantly affect the photometry of the primary, so we have marked it as a possible binary. In total, we classified 56 stars in our sample as binaries. We have marked the 114 remaining stars as singles, 109 of which had already been classified as such in one or several of the previous studies, one had no binarity information in the literature, and the other four had been catalogued as photometric binaries by Douglas et al. (2017).

### 5.4.2 Fits of the Hyades fiducial to the Praesepe cluster

In the $M_v$ vs $B-V$ diagram, represented in the upper part of Figure 5.11, we can see how the fiducial derived from Hyades fits fairly well with the Praesepe cluster as of, approximately, the lower $B-V$ limit established by the fiducial itself ($B-V \gtrsim 0.54$ mag). The single stars that in $M_v$ are located at a greater distance from the fiducial and below it, have $B-V$ values of $\gtrsim 1.4$ mag and only two of them are rapid rotators. As of $B-V \sim 1.35$ mag, several single stars lie above the fiducial, but given the age of the cluster, they would appear not to be pre-main-sequence stars.
On the $M_v$ vs $V-I_c$ diagram, the fit of the Hyades fiducial is also fairly good above the lower limit in $V-I_c$, which was determined by the fiducial ($V-I_c \sim 0.6$ mag). Two single stars from the sample, with $V-I_c \sim 2.2$ mag and $\sim 2.5$ mag, lie slightly below the fiducial but do not possess significantly short rotation period values. Lastly, five single stars with $V-I_c \gtrsim 1.9$ mag, which are situated above the fiducial, are located below it in the previous diagram. Two of these objects are the most rapid rotators situated in the reddest zone of the $M_v$ vs $B-V$ CMD.
The $M_v$ vs $V-K_s$ diagram shows a lesser dispersion than that corresponding to $V-I_c$. It is worth highlighting that the single stars with $V-K_s$ values of $\gtrsim 1$ mag that in this last CMD were below the fiducial in the $V-K_s$ diagram, are found on the fiducial or closer to it, although there does not appear to be a correlation with the period values.

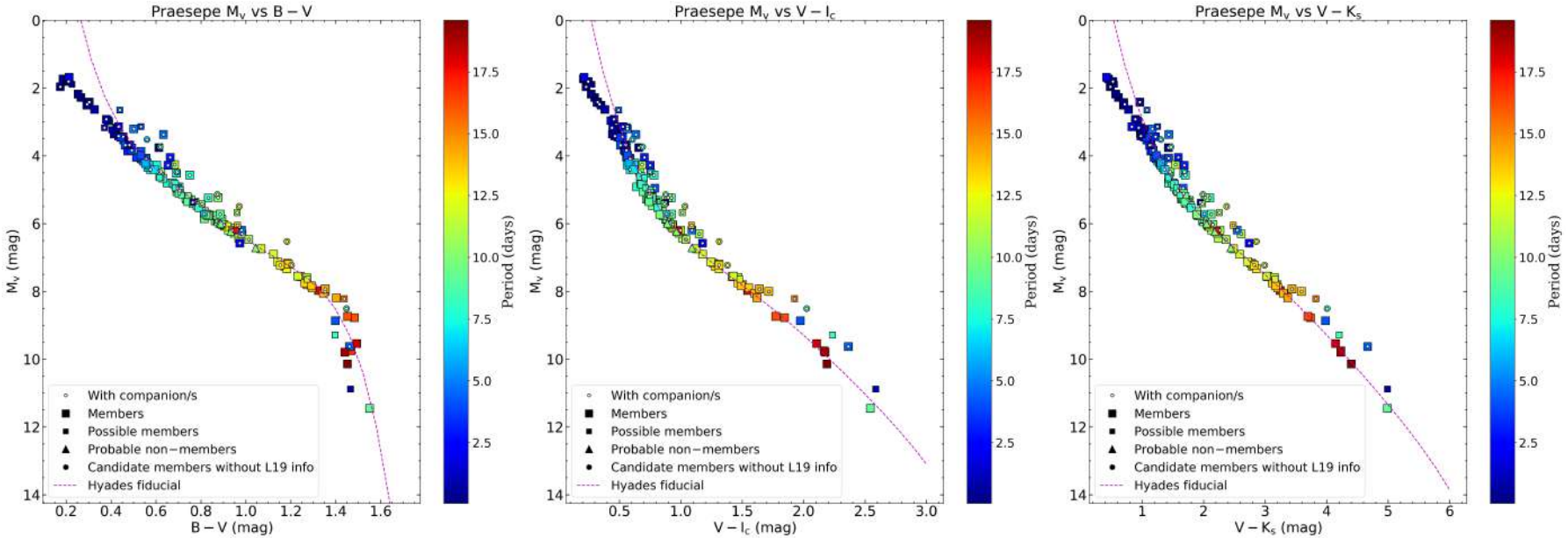


Figure 5.11: Hyades fiducial with stars selected from the Praesepe cluster and their rotation periods. Note that the magnitude and colours were dereddened.

### 5.4.3 Residuals derived from the magnitudes of the Praesepe stars and the Hyades fiducial

Having eliminated the binaries/multiples, probable non-members and candidates without membership information from L19, and having applied the limit imposed by the fiducial, we use a sample with 81 objects from Praesepe. We obtained the correlations for the groups of F/G- and K/M-type stars, and K- and M-type objects separately. In the graph in Figure 5.12, which represents the residuals corresponding to the $M_v$ vs $B-V$ CMD, it shows how some of the F/G stars lie slightly below the fiducial, but do not present any correlation with the rotation periods. Many of the K-type stars behave in a similar way to the F/G stars. However, a small group of K stars have a larger dispersion toward negative residuals, and it also contains a star that shows a slight increase in displacement in the region of positive residuals, but it is not a particularly rapid rotator. In short, the effect under study does not appear to be visible in these stars. In the case of the M-type dwarfs, these do undergo greater dispersion. Two of them are located toward negative residuals and the others in the zone of positive residuals. Although no correlation is perceived between residuals and rotation periods, one of the stars that deviates from the fiducial with positive residuals is that with the second shortest rotation period in the sample, and the star that deviates most in that same zone is the most rapid rotator in the sample.

The residuals corresponding to the $M_v$ vs $V-I_c$ diagram show a larger dispersion in the F/G-type stars, for which we see a slight correlation between lower rotation period values and greater deviation in the region of positive residuals. This subtle correlation seems to be mainly due to the position of a G-type star with a residual of $\Delta V_{Fiducial} \sim 0.5$ mag. In the K and M stars, there is a significant decrease in dispersion compared to the previous diagram. Moreover, we can see three M-stars clearly lying in the region of negative residuals, though in the previous CMD they were situated in the region of positive residuals. Two of these three are the most rapid rotators in the sample.
The residuals in the $M_v$ vs $V-K_s$ diagram show a smaller dispersion than in the previous diagrams. Comparing with the residuals from the $V-I_c$ CMD, the largest change is the decrease in the values of the residuals in most of the stars, but without showing a correlation with the rotation periods noticeably different that the one present in $V-I_c$.

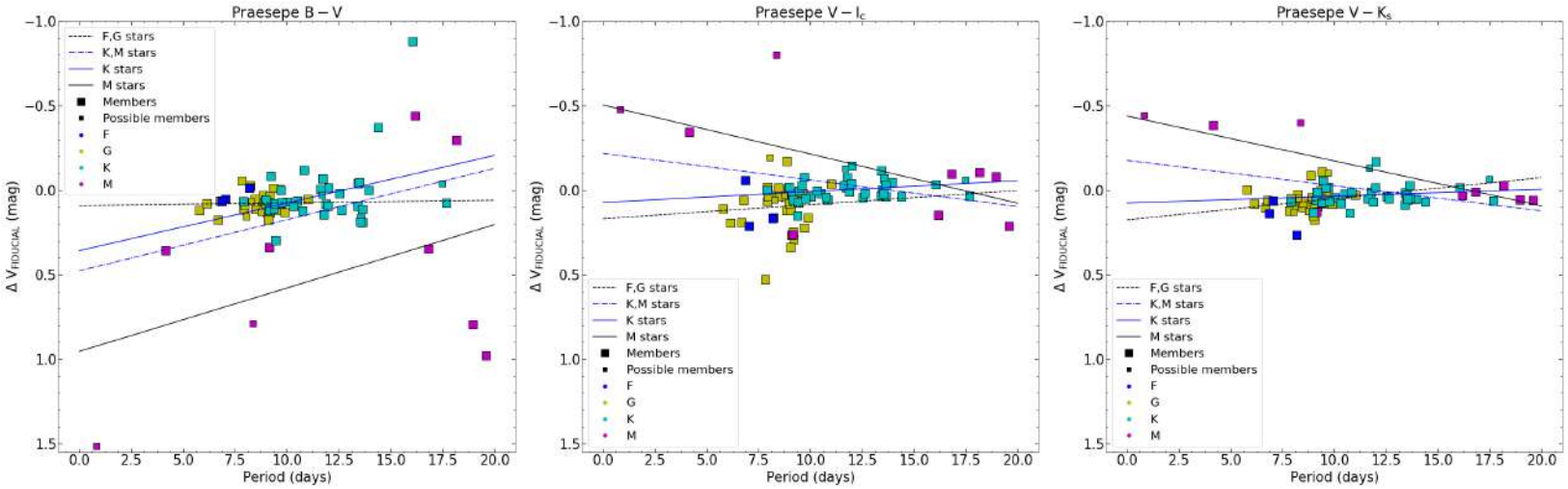


Figure 5.12: Residuals resulting from the differences in $M_v$ between the Praesepe cluster and the Hyades fiducial.

**Histograms of the residuals of Praesepe and the Hyades fiducial**

Figure 5.13 shows the histograms of the residuals for the Praesepe cluster. For late-F, early-G and mid-late-G stars, we see a smaller dispersion in the histograms corresponding to $B - V$ than in those of the $V - I_c$ CMD. The dispersion in $B - V$ starts to increase for the K-type stars (two of which have negative residuals) and becomes more notable for the M-type stars, most of which have positive residuals. Some of these stars present residual values between 0.6 mag and 1.8 mag. In $V - I_c$, these stars present residuals that are close to zero and or negative. Regarding $V - K_s$, the histograms are very similar to those corresponding to $V - I_c$, revealing a higher concentration of stars with residuals around the value zero.

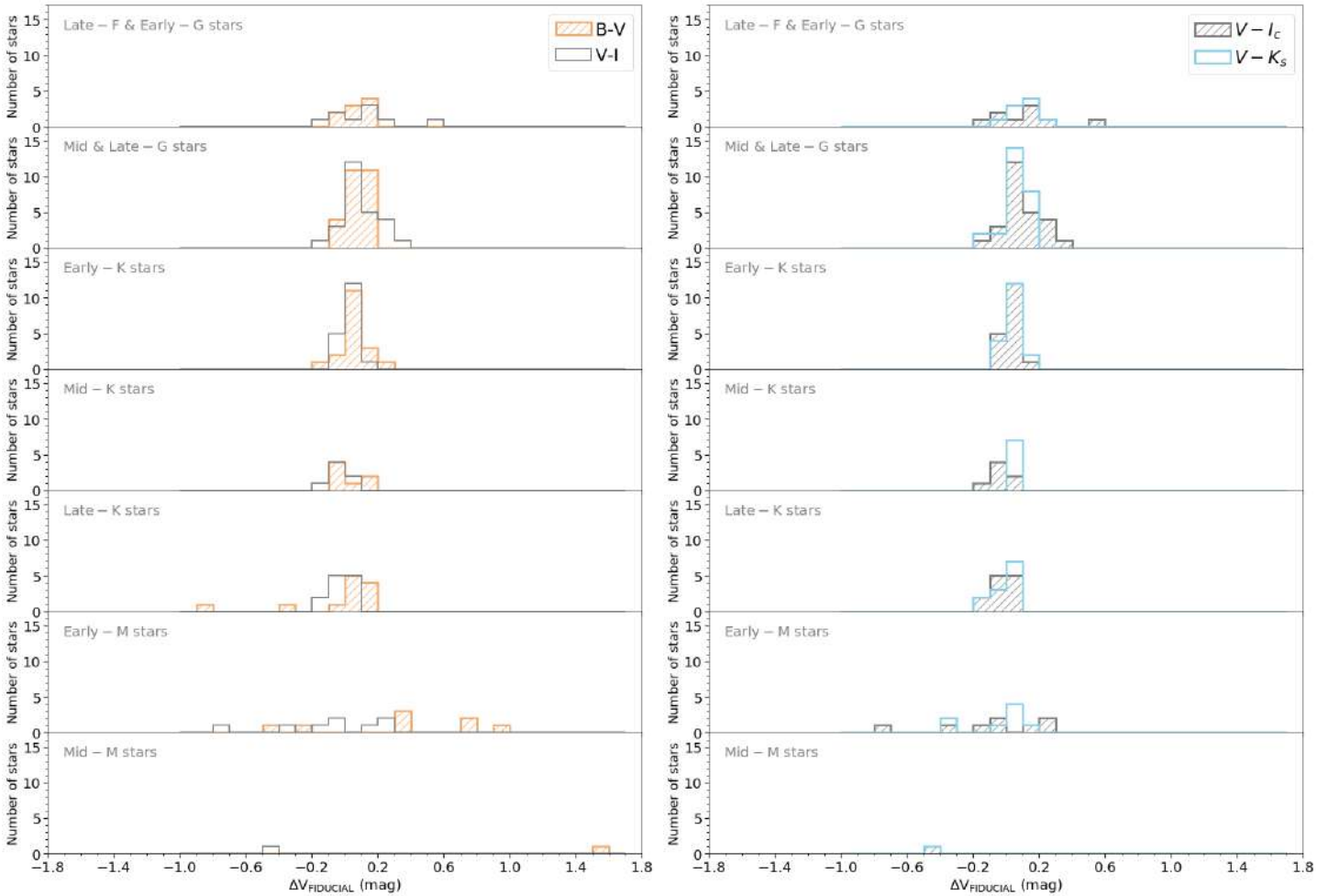


Figure 5.13: Histogram of the residuals for the stars of Praesepe. The residuals corresponding to $B - V$ are represented in orange, $V - I_c$ in grey and $V - K_s$ in blue.

## 5.5 Hyades

### 5.5.1 Binaries in Hyades

Having eliminated those stars classified as non-members in L19H from the initial sample of 75 stars, we are left with 66 objects.

In chapter 4, in order to obtain the fiducial of Hyades, we performed the binarity study for this cluster using data from the literature. Within this sample with 66 objects, 45 have been classified as singles and 14 as binaries. The remaining seven objects do not have multiplicity information from the literature. We proceeded as in previous clusters and checked the four CMDs in order to study the binarity of these stars. We classified five objects as singles and two as binaries in the four CMDs.

Note that the star with no binarity information from the literature that was used to form the fiducial in 4 seems a single star in the four CMDs. We also marked two stars catalogued as single possible members that according to their positions on the CMDs: one star might be binary or non-member and the remaining might be a non-member.

To summarize, in the following section we represent in the CMDs: 48 single stars, 16 binaries, one single star classified as binary or non-member, and one single star that might be a non-member.

### 5.5.2 Fits of the Hyades fiducial to the stars of the same cluster

The diagrams in Figure 5.14 show, as one would expect, few differences between the fiducial and stars of Hyades. The highest distances between the two occur for the stars classified as binaries or that, according to their photometry, could be non-members. Looking at the $M_v$ vs $B-V$ CMD, we should mention one single member and one possible member, both with $B-V$ values of $\sim 1.2$ mag and one single member with $B-V \sim 1.4$ mag that are found below the fiducial, even though they are not rapid rotators.

In the case of the $M_v$ vs $V-I_c$ diagram, barring one star catalogued as a possible member ($V-I_c \sim 2.7$ mag), practically all the single stars classified as members or possible members fit very well with the fiducial. The two member stars that in $M_v$ vs $B-V$ were situated below the fiducial hardly show any differences with it in this diagram.

The $M_v$ vs $V-K_s$ CMD, as with Coma Ber and Praesepe, is very similar to the $V-I_c$ diagram, showing slightly less dispersion as a whole.

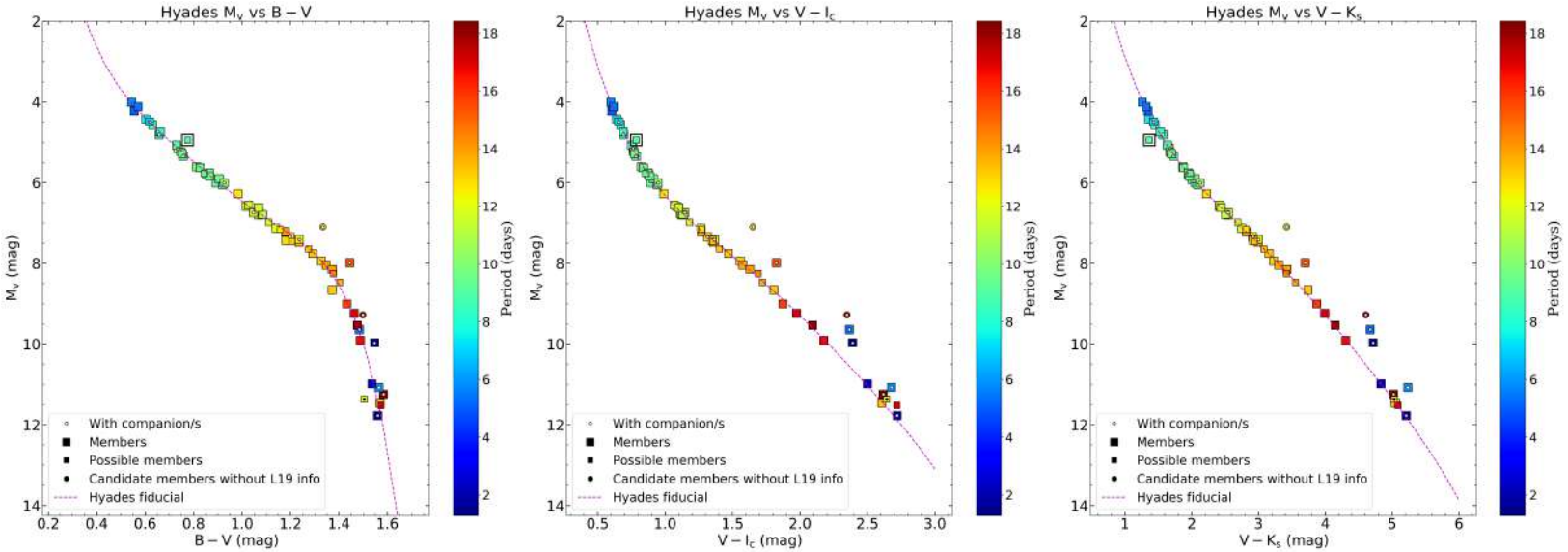


Figure 5.14: CMDs of Hyades stars to which the fiducial has been fitted. The star marked with a black dot is a possible non-member. The star enclosed by a black square is either binary or a non-member. Note that the magnitude and colours were dereddened.

### 5.5.3 Residuals derived from the magnitudes of the stars of Hyades and its fiducial

As we proceeded with previous clusters, in order to derive the residuals, we will eliminate the stars we have identified as binary, those that we have photometrically catalogued as possible non-members, stars identified as probable non-members using the membership information from L19H, and the stars that lack this information. Moreover, we will use the boundaries given by the stars that comprise the fiducial. Lastly, we will represent the residuals for 48 stars of Hyades.

The residuals corresponding to the $M_v$ vs $B-V$ diagram do not reveal a clear trend with regard to the rotation periods; there is larger dispersion in the K and M stars but without indicating a correlation with the rotation periods. Neither do we see a correlation for the F/G-type stars, which show a smaller dispersion than for the K/M stars, particularly the G-types, which keep together close to the fiducial and with very low residuals. Of all the stars that deviate the most, only one (M spectral class) is a rapid rotator, situated in the region of positive residuals.
In the residuals of the $M_v$ vs $V-I_c$ diagram, we can see a clear decrease from the dispersion displayed in the previous diagram in almost all stars, except the F/G-type stars, which maintain a similar dispersion.
The residuals corresponding to $V-K_s$ again show a decrease in dispersion compared with the previous diagrams. When compare with the residuals of $V-I_c$, four M-stars have been reddened (only one object has a short rotation period) and two were displaced towards the positive residuals. There does not appear to be a correlation between the changes of the star positions between $V-I_c$ and $V-K_s$ and the rotation periods.

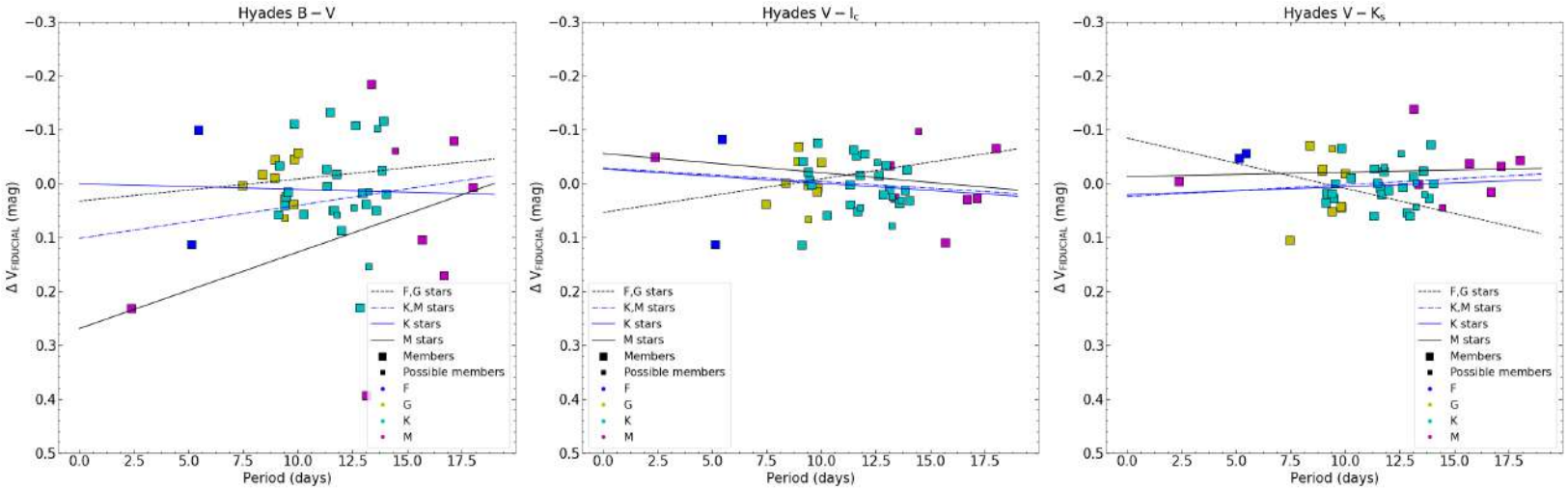


Figure 5.15: Residuals of the differences in $M_v$ between the stars of Hyades and its fiducial.

**Histograms resulting from the residuals of Hyades and its fiducial**

The histogram of the residuals corresponding to the $B - V$ CMD of Figure 5.16 of the Hyades, shows a similar behaviour for the K-type stars as that seen in the histograms for the Praesepe cluster, in which most of the K stars present positive residuals that are close to zero, except for a few objects with negative residuals. Regarding the stars that deviate the most in the region of positive residuals, these are mid-K and early- and mid-M type dwarfs, with values between 0.2 mag and 0.6 mag. As with Praesepe, the early-M stars are those that present the highest values of residuals with respect to the other stars of the cluster.
In the histograms corresponding to the $V - I_c$ CMD, most of the stars have residuals between -0.1 mag and 0.1 mag. Lastly, it should be mentioned that almost no difference is observed in the behaviour of the late-F/early-G and early-late-G stars between the two histograms of the $B - V$ and $V - I_c$ CMDs.
The histograms of $V - K_s$ are very similar to those for $V - I_c$. Aside from the early-K type objects, the other spectral types show either an identical distribution to that observed in $V - I_c$ (as in the case of the late-K and mid-M types), or changes in the residuals of some of the stars, showing negative instead of positive values (four stars).

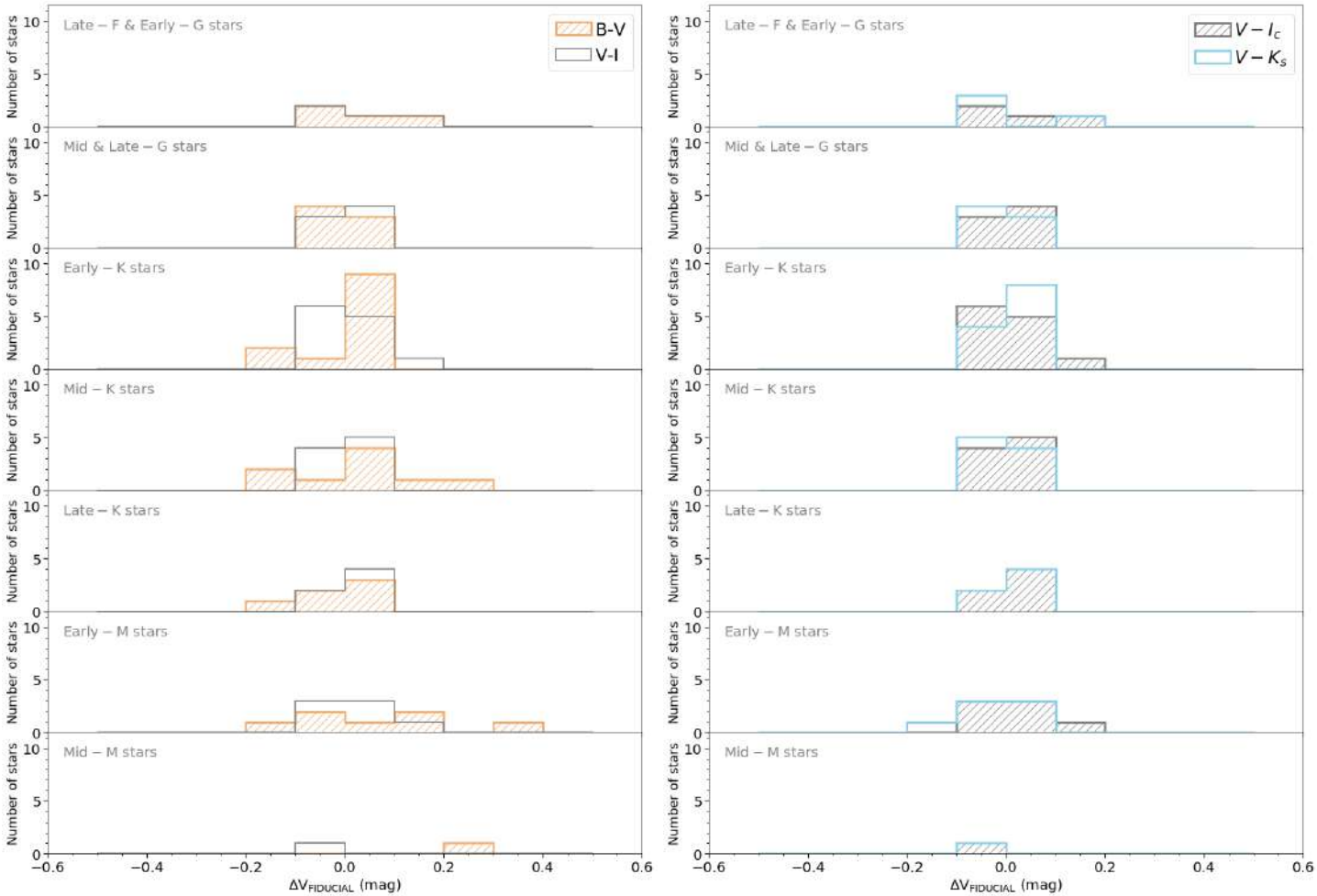


Figure 5.16: Histogram of the resulting residuals for the stars of Hyades. The residuals corresponding to $B - V$ are represented in orange, $V - I_c$ in grey, and $V - K_s$ in blue.

### 5.5.4 Histograms of the stars of the clusters grouped by age range

In this section, we show the histograms of the stars of the clusters grouped according to age. In the graph 5.17a, we have represented the histograms of the stars of the youngest clusters, $\alpha$ Per and Pleiades, with approximate ages of between 70 Myr and 112 Myr. The histograms represented in the graph 5.17b contain the remaining stars of intermediate ages, between 600 Myr and 700 Myr, belonging to Coma Ber, Praesepe and Hyades.
If we compare both Figures 5.17a and 5.17b, we first see a greater dispersion in the residuals of the younger stars, both in the histograms corresponding to $B - V$ and to $V - I_c$.

In the histograms corresponding to $B - V$, we see in the young stars, unlike the intermediate-aged objects, that all the spectral types between late-F and late-K are situated in the region of positive residuals, reaching higher values the later the spectral type. Continuing with the young stars, in the case of the M-types, as we have explained above, a small part of the sample has negative residuals, while the rest have residuals with values between 0 mag and 2.4 mag, reaching the highest values of those obtained for all the stars, both young and intermediate in age. With regard to the histograms of the M-type stars present in the intermediate-age clusters, as with the younger clusters (although to a lesser degree), they undergo a larger dispersion in the residuals compared to the earlier spectral types. Of all the intermediate-age stars, the highest values of the residuals are for an early-M dwarf and a mid-M dwarf star, the latter having the highest, with a value of $\sim$ 1.5 mag.

Regarding the histograms of the residuals corresponding to the $V - I_c$ CMDs, we can see greater differentiation between the distribution of these and those corresponding to $B - V$ for the young stars in comparison with the intermediate-age stars, whose distributions in $B - V$ and $V - I_c$ are similar except for the mid-M stars. Furthermore, for the young stars the decrease in the dispersion in the residuals in $V - I_c$ compared to the histograms of the residuals for $B - V$, it is much clearer for spectral types from late-K to mid-M in comparison with earlier spectral types.

Lastly, the histograms of the $M_v$ vs $V - K_s$ diagrams, both for the young stars and for the intermediate-age stars, show a similar distribution to that observed in $V - I_c$. If we compare the histograms of the two CMDs corresponding to $V - I_c$ and $V - K_s$, for the stars of young clusters, of spectral types between late-F and late-K, we see a higher number of objects situated in the region of negative residuals in the histograms of $V - K_s$. For the groups of early-M and mid-M stars, we observe a higher number of stars in that region in the histograms of $V - I_c$. Regarding the intermediate-age clusters, the histograms of both diagrams are very similar, although for $V - K_s$ the dispersion is even less than that of $V - I_c$. For both the latter and in $V - K_s$ we see the largest dispersion for the M-stars, many of which lie in the region of negative residuals.

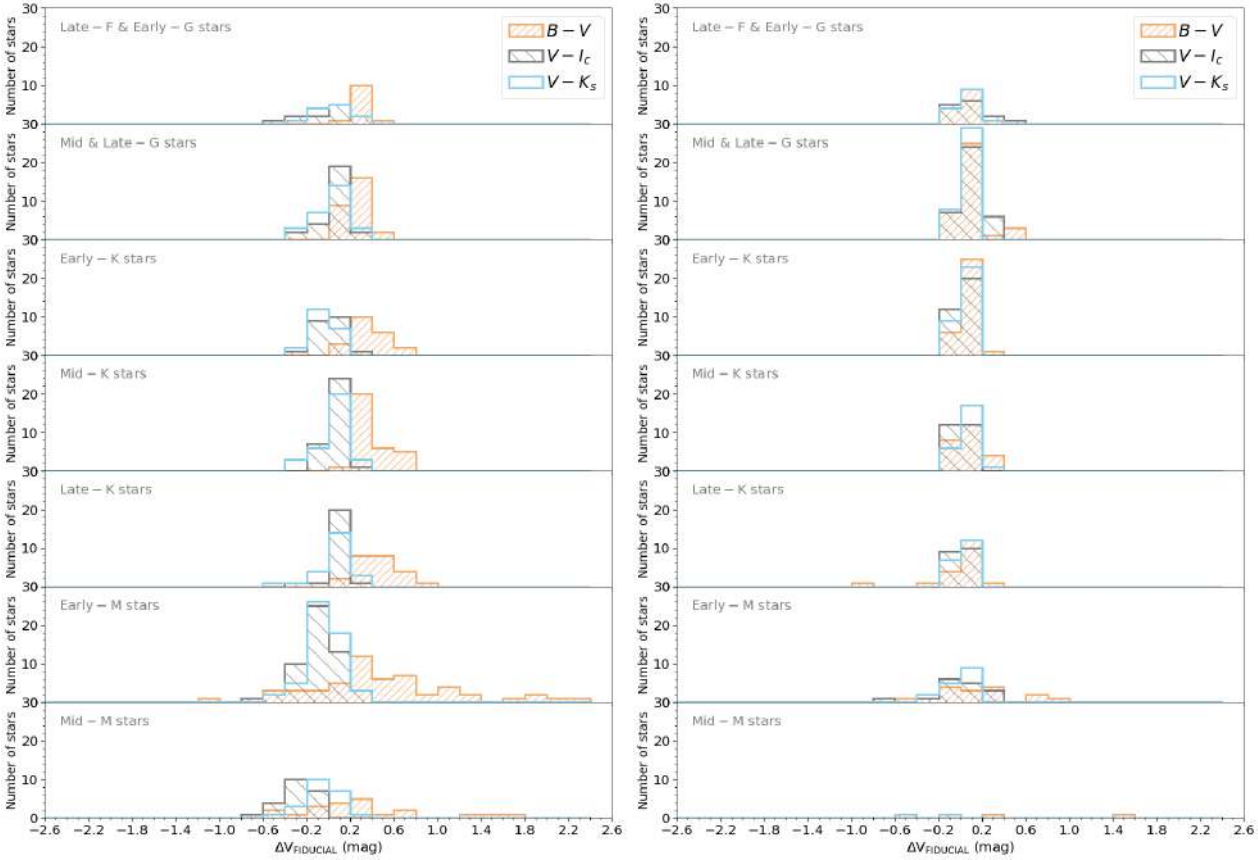


(a) Young stars, corresponding to the clusters $\alpha$ Per and Pleiades.

(b) Intermediate-age stars, belonging to Coma Ber, Praesepe and Hyades.

Figure 5.17: Histograms of the resulting residuals for the stars of the five clusters grouped according to age.

**Box plots of the distributions of the histograms grouped by the age range of the clusters**

We use the box plot statistical tool (see the explanatory graph on the lower right of Figure 5.18) in order to visualize the median of the residuals, represented by a line inside the box. This box contains 50 % of the sample of stars (in this case, each sample is a group of spectral types), and the bars that protrude from each side indicate the range of residuals that contains 24.65 % of the sample stars. Lastly, we represent a much lower percentage, 0.35 %, in grey rhombi.

Figure 5.18 represents three box-plot graphs of the residuals corresponding to the $B-V$, $V-I_c$ and $V-K_s$ CMDs, in which we compare each box plot of the young clusters with that resulting from the intermediate-age clusters. Between the two box plots, we represent the stars corresponding to each spectral group and age group.

The graph corresponding to $B-V$ shows a clear trend of the young stars toward higher positive residuals in comparison with the intermediate ages. However, the mid-M type star group does not follow this trend, since the box plot of the intermediate ages is situated toward higher positive residuals than in the case of the young stars.

The representation of box plots of the residuals for $V-I_c$ show a clearly lower dispersion with regard to $B-V$ and a greater similarity in the positions of the medians among the stars of both age groups.

Regarding $V-K_s$, the graph is very similar to the one represented for $V-I_c$, with an even lower dispersion. We can see with more clarity that the intermediate-age stars are concentrated in a range of residuals that is lower than the range shown in the young stars. Moreover, for the young stars, the positions of the medians in the late-F and early-G up to mid-K spectral groups have shifted slightly toward lower residuals. There appears to be a slight reddening of these spectral-type stars with respect to the $V-I_c$ CMD. This effect is not seen in the intermediate-age stars.

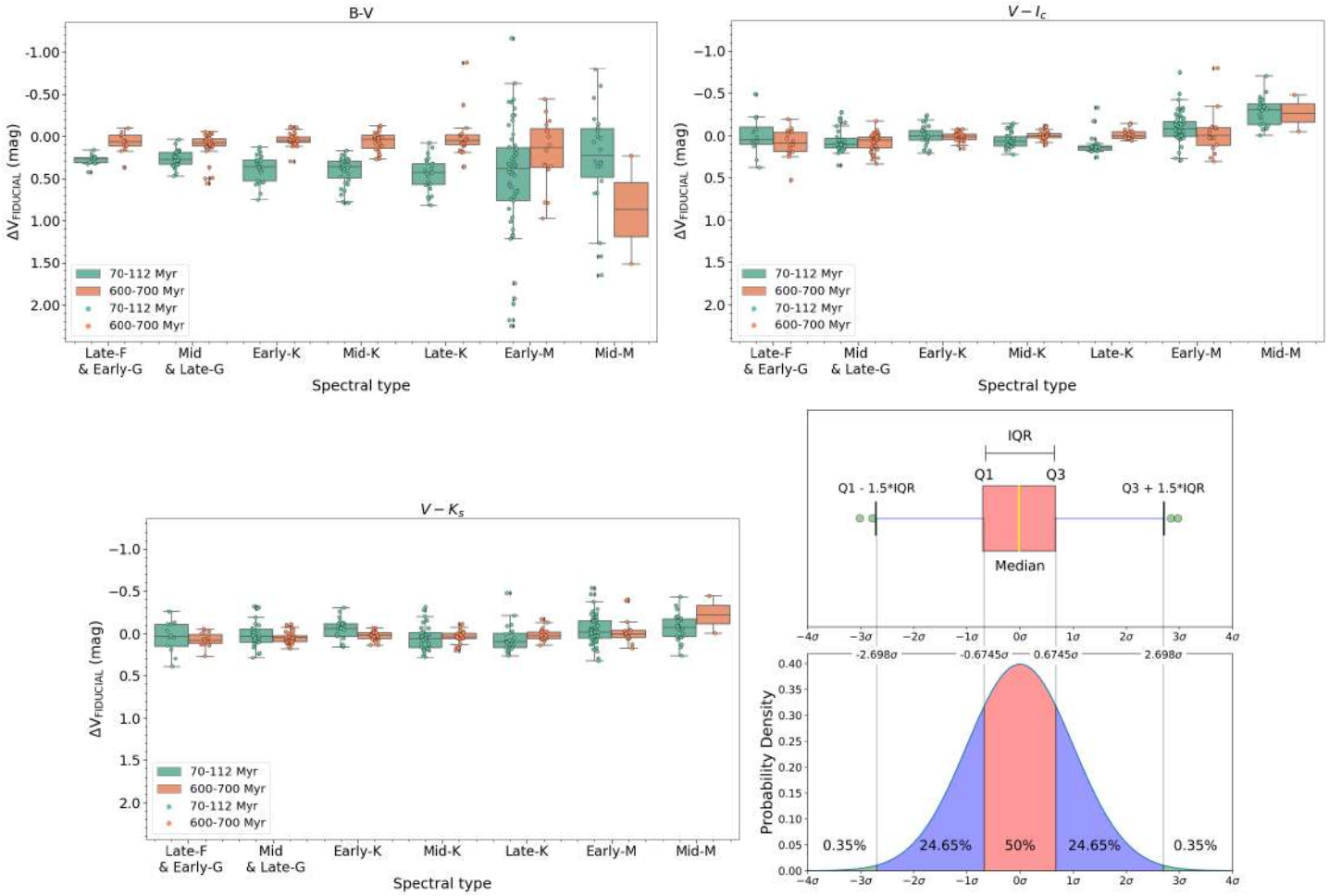


Figure 5.18: Box plots of the residuals of the stars grouped by spectral type and age. The sample of young stars is represented in green and the intermediate-age stars in orange. Each dot located between the two box plots indicates a star.

In this chapter, we have seen how the blueing effect in $B-V$ that we are studying is observed mainly in the younger stellar clusters, being more pronounced in the Pleiades cluster, although the $\alpha$ sample contains much fewer stars. This blueing can also be interpreted as an increase in the $M_v$ absolute magnitude, as other authors have done (Herbig 1962, , etc.). The decrease in brightness could be due to spots that are always seen or to the fact that between some spots and others, many degrees of the star's longitude are covered. The reddening effect in $V-K_s$ can be fairly well seen in the $\alpha$ Per stars with shorter periods, for spectral types from from G to M. In the case of Pleiades, we mainly see this for the K-type stars.

Our initial idea was centred on studying several clusters that had been selected to cover an interval of ages between 70 and 800 Myr. Due to the fact that the age originally estimated for Coma Ber of $\sim$ 400 Myr was a long way off from what was finally established ($\sim$ 600 Myr), we were compelled to divide the study into two age groups: from $\sim$ 70 Myr to $\sim$ 112 Myr, and from $\sim$ 600 Myr to $\sim$ 700 Myr. It is precisely in this gap that we have not been able to cover (112 - 600 Myr) where it is likely that the effect we are studying disappears in in all spectral types except for M-stars . For the M stars in the Praesepe cluster, it appears that the blueing effect can still be discerned slightly, although we have few M stars in that cluster. We intuit a lag in the evolution of the blueing depending on the spectral type, whether G, K or M. In other words, the phenomenon of blueing that we are studying seems to emerge first in the G-type stars (perhaps it is present in the mid- and late-G stars of $\alpha$ Per), then it appears in the K stars (clearly observable in the Pleiades cluster), and possibly afterwards in the M-type dwarfs, although the fact that they are found on the pre-main-sequence in both clusters makes it difficult to discover their position on the CMDs. In the clusters aged between 600 and 700 Myr, the effect does not seem to have completely diminished for the M stars. In the case of the reddening, although we have only observed it clearly in the young clusters, with the results obtained, we have not been able to draw conclusions about the relation between the evolution of this phenomenon and the age of the stars.

As we have restricted the study to stars with photometric measurements with errors less than or equal to 0.04 mag and 0.06 mag (in the $K_s$ band) in the study of blueing and reddening, respectively, we can say that the dispersion that can be seen in the G, K and M stars in the residuals diagrams is real and not a consequence of measurement errors. In the case of the M stars, the fact that the fiducial has such a vertical form in the $B-V$ HR diagram, hinders the analysis of the residuals.

The results that we have obtained for these clusters make it clear that, when studying young clusters, distance, proper motions and radial velocities are good criteria for assigning membership, but not the position in the HR diagram, since there may be G-K-M stars that are displaced with respect to the main sequence of the cluster as a result of the phenomenon of blueing and reddening.

# Chapter 6

# Conclusions

For the purpose of studying the blueing and reddening effects that have been observed in previous studies (Stauffer & Hartmann 1987; Stauffer et al. 2003) for K-type stars belonging to the Pleiades cluster, we studied the position in colour-magnitude diagrams ($M_v$ vs $B-V$, $M_v$ vs $V-I_c$ y $M_v$ vs $V-K_s$) of late spectral type stars located in the clusters $\alpha$ Per, Pleiades, Coma Ber, Praesepe and Hyades. For this, we used photometry from the literature in the bands $BVI_c$, with a minimum accuracy of 0.04 mag, higher than that used by Kamai et al. (2014), and $K_s$ (2MASS) with a minimum accuracy of 0.06 mag. We have also compiled rotation periods in order to study the relation between this parameter and blueing and reddening effects. In order to represent the absolute magnitudes in the $V$ band, we have used the distances derived from the parallaxes of each star provided by *Gaia* DR2. In addition, for stars from the selected clusters that are spectral types from late-G to mid-M, we have obtained $BVR_cI_c$ photometry with a minimum accuracy of 0.04 mag from observations carried out on the 1.5-metre telescope at the Observatorio de Sierra Nevada.

In the context of this study, we have reached the following conclusions:

1. In the study of the Coma Berenices cluster, the distances from *Gaia* DR2 have brought to light giant rapid rotator stars that have been catalogued in other studies as late-type main-sequence stars and members of the cluster.

2. The contamination of giant stars in clusters can present a problem for determining their ages using the technique of gyrochronology. Thus it is important to determine the luminosity of the stars well, as this will be used to derive the ages of the clusters.

3. Having eliminated the giant stars, our sample of Coma Berenices indicates that the age of this cluster is $\sim$ 600 Myr, rather than the age proposed by Tang et al. (2019) of $\sim$ 800 Myr.

4. We have compared the observational data with isochrones derived from stellar models, and we have verified that there is no model that can simultaneously reproduce the behaviour of the cluster stars in the $B-V$ vs $M_v$ and $V-I$ vs $M_v$ diagrams. Therefore, we derived a fiducial for each colour-magnitude diagram ($M_v$ vs $B-V$, $M_v$ vs $V-I_c$ and $M_v$ vs $V-K_s$), making use of the photometry compiled for the single stars of Hyades. We have used this fiducial as a reference to compare with the photometry of the stars of each cluster represented in the three CMDs.

5. We have compared the absolute magnitudes of the single stars that are members and possible members of each cluster and we have confirmed that the blueing effect we are studying is mainly observed in younger stellar clusters. In our sample of $\alpha$ Per containing stars from Early-G to Mid-M, we can see this for stars from G to K types, and slightly in one of the two M stars of the sample. Nonetheless, we do not find a clear relation between this effect and the rotation periods. In Pleiades all the spectral types we studied in our sample (from Late-F to Mid-M) show this effect, and comparing with $\alpha$ Per, it is seen a more clearly relation of the blueward deviation with rotation periods for K- and M-stars: most K-stars with short rotation periods fall further below the fiducial, and we see a larger blueing in a

group of rapidly rotating M stars. Reddening is also perceived for these clusters: in $\alpha$ Per it is observed for stars with short rotation periods and of spectral types from G to M; and in Pleiades we can also see it mainly in K-type rapid rotators.

6. We have divided the ages of the five clusters into two blocks (from 70 Myr to 112 Myr, and from 600 Myr to 700 Myr). In the gap between 112 Myr and 600 Myr, the blueing effect disappears in all the spectral types except for M-stars. It seems that we can still perceive the blueing that we are studying for the M-stars in the Praesepe cluster, although we have few M-stars in this cluster. Regarding reddening, in the intermediate-age clusters it is not clear if this effect is still present. It may be that it disappears before the blueing effect. .

7. Using colour-magnitude diagrams is not recommendable for identifying non-member stars in young clusters whose ages are less than 1 Gyr, unless one takes into account the fact that, depending on the age and spectral type, the stars can present this blueing and/or reddening.

# Appendix A

# Information concerning photometry taken at OSN

## A.1 Coefficients of the photometric calibration

We used the transformation equations developed by Harris et al. (1981), which we explained in chapter 2 (2.1, 2.2, 2.3 and 2.4), for the required Johnson-Cousins filters $BVR_cI_c$. Below we show the coefficients corresponding to each equation and night of observation.

**NIGHT (date): 21/10/2015**

$V$
a1=2.132, a2=0.022, a3=-0.209, a4=0.087, a5=0.026. Extinction value=0.104

$B-V$
b1=0.057, b2=0.091, b3=0.883, b4=-0.030 b5=-0.013. Extinction value=0.054

$V-R_c$
c1=0.245, c2=0.040, c3=1.027, c4=0.0004, c5=0.004. Extinction value=0.040

$V-I_c$
d1=-0.397, d2=0.064, d3=1.041, d4=0.010, d5=0.017. Extinction value=0.078

Airmass ranges:

Alpha Per:1.024-1.13
Pleiades: 1.2875-1.3275
Standard stars: 1.25-2.28

**NIGHT (date): 11/05/2015**

$V$
a1=1.49, a2=0.092, a3=0.863, a4=0.006, a5=-0.443. Extinction value=0.096

$B - V$
b1=-0.046, b2=0.08, b3=1.112, b4=-0.012, b5=-0.146. Extinction value=0.070

$V - R_c$ c1=0.460, c2=0.009, c3=0.221, c4=0.127, c5=0.509. Extinction value=0.133

$V - I_c$
d1=-0.123, d2=0.083, d3=0.475, d4=0.039, d5=0.216. Extinction value=0.143

Airmass ranges:

Coma Ber: 1.036-1.76
Pesebre:1.556-1.736
Standard stars: 1.27-1.86

**NIGHT (date): 26/05/2016**

$V$
a1=1.756, a2=0.215, a3=0.032, a4=-0.039, a5=0.027. Extinction value=0.263

$B - V$
b1=0.048, b2=0.124, b3=0.850, b4=-0.029, b5=0.005. Extinction value=0.093

$V - I_c$
d1=0.014, d2=0.075, d3=0.194, d4=0.032, d5=0.366. Extinction value=0.162

Airmass ranges:
Coma Ber: 1.16-1.178
Standard stars: 1.3-1.59

**NIGHT (date): 10/11/2015**

$V$
a1=1.815, a2=0.154, a3=0.073, a4=-0.037, a5=0.002 Extinction value=
k: 1.117200D-01 k1: 1.084832D+00 k2: -5.131482D-01
$B - V$

b1=0.082, b2=0.075, b3=0.841, b4=-0.014, b5=-0.006. Extinction value=0.059

$V - R_c$
c1=0.261, c2=0.046, c3=0.994, c4=-0.004, c5=0.021. Extinction value=0.043

$V - I_c$

d1=-0.363, d2=0.065, d3=1.034, d4=0.007, d5=0.016. Extinction value=0.074

Airmass ranges:

Alpha:1.03-1.173
Pleiades:1.137-1.3315 SA:1.24-2.84

**NIGHT (date): 11/11/2015**

$V$
a1=1.925, a2=0.090, a3=-0.005, a4=0.021, a5=-0.002. Extinction value=0.110

$B - V$
b1=0.039, b2=0.100, b3=0.861, b4=-0.018, b5=-0.012. Extinction value= 0.079

$V - R_c$
c1=0.279, c2=0.028, c3=0.957, c4=0.024, c5=0.019. Extinction value=0.044

$V - I_c$

d1=-0.311, d2=0.022, d3=1.009, d4=0.008, d5=0.029. Extinction value=0.034

Airmass ranges:

Alpha:1.205-1.624
SA:1.244-1.683

**NIGHT (date): 16/11/2015**

$V$

a1=1.825, a2=1.127, a3=0.079, a4=0.078, a5=-0.074. Extinction value=0.162

$B - V$

b1=-0.059, b2=0.150, b3=0.943, b4=-0.030, b5=-0.037. Extinction value=0.120

$V - R_c$ c1=0.324, c2=0.013, c3=0.904, c4=0.014, c5=0.055. Extinction value=0.022

$V - I_c$

d1=-0.306, d2=0.066, d3=0.925, d4=0.021, d5=0.044. Extinction value=0.094

Airmass ranges:

Alpha Per:1.11-1.25
Hyades:1.2255-1.374
SA:1.26-1.755.

**NIGHT (date): 17/11/2015**

$V$

a1=1.854, a2=0.125, a3=0.072, a4=-0.020, a5=-0.006. Extinction value=0.105

$B - V$

b1=0.067, b2=0.090, b3=0.878, b4=-0.022, b5=-0.018. Extinction value=0.068

$V - R_c$

c1=0.248, c2=0.059, c3=0.987, c4=-0.018, c5=0.041. Extinction value=0.048

$V - I_c$

d1=-0.355, d2=0.120, d3=0.891, d4=-0.004, d5=0.070. Extinction value=0.116

Airmass ranges:

Hyades:1.08-1.65
SA:1.2695-1.936.

**NIGHT (date): 18/11/2015**

$V$

a1=1.629, a2=0.296, a3=0.216, a4=-0.133, a5=-0.007. Extinction value=0.151

$B - V$

b1=-0.022 b2=0.101, b3=0.967, b4=-0.005, b5=-0.058. Extinction value=0.096

$V - R_c$
c1=0.282, c2=0.026, c3=0.956, c4=0.026 c5=0.017. Extinction value=0.044

$V - I_c$
d1=-0.116, d2=-0.056, d3=0.911, d4=-0.006, d5=0.062. Extinction value=-0.064

Airmass ranges:

Alpha Per:1.3-1.64
Hyades:1.089-1.503
SA:1.24-1.508

**NIGHT (date): 19/11/2015**

$V$

a1=1.867, a2=0.127, a3=0.048, a4=-0.024, a5=0.002. Extinction value=0.100

$B - V$

b1=-0.012, b2=0.153, b3=0.916, b4=-0.062, b5=-0.013. Extinction value=0.087

$V - R_c$

c1=0.231, c2=0.070, c3=0.979, c4=-0.029, c5=0.049. Extinction value=0.051

$V - I_c$

d1=-0.370 d2=0.083, d3=0.994, d4=-0.009, d5=0.036. Extinction value=0.071

Airmass ranges:

Alpha Per:1.036-1.17
Hyades: 1.07-2.5325
SA:1.265-1.895

**NIGHT (date): 29/11/2015**

$V$
a1=1.901, a2=0.102, a3=0.017, a4=0.027, a5=-0.014. Extinction value=0.123

$B - V$
b1=0.078, b2=0.086, b3=0.896, b4=-0.0526, b5=-0.009. Extinction value=0.028

$V - R_c$
c1=0.231, c2=0.059, c3=1.076, c4=-0.054, c5=0.019. Extinction value=0.025

$V - I_c$
d1=-0.402, d2=0.094, d3=1.110, d4=-0.046, d5=0.020. Extinction value=0.039

Airmass ranges:

Alpha Per:1.04-1.655
SA:1.24-2.028

**NIGHT (date): 19/12/2015**

$V$
a1=2.438, a2=0.145, a3=0.027, a4=-0.030, a5=0.021. Extinction value=0.312

$B - V$
b1=0.284, b2=0.015, b3=0.893, b4=0.007, b5=-0.025. Extinction value=0.023

$V - R_c$
c1=-0.185, c2=0.042, c3=0.980, c4=0.0002, c5=-0.057. Extinction value=0.042

$V - I_c$
d1=-0.929, d2=0.033, d3=1.150, d4=0.005, d5=-0.025. Extinction value=0.040

Airmass ranges:

Alpha Per:1.12-1.526
Hyades: 1.093-1.745
SA:1.25-2.1255

**NIGHT (date): 29/02/2016**

$V$
a1=-0.375, a2=1.825, a3=3.155, a4=-2.271, a5=0.0129. Extinction value=-0.778

$B-V$
b1=-0.118, b2=0.266, b3=0.365, b4=0.333, b5=-0.018. Extinction value=0.626

$V-I_c$
c1=-1.331, c2=0.873, c3=2.107, c4=-0.907, c5=0.085. Extinction value=-0.472

Airmass ranges:

Pesebre: 1.05-1.43
Standard stars: 1.35-1.40

**NIGHT (date): 01/03/2016**

$V$
a1=2.023, a2=0.115, a3=-0.069, a4=-0.001, a5=0.039. Extinction value=0.114
$B-V$
b1=0.190, b2=0.070, b3=0.768, b4=-0.019, b5=0.018. Extinction value=0.050
$V-I_c$
c1=-0.249, c2=0.086, c3=0.845, c4=-0.006, c5=0.087. Extinction value=0.077

Airmass ranges:

Pesebre:1.05-2.076
Standard stars: 1.26-2.46

**NIGHT (date): 02/03/2016**
We did not use the data corresponding to this night, since the errors are greater than 0.04 mag. In the next section we show the results of the photometry measured for Praesepe during this night.
$V$
a1=2.064, a2=0.089, a3=-0.067, a4=0.008, a5=0.036. Extinction value=0.093

$B-V$
b1=0.068, b2=0.094, b3=0.919, b4=-0.019, b5=-0.034. Extinction value=0.074

$V-I_c$

d1=-0.331, d2=-0.080, d3=-0.999, d4=-0.003, d5=-0.038. Extinction value=0.075

Airmass ranges:

Pesebre:1.059-1.555
Standard stars: 1.26-2.17

**NIGHT (date): 05/01/2017**

$V$
a1=1.969, a2=0.303, a3=0.042, a4=-0.143, a5=0.116. Extinction value=0.292

$B - V$
b1=0.027, b2=0.246, b3=0.999, b4=-0.290, b5=0.064. Extinction value=-0.061

$V - I_c$

d1=-0.295, d2=0.149, d3=0.746, d4=0.010, d5=0.133. Extinction value=0.163

Airmass ranges:

Alpha Per:1.026-1.03
Standard stars: 1.25-1.35

**NIGHT (date): 06/01/2017**

$V$

a1=2.135, a1=0.210, a1=-0.196, a1=-0.0298, a1=0.152. Extinction value=0.197

$B - V$

b1=0.528, b1=-0.142, b1=0.387, b1=0.181, b1=0.057. Extinction value=0.047

$V - I_c$

d1=-0.467, d1=0.321, d1=0.963, d1=-0.225, d1=0.166. Extinction value=0.002

Airmass ranges:

Alpha Per:1.026
Standard stars:1.25-1.37

**NIGHT (date): 07/01/2017**

$V$
a1= 1.815, a2=0.357, a3=0.235, a4=-0.150, a5=-0.006. Extinction value=0.198

$B - V$
b1=0.459, b2=-0.154, b3=0.502, b4=0.215, b5=-0.003. Extinction value=0.097

$V - I_c$
d1=-0.394, d2=0.102, d3=1.286, d4=-0.154, d5=0.010. Extinction value=-0.103

Airmass ranges:

Alpha:1.026-1.368
Standard stars: 1.308-1.556

**NIGHT (date): 15/01/2017**

$V$
a1=2.376, a2=-0.042, a3=-0.205, a4=0.172, a5=-0.004. Extinction value=0.209

$B - V$
b1=0.228, b2=0.053, b3=0.728, b4=0.014, b5=0.012. Extinction value=6.940935D-02

$V - I_c$
d1=0.216, d2=-0.377, d3=0.790, d4=0.211, d5=0.010. Extinction value=-0.071

Airmass ranges:

Alpha:1.44-1.577
Standard stars: 1.26-1.423

**NIGHT (date): 17/03/2017**

$V$
a1=2.353, a2= 0.211, a3=-0.082, a4=0.025, a5=0.032. Extinction value=0.225

$B - V$
b1=0.519, b2=-0.109, b3=0.530, b4=0.128, b5=0.026. Extinction value=0.021

$V - I_c$
d1=-0.290, d2=0.081, d3=0.951, d4=0.037, d5=0.033. Extinction value=0.125

Airmass ranges:
Alpha Per:1.725-1.837
Coma Ber: 1.72-1.84
Standard stars: 1.29-1.84

**NIGHT (date): 18/03/2017**

$V$
a1=2.359, a2=0.072, a3=-0.008, a4=0.036, a5=-0.008. Extinction value=0.100

$B - V$
b1=0.188, b2=0.096, b3=0.819, b4=-0.030, b5=-0.008. Extinction value=0.069

$V - I_c$
d1=-0.285, d2=0.061, d3=1.022, d4=0.017, d5=0.018. Extinction value=0.082

Airmass ranges: Alpha Per:1.658-1.768
Coma Ber: 1.06-1.25
Standard stars: 1.27-1.95

**NIGHT (date): 21/03/2017**

$V$
a1=2.068, a2=0.251, a3=0.193, a4=-0.102, a5=0.001. Extinction value=0.163

$B - V$
b1=0.205, b2=0.079, b3=0.842, b4=-0.040, b5=-0.011. Extinction value=0.044

$V - I_c$

d1=-0.395, d2=0.109, d3=1.186, d4=-0.019, d5=-0.052. Extinction value=0.090

Airmass ranges:
Coma Ber: 1.03-1.65
Standard stars: 1.29-1.86

**NIGHT (date): 04/04/2017**

$V$
a1= 2.275, a2=0.104, a3=0.069, a4=0.034, a5=-0.0356. Extinction value=0.127

$B - V$
b1= 0.670, b2=0.058, b3=-0.340, b4=0.016, b5=0.603. Extinction value=0.055

$V - I_c$
d1=-0.432, d2=0.101, d3= 1.157, d4=0.007, d5=-0.027. Extinction value=0.107

Airmass ranges:
Alpha Per:1.94-2.1 Coma Ber: 1.07-2.14
Standard stars: 1.26-2.3

**NIGHT (date): 05/04/2017**

In order to reduce the upper limit residual values for this night (those were lower than 0.04 mag but higher than expected) we repeated the photometric calibration by dividing the process in two sets: the first set included only the redder stars of Coma Ber and the redder standards stars, and the second one included only the bluer stars for Coma Ber and the bluer standard stars. That way we made two calibrations:

1. Redder stars: Alpha Per ($B - V$ = 1.066 mag), Coma ($B - V$ from 1.02 to 1.1 mag), Standard stars ($B - V$ from 1.024 to 2.192 mag).

V
a1= 2.863, a2=-0.051, a3=-0.340, a4=0.060, a5=0.069. Extinction value=0.017

B-V
b1= -0.299, b2=0.011, b3=1.557, b4=0.026, b5=-0.254. Extinction value=0.042

V-I

d1= -0.310, d2=0.080, d3= 1.040, d4=-0.0001, d5=0.018. Extinction value=0.080

Airmass ranges:
Apha Per: 2.18-2.268
Coma Ber: 1.02-2
Standard stars: 1.25-2.1

2. Bluer stars: Coma ($B - V$ from 0.8 to 0.9 mag), Standard stars ($B - V$ from 0.6 to 0.84).

V
a1= 2.476, a2=0.088, a3=-0.319, a4=0.017, a5=0.230. Extinction value=0.095

B-V
b1= 0.030, b2=0.077, b3=1.431, b4=-0.031, b5=-0.497. Extinction value=0.060

V-I
d1= -0.522, d2=0.034, d3=1.606, d4=0.058, d5=-0.371. Extinction value=0.023

Airmass ranges:
Coma Ber: 1.013-1.017
Standard stars: 1.27-2.1

**NIGHT (date): 06/04/2017**

*V*
a1= 2.271, a2=0.136, a3=-0.058, a4=0.094, a5=-0.014. Extinction value=0.196

$B - V$
b1=0.042, b2=0.213, b3= 1.030, b4=-0.203, b5=0.013. Extinction value=-0.011

$V - I_c$
d1=-0.293, d2=0.076, d3=0.853, d4=0.123, d5=0.024. Extinction value=0.231

Airmass ranges:
Alpha Per:2.03-2.09
Coma Ber: 1.25-1.71
Standard stars: 1.26-1.40

**NIGHT (date): 08/04/2017**

$V$
a1=2.240, a2=0.144, a3=0.112, a4=-0.014, a5=-0.016. Extinction value=0.129

$B - V$
b1=0.159, b2=0.100, b3=0.848, b4=-0.026, b5=-0.010. Extinction value=0.069

$V - I_c$
d1=-0.432, d2=0.120, d3=1.082, d4=0.004, d5=0.006. Extinction value=0.125

Airmass ranges:
Alpha:1.967-2.03
Standard stars: 1.42-2.07

**NIGHT (date): 06/05/2017**

$V$
a1= 2.134, a2=0.047, a3=0.755, a4=0.0252 a5=-0.506. Extinction value=0.057

$B - V$
b1= 0.104, b2=0.155, b3=0.800, b4=-0.003, b5=-0.009. Extinction value=0.153

$V - I_c$
d1=-0.241, d2=-0.009, d3=1.147, d4=0.024, d5=-0.051. Extinction value=0.013

Airmass ranges:
Coma Ber: 1.12-1.21
Standard stars: 1.076-1.21

**NIGHT (date): 07/05/2017**

$V$
a1=2.454, a2=0.037, a3=0.015, a4=0.053, a5=-0.058. Extinction value=0.061

$B - V$
b1=0.348, b2=0.039, b3=0.550, b4=0.013, b5=0.111. Extinction value=0.050
$V - I_c$
c1=-0.355, c2=0.064, c3=1.250, c4=0.0002, c5=-0.103. Extinction value=0.065

Airmass ranges:

Pesebre: 1.48-2.248
Standard stars: 1.38-2.46

## A.2 Photometry measurements of Praesepe stars with errors greater than 0.04 mag

The following table contains the photometry, derived from the observations at OSN, that we did not use in our study, since the errors in the $BVR_cI_c$ filters are greater than 0.04 mag.

| *Name* | $\alpha_{J2000}$ (h:m:s) | $\delta_{J2000}$ ($^\circ$:$'$:$''$) | Date | $B-V$ (mag) | e$B-V$ (mag) | $V$ (mag) | e$V$ (mag) | $V-Rc$ (mag) | e$V-Rc$ (mag) | $V-Ic$ (mag) | e$V-Ic$ (mag) |
|---|---|---|---|---|---|---|---|---|---|---|---|
| JS241 | 08:38:37.47 | 19:15:28.67 | 07/05/2017 | 1.671 | 0.192 | 17.457 | 0.046 | | | 3.124 | 0.0550344 |
| HSHJ229 | 08:38:51.02 | 19:18:33.53 | 07/05/2017 | 5.144 | 3.943 | 19.779 | 0.115 | | | 4.148 | 0.131241 |
| AD2509 | 08:39:06.95 | 19:47:08.03 | 01/03/2016 | 1.705 | 0.179 | 20.430 | 0.089 | | | 3.215 | 0.103085 |
| AD2527 | 08:39:15.37 | 19:19:28.45 | 01/03/2016 | 1.665 | 0.146 | 19.612 | 0.043 | | | 2.954 | 0.0480009 |
| HSHJ256 | 08:39:15.73 | 19:20:02.52 | 01/03/2016 | 1.593 | 0.226 | 19.817 | 0.058 | | | 2.934 | 0.0647384 |
| HSHJ258 | 08:39:18.50 | 19:22:44.26 | 01/03/2016 | 1.650 | 0.180 | 19.945 | 0.056 | | | 2.977 | 0.0632032 |
| JS713 | 08:39:47 | 19:44:12.60 | 01/03/2016 | 1.774 | 0.170 | 19.092 | 0.042 | | | 2.808 | 0.0498913 |
| 2MASSJ08394730+1939344 | 08:39:47.30 | 19:39:34.36 | 01/03/2016 | 1.568 | 0.060 | 18.144 | 0.028 | | | 2.706 | 0.0312075 |
| JS415 | 08:41:10.52 | 18:16:07.05 | 07/05/2017 | 1.630 | 0.137 | 16.631 | 0.028 | | | 2.744 | 0.0346948 |
| HSHJ397 | 08:41:53.59 | 19:36:30.59 | 02/03/2016 | 1.724 | 0.092 | 19.131 | 0.030 | | | 2.868 | 0.0362234 |
| AD3050 | 08:42:04.48 | 19:32:42.72 | 11/05/2015 | 2.718 | 0.368 | 20.787 | 0.058 | 1.225 | 0.083 | 2.733 | 0.073 |

# Appendix B

# Binaries in the five clusters

The following table provides the names of the stars that were classified as binary/multiple and represented in the diagrams of chapter 5. For Hyades cluster we also provided binarity information of several non-member stars.

| $\alpha$ Per | Pleiades | Praesepe | Hyades |
|---|---|---|---|
| HE935 | "Cl* Melotte 22 DH 001" | "Cl* NGC 2632 JS102" | HD285348 |
| HE373 | "Cl* Melotte 22 DH 054" | "Cl* NGC 2632 KW533" | HG7-122 |
| AP41 | "Cl* Melotte 22 DH 056" | "Cl* NGC 2632 KW 16" | HD27732 |
| AP95 | "Cl* Melotte 22 HCG 12" | "Cl* NGC 2632 KW 31" | V*V989Tau |
| AP72 | "Cl* Melotte 22 HCG 16" | "Cl* NGC 2632 VL 465"++ | HD27990 |
| APX158++ | "Cl* Melotte 22 PELS 138" | "V* BR Cnc" | V*V992Tau |
| AP98 | "Cl* Melotte 22 SK787" | "Cl* NGC 2632 KW 47" | HD28099 |
| AP70 | "Cl* Melotte 22 DH 193" | "Cl* NGC 2632 KW 55" | HD286798 |
| AP108 | "Cl* Melotte 22 PELS 028" | "Cl* NGC 2632 KW 79" | HD286820 |
| AP63++ | "Cl* Melotte 22 SK698" | "Cl* NGC 2632 KW100" | HD285828 |
| AP139 | "Cl* Melotte 22 SK671" | "Cl* NGC 2632 KW127" | HD285830 |
| AP127++ | "Cl* Melotte 22 HCG 93" | "Cl* NGC 2632 KW146" | HG7-232 |
| AP139 | "Cl* Melotte 22 PELS 030" | "Cl* NGC 2632 KW563" | V*V918Tau |
| AP201 | "Cl* Melotte 22 HCG 97" | "Cl* NGC 2632 KW566" | HD28344 |
| AP112 | "Cl* Melotte 22 PELS 031" | "Cl* NGC 2632 KW181" | V*V994Tau |
| AP124++ | "Cl Melotte 22 102" | "Cl* NGC 2632 KW184" | HG7-246++ |
| AP101 | "Cl* Melotte 22 SK638" | "Cl* NGC 2632 KW183" | V*V697Tau |
| AP15 | "Cl* Melotte 22 PELS 056" | "Cl* NGC 2632 KW198" | HD285837 |
| AP86 | "Cl Melotte 22 120" | "HD 73616" | TYC677-227-1 |
| AP60 | "Cl Melotte 22 134" | "Cl* NGC 2632 KW236" | UCAC4521-008763++ |
| | "Cl* Melotte 22 HCG 123" | "Cl* NGC 2632 JC 180"++ | TYC694-1183-1 |
| | "Cl Melotte 22 263" | "Cl* NGC 2632 KW244" | HD30246 |
| | "Cl Melotte 22 357" | "Cl* NGC 2632 KW246" | |
| | "Cl* Melotte 22 DH 343" | "Cl* NGC 2632 KW256" | |
| | "Cl Melotte 22 370" | "Cl* NGC 2632 KW257" | |
| | "Cl* Melotte 22 HCG 164"++ | "Cl* NGC 2632 KW272" | |
| | "Cl* Melotte 22 HCG 214" | "Cl* NGC 2632 KW275" | |
| | "Cl* Melotte 22 DH 423" | "Cl* NGC 2632 JS350" | |
| | "Cl Melotte 22 1032" | "Cl* NGC 2632 JS359" | |
| | "Cl Melotte 22 1321"++ | "Cl* NGC 2632 KW297" | |
| | "Cl* Melotte 22 PELS 142" | "Cl* NGC 2632 KW334" | |
| | "Cl Melotte 22 2368" | "Cl* NGC 2632 KW341" | |
| | "Cl* Melotte 22 HCG 376" | "Cl* NGC 2632 KW365" | |
| | "Cl Melotte 22 2462" | "Cl* NGC 2632 KW367" | |
| | "Cl* Melotte 22 HCG 378" | "Cl* NGC 2632 KW368" | |
| | "Cl* Melotte 22 HCG 428" | "Cl* NGC 2632 KW375" | |
| | "Cl* Melotte 22 AK V-088" | "Cl* NGC 2632 JS 428"++ | |
| | "Cl* Melotte 22 DH 794" | "Cl* NGC 2632 KW401" | |
| | "Cl* Melotte 22 AK IV-314" | "Cl* NGC 2632 JS456" | |
| | "Cl* Melotte 22 DH 800" | "Cl* NGC 2632 KW429" | |
| | "Cl* Melotte 22 HCG 489" | "Cl* NGC 2632 KW434" | |
| | "Cl* Melotte 22 HCG 495" | "Cl* NGC 2632 KW439" | |
| | "Cl* Melotte 22 HCG 502" | "Cl* NGC 2632 KW 456" | |
| | "Cl* Melotte 22 PELS 115" | "Cl* NGC 2632 KW466" | |
| | "Cl* Melotte 22 DH 896" | "Cl* NGC 2632 KW474" | |
| | | "Cl* NGC 2632 KW488" | |
| | | "Cl* NGC 2632 KW495" | |
| | | "Cl* NGC 2632 JS516" | |
| | | "Cl* NGC 2632 KW496" | |
| | | "Cl* NGC 2632 JS532" | |
| | | "Cl* NGC 2632 KW515" | |
| | | "Cl* NGC 2632 KW549" | |
| | | "Cl* NGC 2632 JS588" | |
| | | "Cl* NGC 2632 VL 1700" | |
| | | "Cl* NGC 2632 JS600" | |
| | | "Cl* NGC 2632 JS655" | |

Table B.1: Simbad names of the stars catalogued as binaries in each open cluster. The symbol ++ indicates the binaries that were identified photometrically.

# Appendix C

# Fits to the residuals

Below, we show the results of the fits to the residuals represented in chapter 5, corresponding to each cluster, CMD and spectral types. In each column we provide the coefficients $a$, $b$ according to the equation: $\Delta V_{Fiducial}$=$aPeriod$ + $b$; and the root mean square error (RMS) of each fit.

### $\alpha$ Per

| Spectral types | $M_v$ vs $B-V$ | $M_v$ vs $V-I_c$ | $M_v$ vs $V-K_s$ |
|---|---|---|---|
| G-stars | 0.012, 0.287<br>RMS:0.062 | 0.037, -0.027<br>RMS:0.070 | 0.060, -0.311<br>RMS:0.015 |
| K/M-stars | 0.009, 0.415<br>RMS:0.790 | 0.012, -0.034<br>RMS:0.374 | 0.046, -0.237<br>RMS:0.139 |
| K-stars | -0.013, 0.513<br>RMS:0.588 | -0.008, 0.056<br>RMS:0.210 | 0.032, -0.170<br>RMS:0.051 |

### Pleiades

| Spectral types | $M_v$ vs $B-V$ | $M_v$ vs $V-I_c$ | $M_v$ vs $V-K_s$ |
|---|---|---|---|
| F/G-stars | 0.005, 0.238<br>RMS:0.218 | 0.077, -0.292<br>RMS:0.685 | 0.045, -0.141<br>RMS:0.557 |
| K/M-stars | -0.030, 0.541<br>RMS:34.386 | 0.028, -0.170<br>RMS:3.739 | 0.025, -0.102<br>RMS:2.504 |
| K-stars | -0.029, 0.552<br>RMS:1.189 | 0.009, 0.0177<br>RMS:0.745 | 0.033, -0.122<br>RMS:0.931 |
| M-stars | -0.032, 0.536<br>RMS:33.171 | 0.027, -0.237<br>RMS:2.007 | 0.018, -0.100<br>RMS:1.441 |

**Coma Ber**

| Spectral types | $M_v$ vs $B-V$ | $M_v$ vs $V-I_c$ | $M_v$ vs $V-K_s$ |
|---|---|---|---|
| G-stars | 0.076, -0.198 RMS:0.021 | 0.078, -0.509 RMS:0.011 | 0.024, -0.139 RMS:0.002 |
| K-stars | 0.090, -0.827 RMS:0.050 | 0.019, -0.202 RMS:0.030 | 0.025, -0.184 RMS:0.084 |

**Praesepe**

| Spectral types | $M_v$ vs $B-V$ | $M_v$ vs $V-I_c$ | $M_v$ vs $V-K_s$ |
|---|---|---|---|
| F/G-stars | -0.002, 0.091 RMS:0.115 | -0.008, 0.169 RMS:0.663 | -0.012, 0.176 RMS:0.181 |
| K/M-stars | -0.030, 0.478 RMS:5.277 | 0.016, -0.217 RMS:1.085 | 0.015, -0.176 RMS:0.563 |
| K-stars | -0.028, 0.358 RMS:1.117 | -0.006, 0.073 RMS:0.119 | -0.004, 0.077 RMS:0.134 |
| M-stars | -0.037, 0.954 RMS:2.461 | 0.029, -0.504 RMS:0.636 | 0.027, -0.438 RMS:0.150 |

**Hyades**

| Spectral types | $M_v$ vs $B-V$ | $M_v$ vs $V-I_c$ | $M_v$ vs $V-K_s$ |
|---|---|---|---|
| F/G-stars | -0.004, 0.033 RMS:0.0358 | -0.006, 0.054 RMS:0.032 | 0.009, -0.084 RMS:0.031 |
| K/M-stars | -0.006, 0.102 RMS:0.434 | 0.002, -0.028 RMS:0.084 | -0.002, 0.024 RMS:0.056 |
| K-stars | 0.001 , 0.008 RMS:0.172 | 0.003, -0.027 RMS:0.054 | -0.001, 0.021 RMS:0.032 |
| M-stars | -0.014, 0.269 RMS:0.216 | 0.004, -0.055 RMS:0.029 | -0.001, -0.013 RMS:0.021 |

# List of Figures

# List of Tables

# Bibliography


Abramson, G. 2018, Research Notes of the American Astronomical Society, 2, 150

Adams, J. D., Stauffer, J. R., Monet, D. G., Skrutskie, M. F., & Beichman, C. A. 2001, AJ, 121, 2053

Adams, J. D., Stauffer, J. R., Skrutskie, M. F., et al. 2002, AJ, 124, 1570

Adelman-McCarthy, J. K. & et al. 2011, VizieR Online Data Catalog, II/306

Agüeros, M. A., Covey, K. R., Lemonias, J. J., et al. 2011, ApJ, 740, 110

Alam, S., Albareti, F. D., Allende Prieto, C., et al. 2015, ApJS, 219, 12

Allain, S., Fernandez, M., Martin, E. L., & Bouvier, J. 1996, A&A, 314, 173

Allard, F., Hauschildt, P. H., Alexander, D. R., & Starrfield, S. 1997, ARA&A, 35, 137

Allen, C. W. 1973, Astrophysical quantities

An, D., Terndrup, D. M., Pinsonneault, M. H., et al. 2007, ApJ, 655, 233

Angus, R., Aigrain, S., Foreman-Mackey, D., & McQuillan, A. 2015, MNRAS, 450, 1787

Angus, R., Morton, T. D., Foreman-Mackey, D., et al. 2019, AJ, 158, 173

Arenou, F., Luri, X., Babusiaux, C., et al. 2018, A&A, 616, A17

Artyukhina, N. M. 1969, Soviet Ast., 12, 987

Asplund, M., Grevesse, N., Sauval, A. J., & Scott, P. 2009, ARA&A, 47, 481

Aver, E., Olive, K. A., Porter, R. L., & Skillman, E. D. 2013, J. Cosmology Astropart. Phys., 2013, 017

Bailer-Jones, C. A. L., Rybizki, J., Fouesneau, M., Mantelet, G., & Andrae, R. 2018, AJ, 156, 58

Baker, D. E. A., Jameson, R. F., Casewell, S. L., et al. 2010, MNRAS, 408, 2457

Bakos, G., Noyes, R. W., Kovács, G., et al. 2004, PASP, 116, 266

Baraffe, I., Chabrier, G., Allard, F., & Hauschildt, P. H. 1998, A&A, 337, 403

Baraffe, I., Homeier, D., Allard, F., & Chabrier, G. 2015, A&A, 577, A42

Barnes, J. R., Collier Cameron, A., Unruh, Y. C., Donati, J. F., & Hussain, G. A. J. 1998, MNRAS, 299, 904

Barnes, S. A. 2003, ApJ, 586, 464

Barnes, S. A. 2007, ApJ, 669, 1167

Barrado, D., Bouy, H., Bouvier, J., et al. 2016, A&A, 596, A113

Barrado y Navascués, D., Stauffer, J. R., & Jayawardhana, R. 2004, ApJ, 614, 386

Basri, G., Marcy, G. W., & Graham, J. R. 1996, ApJ, 458, 600

Basri, G. & Martín, E. L. 1999, ApJ, 510, 266

Basu, S. & Antia, H. M. 2004, ApJ, 606, L85

Belikov, A. N., Kharchenko, N. V., Piskunov, A. E., et al. 2002, A&A, 384, 145

Bell, C. P. M., Rees, J. M., Naylor, T., et al. 2014, MNRAS, 445, 3496

Bertelli, G., Bressan, A., Chiosi, C., Fagotto, F., & Nasi, E. 1994, A&AS, 106, 275

Bertelli, G., Girardi, L., Marigo, P., & Nasi, E. 2008, A&A, 484, 815

Bertelli, G., Nasi, E., Girardi, L., & Marigo, P. 2009, A&A, 508, 355

Bessell, M. S. 1979, PASP, 91, 589

Bessell, M. S. & Brett, J. M. 1988, PASP, 100, 1134

Bessell, M. S. & Weis, E. W. 1987, PASP, 99, 642

Bihain, G., Rebolo, R., Béjar, V. J. S., et al. 2006, A&A, 458, 805

Bihain, G., Rebolo, R., Zapatero Osorio, M. R., Béjar, V. J. S., & Caballero, J. A. 2010, A&A, 519, A93

Bjork, S. R. & Chaboyer, B. 2006, ApJ, 641, 1102

Bonatto, C., Bica, E., & Girardi, L. 2004, A&A, 415, 571

Borucki, W. J., Koch, D. G., Lissauer, J. J., et al. 2003, in Society of Photo-Optical Instrumentation Engineers (SPIE) Conference Series, Vol. 4854, Future EUV/UV and Visible Space Astrophysics Missions and Instrumentation., ed. J. C. Blades & O. H. W. Siegmund, 129–140

Boss, L. 1908, Popular Astronomy, 16, 566

Boudreault, S., Lodieu, N., Deacon, N. R., & Hambly, N. C. 2012, MNRAS, 426, 3419

Bouvier, J., Forestini, M., & Allain, S. 1997, A&A, 326, 1023

Bouvier, J., Kendall, T., Meeus, G., et al. 2008, A&A, 481, 661

Bouvier, J., Stauffer, J. R., Martin, E. L., et al. 1998, A&A, 336, 490

Bouy, H., Bertin, E., Moraux, E., et al. 2013, A&A, 554, A101

Bouy, H., Bertin, E., Sarro, L. M., et al. 2015, A&A, 577, A148

Brandt, T. D. & Huang, C. X. 2015, ApJ, 807, 58

Bressan, A., Fagotto, F., Bertelli, G., & Chiosi, C. 1993, A&AS, 100, 647

Bressan, A., Marigo, P., Girardi, L., et al. 2012, MNRAS, 427, 127

Burke, C. J., Pinsonneault, M. H., & Sills, A. 2004, ApJ, 604, 272

Caffau, E., Ludwig, H. G., Steffen, M., Freytag, B., & Bonifacio, P. 2011, Sol. Phys., 268, 255

Cantat-Gaudin, T. & Anders, F. 2020, A&A, 633, A99

Carlberg, J. K., Majewski, S. R., Patterson, R. J., et al. 2011, ApJ, 732, 39

Carney, B. W. & Aaronson, M. 1979, AJ, 84, 867

Carrera, R., Bragaglia, A., Cantat-Gaudin, T., et al. 2019, A&A, 623, A80

Casagrande, L., Flynn, C., Portinari, L., Girardi, L., & Jimenez, R. 2007, MNRAS, 382, 1516

Casewell, S. L., Dobbie, P. D., Hodgkin, S. T., et al. 2007, MNRAS, 378, 1131

Casewell, S. L., Jameson, R. F., Burleigh, M. R., et al. 2011, MNRAS, 412, 2071

Casewell, S. L., Jameson, R. F., & Dobbie, P. D. 2006, MNRAS, 365, 447

Castelaz, M. W., Persinger, T., Stein, J. W., Prosser, J., & Powell, H. D. 1991, AJ, 102, 2103

Ceillier, T., Tayar, J., Mathur, S., et al. 2017, A&A, 605, A111

Chabrier, G. & Baraffe, I. 1997, A&A, 327, 1039

Chabrier, G. & Baraffe, I. 2000, ARA&A, 38, 337

Chambers, K. C., Magnier, E. A., Metcalfe, N., et al. 2016, arXiv e-prints, arXiv:1612.05560

Chen, Y., Girardi, L., Bressan, A., et al. 2014, MNRAS, 444, 2525

Choi, J., Dotter, A., Conroy, C., et al. 2016, ApJ, 823, 102

Claret, A. & Torres, G. 2016, A&A, 592, A15

Coc, A., Uzan, J.-P., & Vangioni, E. 2013, arXiv e-prints, arXiv:1307.6955

Collier Cameron, A., Davidson, V. A., Hebb, L., et al. 2009, MNRAS, 400, 451

Copenhagen University, O., Institute, A. O., Cambridge, Uk, & Real Instituto Y Observatorio de La Armada, F. E. S. 2006, VizieR Online Data Catalog, I/304

Cossburn, M. R., Hodgkin, S. T., Jameson, R. F., & Pinfield, D. J. 1997, MNRAS, 288, L23

Covey, K. R., Agüeros, M. A., Law, N. M., et al. 2016, ApJ, 822, 81

Cutri, R. M., Skrutskie, M. F., van Dyk, S., et al. 2003, VizieR Online Data Catalog, II/246

Cutri, R. M., Skrutskie, M. F., van Dyk, S., et al. 2012, VizieR Online Data Catalog, II/281

Cyburt, R. H., Fields, B. D., & Olive, K. A. 2008, J. Cosmology Astropart. Phys., 2008, 012

Dahm, S. E. 2015, ApJ, 813, 108

D'Antona, F. & Mazzitelli, I. 1994, ApJS, 90, 467

De Gennaro, S., von Hippel, T., Jefferys, W. H., et al. 2009, ApJ, 696, 12

Deacon, N. R. & Hambly, N. C. 2004, A&A, 416, 125

Delorme, P., Cameron, A. C., Hebb, L., et al. 2011a, in Astronomical Society of the Pacific Conference Series, Vol. 448, 16th Cambridge Workshop on Cool Stars, Stellar Systems, and the Sun, ed. C. Johns-Krull, M. K. Browning, & A. A. West, 841

Delorme, P., Collier Cameron, A., Hebb, L., et al. 2011b, MNRAS, 413, 2218

Dias, W. S., Monteiro, H., Caetano, T. C., et al. 2014, A&A, 564, A79

Dickens, R. J., Kraft, R. P., & Krzeminski, W. 1968, AJ, 73, 6

Dobbie, P. D., Pinfield, D. J., Jameson, R. F., & Hodgkin, S. T. 2002, MNRAS, 335, L79

Dotter, A., Chaboyer, B., Ferguson, J. W., et al. 2007, ApJ, 666, 403

Dotter, A., Chaboyer, B., Jevremović, D., et al. 2008, ApJS, 178, 89

Douglas, S. T., Agüeros, M. A., Covey, K. R., et al. 2014, ApJ, 795, 161

Douglas, S. T., Agüeros, M. A., Covey, K. R., et al. 2016, ApJ, 822, 47

Douglas, S. T., Agüeros, M. A., Covey, K. R., & Kraus, A. 2017, ApJ, 842, 83

Douglas, S. T., Curtis, J. L., Agüeros, M. A., et al. 2019, ApJ, 879, 100

Duchêne, G. & Kraus, A. 2013, ARA&A, 51, 269

Eddington, A. S. 1910, MNRAS, 71, 43

Eddington, A. S. 1926, The Internal Constitution of the Stars

Eggen, O. J. 1982, ApJS, 50, 221

Eichhorn, H., Googe, W. D., Lukac, C. F., & Murphy, J. K. 1970, MmRAS, 73, 125

Feiden, G. A. & Chaboyer, B. 2014, ApJ, 789, 53

Festin, L. 1998, A&A, 333, 497

Fossati, L., Bagnulo, S., Landstreet, J., et al. 2008, A&A, 483, 891

Gaia Collaboration, Babusiaux, C., van Leeuwen, F., et al. 2018a, A&A, 616, A10

Gaia Collaboration, Brown, A. G. A., Vallenari, A., et al. 2018b, A&A, 616, A1

Gaia Collaboration, Brown, A. G. A., Vallenari, A., et al. 2016, A&A, 595, A2

Gaia Collaboration, van Leeuwen, F., Vallenari, A., et al. 2017, A&A, 601, A19

Gennaro, M., Prada Moroni, P. G., & Degl'Innocenti, S. 2010, A&A, 518, A13

Gingerich, O. 2013, in Astronomical Society of the Pacific Conference Series, Vol. 471, Origins of the Expanding Universe: 1912-1932, ed. M. J. Way & D. Hunter, 205

Girardi, L., Bressan, A., Bertelli, G., & Chiosi, C. 2000, A&AS, 141, 371

Goldman, B., Röser, S., Schilbach, E., et al. 2013, A&A, 559, A43

Gossage, S., Conroy, C., Dotter, A., et al. 2018, ApJ, 863, 67

Grevesse, N. & Sauval, A. J. 1998, Space Sci. Rev., 85, 161

Hambly, N. C., Hawkins, M. R. S., & Jameson, R. F. 1993, A&AS, 100, 607

Hambly, N. C., Hodgkin, S. T., Cossburn, M. R., & Jameson, R. F. 1999, MNRAS, 303, 835

Hanson, R. B. 1975, AJ, 80, 379

Haro, G., Chavira, E., & Gonzalez, G. 1982, Boletin del Instituto de Tonantzintla, 3, 3

Harris, W. E., Fitzgerald, M. P., & Reed, B. C. 1981, PASP, 93, 507

Harris, W. E. & Racine, R. 1979, ARA&A, 17, 241

Hartman, J. D., Bakos, G. Á., Kovács, G., & Noyes, R. W. 2010, MNRAS, 408, 475

Hartman, J. D., Bakos, G. Á., Noyes, R. W., et al. 2011, AJ, 141, 166

Hartmann, L. 2009, Accretion Processes in Star Formation: Second Edition

Herbig, G. H. 1962, ApJ, 135, 736

Hertzsprung, E. 1911, Publikationen des Astrophysikalischen Observatoriums zu Potsdam, 22, A1

Hertzsprung, E. 1947, Annalen van de Sterrewacht te Leiden, 19, A1

Hillenbrand, L. A., Zhang, C., Riddle, R. L., et al. 2018, AJ, 155, 51

Høg, E., Fabricius, C., Makarov, V. V., et al. 2000, A&A, 355, L27

Howell, S. B., Sobeck, C., Haas, M., et al. 2014, PASP, 126, 398

Irwin, J. & Bouvier, J. 2009, in The Ages of Stars, ed. E. E. Mamajek, D. R. Soderblom, & R. F. G. Wyse, Vol. 258, 363–374

Jackson, R. J. & Jeffries, R. D. 2010, MNRAS, 402, 1380

Jameson, R. F., Dobbie, P. D., Hodgkin, S. T., & Pinfield, D. J. 2002, MNRAS, 335, 853

Jameson, R. F. & Skillen, I. 1989, MNRAS, 239, 247

Johnson, H. L. 1952, ApJ, 116, 640

Johnson, H. L. & Knuckles, C. F. 1955, ApJ, 122, 209

Johnson, H. L., Mcarthur, J. W., & Mitchell, R. I. 1968, ApJ, 152, 465

Johnson, H. L. & Mitchell, R. I. 1958, ApJ, 128, 31

Johnson, H. L., Mitchell, R. I., Iriarte, B., & Wisniewski, W. Z. 1966, Communications of the Lunar and Planetary Laboratory, 4, 99

Joner, M. D., Taylor, B. J., Laney, C. D., & van Wyk, F. 2006, AJ, 132, 111

Jones, B. F. 1981, AJ, 86, 290

Jones, B. F. & Cudworth, K. 1983, AJ, 88, 215

Jones, B. F. & Stauffer, J. R. 1991, AJ, 102, 1080

Kaiser, N., Aussel, H., Burke, B. E., et al. 2002, in Society of Photo-Optical Instrumentation Engineers (SPIE) Conference Series, Vol. 4836, Survey and Other Telescope Technologies and Discoveries, ed. J. A. Tyson & S. Wolff, 154–164

Kamai, B. L., Vrba, F. J., Stauffer, J. R., & Stassun, K. G. 2014, AJ, 148, 30

Kawaler, S. D. 1989, ApJ, 343, L65

Khalaj, P. & Baumgardt, H. 2013, MNRAS, 434, 3236

Kharchenko, N. V. 2001, Kinematika i Fizika Nebesnykh Tel, 17, 409

Kharchenko, N. V., Piskunov, A. E., Röser, S., Schilbach, E., & Scholz, R. D. 2005, A&A, 438, 1163

Kharchenko, N. V., Piskunov, A. E., Röser, S., et al. 2009, A&A, 504, 681

Kippenhahn, R., Weigert, A., & Hofmeister, E. 1967, Methods in Computational Physics, 7, 129

Klein Wassink, W. J. 1924, Bull. Astron. Inst. Netherlands, 2, 183

Klein Wassink, W. J. 1927, Publications of the Kapteyn Astronomical Laboratory Groningen, 41, 1

Kopytova, T. G., Brandner, W., Tognelli, E., et al. 2016, A&A, 585, A7

Kovács, G., Hartman, J. D., Bakos, G. Á., et al. 2014, MNRAS, 442, 2081

Kraus, A. L. & Hillenbrand, L. A. 2007, AJ, 134, 2340

Krełowski, J., Strobel, A., Galazutdinov, G. A., Bondar, A., & Valyavin, G. 2019, MNRAS, 486, 112

Landolt, A. U. 1992, AJ, 104, 340

Landolt, A. U. 2009, AJ, 137, 4186

Landolt, A. U. 2013, AJ, 146, 131

Law, N. M., Kulkarni, S. R., Dekany, R. G., et al. 2009, PASP, 121, 1395

Lawrence, A., Warren, S. J., Almaini, O., et al. 2013, VizieR Online Data Catalog, II/319

Lebreton, Y. 2005, in ESA Special Publication, Vol. 576, The Three-Dimensional Universe with Gaia, ed. C. Turon, K. S. O'Flaherty, & M. A. C. Perryman, 493

Lebreton, Y., Fernandes, J., & Lejeune, T. 2001, A&A, 374, 540

Lebreton, Y., Goupil, M. J., & Montalbán, J. 2014, in EAS Publications Series, Vol. 65, EAS Publications Series, 99–176

Leggett, S. K., Harris, H. C., & Dahn, C. C. 1994, AJ, 108, 944

Li, J., Smith, M. C., Zhong, J., et al. 2016, ApJ, 823, 59

Lodieu, N. 2020, Mem. Soc. Astron. Italiana, 91, 84

Lodieu, N., Deacon, N. R., & Hambly, N. C. 2012, MNRAS, 422, 1495

Lodieu, N., Dobbie, P. D., Deacon, N. R., et al. 2007, MNRAS, 380, 712

Lodieu, N., McCaughrean, M. J., Barrado Y Navascués, D., Bouvier, J., & Stauffer, J. R. 2005, A&A, 436, 853

Lodieu, N., Pérez-Garrido, A., Smart, R. L., & Silvotti, R. 2019a, A&A, 628, A66

Lodieu, N., Rebolo, R., & Pérez-Garrido, A. 2018, A&A, 615, L12

Lodieu, N., Smart, R. L., Pérez-Garrido, A., & Silvotti, R. 2019b, A&A, 623, A35

Loktin, A. V. & Beshenov, G. V. 2001, Astronomy Letters, 27, 386

Loktin, A. V., Gerasimenko, T. P., & Malysheva, L. K. 2001, Astronomical and Astrophysical Transactions, 20, 607

Luri, X., Brown, A. G. A., Sarro, L. M., et al. 2018, A&A, 616, A9

Maeder, A. & Mermilliod, J. C. 1981, A&A, 93, 136

Makarov, V. V. 2006, AJ, 131, 2967

Mamajek, E. E. & Hillenbrand, L. A. 2008, ApJ, 687, 1264

Marigo, P. 2001, A&A, 370, 194

Marilli, E., Catalano, S., & Frasca, A. 1997, Mem. Soc. Astron. Italiana, 68, 895

Martín, E. L., Dahm, S., & Pavlenko, Y. 2001, in Astronomical Society of the Pacific Conference Series, Vol. 245, Astrophysical Ages and Times Scales, ed. T. von Hippel, C. Simpson, & N. Manset, 349

Martín, E. L., Lodieu, N., Pavlenko, Y., & Béjar, V. J. S. 2018, ApJ, 856, 40

Martin, E. L., Zapatero Osorio, M. R., & Rebolo, R. 1998, in Astronomical Society of the Pacific Conference Series, Vol. 134, Brown Dwarfs and Extrasolar Planets, ed. R. Rebolo, E. L. Martin, & M. R. Zapatero Osorio, 507

Mason, B. D., Wycoff, G. L., Hartkopf, W. I., Douglass, G. G., & Worley, C. E. 2001, AJ, 122, 3466

Mazzei, P. & Pigatto, L. 1989, A&A, 213, L1

McNally, D. 1965, The Observatory, 85, 166

Meibom, S., Mathieu, R. D., & Stassun, K. G. 2009, ApJ, 695, 679

Melis, C., Reid, M. J., Mioduszewski, A. J., Stauffer, J. R., & Bower, G. C. 2014, Science, 345, 1029

Melnikov, S. & Eislöffel, J. 2012, A&A, 544, A111

Melnikov, S. & Eislöffel, J. 2018, A&A, 611, A34

Mendoza, E. E. 1967, Boletin de los Observatorios Tonantzintla y Tacubaya, 4, 149

Mermilliod, J. C. 1981, A&A, 97, 235

Mermilliod, J. C., Grenon, M., & Mayor, M. 2008, A&A, 491, 951

Mermilliod, J. C., Mayor, M., & Udry, S. 2009a, A&A, 498, 949

Mermilliod, J. C., Mayor, M., & Udry, S. 2009b, A&A, 498, 949

Mermilliod, J. C., Weis, E. W., Duquennoy, A., & Mayor, M. 1990, A&A, 235, 114

Messina, S., Pizzolato, N., Guinan, E. F., & Rodonò, M. 2003, A&A, 410, 671

Messina, S., Rodonò, M., & Guinan, E. F. 2001, A&A, 366, 215

Meynet, G., Mermilliod, J. C., & Maeder, A. 1993, A&AS, 98, 477

Moffat, A. F. J. 1969, A&A, 3, 455

Moraux, E., Bouvier, J., & Stauffer, J. R. 2001, A&A, 367, 211

Moraux, E., Bouvier, J., Stauffer, J. R., & Cuilland re, J. C. 2003, A&A, 400, 891

Morzinski, K. M. 2011, in American Astronomical Society Meeting Abstracts, Vol. 217, American Astronomical Society Meeting Abstracts #217, 226.02

Mowlavi, N., Eggenberger, P., Meynet, G., et al. 2012, A&A, 541, A41

Netopil, M., Paunzen, E., Heiter, U., & Soubiran, C. 2016, A&A, 585, A150

Nunez, A. 2018, PhD thesis, Columbia University

O'dell, M. A. & Collier Cameron, A. 1993, MNRAS, 262, 521

O'dell, M. A., Hendry, M. A., & Collier Cameron, A. 1994, MNRAS, 268, 181

O'dell, M. A., Hilditch, R. W., Collier Cameron, A., & Bell, S. A. 1997, MNRAS, 284, 874

Olivares, J., Moraux, E., Sarro, L. M., et al. 2018, A&A, 612, A70

Pace, G., Melendez, J., Pasquini, L., et al. 2009, A&A, 499, L9

Pace, G. & Pasquini, L. 2004, A&A, 426, 1021

Palmer, M., Arenou, F., Luri, X., & Masana, E. 2014, A&A, 564, A49

Patenaude, M. 1978, A&A, 66, 225

Patience, J., Ghez, A. M., Reid, I. N., & Matthews, K. 2002, AJ, 123, 1570

Patience, J., Ghez, A. M., Reid, I. N., Weinberger, A. J., & Matthews, K. 1998, AJ, 115, 1972

Paxton, B., Bildsten, L., Dotter, A., et al. 2011, ApJS, 192, 3

Paxton, B., Cantiello, M., Arras, P., et al. 2013, ApJS, 208, 4

Paxton, B., Marchant, P., Schwab, J., et al. 2015, ApJS, 220, 15

Pecaut, M. J. & Mamajek, E. E. 2013, ApJS, 208, 9

Pecaut, M. J., Mamajek, E. E., & Bubar, E. J. 2012, ApJ, 746, 154

Perryman, M. A. C., Brown, A. G. A., Lebreton, Y., et al. 1998, A&A, 331, 81

Perryman, M. A. C., Lindegren, L., Kovalevsky, J., et al. 1997, A&A, 500, 501

Pinfield, D. J., Hodgkin, S. T., Jameson, R. F., et al. 2000, MNRAS, 313, 347

Pinsonneault, M. H., Stauffer, J., Soderblom, D. R., King, J. R., & Hanson, R. B. 1998, ApJ, 504, 170

Pinsonneault, M. H., Terndrup, D. M., Hanson, R. B., & Stauffer, J. R. 2004, ApJ, 600, 946

Pizzolato, N., Maggio, A., Micela, G., Sciortino, S., & Ventura, P. 2003, A&A, 397, 147

Pojmanski, G. 2002, Acta Astron., 52, 397

Pollacco, D., Skillen, I., Collier Cameron, A., et al. 2006, Ap&SS, 304, 253

Prosser, C. F. 1992, AJ, 103, 488

Prosser, C. F. & Grankin, K. N. 1997, Rotation Periods of Open Cluster Stars. IV., Center for Astrophysics Preprint Series No. 4539

Prosser, C. F., Schild, R. E., Stauffer, J. R., & Jones, B. F. 1993a, PASP, 105, 269

Prosser, C. F., Shetrone, M. D., Dasgupta, A., et al. 1995, PASP, 107, 211

Prosser, C. F., Shetrone, M. D., Marilli, E., et al. 1993b, PASP, 105, 1407

Prosser, C. P. & Randich, S. 1998, Astronomische Nachrichten, 319, 201

Radick, R. R., Lockwood, G. W., Skiff, B. A., & Thompson, D. T. 1995, ApJ, 452, 332

Radick, R. R., Skiff, B. A., & Lockwood, G. W. 1990, ApJ, 353, 524

Radick, R. R., Thompson, D. T., Lockwood, G. W., Duncan, D. K., & Baggett, W. E. 1987, ApJ, 321, 459

Rau, A., Kulkarni, S. R., Law, N. M., et al. 2009, PASP, 121, 1334

Rebull, L. M., Stauffer, J. R., Bouvier, J., et al. 2016, AJ, 152, 113

Rebull, L. M., Stauffer, J. R., Hillenbrand, L. A., et al. 2017, ApJ, 839, 92

Reid, N. 1992, MNRAS, 257, 257

Robichon, N., Arenou, F., Mermilliod, J. C., & Turon, C. 1999, A&A, 345, 471

Roeser, S., Demleitner, M., & Schilbach, E. 2010, AJ, 139, 2440

Röser, S., Schilbach, E., Piskunov, A. E., Kharchenko, N. V., & Scholz, R. D. 2011, A&A, 531, A92

Russell, H. N. 1913, The Observatory, 36, 324

Sampedro, L., Dias, W. S., Alfaro, E. J., Monteiro, H., & Molino, A. 2017, MNRAS, 470, 3937

Sandage, A. 1962, ApJ, 135, 349

Sanner, J. & Geffert, M. 2001, A&A, 370, 87

Sarro, L. M., Bouy, H., Berihuete, A., et al. 2014, A&A, 563, A45

Scholz, A., Irwin, J., Bouvier, J., et al. 2011, MNRAS, 413, 2595

Sestito, P. & Randich, S. 2005, A&A, 442, 615

Silaj, J. & Landstreet, J. D. 2014, A&A, 566, A132

Simons, D. A. & Becklin, E. E. 1992, ApJ, 390, 431

Skrutskie, M. F., Cutri, R. M., Stiening, R., et al. 2006, AJ, 131, 1163

Skumanich, A. 1972, ApJ, 171, 565

Soderblom, D. R. 2010, ARA&A, 48, 581

Soderblom, D. R., Jones, B. F., Balachand ran, S., et al. 1993, AJ, 106, 1059

Spada, F., Demarque, P., Kim, Y. C., Boyajian, T. S., & Brewer, J. M. 2017, ApJ, 838, 161

Stauffer, J. 1982a, PASP, 94, 678

Stauffer, J., Hamilton, D., Probst, R., Rieke, G., & Mateo, M. 1989a, ApJ, 344, L21

Stauffer, J., Klemola, A., Prosser, C., & Probst, R. 1991, AJ, 101, 980

Stauffer, J. R. 1982b, AJ, 87, 1507

Stauffer, J. R. 1984, ApJ, 280, 189

Stauffer, J. R., Barrado y Navascués, D., Bouvier, J., et al. 1999, ApJ, 527, 219

Stauffer, J. R. & Hartmann, L. W. 1987, ApJ, 318, 337

Stauffer, J. R., Hartmann, L. W., Burnham, J. N., & Jones, B. F. 1985, ApJ, 289, 247

Stauffer, J. R., Hartmann, L. W., Fazio, G. G., et al. 2007, ApJS, 172, 663

Stauffer, J. R., Hartmann, L. W., & Jones, B. F. 1989b, ApJ, 346, 160

Stauffer, J. R., Jones, B. F., Backman, D., et al. 2003, AJ, 126, 833

Stauffer, J. R., Liebert, J., & Giampapa, M. 1995, AJ, 109, 298

Stauffer, J. R., Liebert, J., Giampapa, M., et al. 1994, AJ, 108, 160

Stauffer, J. R., Schild, R., Barrado y Navascués, D., et al. 1998a, ApJ, 504, 805

Stauffer, J. R., Schild, R. A., Baliunas, S. L., & Africano, J. L. 1987, PASP, 99, 471

Stauffer, J. R., Schultz, G., & Kirkpatrick, J. D. 1998b, ApJ, 499, L199

Steele, I. A., Jameson, R. F., & Hambly, N. C. 1993, MNRAS, 263, 647

Tabernero, H. M., Montes, D., & González Hernández, J. I. 2012, A&A, 547, A13

Tang, S.-Y., Chen, W. P., Chiang, P. S., et al. 2018, ApJ, 862, 106

Tang, S.-Y., Pang, X., Yuan, Z., et al. 2019, ApJ, 877, 12

Terrien, R. C., Mahadevan, S., Deshpande, R., et al. 2014, ApJ, 782, 61

Trumpler, R. J. 1921, Lick Observatory Bulletin, 333, 110

Trumpler, R. J. 1938, Lick Observatory Bulletin, 494, 167

Turner, D. G. 1979, PASP, 91, 642

Upgren, A. R., Weis, E. W., & Deluca, E. E. 1979, AJ, 84, 1586

Upgren, A. R., Weis, E. W., & Hanson, R. B. 1985, AJ, 90, 2039

van Leeuwen, F. 1999, in Astronomical Society of the Pacific Conference Series, Vol. 167, Harmonizing Cosmic Distance Scales in a Post-HIPPARCOS Era, ed. D. Egret & A. Heck, 52–71

van Leeuwen, F. 2009, A&A, 497, 209

van Leeuwen, F., Alphenaar, P., & Brand, J. 1986, A&AS, 65, 309

VandenBerg, D. A., Bergbusch, P. A., & Dowler, P. D. 2006, ApJS, 162, 375

Vandenberg, D. A. & Bridges, T. J. 1984, ApJ, 278, 679

VandenBerg, D. A. & Clem, J. L. 2003, AJ, 126, 778

Wang, P. F., Chen, W. P., Lin, C. C., et al. 2014, ApJ, 784, 57

Weis, E. W. 1981, PASP, 93, 437

Weis, E. W., Deluca, E. E., & Upgren, A. R. 1979, PASP, 91, 766

Weis, E. W. & Hanson, R. B. 1988, AJ, 96, 148

Weis, E. W. & Upgren, A. R. 1977, in Bulletin of the American Astronomical Society, Vol. 9, 332

Weis, E. W. & Upgren, A. R. 1982, PASP, 94, 475

Wenger, M., Ochsenbein, F., Egret, D., et al. 2000, A&AS, 143, 9

Willliams, D. M., Boyle, R. P., Morgan, W. T., et al. 1996, ApJ, 464, 238

Wright, E. L., Eisenhardt, P. R. M., Mainzer, A. K., et al. 2010, AJ, 140, 1868

Yi, S. K., Demarque, P., & Kim, Y.-C. 2003, in Extragalactic Globular Cluster Systems, ed. M. Kissler-Patig, 255

Yoon, S. C., Dierks, A., & Langer, N. 2012, A&A, 542, A113

Zacharias, N., Finch, C. T., Girard, T. M., et al. 2013, AJ, 145, 44

Zapatero Osorio, M. R., Béjar, V. J. S., Lodieu, N., & Manjavacas, E. 2018, MNRAS, 475, 139

Zapatero Osorio, M. R., Gálvez Ortiz, M. C., Bihain, G., et al. 2014, A&A, 568, A77

Zapatero Osorio, M. R., Martin, E. L., & Rebolo, R. 1997a, A&A, 323, 105

Zapatero Osorio, M. R., Rebolo, R., & Martin, E. L. 1997b, A&A, 317, 164

Zapatero Osorio, M. R., Rebolo, R., Martín, E. L., et al. 1997c, ApJ, 491, L81

Zapatero Osorio, M. R., Rebolo, R., Martín, E. L., et al. 1999, A&AS, 134, 537

Zuckerman, B., Melis, C., Rhee, J. H., Schneider, A., & Song, I. 2012, ApJ, 752, 58